STUDIES TOWARDS DEVELOPMENT OF IMPROVED MODELLING AND SCALE-UP PROCEDURES FOR DENSE-PHASE PNEUMATIC CONVEYING OF FINE POWDERS

A thesis submitted in fulfilment of the requirements
for the award of the degree of

DOCTOR OF PHILOSOPHY

Submitted by

KAPIL SHARMA

Registration No.: 901508009

DEPARTMENT OF MECHANICAL ENGINEERING

THAPAR INSTITUTE OF ENGINEERING & TECHNOLOGY

(Deemed to be University)

PATIALA-147004,

PUNJAB, INDIA

February 2020

This thesis is dedicated to my parents,

Shukla Sharma and Vijay Sharma, my sister Sunita Sharma and my nephew Parav

Sharma for their love, support and patience

THESIS CERTIFICATION

I, Kapil Sharma, hereby certify that the work which is being presented in this thesis report entitled **"Studies Towards Development of Improved Modelling and Scale-up Procedures for Dense-Phase Pneumatic Conveying of Fine Powders"** submitted in fulfilment of the requirements for the award of the degree of **Doctor of Philosophy** in Department of Mechanical Engineering, Thapar Institute of Engineering and Technology, Patiala, Punjab, India, is an authentic record of my own work carried out under the supervision of Dr. S.S. Mallick, Associate Professor and Dr. Anu Mittal, Assistant Professor, Department of Mechanical Engineering, Thapar Institute of Engineering and Technology, Patiala, Punjab, India from Jan 2016 to Jun 2019. The matter presented in this thesis work has not been submitted in any other University / Institute for the award of any other degree.

Kapil Sharma

Kapil Sharma Date: February 18, 2020

Registration No.: 901508009

This is to certify that the above statement made by the student is correct to the best of my knowledge and belief.

Dr. S.S. Mallick, PhD Supervisor
(Associate Professor)

Dr. Anu Mittal, PhD Supervisor
(Assistant Professor)

Department of Mechanical Engineering, Thapar Institute of Engineering and Technology, Patiala, Punjab, India

ACKNOWLEDGEMENTS

With deep sense of gratitude, I express my sincere thanks to my supervisors Dr. S.S. Mallick, Associate Professor and Dr. Anu Mittal, Assistant Professor, Mechanical Engineering Department (MED), Laboratory for Particle and Bulk Solids Technologies, Thapar Institute of Engineering and Technology, Patiala, Punjab, India for their valuable guidance, constructive suggestions/ideas and constant encouragement during the course of my Ph.D. research work. It has been a great honor for me to be a student of Dr. S.S. Mallick and Dr. Anu Mittal.

I am thankful to Prof. Dr. Peter Wypych of University of Wollongong, Australia and Dr. Renhu Pan of Fujian Longking Co., China, for their valuable guidance at times and support.

I also express my gratitude to my Master degree supervisor, Dr. Kundan Lal Rana (Assistant Professor, Thapar Institute of Engineering and Technology, Patiala, Punjab, India) for inspiring me to go for Doctorate research. He has always been a source of great motivation for me. In addition, I would like to thank him for the continuous encouragement and kind support.

I also pay thanks to Mr. Atul Sharma, Lecturer and Dr. Gautam Setia, Assistant Professor, Mechanical Engineering Department (MED), Laboratory for Particle and Bulk Solids Technologies, Thapar Institute of Engineering and Technology, Patiala, Punjab, India, for their moral support at times, providing guidance and help during the experimental trials.

I am highly indebted to National Thermal Power Corporation (NTPC), A Maharatna Company (A Government of India Enterprise) (PI: Dr. S.S. Mallick), for providing the financial support to carry out the Ph.D. research work.

My sincere and grateful thanks to Dr. T. P. Singh, Professor and Head, Mechanical Engineering Department (MED), Dr. D. Gangacharyulu, Professor, Chemical Engineering Department (CHED), Dr. Vikrant Khullar, Assistant Professor, Mechanical Engineering Department (MED), members of the doctoral committee for their technical as well as moral support during my research work.

I would like to thank the "Thapar Institute of Engineering and Technology," Patiala, Punjab, India, for providing me such a great environment to learn and perform my research. I also extend my thanks to the mechanical engineering laboratory staff and the library staff of the "Thapar Institute of Engineering and Technology," Patiala, Punjab, India.

I am grateful to my parents for giving me inspiration and moral support, which enable me to pursue my studies.

Above all, I express my thanks to the "ALMIGHTY" for blessings and kindness.

ABSTRACT

This thesis aims to provide an improved model for solids friction factor and particle velocity for fluidized dense-phase pneumatic conveying of fine powders. Due to the highly turbulent and concentrated moving dunes, only limited progress has been attained so far towards understanding the flow mechanism of fluidized dense-phase pneumatic conveying of fine powders. A new test facility has been developed for the pneumatic conveying of fine powders. Fine powders such as cement and fly ash were tested for their apparent rheology in a rotational powder rheology tester. Tests were carried out with different rotational speeds and fluidization air quantities. Governing equations for solids-gas flow for fluidized dense-phase pneumatic conveying of powders have been developed considering one-directional steady-state flow, and the same were solved by using Fourth-fifth-order Runge-Kutta-Fehlberg (RKF45) method for various solids flow and airflow rates for constant and variable fluidized bulk densities to determine particle and actual gas velocities. The results have shown an increasing trend of particle and actual gas velocities and decreasing trend of solids volumetric concentration in the direction of flow. From the numerically obtained values, a model for particle velocity has been obtained using solids loading ratio, dimensionless velocity, dimensionless diameter and dimensionless density terms covering flow, pipe and particle properties. An improved model for solids friction factor has been developed by incorporating an additional collision term representing energy loss due to particle-particle impact during conveying. The new solids friction factor model has been validated by using it to predict total pipeline pressure drop for length and diameter scale-up conditions and comparing the predicted pneumatic conveying characteristics against the experimental plots. The results confirm the improved prediction capability of the new solids friction factor model. The model has been further improved by incorporating apparent powder rheology terms in the expression for solids

friction factor model. Two different formats for modelling solids friction factor were evaluated; one format is scientifically more appropriate, whereas the other format provides practical convenience of testing and modelling. A comprehensive scale-up evaluation has shown that the format with convenience can provide satisfactory results from an industrial design point of view.

Keywords: Solids friction factor, Pneumatic conveying, Powder rheology, Runge-Kutta-Fehlberg, Particle velocity

TABLE OF CONTENTS

Page No.

LIST OF FIGURES

Page No.

CHAPTER 2

CHAPTER 3

CHAPTER 4

CHAPTER 5

ANNEXURE A1

ANNEXURE A2

ANNEXURE A3

LIST OF TABLES

Page No.

CHAPTER 5

ANNEXURE A2

LIST OF SYMBOLS AND ABBREVIATIONS

A	Cross-sectional area of control volume or pipe wall [m^2]
A_{sp}	Half pressure gradient from the power-law fluid [Pa/m]
A_{sy}	Half pressure gradient from the yield power-law fluid [Pa/m]
Ar	Archimedes Number
C	Particle velocity [m/s]
D	Internal diameter of pipe [m]
d_s, d_p	Particle diameter [μm]
d_{50}, D_{50}	Median particle diameter [μm]
E_L	Energy loss (K.E.) due to particle impact against other particles [Joule]
$F_r = V/(gD)^{0.5}$	Froude number of flow
$Fr_i = V_i/(gD)^{0.5}$	Froude number of flow at the beginning of the pipe
$Fr_s = w_{fo}/\sqrt{gd_{50}}$	Particle Froude number
Fr_m	Mean Froude number related to the section of pipe
F_a	Frictional force due to air phase [N]
F_s	Frictional force due to solids phase [N]
f_a	Frictional force per unit volume due to air phase [N/m^3]
f_s	Frictional force per unit volume due to solids phase [N/m^3]
g	Acceleration due to gravity [m/s^2]
K	Coefficient of power function

K_{st}	pressure drop coefficient for straight pipe sections
L	Total length of the pipe [m]
L_h	Length of horizontal pipe or test section [m]
L_v	Length of vertical pipe or test section [m]
m_p	Mass of each particle [kg]
m_f, m_a	Mass flow rate of air [kg/s]
m_s	Mass flow rate of solids [kg/s]
$m^* = m_s/m_a$	Solids loading ratio
ΔM_p	Total mass of particles in a control volume [kg]
$N.B.$	Number of bends
n	Number density of particles in the gas
N	Total number of particles in a control volume
P	Pressure [Pa]
ΔP_m	Change in momentum delivered by the particle [kg-m/s]
ΔP, ΔP_{st}	Pressure drop through a straight horizontal pipe or pipe section [Pa]
ΔP_{Total}	Total pipeline pressure drop [Pa]
ΔP_{accel}	Pressure drop due to initial acceleration [Pa]
ΔP_b	Pressure drop due to the bends [Pa]
ΔP_v	Pressure drop due to the verticals [Pa]
Stk	Stokes Number
t	Time [s]

u_a, u_g	Actual gas velocity [m/s]
u_s	Particle velocity [m/s]
V	Superficial air or gas velocity [m/s]
V_T	Total volume of gas [m^3]
V_{sp}	Specific volume [m^3]
$V_a = m_a/\rho_a$	Volumetric flow rate of air [m^3/s]
$V_s = m_s/\rho_{fl}$	Volumetric flow rate of solids [m^3/s]
$VLR =$ $\{(m_s/\rho_{fl})/(m_a/\rho_a)\}$	Volumetric loading ratio
w_f	Particle settling velocity in a cloud [m/s]
w_{fo}	Free settling velocity of an isolated particle [m/s]
w_{fo}/V	Dimensionless velocity

Greek symbols

λ_f	Air/gas only friction factor
λ_s	Solids friction factor through a straight pipe
λ_T	Combined solids-air friction factor
λ_s^*	Impact and friction factor for solids
$\varepsilon_a = V_a/(V_a + V_s)$	Volume fraction of air
$\varepsilon_s = V_s/(V_a + V_s)$	Volume fraction of solids
ε	Voidage
ρ, ρ_a	Density of air [kg/m^3]

ρ_s	Particle density [kg/m^3]
ρ_b	Loose-poured bulk density [kg/m^3]
ρ_{fl}	Fluidized bulk density [kg/m^3]
ρ_{sus}	Suspension density of the gas-solid mixture [kg/m^3]
μ	Dynamic viscosity of air [kg/ms]
$d\varphi$	Differential particle flux
$\Delta x, \Delta L$	Length of control volume [m]
β_o	Velocity ratio related to particle fall velocity in the undisturbed fluid $\left(\beta_o = {}^{w_{fo}}/_{V}\right)$
τ_1	Shear stress on the pipe wall due to the non-suspension layer in dense-phase regime [Pa]
τ_2	Shear stress on the pipe wall due to suspension layer in dense-phase regime [Pa]
τ	Shear Stress [Pa]

Abbreviations

3-D	Three Dimensional
BD	Bottom Discharge
CFD	Computational Fluid Dynamics
CFBR	Couette Fluidized-Bed Rheometer
DEM	Discrete Element Method
ESP	Electrostatic Precipitator

I.D.	Internal Diameter
IGT	Institute of Gas Technology
IPFs	Inter Particle Forces
MSFBR	Mechanically Stirred Fluidized Bed Rheometer
NRV	Non-return Valve
NTPC	National Thermal Power Corporation
ODE	Ordinary Differential Equation
PC	Personnel Computer
PCC	Pneumatic Conveying Characteristics
PIV	Particle Image Velocimetry
PRV	Pressure Reducing Valve
P&ID	Process and Instrumentation Diagram
RPM	Revolution Per Minute
RKF45	Runge-Kutta-Fehlberg
SEM	Scanning Electron Microscope
TD	Top Discharge
VLR	Volumetric Loading Ratio

Subscripts

$accel$	acceleration
b	bend
f, a	air/gas
fl	fluidized

i	initial condition
s, p	solid/particle
s_1	pure non-suspension layer (dense-phase)
s_2	suspension layer (dilute-phase)
T	Total
v	vertical
x, y, z	directions

Superscripts

a, b, c	Exponents of the power function

CHAPTER 1

INTRODUCTION AND OBJECTIVES

1.1 Introduction

Transportation of fine powders, such as cement, pulverized coal, fly ash, food products, chemical powders, pulverized coal, calcium carbonate, plastic pellets, etc. through pipelines by using gas as the conveying medium is mostly preferred in various industries including cement, chemical, coal-fired thermal power plants, pharmaceutical, petrochemical plants, calcium carbonate to list a few. Out of the various modes of conveying, for the transport of fine powders (fly ash, cement, alumina, barytes, pulverized coal), which have good air retention capabilities, the fluidized dense-phase method is preferred over the conventional dilute-phase flow. This is due to the fact that the fluidized dense-phase flow is characterized by high solids to gas mass flow rate ratio (can go up to 100) and because of that the following advantages are obtained: lower conveying velocity requirements at feed points due to the non-suspension nature of transportation, reduced airflow and size of air compressors, savings in operating power (can go up to 50% energy saving), lower wear rate of pipelines and bends, reduced size of solids-gas separation equipment, reduced size of pipes, and decreased rate of particles attrition and product degradation (Klinzing et al., 2010; Mallick, 2009). In order to ensure that the guaranteed amount of material is transported without flow blockage, designing of the fluidized dense-phase system is based on the estimation of two main parameters, which are the total pipeline pressure drop and minimum airflow rate requirement. Over-prediction of the total pipeline pressure drop would cause the use of large size of air movers, which would result in initial and operating cost increment. On the other hand, the reduced flow rate of material would be observed with the under-prediction of total pipeline pressure drop. Saltation in the pipeline, product build-up, unstable flow, and ultimately, pipeline blockage is caused by the underestimation of the reliable transport boundary (Wypych, 1989). The pressure

loss for solids-gas flow through a straight horizontal section of pipe can be expressed using equation (1.1), as given by Barth (1958).

$$\Delta P = \frac{\left(\left(\lambda_f + m^* \lambda_s\right)\rho_a L V^2\right)}{2D} \tag{1.1}$$

where 'ΔP' is the pressure drop in the horizontal section, 'λ_f' is the air (gas) only friction factor, 'm^*' is the solid loading ratio, 'λ_s' is the solids friction factor, 'ρ_a' is the density of air, 'L' is the total length of the pipe, 'V' is the superficial air velocity, and 'D' is the internal diameter of the pipe. The above equation (1.1) considers the pressure losses due to the gas and solids phases separately. In the above equation, it is relatively easier to calculate the other terms, such as air/gas-only friction factor (λ_f), solids loading ratio (m^*), the density of air (ρ_a), gas velocity (V) using the well-established models of thermos-fluids, but a precise estimation of solids friction factor is a challenging task due to the limited progress made so far towards understanding the fundamentals of changing flow mechanisms in fluidized dense-phase. The solids friction factor term is a combined depiction of loss of energy due to solids to solids, solids to gas, and solids to pipe wall interactions (Klinzing et al., 2010; Mallick, 2009). Weber (1981) used the expression represented in the equation (1.1) for coarse-grained particles, which are likely to be conveyed in the suspension flow mode (i.e., dilute-mode of flow). For certain products and types of flows, such as low-velocity slug-flow of granular products (Mi and Wypych, 1994; Mi and Wypych, 1995; Pan and Wypych, 1997) or the suspension flow mode (i.e., dilute flow mode) of bulk solids, fundamental modelling approaches based on the concept of empirical powder-function based mechanics have been developed in relatively more detail, because it is relatively easier to model this type of flow mechanism (Mallick, 2009). Also, the flow physics of energy required to lift the particles is well

defined (Pan, 1992). However, the accurate modelling of solids friction factor for the fluidized dense-phase conveying of fine powders as compared to the dilute-phase has been a far more challenging task to be solved at a similar level of accuracy. This occurs due to the highly concentrated, turbulent and complex nature of the gas-solids mixture moving in the fluidized bed (non-suspension mode) of fine powders under high solids to gas mass flow rate ratio, which makes it difficult to connect the particle and bulk properties during actual flow operating conditions and the subsequent accuracy of modelling and scale-up is compromised (Mallick, 2009).

Stegmaier (1978) developed a power function-based model to estimate solids friction factor for fly ash, alumina, quartz powder, sand, catalyst for horizontal transport with average particle size ranging from 15 to 112 μm and particle density from 1500 to 4100 kg/m^3, respectively for a range of flow conditions (dense- to dilute-phase). The developed model is presented in equation (1.2).

$$\lambda_s = 2.1\ (m^*)^{-0.3}\ (Fr)^{-2}\ (Fr_s)^{0.5}\ (D/d_s)^{0.1} \tag{1.2}$$

Rizk (1982) identified the various factors that contributed to the overall solids friction factor (λ_s). The developed model for solid friction factor (λ_s) worked well in the dilute phase. He mentioned 'λ_s' can be separated into two terms provided by the equation (1.3).

$$\lambda_s = \lambda_s{}^* \left(\frac{C}{V}\right) + 2\left(\frac{w_f}{V}\right)\Big/\left(\frac{C}{V}\right) Fr^2 \tag{1.3}$$

Where, $\lambda_s{}^*$ is related to the impact and friction of the solid particles (particle to particle/wall). The term $2\left(\frac{w_f}{V}\right)/\left(\frac{C}{V}\right) Fr^2$ is related to the energy loss due to keeping the particles in suspension.

Wypych et al. (1990, 1990a) presented a dilute-phase model, which was based on equation (1.3), and termed it as Weber A4 model, which was originally presented by Rizk (1982). However, the authors replaced the term $\beta = \frac{w_f}{V}$ by $\beta_o = \frac{w_{fo}}{V}$. Other empirical power function-based models have been popularly used over the years by several researchers, such as Pan and Wypych (1992), Pan (1992), Jones and Williams (2003), using dimensionless numbers, as given by equation (1.4).

$$\lambda_s = K(m^*)^a(Fr)^b \tag{1.4}$$

Pan and Wypych (1998) added the term, i.e., "particle to air density ratio" in the format given above (provided by equation 1.4) in order to incorporate the changes occurred in the "gas density" term along the pipeline (due to gas expansion), is given by equation (1.5). Four different fly ash samples were transported with average particle size ranging from 4 to 58 μm, particle density from 2197 to 2540 kg/m^3, and bulk density from 634 to 955 kg/m^3 for respective internal diameter taken from 52.5 to 105 mm and length from 70 to 564 m.

$$\lambda_s = K(m^*)^a(Fr)^b \left(\rho_a/\rho_s\right)^c \tag{1.5}$$

Ratnayake and Datta (2007) and Sæther et al. (2009) provided a model format to determine straight pipe pressure drop where the solids-air mixture has been considered as a single-phase (instead of treating solids and air separately). The total pressure drop due to solids-air mixture has been given by equation (1.6), and an expression of suspension density has been provided by equation (1.7).

$$\Delta P_{st} = \frac{1}{2}(K_{st})(\rho_{sus})\left(V^2{}_{entry}\right)\left(\frac{\Delta L}{D}\right) \tag{1.6}$$

$$\rho_{sus} = \frac{m_s + m_a}{V_s + V_a} \tag{1.7}$$

Mallick (2009) evaluated the above various mentioned existing models or model formats for solids friction for scale-up accuracy and stability. He found that the above formats of solids friction factor can surprisingly result in gross inaccurate predictions under significant scale-up conditions of pipeline lengths and diameters. Mallick (2009) modified an existing dilute phase model known as Weber A4 model to dense-phase model, which he termed as modified Weber-A4 model. The newly developed model was claimed to be more appropriate for dense-phase conditions by changing the term from w_{fo} (settling velocity of a single particle) to w_f (settling velocity of a particle in a cloud). The results revealed an improvement in the overall accuracy of predictions under scale-up conditions for fly ash, ESP dust, pulverized coal, and fly ash/cement mixture. The modified Weber-A4 model is essentially a Rizk (1982) model, but Mallick (2009) used it for fine powders, and Rizk (1982) used it for coarse particles. Mallick (2009) developed another method of representing the solid friction factor using the concept of "two-layer" slurry flow modelling (suspension flow occurring on top of a non-suspension layer), but he could not further proceed to actually test the accuracy of the two-layer concept because he did not have the experimental data of rheological properties of fine powders. During pneumatic conveying trials through sight glass observation, it was found that there is a suspension layer that flows on the top over the bottom non-suspension layer. Therefore, the "two-layer" concept was believed to be the more appropriate form to represent the actual flow conditions under dense-phase conveying.

Setia et al. (2015) introduced a new model format by incorporating the terms such as volumetric loading ratio and dimensionless velocity, as these were believed to be the more appropriate flow defining parameters. In the opinion of Setia et al. (2015), Volumetric Loading Ratio (VLR) is used to include the partial occupancy of pipe volume by the solids in the dense phase. As per Setia et al. (2015), for fluidized non-suspension (dense) type of flows, a considerable portion of the pipe volume is occupied by the dunes, and hence, the lack of cross-section available for the flow of gas-phase was not ignored. The term $\frac{w_{fo}}{V}$ attempts to indicate dense- to dilute-phase transition phenomenon. Larger sized and/or higher particle density products will have increased free settling velocity, and higher velocity will be required to keep them in suspension.

The model for estimating the solids friction factor was provided in the equation (1.8) as follows,

$$\lambda_s = K\ (VLR)^a\ \left(\frac{w_{fo}}{V}\right)^b \tag{1.8}$$

where

$$VLR = \left({}^{V_s}/_{V_a}\right) = \{(m_s/\rho_s)/(m_a\ /\rho_a)\} \tag{1.9}$$

The above presented Volumetric Loading Ratio model (in equation 1.8) did not work well in the scale-up evaluation and provided under-prediction. This model worked well in dense-phase, but it did not work in the dilute phase. This could be due to the fact that in dilute-phase, the partial occupancy of pipe volume covered by the solids is less or should be ignored as compared to the dense-phase flow, as the remaining volume available for gas flows is more in the former case. The

above model presented in equation (1.8) was found to be better than other existing models (refer equations 1.2 to 1.5). Earlier the term solids loading ratio (m^*) (mass flow rate ratio of solids to air) was used to represent the flow condition that occurred in the pipeline (Mallick, 2009; Pan and Wypych, 1992; Setia and Mallick, 2015a; Jones and Williams, 2003; Williams and Jones, 2004; Ratnayake et al., 2007; Chunhui et al., 2012; Behera et al., 2013; Cai et al., 2014; Behera et al., 2015). Setia et al. (2015) introduce the term volumetric loading ratio (VLR), which mainly incorporates the effect of product volume occupancy inside the pipeline, which in turn was considered to be the better representation for the flow conditions. This term was assuming a uniform distribution of solids across the pipe cross-section. On the other hand, always there is a transition phase that exists during the flow conditions in the pipeline. Therefore, to incorporate the transition phase from dense- to dilute-phase the dimensionless velocity term $\left({}^{w_{fo}}/_{V}\right)$ was used (Setia et al., 2015).

Subsequently, Setia et al. (2016) provided a new two-layer based model format (suspension flow occurring on top of a non-suspension layer) to determine solids friction factor, which included separate contributory terms for the non-suspension and suspension flows. The work has been carried out on the fine powders such as fly ash, cement, ESP dust. The format is provided in the following:

$$\lambda_s = \tau_1 \left[K(VLR)^a \left(\frac{w_{fo}}{V}\right)^b \right] + \tau_2 \left[\lambda_s^* \left(\frac{C}{V}\right) + \left({}^{2\beta_o}\Big/_{\left(\frac{C}{V}\right) Fr^2} \right) \right] \quad (1.10)$$

where K is the coefficient, and 'a' and 'b' are the exponents of power function format and $'\tau_1'$ and $'\tau_2'$ denote the relative contributions of non-suspension and suspension layers, respectively. The first term in equation (1.10), i.e., $\tau_1 \left[K(VLR)^a \left(\frac{w_{fo}}{V}\right)^b\right]$ represents the contribution of dense phase flow (non-suspension layer), whereas the second term, i.e., $\tau_2 \left[\lambda_s^* \left(\frac{C}{V}\right) + \left({2\beta_o}/{\left(\frac{C}{V}\right) Fr^2}\right)\right]$ represents the contribution of dilute-phase flow (suspension layer) (Wypych et al., 1990; 1990a). The two layers mentioned here (suspension and non-suspension layer) were physically observable, and to represent these two layers, two distinct models were required. The second portion of this equation has been taken from a pure dilute-phase model (suspension flow type), known as "Weber A4" model (Wypych, 1990). This model (Weber A4) has been reported (Mallick, 2009; Wypych, 1990) to provide better predictions for dilute-phase flow for different pipeline configurations. The predicted results of pneumatic conveying characteristics have displayed 'U'-shaped trends that were very close to the shapes of experimental pneumatic conveying characteristics in comparison to the uniform flow model presented in equation (1.8). The results revealed that the two-layer model could provide better reliable scale-up predictions as compared to the uniform model (equation 1.8) and other existing correlations in the literature, but it showed some inaccurate results for scale-up predictions in the step-up pipelines. Overall, preliminary validations of a two-layer model have indicated a good potential from dense to the dilute-phase regime. On the other hand, in realistic situations, there is some influence of solid particles (particle to particle/wall) in the entire pipeline, which creates some frictional effects. Therefore, in the present thesis, the term $'\lambda_s^{*}'$ is used to incorporate impact and friction effects caused by the solids.

There is another approach to designate the pressure drop in the pipeline, which is given by Weber (1991). In that approach, he did not consider separately the air only and the solid component of the pressure drop. Weber (1991) suggested that the pressure drop of the solids air mixture was integral in nature. In his opinion, it is individually difficult to separate the pressure drop caused by air-only and solids-only due to the intense mixing nature of the dense phase flow. He considered that the entire pressure drop of solid and air could be represented by the following new model format, as provided by the equation (1.11).

$$\Delta P = \frac{\lambda_T \rho V^2 L}{2D} \tag{1.11}$$

The model format presented in the equation (1.11) has been validated by Mallick (2009) under scale-up conditions of diameter and length. He validated with the aid of using dimensionless numbers such as solid loading ratio (m^*), mean Froude number (Fr_m) terms. The model is given by equation (1.12):

$$\lambda_T = K(m^*)^a (Fr_m)^b \tag{1.12}$$

where *'K'* is the coefficient, and *'a'* and *'b'* are the exponents of power function format. It has been found that using the above model (i.e., equation 1.12), pressure drop predictions under scale-up conditions did not come well (i.e., largely inaccurate). However, an attempt should be made to explore the use of other dimensionless terms such as Volumetric Loading ratio and w_{fo}/V (instead of m* and Fr), because Setia et al. (2016) have shown that this method seems to have better potential to provide reliable scale-up predictions. Therefore, using the same format with different

dimensionless terms needs to be addressed in the future. Moreover, there is a possibility that the format given by equation (1.8) is internally more suitable for fluidized dense-phase flow, and it is only the choice of dimensionless terms that are causing the inaccuracies associated with equation (1.4).

Unfortunately, many of the existing models do not consider the particle velocity term (C) (refer equations 1.4, 1.5, and 1.8). In the solid friction factor modelling, particle velocity term (C) is an important parameter, because it is considered to be an important particle flow characteristic and hence needed to be included in the model. Particle velocity term $'C'$ has been used by Setia et al. (2016) in the two-layer model. They have used $C/V = 1$, which may not be good for dense-phase, because Mallick (2009) considered that at low superficial air velocity range, the value of C/V would be less than that of dilute-phase. Therefore, due to such an assumption made in the existing two-layer model, an accurate estimation of particle velocity had not been possible. Most of the existing models, e.g., equations (1.4) and (1.5), do not address particle velocity and the slip velocity (the difference between gas and particle velocities) and relies on the superficial velocity of the gas. Therefore, it is considered that it would be prudent to include the particle velocity term, which is considered to be the most important parameter to represent the dune flow. However, experimental measurement of dune velocity for fine powders during actual flow conditions is a difficult task. The reason for this is, it is difficult to analyze the structure (i.e., movement) of the dunes between the sensors because the fine powders coat the sight glass.

Kaur et al. (2017) solved one-dimensional governing equations of flow for dense-phase pneumatic conveying of fly ash using the Runge-Kutta-Fehlberg (RKF45) method. Using numerical analysis,

Kaur et al. (2017) developed a new correlation of determining particle velocity. This work was done on the limited data (only fly ash), which needs to be further validated for other types of products. The model is provided by equation (1.13).

$$\frac{u_s}{u_a} = 10^{-3.227}(m^*)^{1.212}\left(\frac{w_{fo}}{V}\right)^{-0.385} \tag{1.13}$$

Kaur et al. (2017) considered a constant value of fluidized bulk density, but it may be expected to vary along the length of the pipe (possibly decreasing). Because of the expansion of gas, more mixing of gas by the transport and the intense blending that can happen over the bend. In their model, they did not consider any concentration gradient of the particles across the diameter of the pipe and coupling between solid to solid and gas to solid particles. Therefore, the effects of varying fluidized bulk density, concentration gradient, and coupling parameters need to be included in the future model of particle velocity. As compared to the existing models of particle velocity mentioned below in equations (1.14) and (1.15), it was claimed that the model developed holds good for dense phase. The new model (Kaur et al. 2017) was validated against two existing models (Klinzing et al. 1989; Hong and Shen 1994), which are given by:

$$u_s = \left(u_a - w_{fo}^{0.71}\right)D^{0.019} \tag{1.14}$$

$$u_s = u_a\left[1 - 0.533\left(\frac{1000\rho_a}{\rho_s}\right)^{1.093}\left(\frac{D}{100d_p}\right)^{-0.721}\right] \tag{1.15}$$

The model given by equation (1.14) was developed by Klinzing et al. (1989) (as reported by Wei et al. 2011), which was only suitable for the dilute-phase system and has been applicable for the particle size range of 67 to 900 μm. The model given by equation (1.15) was developed by Hong and Shen (1994) (as reported by Wei et al. 2011). They used a particle density term in their model and reported that the model is appropriate for "High solid-gas ratio and for fine powder." The existing models presented in the equations (1.14) and (1.15) seems to be applicable for fine powders to estimate particle velocity term. Therefore, Kaur et al. (2017) used these two models to predict particle velocity for fine powders for validation purposes only. It has been found that the values of particle velocity obtained with the aid of using the numerical model lie in between the two sets of the predicted existing model presented in equations (1.14) and (1.15).

The aerated powders conveyed in fluidized dense-phase behave as pseudo-fluid (fluid-like appearance). However, none of the existing models for solid friction factor or pressure drop considers fluid bed rheology (or apparent viscosity). Readdressing the issue of two-layer modelling (Mallick, 2009), apparent rheology is considered to be a significant parameter in order to understand the flow mechanism and modelling fluidized dense-phase type of conveying. Anjaneyulu and Khakhar (1994) experimentally studied the rheology of granular materials (glass beads) with Brookfield, Synchro-Lectric viscometer. However, their scope of work was limited up to granular products only, and hence, no data was generated to study the rheology of fine powders. Bruni et al. (2007, 2007a) studied the rheological characteristics (torque vs. impeller depth) for aerated fine powders and addressed the issue of the influence of inter-particle forces on the fluidization behaviour of fine powders. However, they did not model the pressure drops of fine powders at different aeration conditions in relation to pneumatic conveying.

Chen (2013) designed a testing apparatus using a combination of a fluidization chamber and a rotary viscometer, which utilized the Couette method to measure the rheology of gas-solid systems. In his present set-up, only the rheology of homogenous laminar flow was considered, but actually, in the case of aerated powder, the flow is heterogeneous (i.e., turbulent in nature), which requires further investigations. Therefore, rheological data should be obtained from a set-up where turbulent flow condition (turbulent fluidized bed condition) is prevailing. Chen (2013) carried out rheology testing of fine powders such as fly ash and cement. However, he could not carry out comprehensive validation on the usability of such data to model solid friction factor. This is due to the fact that he only validated on a 7-meter long pilot-scale pneumatic conveyor, which is too short for validation purposes with any degree of reliability for practical usefulness. Further improvements and modifications are required to evaluate the flow behaviour under conveying conditions having the scale of practical relevance.

Chaudhry (2015) tried to investigate the rheology of fine powders, i.e., the yield stress of fine powders for modelling fluidized dense-phase pneumatic conveying. She attempted to develop a powder rheological tester by having a 4-inch diameter tube attached to the bottom with aeration arrangement provided in the distributor plate with the help of a compressor supply fixed to it. However, she found that with such a set-up, getting a reliable and stable result is an extremely difficult task because of the experimental challenges, such as non-uniform fluidization, channelling, etc.

The existing models for pressure drop are often based on Barth's approach (Barth 1958) and using the "straight pipe" pressure drop data for modelling of solids friction (Mallick 2009). Barth

equation considers a linear dependency of solids loading ratio, which is then multiplied by solids friction factor (which again may have a direct or indirect inclusion of solids loading ratio term) (Mallick, 2009). As a result, it is thought that the Barth equation is always inherently influenced by solids loading ratio. Therefore, it is important to evaluate a model format that will not include solids loading ratio. A proposed format is provided in the following, which is the termed here as the amended Barth format:

$$\Delta P = \frac{\left((\lambda_f + \lambda_s)\rho_a L V^2\right)}{2D} \tag{1.16}$$

The "straight pipe" pressure drop data (obtained from the differences of static pressure values measured across a straight pipe section between two tapping points) are a presumably better selection of data for modelling straight pipe losses as compared to the "back-calculation" method (Jones and Williams 2003). It can be a difficult task to obtain a consistently good straight-pipe data, due to the frequent choking of the filters installed in the various pressure tapping points in the entire pipeline (Mallick, 2009; Setia, 2016a). Also, it becomes a very challenging work to set-up a typical mean value of static pressures, due to the highly fluctuating nature of the pressure signals. Additionally, if the distance between tapping points is comparatively small, it may be hard to obtain reliable pressure difference values (due to the highly fluctuating nature of signals). On the other hand, too long a distance between the tapping points may result in the transformation of dune properties between the tapping points. Therefore, in spite of the "straight-pipe" method being preferably suitable for the modelling purposes, this approach of data measurement and modelling is having certain practical drawbacks (as discussed above). In the "back-calculation" method, the pressure loss in the straight pipe is determined by subtracting losses occurring in the bends,

verticals and that due to initial acceleration from the total pipeline pressure drop. Therefore, the "back-calculation" method is indirectly dependent on the accuracy of reliable bend/vertical/acceleration models (the development of these models is still under the research stage). However, according to the practical point of view, this method has the main benefit that only one pressure transducer is required, and that too is installed on the clean airline (located on the compressed air line and just before the blow tank). The transducer on clean airline does not require frequent cleaning and provides data with less pressure fluctuation (compared to particle-laden flow areas where transducers are installed in a "straight pipe" approach). Mallick (2009) demonstrated that the solids friction factor models developed using the "back-calculation" method can provide grossly inaccurate results when tested under scale-up conditions of pipeline length and diameter. However, it should be noted that Mallick (2009) carried out the evaluation work using a format of solids friction factor as given by equation (1.4). This power function format uses solids loading ratio and Froude number as the dimensional terms, and it has been demonstrated that this format can provide grossly inaccurate scale-up predictions (Mallick, 2009). Therefore, it would be very difficult to predict, whether the large inaccuracy of "back-calculation" method under the scale-up configurations is due to its indirect approach of estimating the solids friction factor with dependency on bend/vertical/acceleration losses or if it is due to the selection of unsuitable solids friction factor model format (i.e., the dimensionless terms). There may be a possibility that the reliable solids friction factor model, such as the two-layer model format of Setia et al. (2016), could provide better-quality predictions even with the "back-calculation" approach. Therefore, it is essential to generate a solids friction factor model using the combination of a two-layer format of Setia et al. (2016) and back-calculation method and test the model for its scale-up accuracy.

Based on the above discussion, the following are the three critical areas that require further attention.

- Development of a validated particle velocity model (of practical use) using the numerical technique by considering the effect of change in particle concentration along the pipeline diameter and varying fluidized bulk density (along with the flow).

- Development of pressure drop models using different model formats, such as combined gas-solid phase approach, amended Barth technique, and back-calculation method (with relatively established reliable solids friction factor model format).

- Development of a pressure drop model using rheological parameters of aerated fine powders.

Therefore, further work is required to be carried out in the above mentioned critical areas: In the view of the above, the following are the objectives.

1.2 Research objectives

Specific research objectives include:

1. To develop dense-phase pneumatic conveying test facility.

2. To experimentally determine shear stress and apparent viscosity of aerated powder bed under different conditions of aeration, shear rate and type of powders and to convey fine powders (Group-A fine powder) through pneumatic conveying test rig.

3. To carry out scale-up evaluation of pressure drop models developed using different model formats, such as combined gas-solid phase approach, amended Barth technique and back calculation method (with relatively established reliable solids friction factor model format).

4. To numerically determine particle velocity for Group-A fine powders and use the same to develop validated solids friction model and validate the numerically developed particle velocity model with predictions obtained using existing empirical models.

5. To develop validated model for solids friction, using rheological data of fine powders (Group-A fine powders) and the pseudo-fluid flow concept for dune transport.

The outcome of the present thesis work would provide a better understanding of the fundamentals of changing flow mechanisms in the fluidized dense-phase flow of powders. The newly developed validated modelling and scale-up procedure would benefit the industrial sector in the following ways:

- The reduced flow rate of air, which leads to the reduced consumption of power and the sizing of the compressor.
- Pipe sizing calculations getting optimized to a greater extent for a given product and layout.
- The troubleshooting of the entire installed pneumatic transport system getting easier.
- Reduced size of the solids-gas separation equipment.
- Estimated prediction of pressure drop in a precise manner - design getting optimized.
- Fluidized dense-phase system emerging as a promising method to transport fine powders in the industry.

Chapter 1 presents the introduction to the subject and need of the research work. It comprises of the need of work and specific research objectives. In this thesis, a formal 'literature review' chapter has not been provided, but the contents of the same have been included in different chapters covering respective domains. Chapter 2 covers details of the experimental set up/test facilities developed and test programs. Chapter 3 evaluates two methods of modelling solids friction factor – one method is scientifically more accurate, but the other method has practical advantages. Chapter 4 contains governing equations for gas-solids flow and results of numerical modelling to solve for particle velocity under different flow conditions. Chapter 5 introduces a new scale-up validated modelling procedure in which the particle-particle collision effect has been considered. It also includes apparent rheological properties of powdered bed into modelling solids friction factor. Chapter 6 includes the conclusion and future scope of work. Note: some of the initial thought research issues, such as combined air and solids friction factor or amended Barth's equation approach, did not result in reliable predictions. Hence, the same has been placed in Annexure.

CHAPTER 2

EXPERIMENTAL WORK

The scope of the present thesis includes the development of improved modelling and scale-up procedures for dense-phase pneumatic conveying of fine powders. Steady-state data of pressure drop of fine powders (such as cement, fly ash, ESP dust, etc.) pneumatically conveyed in recent past by Setia (2016a), Mallick (2009) and before by Pan (1992) have been primarily used for modelling solids friction, particle velocity, and scale-up validations. In addition, fine powders, such as fly ash and cement, conveyed through the test rigs of Particle and Bulk Solids Technologies Laboratories (53 mm I.D. x 70 m long and 105 mm I.D. x 130 m long pressure conveying rigs) of Thapar Institute, were used for specific investigations. Rheological parameters of fine powders, such as fly ash and cement, have been experimentally determined in the rotational Powder Rheometer.

2.1 Pneumatic conveying through existing test facilities

White cement powder was conveyed from fluidized dense-phase to dilute phase regime through 53 mm I.D. × 69 m long test rig at Thapar Institute of Engineering and Technology. A schematic of this test rig is shown in Figure 2.1. Different pneumatic conveying trials were conducted corresponding to different air and solids mass flow rates. The purpose of testing at Thapar Institute of Engineering and Technology test rig was to evaluate the extent of powder deposition on the surface of filters of static pressure transducers. Static pressure transducers were located along the pipeline from P1 (beginning of pipeline) to P8 (last transducers in the line, towards the end of pipeline). Figure 2.2 shows the pictorial representation of transducers installed in the dirty line (cement-airflow line) after 10^{th} and 25^{th} conveying cycle at P2 (the second transducer in the line after P1) and P8 (the last transducer in the line) locations. The test set-up consists of a 0.2 m^3

bottom-discharge type blow tank (A) feeding system. A receiving bin (B) with a capacity of 0.65 m^3 was installed on the top of the blow tank. The receiver bin was fitted with bag filters (C) having a reverse pulse jet type cleaning mechanism.

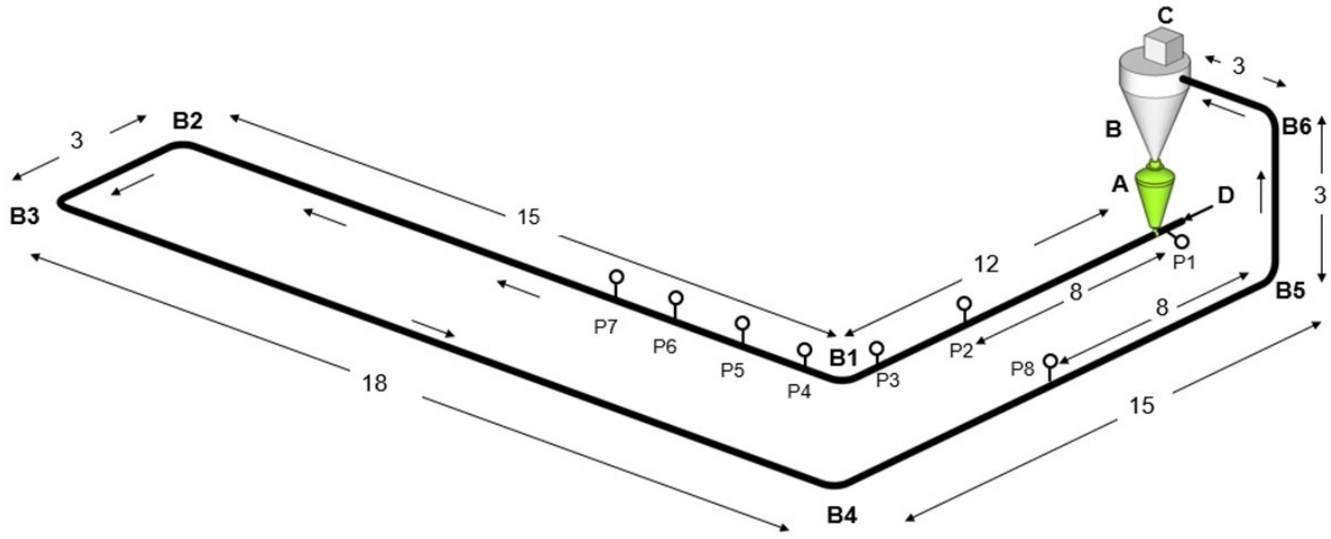

Figure 2.1: Schematic diagram (isometric view) of the existing test rig (53 mm I.D. × 69 m long)

In order to supply the compressed air (D) at a maximum pressure of approximately 750 kPa-g, Kirloskar made electric-powered Model KES 18-7.5, 3.37 m^3/min free air delivery rotary screw compressor was used. Pipes and bends used in the pilot plant were made of mild steel. The pipeline included a 3 m vertical lift, six 1 m radius of curvature, and 90° angle bends. To measure static pressure in the horizontal straight sections of the pipeline, eight static pressure transducers were employed along with all the pipelines (P1 to P8). The static pressure transducers had the following specification: manufacturer: Endress & Hauser, model: Cerabar PMC131, pressure range: 0–2 bar, maximum pressure: 3.5 bar (absolute), current signal: 4–20 mA. Other required instruments, such as PRV (pressure reducing valve), flow meter (vortex type), NRV (non-return valve), flow control

valve, pressure gauge, etc. were suitably placed in the appropriate locations. The calibration of the static pressure transducers (P1 to P8), load cells, and airflow meter was performed using the standard calibration procedure (Mallick, 2009). The pressure transducers were installed in near the blow tank (P1) and to the end of the pipeline (P8) in the ash conveying lines. Shear beam type load cells were placed on the top side of the blow tank and receiver bin. The pressure readings were obtained in P1 to P8 locations in the pipeline, and load cells were used to calculate the mass of material accumulated in and discharged from the blow tank and receiver bin. A portable PC compatible data logger (make: National Instruments) was used to record the electrical output signals from the load cells, pressure transducer, and flow meters. The installed data logger was a high-speed unit featuring 14-bit resolution and had 16 different channels. It must be emphasized that the purpose of carrying tests in the existing set-up was not for modelling solids friction but to investigate into the extent of powder deposition on the filters of static pressure transmitters, which may compromise with the quality data. Later in this thesis, the author has described in much detail the practical challenges of pressure measurements by static pressure transmitters on conveying ("dirty") lines. For this investigation, cement was conveyed through the 70 m test rig at 6.1 t/h using an airflow of 0.027 kg/s. Twenty-five conveying trials were conducted. Figure 2.2 shows the condition of filters at the beginning of conveying, after 10 and 25 cycles at P1 and P8 locations. It can be seen that there was significant chocking of filters even after ten cycles. This would require the periodic opening of the pressure measurement assembly and cleaning of the filters. Table 2.1 includes the physical properties of the cement conveyed for the above-described purpose through the existing pneumatic conveying test rig. Particle size distribution was measured using the laser diffraction method.

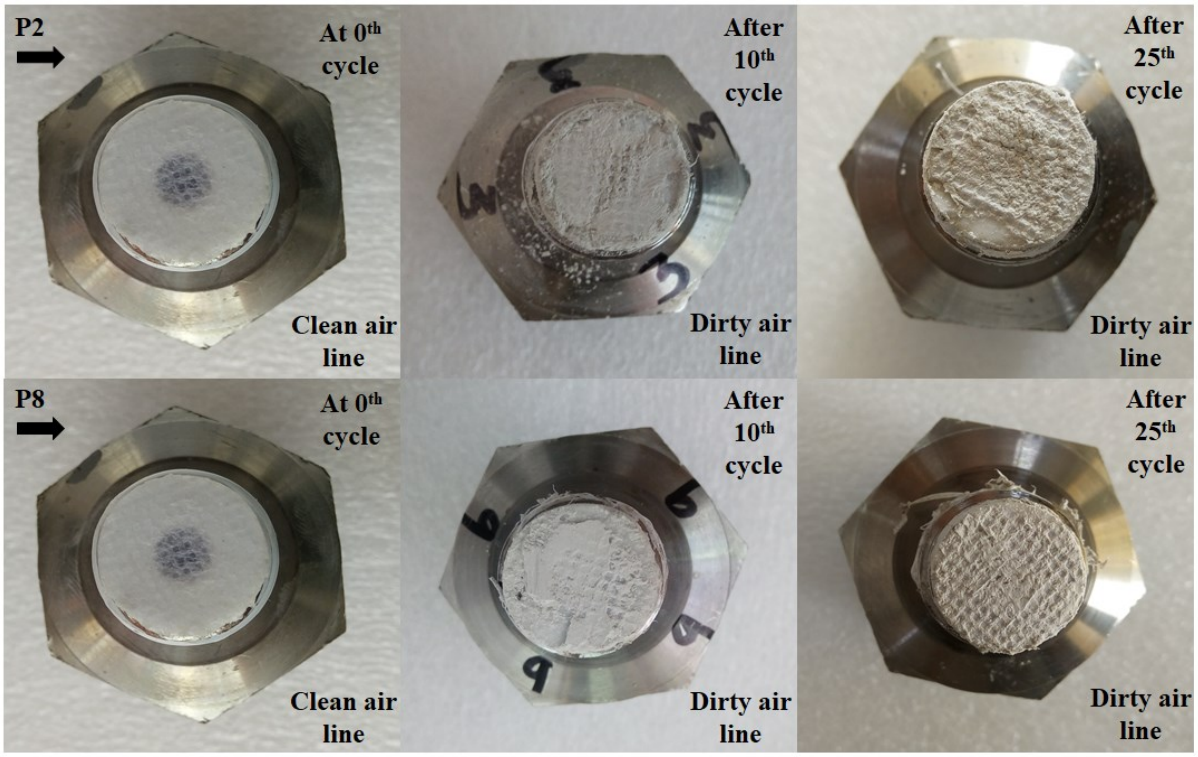

Figure 2.2: Pictorial representation of transducers showing filter conditions after 0th (before the start of conveying), 10^{th} and 25^{th} conveying cycles installed in P2 and P8 locations

Table 2.1: Physical properties of product conveyed through existing pneumatic conveying set up

Powder	d_{10} **(µm)**	d_{50} **(µm)**	d_{90} **(µm)**	ρ_s **(kg/m^3)**	ρ_b **(kg/m^3)**
Cement (white)	5	27	80	2000	1280

2.2 Development of new pneumatic conveying test facility

Towards the later stages of the Ph.D. tenure, a new pneumatic conveying test facility was built at the Particle and Bulk Solids Technologies Laboratory of Thapar Institute of Engineering &

Technology through research project sponsored by NTPC (previously known as National Thermal Power Corporation). Figure 2.3 shows a schematic of the new facility. The new facility comprised of a multistage screw compressor (equipped with air receiver and drier), having the maximum delivery pressure of approximately 700 kPa-g; it is a Chicago Pneumatic Compressors, a division of Atlas Copco India Ltd. Model CPD 75 G 7 having a capacity of 605 m^3/hr (Free Air Delivery). A bottom-discharge type blow-tank (A) having 0.8 m^3 empty volume was used to feed the product into the pipeline. On the top of the blow tank, a receiver bin (B) with insertable pulse jet dust filter of capacity 2.5 m^3 capacity was installed. The receiver bin was fitted with bag filters (C) having a reverse pulse jet type cleaning mechanism. The test rig is of 130 m of length and having 100 NB pipeline bore and includes 12 number of bends (90^o bends of 1 m radius of curvature) and a vertical lift of height 5 m. To measure static pressure in the horizontal straight sections of the pipeline, seven static pressure transducers were employed along with all the pipelines, i.e., P8, P1 to P6 (see Figure 2.3). The static pressure transducers had the following specification: manufacturer: Wika, model: S-20, pressure range: 0-10 and 0-2.5 bar-g, maximum pressure: 40 bar (absolute), current signal: 4 to 20 mA. The P8 transducer was used to measure the total pipeline pressure drop, whereas P1-P6 tapping points were installed to provide static pressures along the pipeline. All other necessary instrumentation, such as the pressure-reducing valve, flow meter (orifice type), non-return valve, flow-control valve, pressure gauge, etc. were installed in suitable locations. Process and Instrumentation Diagram (P&ID) of the new set up is shown in Figure 2.4. The standard calibration procedure was used to calibrate the pressure transducers, load cells, and flow meter (Mallick, 2009). The pressure transducers were installed in the clean airline (P8) near the blow tank and the ash conveying lines (P1 to P6). The receiver bin and blow tanks were supported on load cells (shear beam type) to determine mass flow rates of solids. To achieve a wide range of

airflow, a flow control valve was used to change the air mass flow rate. Variation of solids flow rates was achieved through different blow tank pre-pressurization and combinations of different amounts of blow tank aeration and transport air. A portable PC compatible data logger (Data Taker 80 or DT80 and CEM 20 of Data electronics) was used to record the electrical output signals from the load cells, static pressure transducer, and airflow meters. DT80 is a high-speed unit featuring 18-bit resolution. This has 39 analogue inputs. Various samples of fly ash obtained from different power-stations were conveyed in fluidized dense through the newly developed test facility. In this thesis, the solids friction factor model generated for one such product has been provided. Physical properties of this product are provided in Table 2.2.

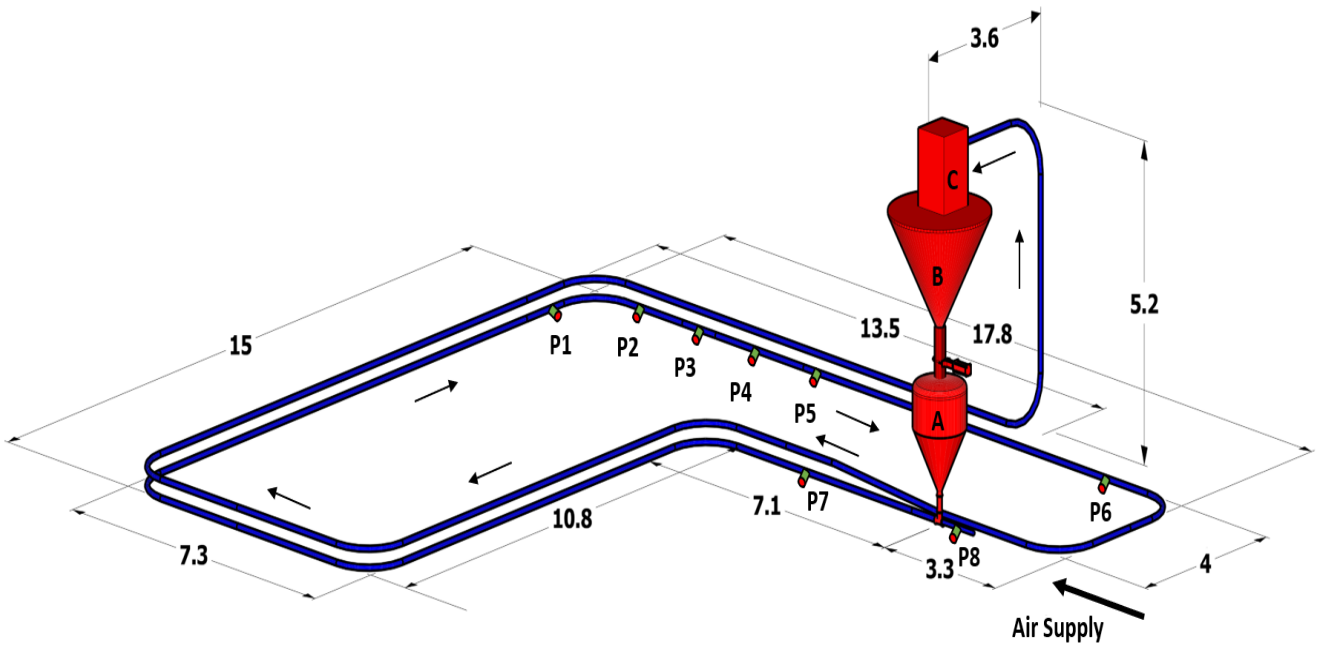

Figure 2.3: Schematic diagram of the new test facility with pipeline dimensions

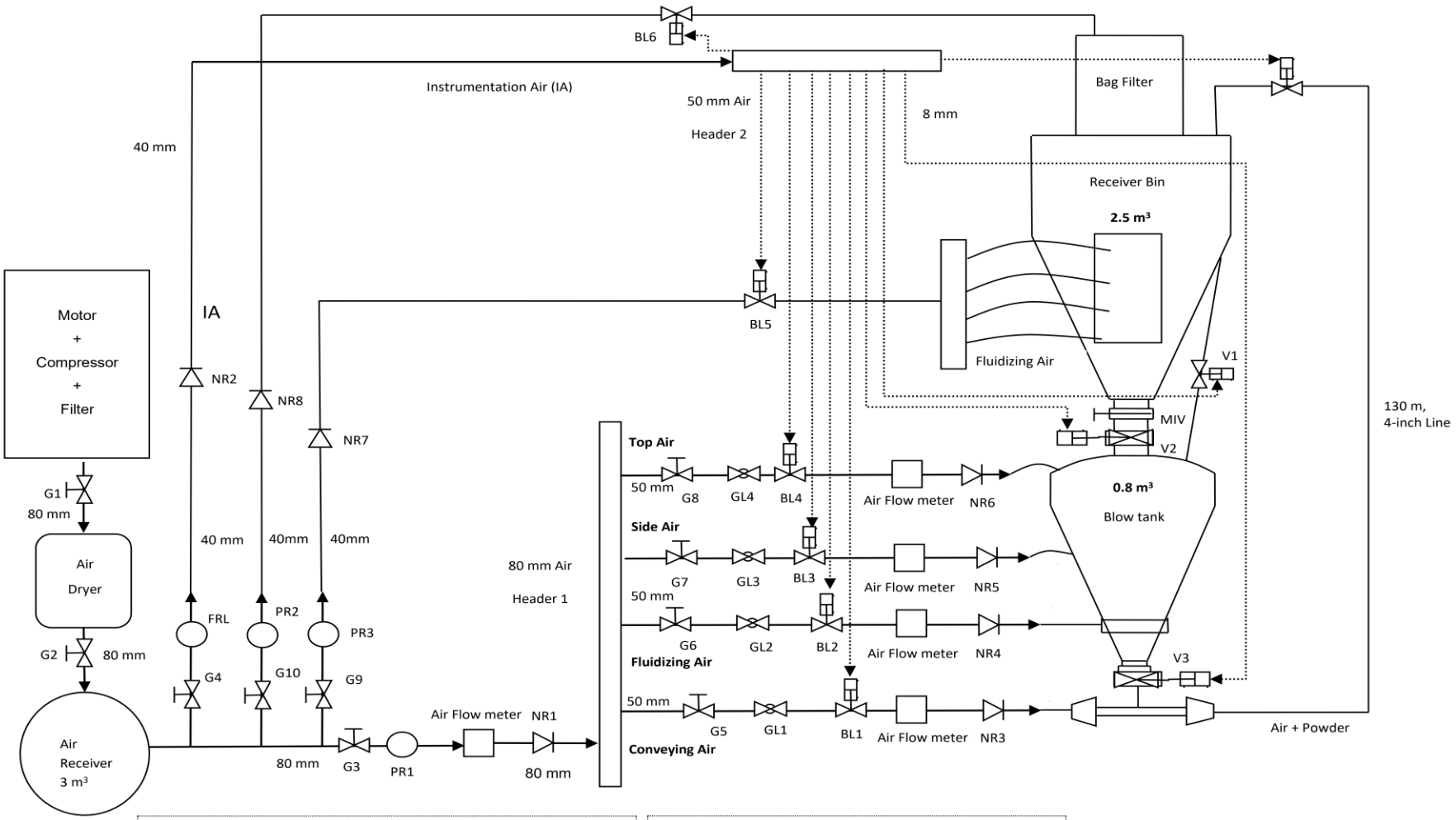

Legend and Abbreviations	
Symbol	**Name**
G1, G2.....	Manually operated Air Flow On /Off Valves
GL1, GL2.....	Air Flow Control Valves (Globe)
PR1, PR2.....	Pressure Regulator Valves
BL1, BL2.....	Automated Blow off Valves
NR1, NR2.....	Non-Return Valves

Legend and Abbreviations	
Symbol	**Name**
MIV	Manually operated Material Intake Valve
V1	Vent off Valve
V2	Material Intake Valve
V3	Blow Tank Discharge Valve

Figure 2.4: P&ID for the newly developed pneumatic conveying test rig

Table 2.2: Physical properties of product conveyed through new pneumatic conveying set up

Powder	d_{10} (µm)	d_{50} (µm)	d_{90} (µm)	ρ_s (kg/m^3)	ρ_b (kg/m^3)	w_{fo} (m/s)
Fly ash	5	44	171	2104	1000	0.123

2.3 Apparent rheology measurement for fluidized powders

Apparent rheology of dry and fine powders was measured using a powder rheometer ("MCR 702 Twin Drive") machine at Anton Paar, Gurugram, India. The "Powder Cell" is an instrument for the study of dry granular flows, especially in the fluidized or near fluidized conditions. The "MCR 702 Twin Drive" combines a traditional stress-controlled rheometer and a strain-controlled rheometer in a single instrument. The experimental set-up of the Anton Paar powder cell is shown in Figure 2.5. The "powder measuring cell" is comprised of a 50 mm internal diameter glass cylinder of capacity 140 ml, provided with a porous plate for the uniform distribution of airflow to aerate the powder below and above the minimum fluidization conditions. In general, the rheometer device has been equipped with impellers of different shapes (such as circular, flat or cylindrical), but in the present investigation, in order to carry out the modelling and rheology trials, flat (10 mm) shaped type of impeller (stirrer ST36-2V type) has been employed as shown in Figure 2.5. The instrument is provided with a torque sensor able to accurately measure the torque in single-drive mode (between 1×10^{-9} to 0.23 Nm) and twin drive mode (between 5×10^{-9} to 0.23 Nm). These wide ranges of measurable torque values make this torque sensor capable of measuring the torques in both fluidized and non-fluidized state for powders. In the present rheology trials, the

rotational speed of the impeller has been continuously regulated between 0 to 200 rpm in linear steps. The equipment is provided with an air mass flow controller (ranging from 0 L/min to 15 L/min). There is a pressure sensor that is used to characterize the pressure drop across the powdered bed. The rheometer is provided with a dust protection hood (to catch powders having size of more than 5 µm, which allows the measurements of Geldart Group A powders. Test data and results obtained from this equipment have been provided in detail in a later chapter. The details of the experimental conditions are given in Table 2.3.

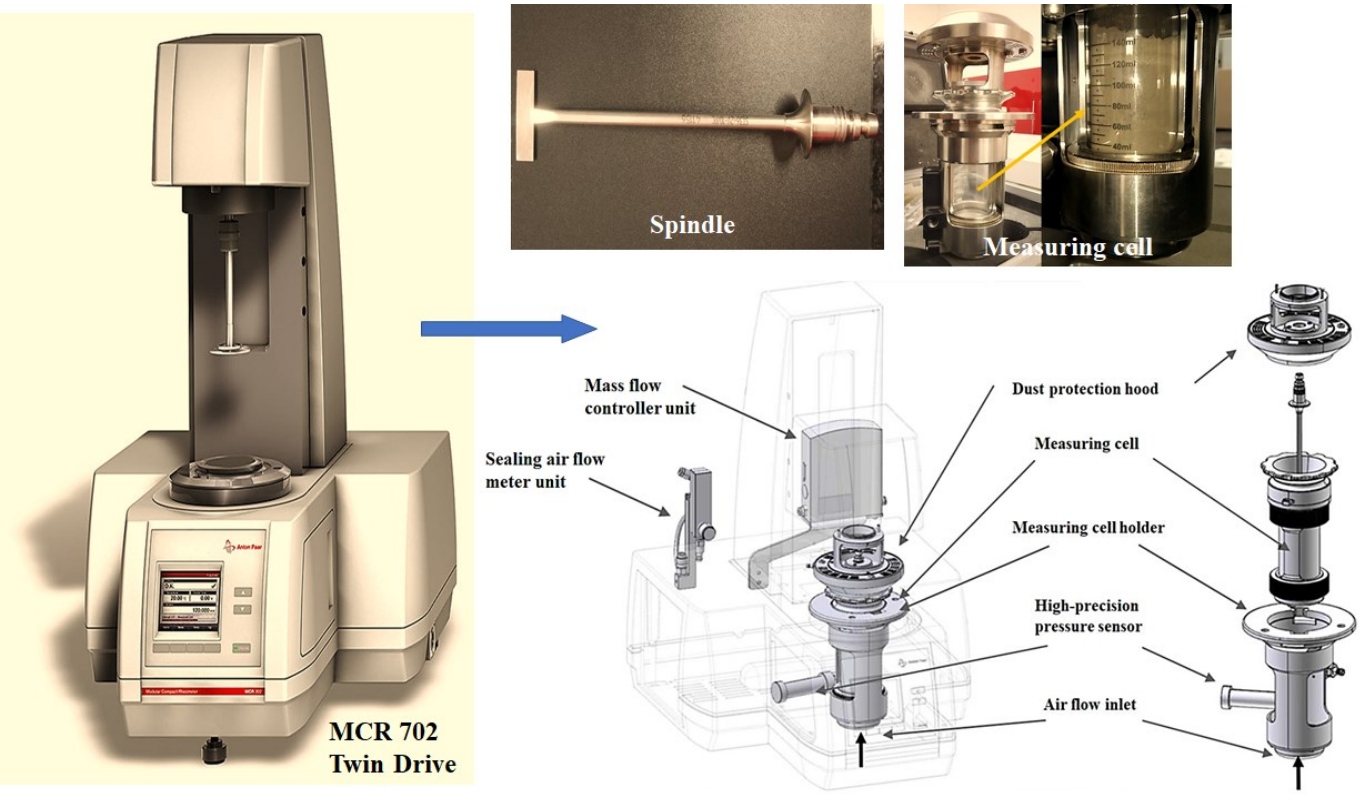

Figure 2.5: Schematic diagram of MCR 702 Twin Drive" Rheometer at Anton Paar Laboratory, Gurugram, India

Table 2.3: Details of experimental conditions

Flow Rate (l/min)	**Spindle rotational speed (rpm) - low to high airflow in linear steps**	**Spindle rotational speed (rpm) - high to low airflow in linear steps**
0 to 15 (in steps of 3 l/min)	0 to 200	200 to 0

Table 2.4: Details of products tested for apparent powder rheology

Powder	d_{10} **(µm)**	d_{50} **(µm)**	d_{90} **(µm)**	ρ_s **(kg/m^3)**	ρ_b **(kg/m^3)**	w_{fo} **(m/s)**
Cement (white)	3	19	50	2720	1028	0.03
Cement (grey)	4	18	54	2680	1020	0.0262
Fly ash	9	65	206	1900	950	0.242
Fly ash	4	22	79	2370	660	0.038
Cement (grey)	3	19	75	2910	1080	0.036

Table 2.4 shows the details of products tested for apparent powder rheology in powder Rheometer. In Chapter 5, cement (grey) (average particle size: 18 µm), fly ash (average particle size: 65 µm), fly ash (average particle size: 22 µm) and cement (grey) (average particle size: 19 µm) is designated as grey cement 2, fly ash 2, fly ash 1, grey cement 1. It is to be noted that fly ash 1 and cement (grey) 1 were pneumatically conveyed in the laboratory of Fujian Longking Co., China (Setia, 2016a). Samples of these powders were tested for their apparent rheology in the present work.

Whereas, fly ash 2 was obtained for an Indian power station. This product was used in the present thesis to generate data for apparent powder rheology. In addition to this, SEM images are provided in Figures 2.6 to 2.10. The SEM image analysis gives an idea of the shape of the bulk material. SEM images were captured at the Sophisticated Analytical Instruments Laboratory of TIET, Patiala. It has been evident from the figures that some of the samples have a spherical shape, and some of them having a polyhedral shape. This is an important consideration in fluidization and conveying of particles. The polyhedral structure of the powder samples contributes to the challenges in conveying and fluidizing phenomenon in comparison to the spherical structure.

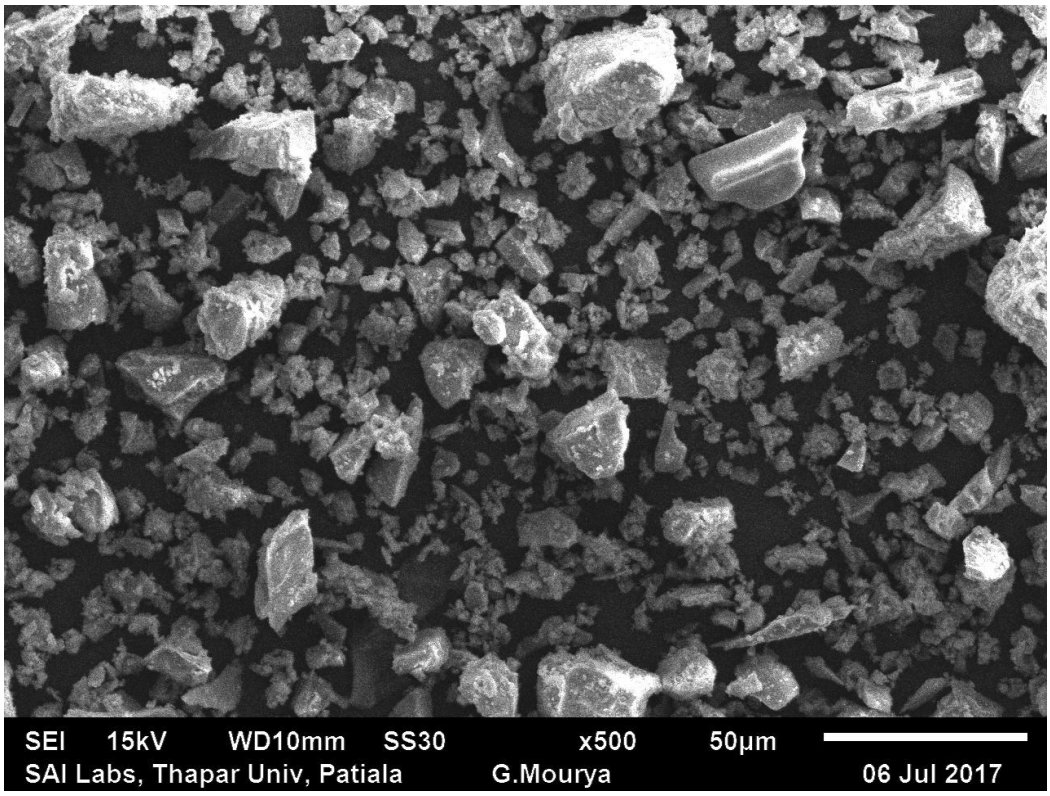

Figure 2.6: SEM image of cement **(**white) (conveyed at TIET)

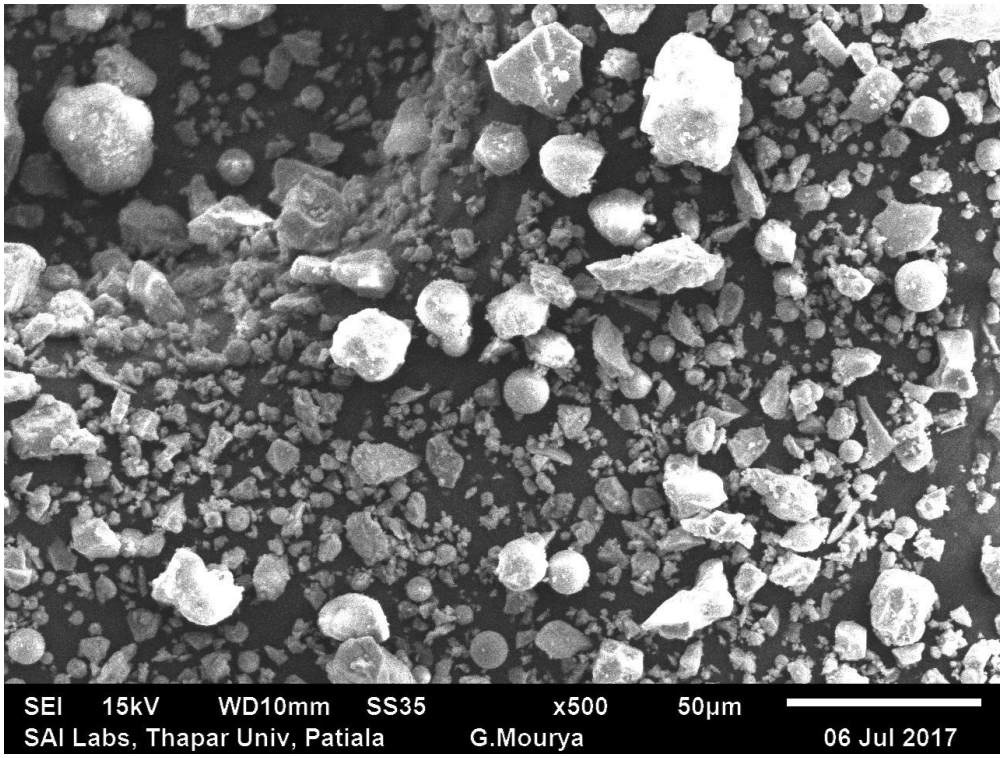

Figure 2.7: SEM image of grey cement (conveyed at TIET)

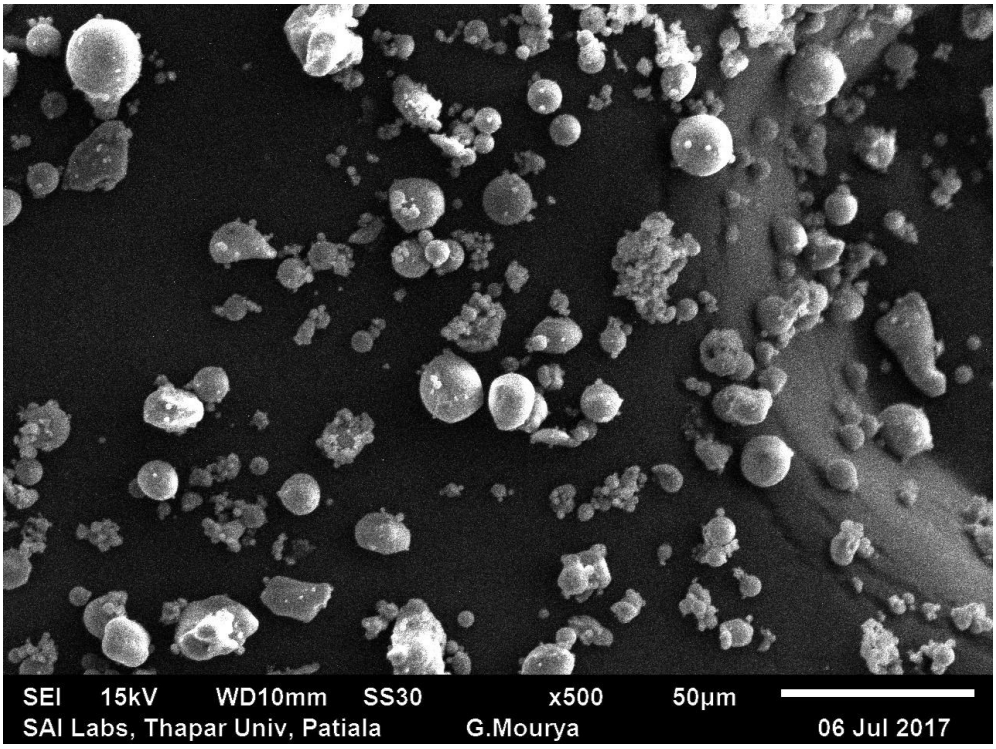

Figure 2.8: SEM image of fly ash (conveyed at TIET)

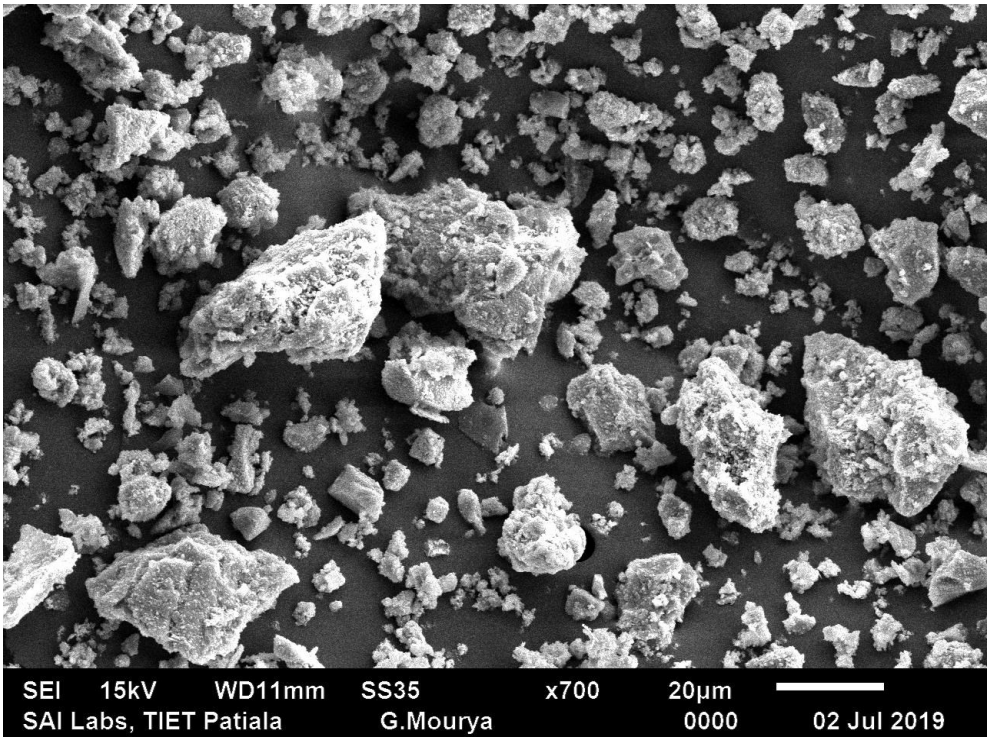

Figure 2.9: SEM image of fly ash (conveyed in Fujian Longking, China)

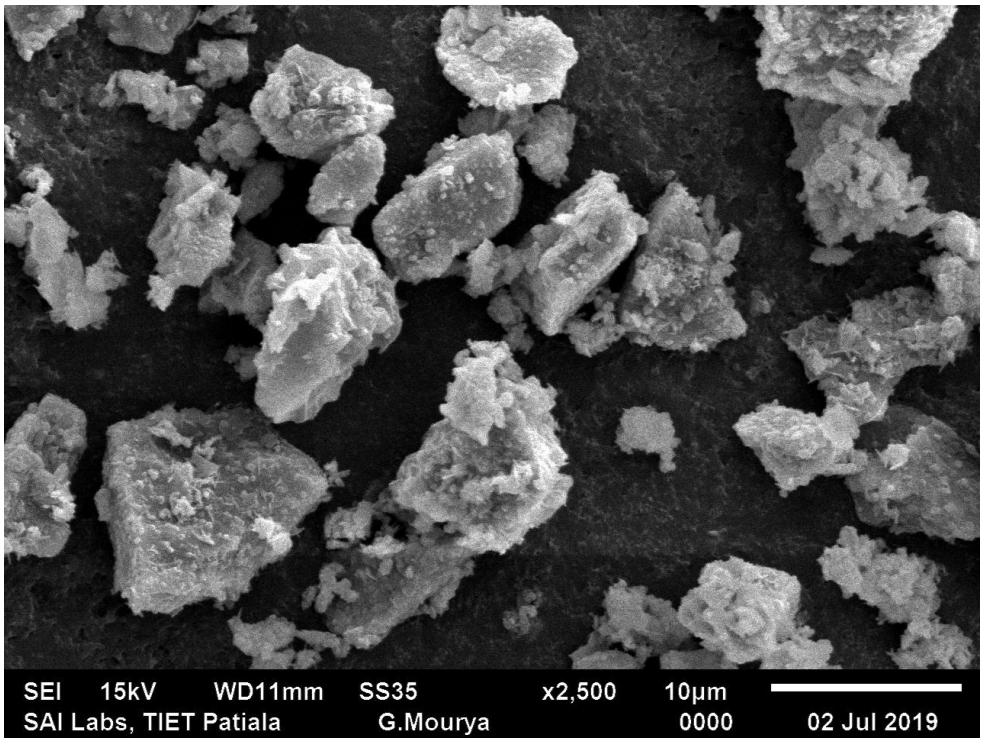

Figure 2.10: SEM image of grey cement ((conveyed in Fujian Longking, China)

2.4 Test data of other researchers used for modelling and scale-up purpose

Pneumatic conveying test data provided in Mallick (2009) and Setia et al. (2016) for two samples of fly ash, ESP dust, and cement have been used in this thesis for modelling solids friction and diameter and length scale-up prediction/validation. Physical properties and pipeline conditions of these products are provided in Table 2.5. Schematic of such test rigs are provided in Figures A1.1 to Figures A1.4 (Annexure 1). As mentioned before, steady-state straight pipe and total pipeline data of these set-ups have been used the author to develop the majority of solids friction factor models and scale-up validations for fly ash, ESP dust, and cement. Detail description of the experimental test set-up is described in Mallick (2009) and Setia (2016a). In addition to this, the fluidization and de-aeration test set up from which the values of fluidized bulk density were obtained is given in Figure A1.5 (Annexure 1). The obtained values of fluidized bulk density were used in the modelling for particle velocity.

The three-particle diameters (d_{10}, d_{50}, d_{90}) have been obtained from the Malvern particle size analyzer equipment. Out of these three different diameters $'d_{10}'$ is meant for the very fine/cohesive particles (which stick with the pipe walls) and $'d_{90}'$ is meant for the very coarse particles (that can cause blockage in the pipeline) in the entire pipeline. On the other hand, $'d_{50}'$ represents the median/average particle diameter (neither very fine/cohesive nor coarse). In order to avoid very much complex flow phenomenon and to represent better flow conditions, for the sake of simplicity, the term $'d_{50}'$ has been employed for modelling purposes. In addition to this for the modelling purposes, the consideration of the spherical shape of particles have been taken into account which is merely represented by the median/average particle diameter (d_{50}).

Table 2.5: Physical properties of products and pipeline configurations

Product	**Originally conveyed in laboratory**	d_{10} **(µm)**	d_{50} **(µm)**	d_{90} **(µm)**	ρ_s **(kg/m^3)**	ρ_b **(kg/m^3)**	w_{fo} **(m/s)**	D **(mm)**	L **(m)**	L_h **(m)**	L_v **(m)**	**No. of Bends** ***(N.B.)***
Fly ash (Mallick, 2009)	University of Wollongong, Australia	2	30	110	2300	700	0.06	69 105 69	168 168 554	161 161 547	7 7 7	5 5 17
ESP dust (Mallick, 2009)	University of Wollongong, Australia	3	7	25	3637	610	0.005	69 105 69	168 168 554	161 161 547	7 7 7	5 5 17
Fly ash (Setia et al., 2016)	Fujian Longking Co., Ltd., China	4	22	79	2370	660	0.038	65 80/100	254 407	241 382	13 25	10 14
Cement (Setia et al., 2016)	Fujian Longking Co., Ltd., China	3	19	75	2910	1080	0.036	65 80/100	254 407	241 382	13 25	10 14

Product	**Originally conveyed in laboratory**	d_{10} **(μm)**	d_{50} **(μm)**	d_{90} **(μm)**	ρ_s **(kg/m^3)**	ρ_b **(kg/m^3)**	w_{fo} **(m/s)**	D **(mm)**	L **(m)**	L_h **(m)**	L_v **(m)**	**No. of Bends** ***(N.B.)***
Fly ash (Pan, 1992)	University of Wollongong, Australia	-	16	-	2197	634	0.0158	69 69	172 554	165 547	7 7	5 17
Pulverized brown coal (Pan, 1992)	University of Wollongong, Australia	-	26	-	1488	437	0.0299	69 69	172 554	165 547	7 7	5 17
Fly ash (89% weight) and cement (11% weight) mixture (Wypych, 1989)	University of Wollongong, Australia	-	19 20	-	2130 3100	700 950	0.0232 0.0375	60 105	162 554	158 547	4 7	5 17

CHAPTER 3

AN EVALUATION OF MODELLING FORMAT FOR INDUSTRIAL DESIGN - ENGINEERING CONVENIENCE VERSUS RESEARCH ACCURACY

3.1 Modelling solids friction factor using "back-calculation" method versus "straight pipe" method

An accurate modelling of solids friction factor is a challenging task due to the limited development achieved so far towards understanding the basics of flow mechanisms of highly turbulent, complex, and high concentration powdered bed. The loss of energy takes place in the entire pipeline due to the collisions between solids and solids, solids and gas and solids and pipe wall, and these losses together constitute a friction factor term known as solids friction factor (Klinzing et al., 2010; Mallick, 2009). Various researchers have provided expressions for the solids friction factor to determine the pressure drop in the gas-solids flows. Empirical models based on power function formats have been popularly used over the years by several investigators (Mallick, 2009; Pan and Wypych, 1992; Setia and Mallick, 2015a; Jones and Williams, 2003; Williams and Jones, 2004; Ratnayake et al., 2007; Chunhui et al., 2012; Behera et al., 2013; Cai et al., 2014; Behera et al., 2015) using dimensionless numbers. Mallick (2009) carried out the evaluation of solids friction factor model developed using the "straight-pipe" data obtained from a set of two pressure transduces strategically placed on the straight-pipe section for fly ash and ESP dust using solid loading ratio and gas Froude number as the dimensionless parameters (refer equation 1.4). Model for solids friction factor using the format using the above parameters (solid loading ratio and gas Froude number) was also developed using the "back-calculation" method using the total pipeline pressure drop data obtained from the transducer located at the beginning of the pipe (Mallick, 2009). Losses occurred due to the bends, verticals, and initial acceleration were determined using models available in the literature (Mallick, 2009). Both the methods (i.e., models for solids friction developed using "straight pipe" and "back-calculation" methods) resulted in inaccurate predictions

when used to predict the total pipeline pressure drop for larger and longer pipelines. The ranges of inaccuracies were much higher for the models developed using the "back-calculation" method (in the range of 40 to 150% depending on the pipeline and product).

Recently, Setia et al. (2016) developed an improved method to model solids friction factor (refer equation 1.10). A two-layer based model was provided in which the authors considered the solids friction contributions of the non-suspension bed of powders flowing along the bottom of the pipe and the suspension of particles occurring on top of the non-suspension layer. Volumetric loading ratio and dimensionless velocity (ratio of free settling velocity to superficial air velocity) have been used to represent the non-suspension flow of the dune layer. A solids impact and friction term have been employed to represent the dilute-phase flow due to its established reliability. The validation of the two-layer model was carried out against the experimental pressure loss data of two samples of fly ash, ESP dust, and cement under the scale-up conditions of pipeline lengths and diameters. The predicted results of pneumatic conveying characteristics with two-layer modelling approach (Setia et al., 2016) have displayed 'U'-shaped trends that were very close to the shapes of experimental pneumatic conveying characteristics in comparison to the earlier model of Mallick (2009) having solids friction factor and Froude number as dimensionless parameters. The new developed two-layer model resulted in predictions within 12% accuracy for a wide range of scale-up conditions resulting in better reliability of predictions.

In order to comment on the apparent lack of reliability of the "back-calculation" approach, it should be remembered that the format of solids friction factor using solid loading ratio and Froude number (Mallick, 2009) provided grossly inaccurate scale-up predictions of about 60% (Mallick, 2009)

even when the "straight-pipe" modelling approach was adopted (compared to only 12% inaccuracy provided by the improved two-layer format). Therefore, it would not be conclusive to state whether that the failure of "back-calculation" method is attributed to its indirect approach of determining solids friction factor with dependency on bend/vertical/acceleration loss models or if it is due to the selection of inappropriate solids friction factor model format (i.e., the dimensionless terms). It could happen that a robust solids friction factor model, such as the two-layer model (Setia et al., 2016), could provide much improved predictions even with the "back-calculation" approach. Therefore, there is a need to develop solids friction factor model using the combination of two-layer format (Setia et al., 2016) and back-calculation method and to put the model so developed under scale-up testing. Therefore, an attempt has been made in this chapter to evaluate the true accuracy of the "back-calculation" method as it offers various practical merits over the "straight pipe" method.

There are two methods to determine the solids friction factor; one is the "straight pipe" method (Mallick, 2009; Wypych, 1989; Setia et al., 2016; Pan and Wypych, 1992; Setia and Mallick, 2015; Pan, 1992; Wypych et al., 1990; Wypych et al., 1990a; Pan and Wypych, 1998; Setia and Mallick, 2015a) and the other is known as "back-calculation" approach (Jones and Williams, 2003; Williams and Jones, 2004). In the "straight pipe method," pressure drop data obtained from the differences of static pressure values measured across a straight pipe section between two tapping points are used by for modelling of solids friction. It has been experienced (Mallick, 2009; Setia, 2016a) that getting reliable straight-pipe data can be a challenging task due to the frequent choking of the filters used in pressure tapping points. Also, due to the highly fluctuating pressure signals (caused by the presence of turbulent and concentrated moving dunes), it is often difficult to

establish a representative mean value of static pressure (Mittal, 2016). Furthermore, if the distance between the tapping points is relatively small, it may be difficult to obtain reliable pressure difference values between the tapping points due to the highly fluctuating nature of signals and the pressure differentials may lie in the tolerance ranges of the pressure transducers. A combination of all these could easily result in inaccuracies in the range of 1 to 5 kPa (as an example) in the value of pressure differential across a 10 m long (typical) pipe section (considering two static pressure transducers have been installed across such short pipe section). Such inaccurate test data would result in the development of an inaccurate model for solids friction factor (inheriting under- or over-prediction characteristics), which, when scaled up to predict pressure drops in larger or longer pipelines (e.g., 500 m long), could provide gross over/under-predictions. On the contrary, too long a distance between the tapping points may result in a change in dune characteristics along the length. Therefore, in spite of the "straight-pipe" approach being fundamentally preferable, this method of data measurement and modelling is having certain practical limitations (as mentioned above). In the "back-calculation" method, straight pipe loss is calculated using the following equation (3.1), given as:

$$(\Delta P)_{st} = (\Delta P)_{Total} - (\Delta P)_b + (\Delta P)_v + (\Delta P)_{accel} \tag{3.1}$$

where, '$(\Delta P)_{st}$' is the pressure drop due to the straight pipe section, '$(\Delta P)_{Total}$' is the total pipeline pressure drop, '$(\Delta P)_b$' is the pressure drop due to the bends, '$(\Delta P)_v$' is the pressure drop due to the verticals and '$(\Delta P)_{accel}$' is the pressure drop due to initial acceleration. In the back-calculation method, losses due to bends, vertical and initial acceleration is first estimated (using available models provided in literature) to subsequently determine the straight pipe loss for the

entire pipe. This method bears the criticism (Mallick 2009) that till date reliable models to calculate bend, vertical and initial acceleration losses have not been developed (these are still under research stage) and hence the theoretically calculated component losses may be erroneous, which would, in turn, affect the accuracy of the straight pipe losses obtained from "back-calculation" method. In other words, the "back-calculation" method is an indirect method and depends on the accuracy of bend/vertical/acceleration loss models (which are still being researched). However, for practical purposes, this method has some major advantages that only one pressure transducer is required in this approach and that too is installed on the clean airline (on the compressed air line and just before the blow tank denoted by location P8 in the Figure A1.1) and it leads to less maintenance because it is well calibrated and free from the contact of particles. Transducer installed on clean airline does not require any frequent cleaning, and it provides data with reduced pressure fluctuation (due to "air only" flow); thus less manpower is required and is cost-effective due to the use of only a single transducer in the entire pipeline in comparison to the straight pipe method (where at least an additional pair of transducers with filters are required). Moreover, as the single pressure transducer is recording total pipeline pressure drop data, which is much larger in magnitude compared to the pressure differential data obtained in the "straight-pipe" method across a shorter pipe section. Total pipeline pressure drop data, being large in magnitude, is less affected by the tolerances and possible inherent inaccuracies of the combination of pressure transducer-filter-data logging arrangements.

In this chapter, the "back-calculation" approach of modelling solids friction factor has been employed using a two-layer model format (refer equation 1.10) multiple regression technique for the fly ash, ESP dust, and cement (mentioned in Table 3.1). Models have been developed using

the total pipeline pressure drop pneumatic conveying characteristics provided in Mallick (2009) and Setia (2016a) and by subtracting the losses occurred due to initial acceleration, verticals, and bends from the total pipeline pressure drop data. These losses were calculated using the following equations 3.2 to 3.4:

Acceleration loss : $\Delta P_{accel} = \rho_a V^2 (1 + 2m^* C/V)/2$ (3.2)

where, 'ΔP_{accel}' is the pressure drop due to initial acceleration, 'ρ_a' is the density of air, *'V'* is the superficial air or gas velocity, 'm^*' is the solids loading ratio, and *'C'* is the particle velocity.

Vertical loss : $\Delta P_V = m^* \rho_a g L_V V/C$ (3.3)

where, 'ΔP_V' is the pressure drop due to the verticals, 'm^*' is the solids loading ratio, 'ρ_a' is the density of air, 'g' is the acceleration due to gravity, 'L_V' is the length of vertical pipe or test section, 'V' is the superficial air or gas velocity, and 'C' is the particle velocity.

Bend loss : $\Delta P_b = NB(1 + m^*)\rho_a V^2/2$ (3.4)

where, 'ΔP_b' is the pressure drop due to the bends, 'NB' is the number of bends, 'm^*' is the solids loading ratio, 'ρ_a' is the density of air, 'V' is the superficial air or gas velocity.

The values of power function constant ('K'), exponents ('a' and 'b'), w_{fo}, λ_s^* of the developed models are provided in Table 3.1. These have been obtained using the "back-calculation"

modelling approach and “two-layer” format employed in the present study using the format of equation (1.10). Table 3.1 also contains values of the same parameters obtained by Setia et al. (2016), who used the “straight pipe” modelling approach using a “two-layer” format (refer equation 1.10). The high values of R^2 indicate a good fit of the model to experimental data, which has been used to develop models.

Table 3.1: Models developed using "back-calculation" versus "straight pipe" methods (both using "two-layer" format, equation 1.10)

Product reference	**Pipeline data used for modelling**	**Models (as per the format provided by equation 1.10)**					**R^2**
		K	a	b	λ_s^*	w_{fo} (m/s)	
Models developed using "back-calculation" approach in the present study							
Fly ash (Mallick, 2009)	69 mm I.D. × 168 m	5.5	−0.48	1.55	0.0055	0.06	0.96
ESP dust (Mallick, 2009)	69 mm I.D. × 168 m	224	−0.32	1.40	0.0060	0.005	0.97
Fly ash (Setia et al, 2016)	65 mm I.D. × 254 m	19.95	−0.75	1.73	0.00529	0.038	0.96
Cement (Setia et al., 2016)	65 mm I.D. × 254 m	7	−0.49	1.41	0.00588	0.036	0.95
Fly ash (Pan, 1992)	69 mm I.D. × 172 m	192	-0.31	1.71	0.00599	0.0158	0.99
Pulverized brown coal (Pan, 1992)	69 mm I.D. × 172 m	0.138	-0.097	0.52	0.00579	0.0299	0.97

Fly ash (89% weight) and cement (11% weight) mixture (Wypych, 1989)	60 mm I.D. × 162 m	115	-0.42	1.79	0.00389	0.0232 0.0375	0.99
Models developed using a "straight pipe" approach (Setia et al., 2016)							
Fly ash (Mallick, 2009)	69 mm I.D. × 168 m	8.04	−0.22	1.48	0.0043	0.06	0.98
ESP dust (Mallick, 2009)	69 mm I.D. × 168 m	3018	−0.20	1.72	0.0135	0.005	0.99
Fly ash (Setia et al., 2016)	65 mm I.D. × 254 m	23.54	−0.61	1.71	0.0074	0.038	0.99
Cement (Setia et al., 2016)	65 mm I.D. × 254 m	17.31	−0.40	1.54	0.0081	0.036	0.98

3.2. Scale-up validation of models

The models developed using "back-calculation" approach using the experimental data of 69 mm I.D. × 168 m long pipe (Mallick 2009) for fly ash and ESP dust (Mallick 2009) and 65 mm I.D. × 254 m long for the other sample of fly ash and cement (Setia et al., 2016) have been validated for longer and larger scale-up pipeline configurations (105 mm I.D. × 168 m long and 69 mm I.D. × 554 m long pipelines for fly ash and ESP dust, 80/100 mm I.D. × 407 m long step-up pipeline for the other fly ash sample and cement) for different air and solids mass flow rates by comparing the predicted pneumatic conveying characteristics against the experimental plots. An iterative solution-based program has been developed to estimate the total pipeline pressure drop by dividing the total pipeline into several smaller straight pipe segments and bends. The program commences from the exit section of the pipe and gradually calculates the pressure losses in different pipe segments up to the blow tank. The program begins with a known condition, which corresponds to the discharge or the atmospheric condition and proceeds section by section and terminates at the blow tank location of the pipe. While Chambers and Marcus (1986) models have been used to determine the pressure drops due to initial acceleration, verticals, and bends (equations 3.2 to 3.4), models provided in Table 3.1 have been used to determine the losses that occurred in the straight horizontal pipes. The results are provided in Figures 3.1 to 3.6.

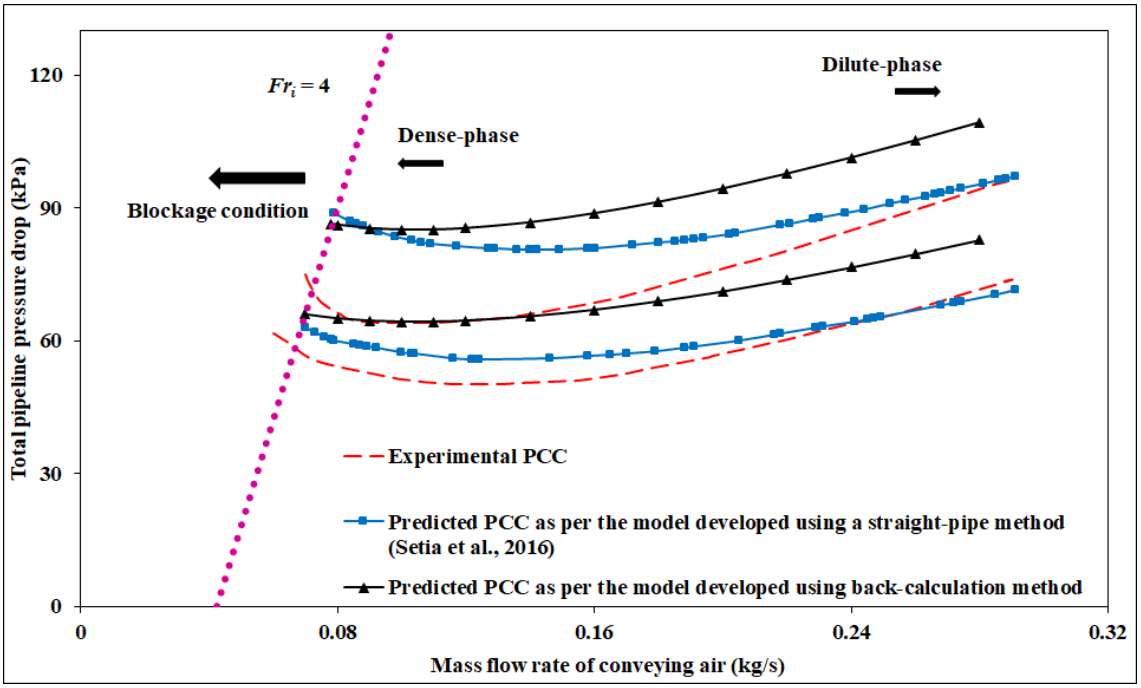

Figure 3.1: Scale-up evaluation of models based on "back-calculation" versus "straight pipe" methods for fly ash through 105 mm I.D. × 168 m long pipe

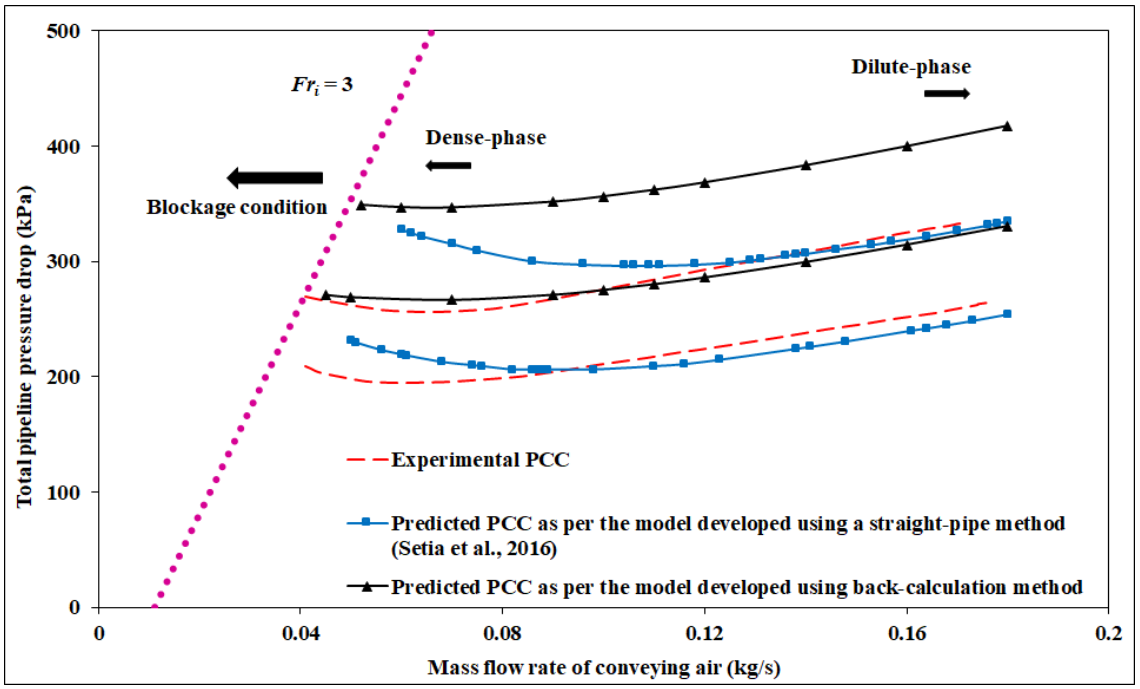

Figure 3.2: Scale-up evaluation of models based on "back-calculation" versus "straight pipe" methods for fly ash through 69 mm I.D. × 554 m long pipe

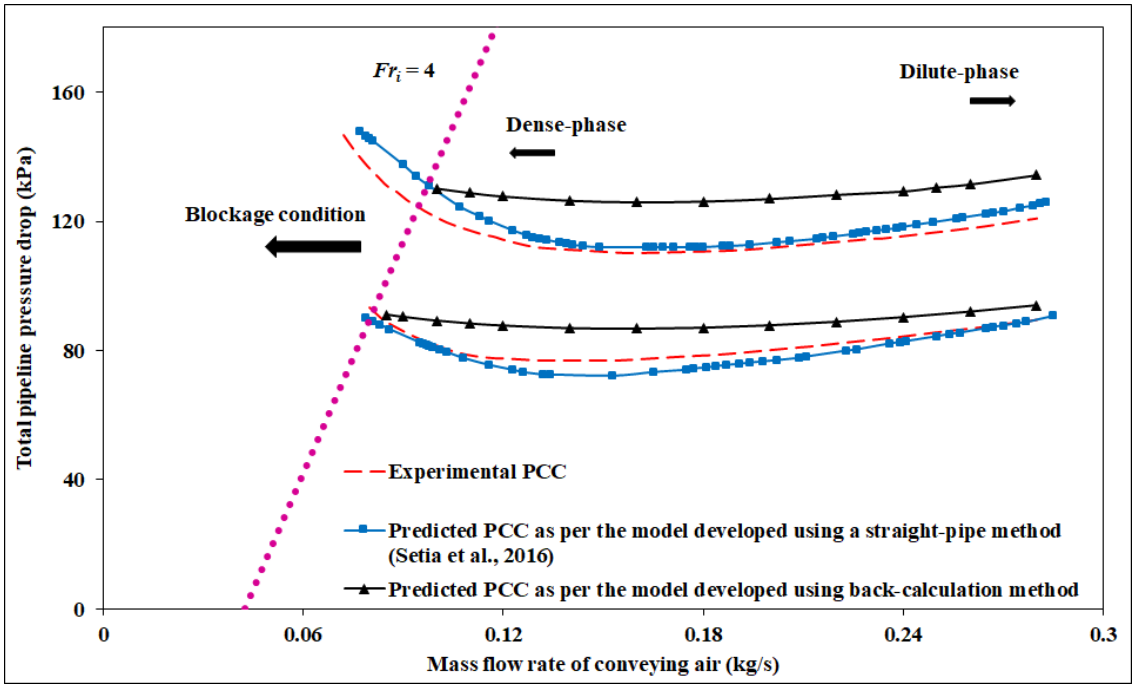

Figure 3.3: Scale-up evaluation of models based on "back-calculation" versus "straight pipe" methods for ESP dust through 105 mm I.D. × 168 m long pipe

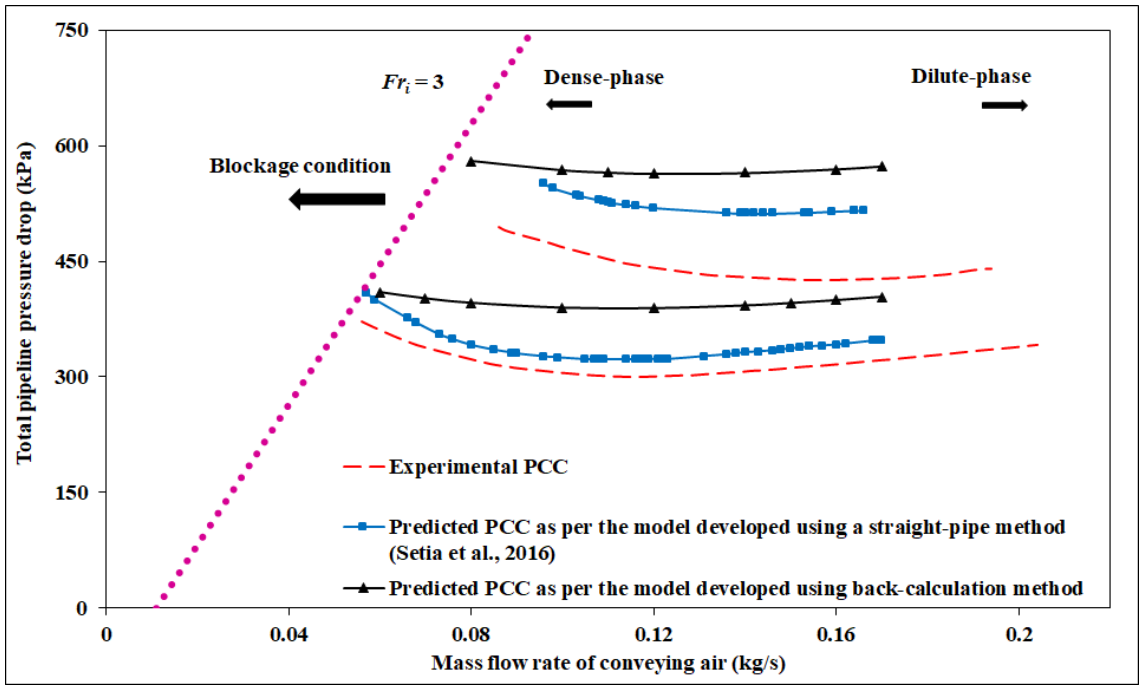

Figure 3.4: Scale-up evaluation of models based on "back-calculation" versus "straight pipe" methods for ESP dust through 69 mm I.D. × 554 m long pipe

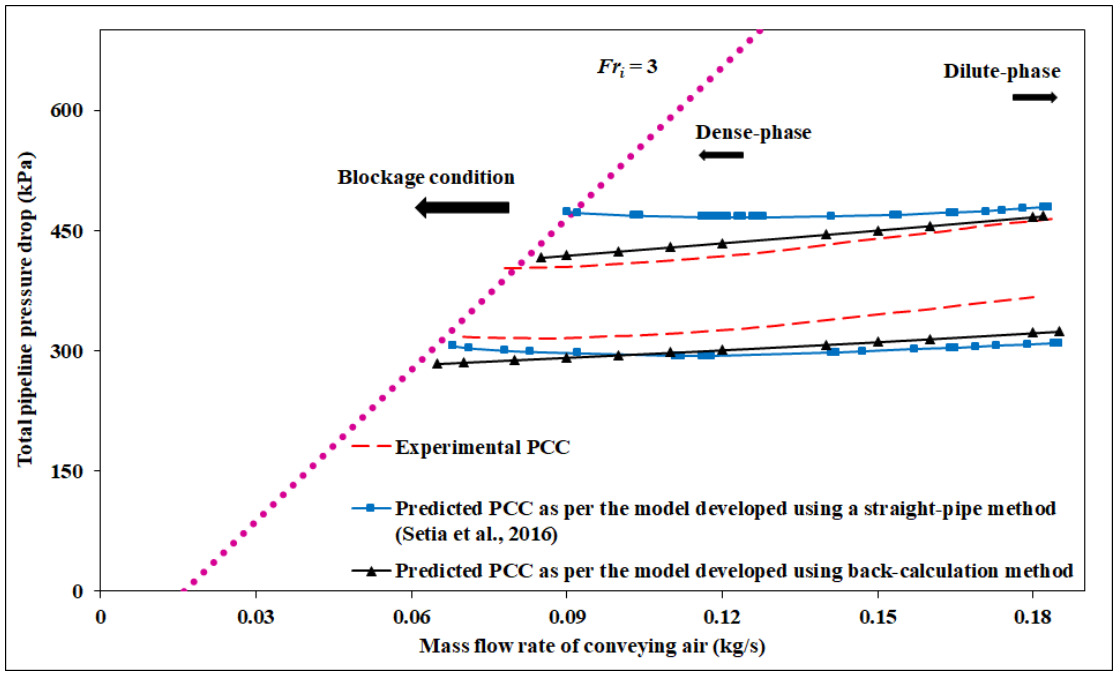

Figure 3.5: Scale-up evaluation of models based on "back-calculation" versus "straight pipe" methods for cement through 80/100 mm I.D. × 407 m long pipe

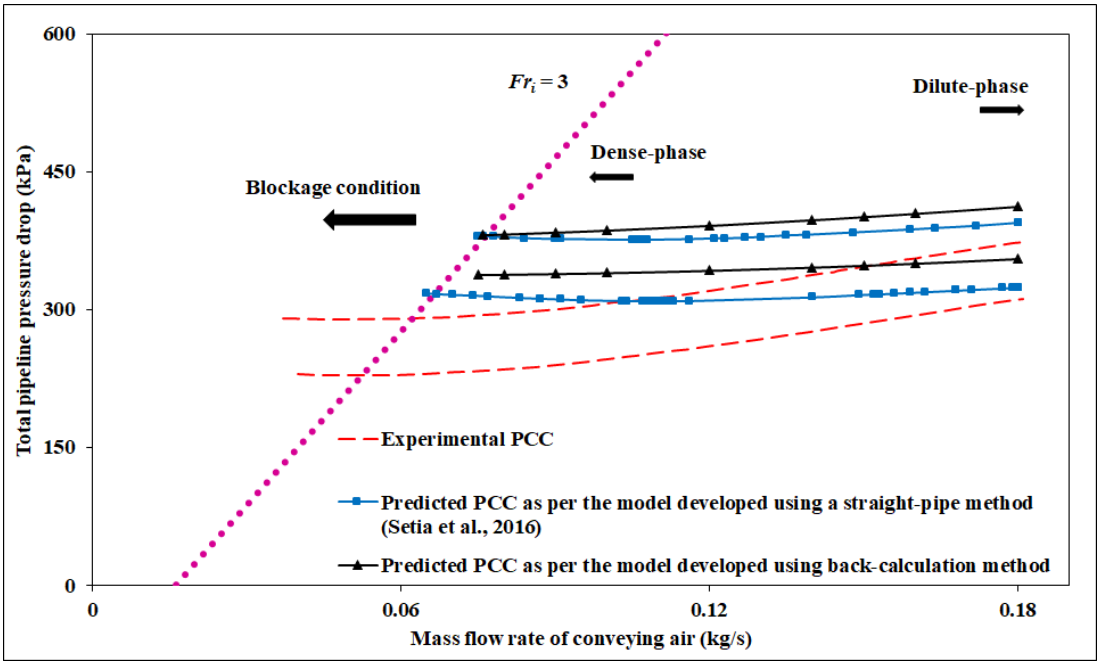

Figure 3.6: Scale-up evaluation of models based on "back-calculation" versus "straight pipe" methods for fly ash through 80/100 mm I.D. × 407 m long pipe

The results show that for fly ash and 105 mm I.D. × 168 m long pipeline (18 t/h: bottom lines and 28 t/h: top lines) (Figure 3.1), the new model developed using "back-calculation" method and the "straight-pipe" model of Setia et al. (2016), i.e., two-layer format, provided almost similar predictions in very dense-phase (low-velocity zone), while on the other hand, the new model provided some over-prediction in dilute-phase in comparison to the existing two-layer model format developed by Setia et al. (2016) for a higher mass flow rate of solids (i.e., 28 t/h). In dense-phase or low-velocity flow regime, the relative error shown by the straight pipe approach (Setia et al., 2016) is 29%, while 32% is shown by the back-calculation approach; i.e., both the approaches have provided similar levels of accuracy. However, for a lower mass flow rate of solids (i.e., 18 t/h), the new model developed using "back-calculation" method provided some over-prediction from dense- to the dilute-phase region in comparison to the existing two-layer model format developed by Setia et al. (2016). For the 69 mm I.D. × 554 m long pipe, i.e., for length scale-up (7 t/h: bottom lines and 11 t/h: top lines) (Figure 3.2), the results show that the "back-calculation" method provides over-predictions from dense- to dilute-phase in comparison to the existing Setia et al. (2016) two-layer model format for both mass flow rate of solids (i.e., lower: 7 t/h and higher: 11 t/h). In the dense-phase flow regime, the relative error shown by the straight pipe approach (Setia et al., 2016) is 23%, while 35% is shown by the back-calculation approach. Figure 3.3 shows that for ESP dust and diameter scale-up (105 mm I.D. × 168 m long pipeline) (15 t/h: bottom lines and 25 t/h: top lines), the new model (developed through "back-calculation" method) provides almost similar predictions in very dense-phase and some over-prediction in dilute-phase in comparison to the "straight pipe" model of Setia et al. (2016), i.e., two-layer format, for both mass flow rate of solids (i.e., lower: 15 t/h and higher: 25 t/h). In the dense-phase flow regime, the relative error shown by the straight pipe approach (Setia et al., 2016) is 5%, while 12% is shown

by the back-calculation approach. For ESP dust and length scale-up (69 mm I.D. × 554 m long pipe) (6 t/h: bottom lines and 10 t/h: top lines) the "back-calculation" method based model provides over-predictions from dense- to dilute-phase in comparison to the "straight-pipe" model of Setia et al. (2016) (Figure 3.4) for both mass flow rate of solids (i.e., lower: 6 t/h and higher: 10 t/h). The relative error shown by the straight pipe approach (Setia et al., 2016) is 14%, while 18% is shown by the back-calculation approach in the dense-phase zone. Figure 3.5 shows the results of scale-up evaluations for cement conveyed through the 80/100 mm I.D. × 407 m long step-up pipeline (18 t/h: bottom lines and 36 t/h: top lines). The results for cement (for 80/100 mm I.D. × 407 m long step-up pipeline) indicate that in dense-phase flow regime, the relative error shown by the straight pipe approach (Setia et al., 2016), i.e., two-layer format is 14%, while 5% is shown by the back-calculation approach, i.e., the back-calculation approach has provided more accurate predictions, while on the other hand, the new model (developed through "back-calculation" method) provided almost similar predictions in dilute-phase with the existing two-layer model format developed by Setia et al. (2016) for higher mass flow rate of solids (i.e., 36 t/h). However, for a lower mass flow rate of solids (i.e., 18 t/h), the new model developed using the "back-calculation" method provided almost similar predictions from dense- to dilute-phase region with the existing two-layer model format developed by Setia et al. (2016). Figure 3.6 shows the results of scale-up evaluations for fly ash conveyed through the 80/100 mm I.D. × 407 m long step-up pipeline (20 t/h: bottom lines and 30 t/h: top lines). In the dense-phase flow regime, the relative error shown by the straight pipe approach (Setia et al., 2016) is 22%, while 26% is shown by the back-calculation approach. Hence, the new model (developed through "back-calculation" method) shows almost similar results to some extent in dense-phase flow regime and some over-prediction in dilute-phase in comparison to the existing two-layer model format developed by Setia et al.

(2016) for higher mass flow rate of solids (i.e., 30 t/h). However, for a lower mass flow rate of solids (i.e., 20 t/h) the new model developed using the "back-calculation" method provided over-predictions from dense- to dilute-phase region in comparison to the existing two-layer model format developed by Setia et al. (2016). Table 3.2 shows the complete detail of relative error values in predictions obtained using the "back-calculation" versus "straight pipe" approach of modelling for different mass flow rates of solids and air in different pipes in both low velocity and high-velocity region. The relative error is calculated based on the following equation (3.5) and uses the absolute values:

$$\%\ \text{Relative Error} = \left(\frac{\text{Experimental data} - \text{Predicted value}}{\text{Experimental value}}\right) \times 100 \qquad (3.5)$$

Table 3.2: Comparison of relative errors of predictions between models developed using "back-calculation" and "straight pipe" methods

Product	**Pipe diameter and length**	**Mass flow rate of solids (t/h)**	**Mass flow rate of air (kg/s)**	**Relative error % of model developed using a "straight pipe" method**	**Relative error % of model developed using "back-calculation" method**
Fly ash (Mallick, 2009)	105 mm I.D. × 168 m long	28 18	0.10 0.26	29 3	32 18
ESP dust (Mallick, 2009)	105 mm I.D. × 168 m long	25 15	0.12 0.26	5 2	12 6
Fly ash (Mallick, 2009)	69 mm I.D. × 554 m long	11 7	0.07 0.16	23 6	35 21
ESP dust (Mallick, 2009)	69 mm I.D. × 554 m long	10 6	0.1 0.16	14 6	18 21

Product	**Pipe diameter and length**	**Mass flow rate of solids (t/h)**	**Mass flow rate of air (kg/s)**	**Relative error % of model developed using a "straight pipe" method**	**Relative error % of model developed using "back-calculation" method**
Cement (Setia et al., 2016)	80/100 mm I.D. × 407 m long	36 18	0.1 0.17	14 16	5 11
Fly ash (Setia et al., 2016)	80/100 mm I.D. × 407 m long	30 20	0.1 0.17	22 7	26 17

It can be seen from Table 3.2 that the relative error values of predictions obtained using the "back-calculation" method are generally larger than that obtained using the "straight pipe" method of Setia et al. (2016) by a maximum of 15%. Also, the maximum error value obtained with the "back-calculation" method has been found to be within 3 to 35% range when compared with the experimental pressure drop values. This is certainly a significant improvement considering the 40 to 150% range of error values in predictions obtained by Mallick (2009) using the "back-calculation" technique in his earlier work. This shows that selection of an improved format of model for solids friction factor (e.g., two-layer format) could significantly improve the reliability of "back-calculation" method and considering the other benefits that the "back-calculation" method provides (such as less number of pressure transducer requirement and is to be installed on clean pipe, no requirement of periodic change of filters, less pressure fluctuation, etc.), this could promote the "back-calculation" approach as a quicker, yet being a reliable method to carry out testing and modelling pressure drop for industrial designs. Also, the accuracy of the prediction of pressure drop is more in the dense-phase region, where the bend loss effects are comparatively less than dilute-phase conveying. The accuracy of the "back-calculation" approach has been tested for other products and pipeline configurations shown in Figures 3.7 to 3.9. Figure 3.7 shows the results of scale-up evaluations for fly ash (Pan, 1992) conveyed through the 69 mm I.D. × 554 m long pipeline (7.2 t/h: bottom lines and 14.4 t/h: top lines). The results show that the "back-calculation" method shows better predictions in the very dense-phase region, and it shows slight over predictions in the dilute-phase region for both solid flow rates (i.e., lower: 7.2 t/h and higher: 14.4 t/h). Figure 3.8 shows the results of scale-up evaluations for pulverized brown coal (Pan, 1992) conveyed through the 69 mm I.D. × 554 m long pipeline (1.8 t/h: bottom lines and 9 t/h: top lines). The results show that the "back-calculation" method works well for lower solid flow rate (1.8 t/h)

from dense to dilute-phase region whereas, it shows better predictions in the dense-phase region and slight overprediction in the dilute-phase region for higher solid flow rate (9 t/h). Figure 3.9 shows the results of scale-up evaluations for fly ash and cement mixture (Wypych, 1989) conveyed through the 105 mm I.D. × 168 m long pipeline (36 t/h: bottom lines and 72 t/h: top lines). The results show that the "back-calculation" method works well in the dense-phase region and shows slight over predictions in dilute-phase for both solid flow rates (i.e., lower: 36 t/h and higher: 72 t/h). The bend loss is a more significant factor in dilute-phase conveying. The primary regime of the study of the present chapter is the fluidized dense-phase system. In this regime (dense-phase), the bend losses are expected to be relatively less dominant, and pressure drop through the straight pipe is supposed to be a more significant factor. Nonetheless, future research is to be carried out in modelling and prediction of bend loss for different powders and pipe layout.

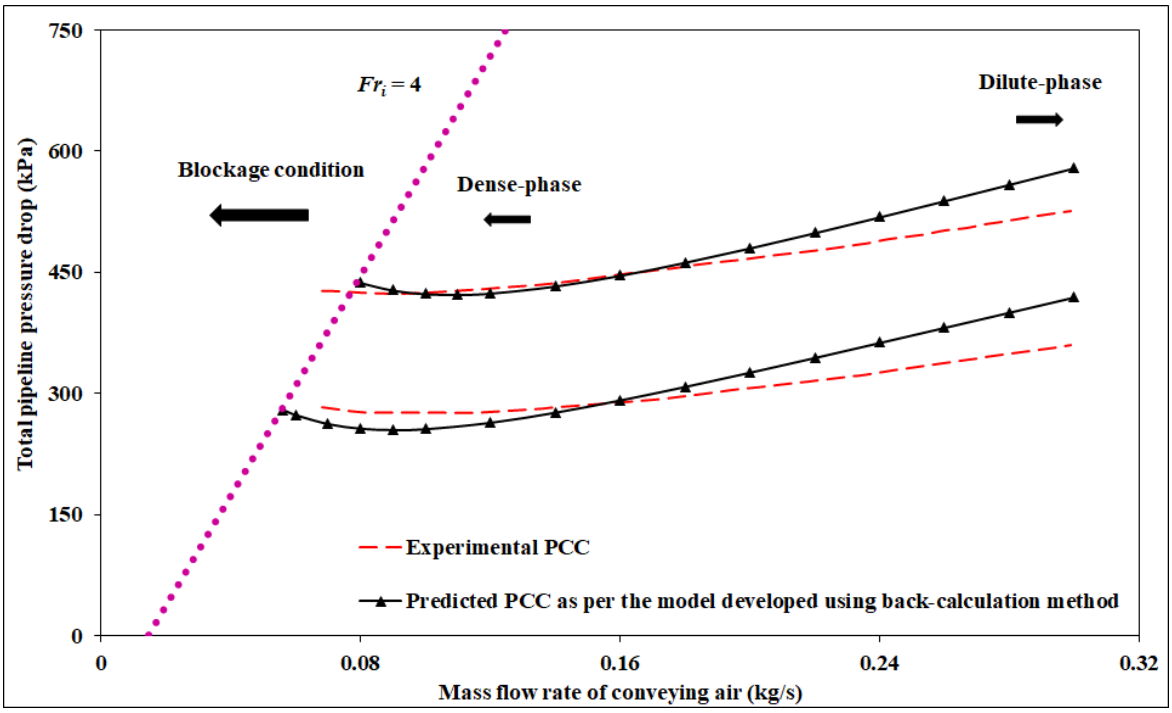

Figure 3.7: Scale-up evaluation of "back-calculation model" with Experimental PCC for fly ash (Pan, 1992) through 69 mm I.D. × 554 m long pipe

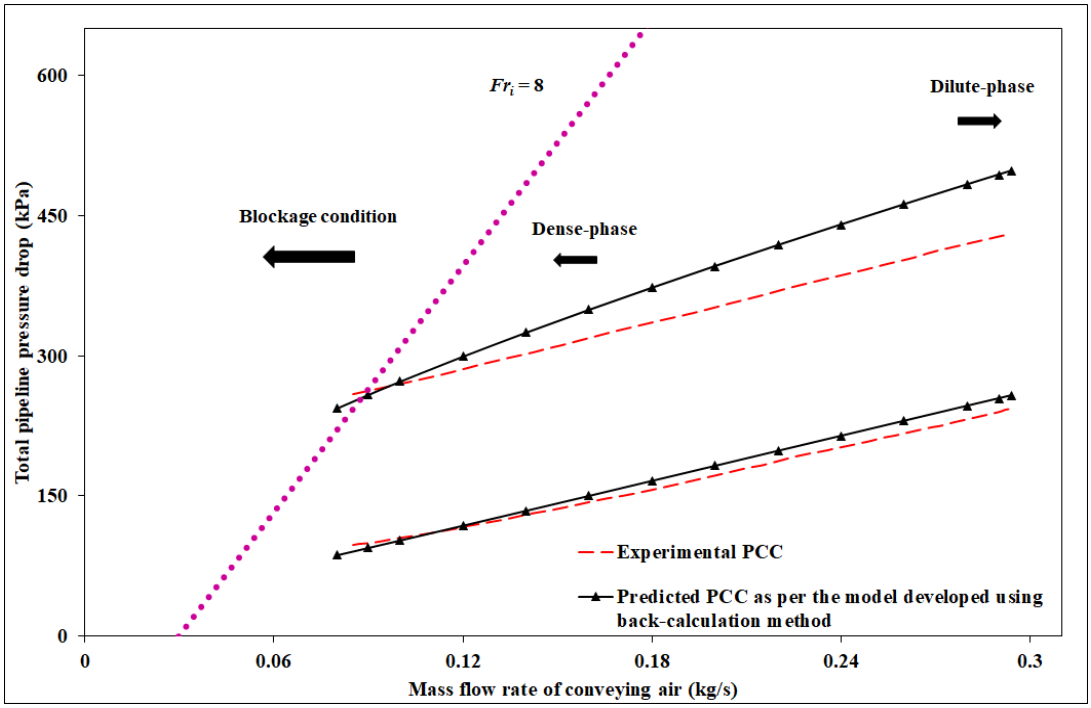

Figure 3.8: Scale-up evaluation of "back-calculation model" with Experimental PCC for pulverized brown coal (Pan, 1992) through 69 mm I.D. × 554 m long pipe

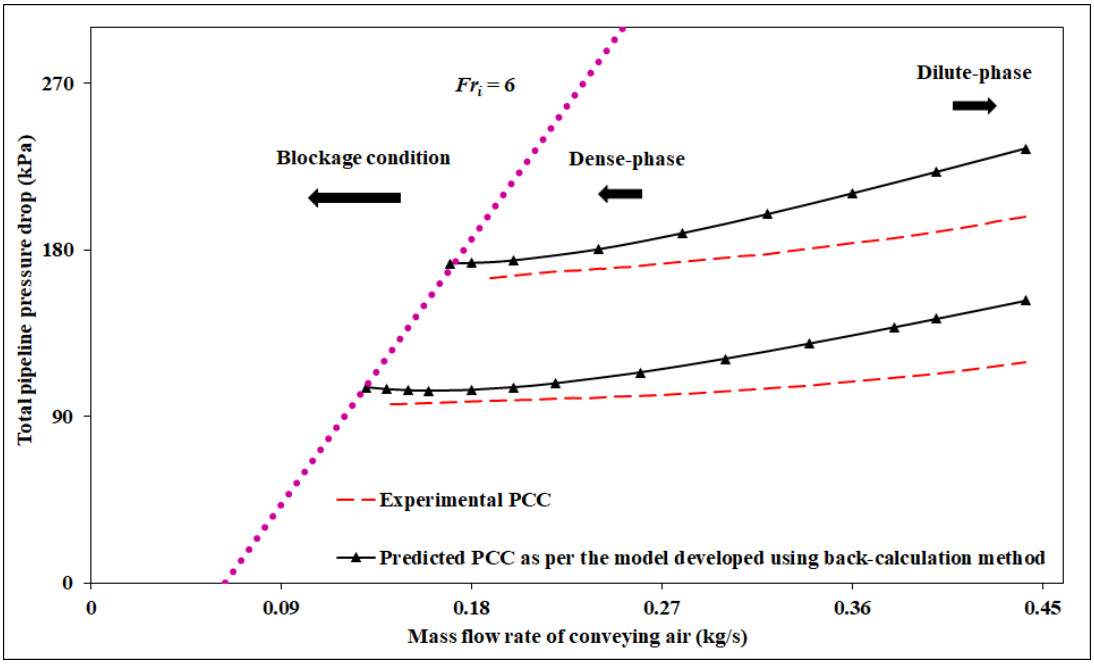

Figure 3.9: Scale-up evaluation of "back-calculation model" with Experimental PCC for fly ash and cement mixture (Wypych, 1989) through 105 mm I.D. × 168 m long pipe

The relative error values of predictions obtained using the “back-calculation” method are generally larger than that obtained using a “straight pipe” method by a maximum of 15%. The absolute error values obtained using the “back-calculation” method have been drastically reduced to a range of 3 to 35% from the earlier reported values of 40 to 150% inaccuracy. This significant improvement has been made possible due to the selection of an accurate format of modelling solids friction factor (two-layer modelling format) in the first place. While the “straight pipe” modelling approach will remain as the preferred method for studying pneumatic conveying and solids friction from a more research/fundamental point of view, the significant improvement of accuracy of “back-calculation” technique could promote the “back-calculation” approach as a quicker method for conducting testing and modelling pressure drop for industrial designs considering the several practical benefits of performing pneumatic conveying trails, data analysis, cost, time, etc. associated with “back-calculation method”. Based on the results presented in this chapter, it can be said that the “back-calculation” method generally provides up to 15% over-prediction compared to the straight-pipe model. This could be beneficial from an industrial system design point of view as this could provide a natural safety factor in predicting total pipeline pressure drop. However, while developing solids friction factor model using the “back-calculation” method, the pilot plant in the laboratory should not have too many bends or verticals, and the significant amount of pressure drops should come from the straight-horizontal pipe sections.

CHAPTER 4

NUMERICAL MODELLING OF PARTICLE VELOCITY

This chapter discusses the particle velocity estimation using numerical modelling technique. The detailed discussion has been made on the results obtained with the help of a MATLAB based program and on the validation of the newly developed particle velocity model. In the first half of the chapter, examinations have been made on the importance of using the particle velocity model in the existing two-layer model format, which was originally developed by Setia et al. (2016). A precise review of the existing literature related to particle velocity estimation for pneumatic conveying has also been presented. In the later part of this chapter, the newly developed particle velocity model has been used in the existing two-layer flow model format to estimate the solids friction factor under scale-up conditions of various pipeline lengths and diameters, respectively. The newly developed numerical particle velocity model has been validated using existing empirical models in the two-layer flow model format for scale-up configurations of various pipeline lengths and diameters, respectively.

4.1 Particle velocity and numerical simulation in gas-solids flows

Tsuji et al. (1985) used a numerical simulation technique for pneumatic conveying to study the behaviour of solids in a horizontal pipe channel. Polyethylene pellets were transported with an average particle size of 1.1 mm, particle density of 923 kg/m^3, air velocity ranging from 7 to 20 m/s, and mass flow ratio of less than 10. In their work, the various parameters, such as fluid drag, lift force due to particle rotation and torque on the rotating particles, were taken into consideration. The friction loss occurred due to the collision of particles with a surface of the pipe wall was also estimated. Frank et al. (1993) studied the motion of solid particles in a horizontal, two-dimensional, turbulent channel flow with the aid of experimental investigations and numerical

simulation. The numerical simulation was based on the Lagrangian approach. In the present work, glass particles were taken into account with average particle size: 115 μm and particle density: 2500 kg/m^3 for the respective horizontal channel of length: 4 m (approx.). The collision of glass particles (spherical in shape) with a pipe wall was investigated. It was found that the results obtained from the numerical method are in close agreement with the experimental investigations. Levy (2000) attempted to model the plug flow in a horizontal pneumatic conveying pipeline with the aid of using the two-fluid approach. To simulate the dense-phase flow conditions, a three-dimensional (3-D) model for the horizontal pipe of the respective internal diameter: 80 mm and length: 10 m was developed. In order to carry out the numerical simulations, polyethylene pellets (mono-sized and spherical in shape) with average particle size: 3 mm and particle density: 880 kg/m^3 were taken into consideration. The finite volume numerical method was used to solve the conservation equations for mass and momentum for the gas and solids phases. Along the horizontal pipe channel, the formation and deformations of plugs were demonstrated with the help of using numerical simulations. In the present investigation, axial and radial pressure drops were inspected and compared with the obtained experimental data. It was concluded that due to plug formation and deformation, it is not possible to obtain the plug velocity by cross-correlation between radial or axial pressure drops. Pu et al. (2008) studied the dense phase pneumatic conveying of pulverized coal at high pressure in a vertical pipe with the aid of three-dimensional numerical simulation. Pulverized coal was conveyed between two pressurized hoppers with an average particle size of 37 μm, particle density of 1350 kg/m^3 for respective internal diameter: 10 mm and length: 53 m. It was observed that as the superficial velocity increased, the pressure gradient decreased first and then subsequently increased, and as the transport pressure decreased, the pressure gradient also decreased. It was also concluded that there is a great influence of particle turbulence on dense

phase pneumatic conveying at high-pressure conditions. Pu et al. (2010) studied the dense phase pneumatic conveying of pulverized coal at high pressure in a horizontal pipe with the aid of numerical simulation. Pulverized coal was transported between two pressurized hoppers with an average particle size of 37 μm, particle density of 1350 kg/m^3 for pipe internal diameter: 10 mm and length: 53 m. It was observed that as the superficial velocity increased, the pressure gradient decreased first and then subsequently increased after reaching a minimum point. It has also been observed that in the horizontal pipe section in dense phase pneumatic conveying at high pressure, the pulverized coal deposited in the lower portion of the pipe surface and the upper surface of the settled layer had a distinct concave. Liu et al. (2011) numerically simulated the dense-phase pneumatic conveying for long-distance pipes in a horizontal channel. Fly ash was transported from the feeder vessel into the receiver bin in dense-phase, with an average particle size of 60 μm, bulk density of 770 kg/m^3 for respective internal diameter: 80 mm and length: 203 m. It was observed that the gas and particle velocity increased along the pipeline length, and the velocity on the upper surface of the pipe was larger than that at the bottom surface of the pipe and along pipe axial direction, pressure and pressure gradient decreased, and dynamic pressure increased gradually. Tripathi and Khakhar (2011) numerically simulated the sedimentation of a sphere of higher mass in a steady, gravity-driven granular flow of identical spheres, on a rough inclined plane. Behera et al. (2013, 2013a) solved one-dimensional governing equations of flow and developed a model to simulate fluidized dense-phase pneumatic conveying of fine powders through straight pipelines. Five different powder samples were transported, such as fly ash, alumina and cement meal with average particle size varying from 11 to 75 μm, particle density from 2096 to 3000 kg/m^3 for the respective pipeline of internal diameter: 63 mm and length: 173 m. It was found that for all five powders, the error between the numerically predicted and experimental values of inlet pressure lie

within acceptable margins, ranging from 13 to 25 %. The developed model has also been simulated for a pipeline configuration of different pipeline length and diameter. It has been found that the error between the predicted and the experimental pressure drop for the scale-up configurations was within ±10% for their set of data. Kuang et al. (2013) attempted to examine the gas-solid flow behaviour for coarser particles, using the combined approach of computational fluid dynamics and the discrete element method (CFD-DEM). In the present investigation, the applied simulation conditions were as follows; the pipe of internal diameter ranging from 49 to 51 mm, pipe length ranging from 6 to 14 m, average diameter of particle ranging from 2 to 5 mm, density ranging from 880 to 1350 kg/m^3. Kaur et al. (2017) **s**olved one-dimensional governing equations of flow for fluidized dense-phase pneumatic conveying using the Runge-Kutta-Fehlberg (RKF45) method. Fly ash was conveyed from the feeder vessel into the receiver bin in dense phase, with an average particle size of 30 μm, particle density of 2300 kg/m^3, bulk density of 700 kg/m^3 for respective internal diameter: 69 mm and length: 168 m. Using numerical analysis, Kaur et al. (2017) developed a correlation for determining particle velocity. The model is provided in Chapter 1 in equation (1.13).

Subsequently, Kaur et al. (2017a) solved one-dimensional governing equations of flow for fluidized dense-phase pneumatic conveying of fine powders using Runge-Kutta-Fehlberg (RKF45) method using the different sample of fly ash. The product (i.e., fly ash) was transported from the feeder vessel into the receiver bin in dense phase, with average particle size of 22 μm, particle density of 2370 kg/m^3, bulk density of 660 kg/m^3 for respective internal diameter: 65 mm and length: 254 m. Using numerical analysis, Kaur et al. (2017a) developed a new correlation of estimating particle velocity. The model is provided by equation (4.1).

$$\frac{u_s}{u_a} = 10^{-2.026}(m^*)^{0.912}\left(\frac{W_{fo}}{V}\right)^{-0.135} \quad (4.1)$$

In both of the above investigations done by Kaur et al. (2017; 2017a), the results revealed that the particle and actual gas velocities and the ratio of the two velocities increase in the direction of flow. The newly developed particle velocity model, when incorporated in the solids friction factor format, resulted in reliable predictions for scale-up configurations of various diameters and lengths, respectively. These investigations were done on the limited data (only fly ash), which needs to be further validated for other types of products. Vango et al. (2018) presented a coupled CFD-DEM model to study the multiphase flows in densely packed beds. Various existing models in the literature (Mallick, 2009; Barth, 1958; Setia and Mallick, 2015; Jones and Williams, 2003; Pan and Wypych, 1998; Setia et al., 2014) to estimate the solids friction factor term use "superficial gas velocity", in place of actual gas velocity, which is a valid assumption for suspension type of flow (i.e., dilute-phase flow regime). Since the volume of the entire pipeline occupied by the particles is significantly less as compared to the remaining residual volume available for gas flows. However, for fluidized non-suspension (dense) type of flows under a high solid loading ratio, a considerable portion of the pipe volume is occupied by the dunes, and hence, the lack of cross-section of pipe area available for the flow of gas-phase should not be ignored. Thus, in such cases to represent actual gas velocity (u_a) with superficial velocity (V) term could lead to gross inaccuracies in the model in fluidized dense phase mode of conveying. The existing empirical models for solids friction factor (equations 1.2 to 1.5, 1.8 and 1.10) do not address the particle or dune velocity and the slip velocity (the difference between gas and particle velocities) and totally depend on the superficial velocity of the gas. Nonetheless, it should not be overlooked that particle velocity estimation is important in order to better understand the gas-solids flow mechanism.

Over the years, researchers have made attempts to determine the particle velocity using various experimental techniques. To measure particle velocity in dilute gas-particle two-phase flows, particle image velocimetry (PIV) technique was developed. Miyazaki et al. (1999) first measured the particle velocity of glass beads (average diameter: 2.9-3.9 mm) in gas-solids two-phase flow by using particle image velocimetry (PIV) method. The main limitation of this technique is that it is limited to dilute-phase particulate flow (higher air velocity or suspension flow) only. However, limited research has been reported so far in the area of applying particle image velocimetry for estimating particle velocity in the dense-phase pneumatic conveying. Li and Tomita (2000) have carried out measurements to estimate particle velocity using the photographic image technique. For testing purposes, two test products, i.e., polyethylene (average diameter: 3.13 mm) and polyvinyl (average diameter: 4.26 mm), were used. Wei et al. (2011) determined the particle velocity of quartz sand (average diameter: ranging from 60 to 350 μm) and pulverized coal (average diameter: ranging from 75 to 300 μm) using optical fiber probe technique. Yan and Rinoshika (2011) attempted to determine the particle velocity of polyethylene particles (average diameter: 2-3 mm) using particle image velocimetry (PIV) technique for low-velocity flows. It is evident from the existing literature that the majority of the attempts have been made towards the estimation of particle velocity considering the coarser particles (i.e., applicable for dilute phase mode) and very little work has been reported so far in the area of measurement of particle velocity for fine powders. Limited attempts have been made to experimentally determine the particle velocity for fine powders due to various challenges associated with fine powders such as (1) fine powders have high turbulent nature of flow, and it is difficult to analyze the structure (i.e., movement) of the dunes between the sensors; (2) fine powders tend to coat the sight glass thus making it difficult to see through the glass. Therefore, researchers have largely relied on empirical

models such as Klinzing et al. (1989), Hong and Shen (1994), Hinkle (1953), Arastoopour et al. (1979), IGT (Klinzing et al., 1987), Tripathi et al. (2018), Santo et al. (2018) for particle velocity estimation. Table 4.1 shows the various gas-solids velocity correlations in horizontal dilute phase pneumatic conveying. Most of these empirical models are valid only for coarser particles, which are being transported in dilute-phase only (Li et al., 2014). Kaur et al. (2017; 2017a) carried out particle velocity estimations using numerical procedures for fly ash. However, the work was carried out for limited test products (only for fly ash), which needs to be further validated for other types of products. Hence, there is a need to carry out further research to validate the preliminary findings and to use the results of an improved particle velocity model.

Table 4.1: Gas–solids velocity correlations in horizontal dilute-phase pneumatic conveying

Author	Empirical correlations	Data range
Hinkle (1953)	$u_s = u_g\left(1 - 0.1344 {d_s}^{0.3} {\rho_s}^{0.5}\right)$	0.36 mm $< d_s <$ 8.38 mm 1048 kg/m^3 $< \rho_s <$ 1808 kg/m^3
Arastoopour et al. (1979)	$u_s = u_g\left(1 - 0.044 {d_s}^{0.3} {\rho_s}^{0.5}\right)$	Same as Hinkle (1953)
IGT (Klinzing et al., 1987)	$u_s = u_g\left(1 - 0.68 {d_s}^{0.92} {\rho_s}^{0.5} {\rho_a}^{-0.2} D^{-0.54}\right)$	Not given
Klinzing et al. (1989)	$u_s = \left(u_g - {w_{fo}}^{0.71}\right) D^{0.019}$	67 µm $< d_s <$ 900 µm 2395 kg/m^3 $< \rho_s <$ 5004 kg/m^3
Hong and Shen (1994)	$u_s = u_g \left[1 - 0.533 \left(\frac{1000\rho_a}{\rho_s}\right)^{1.093} \left(\frac{D}{100 d_p}\right)^{-0.721}\right]$	High solid-gas ratio, fine powder
Tripathi et al. (2017)	$\frac{u_s}{u_g} = 1 - 0.072 \left[Ar \left(\frac{\rho_p - \rho_a}{\rho_a}\right)\right]^{0.091}$	0.23 mm $< d_s <$ 4 mm 940 kg/m^3 $< \rho_s <$ 3794 kg/m^3
Santo et al. (2018)	$\frac{u_s}{u_g} = 1 - 0.02 \left[Ar \left(\frac{\rho_p - \rho_a}{\rho_a}\right) \left(\frac{D}{D_{50}}\right)^{-2}\right]^{0.14}$	0.06 mm $< d_s <$ 4 mm 940 kg/m^3 $< \rho_s <$ 5800 kg/m^3

4.2 Numerical solution for particle velocity for constant fluidized bulk density

In order to develop the governing equations for solids-gas through a horizontal section of the pipeline, the following assumptions have been made:

- The flow is considered to be occurring in the steady-state condition.
- The flow is one-dimensional (i.e., in the x-direction of bulk flow).
- The system is isothermal, and the gas phase obeys the ideal gas equation of state.
- There is no heat and mass transfer between the phases.
- The composition of the solids-gas mixture in a finitely small control volume is uniform.
- There is no concentration gradient of particles taken across the pipe diameter.
- Fluidized bulk density is taken in place of particle density.
- Fluidized bulk density is assumed to be constant in the entire cross-section of the pipeline.

In the present thesis, the maximum length of the pipe for model prediction purposes has been taken as 554 m. As the length of the pipe is very large with the same diameter, the fluctuations in the pipe will come into existence, and it majorly influences the flow conditions. Therefore, it is difficult to incorporate energy losses, turbulence created by the fluctuations that occurred in the entire pipeline in a 3D numerical model. Hence, it is beyond the scope of the numerical work presented in this chapter. Therefore, the flow is considered to be happening only in one direction (x-direction). However, Chapter 5 deals with the model prediction considering the energy losses/turbulence occurred in the pipeline.

In the present investigation, the term ‘particle density’ has been replaced by the term ‘fluidized bulk density’ because the latter term shows better flow representation of moving dunes in the pipeline for the fluidized dense-phase conditions. For developing the energy equation, energy balance across a control volume is as given below (Figure 4.1).

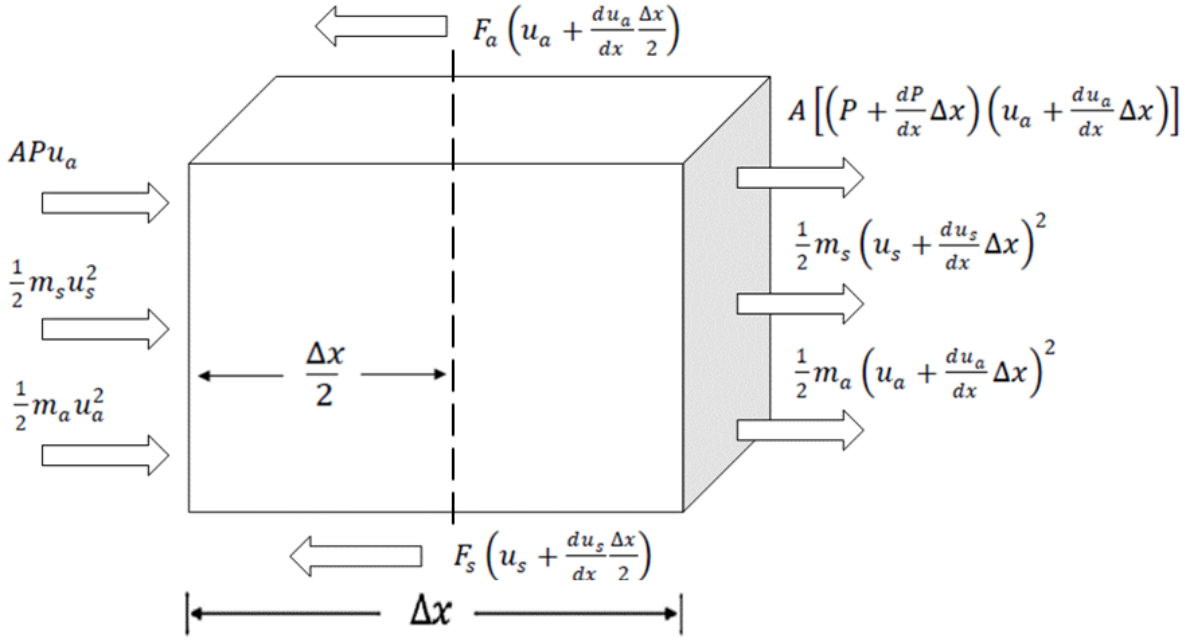

Figure 4.1: Mass and momentum interactions across a control volume

Conservation of mass for the gas-phase is represented by equation (4.2), and the solids phase is represented by equation (4.3), respectively.

$$\frac{d}{dx}(\varepsilon_a \rho_a u_a) = 0 \tag{4.2}$$

$$\frac{d}{dx}(\varepsilon_s \rho_{fl} u_s) = 0 \tag{4.3}$$

To obtain conservation of momentum per unit time equation (i.e., force balance equation), the equation (4.4) has been derived from the control volume shown in Figure 4.1, as shown below:

$$\left[(\rho_a \varepsilon_a A u_a)\left(u_a + \frac{du_a}{dx}\Delta x\right) - (\rho_a \varepsilon_a A u_a)u_a\right] + \left[(\rho_{fl} \varepsilon_s A u_s)\left(u_s + \frac{du_s}{dx}\Delta x\right) - (\rho_{fl} \varepsilon_s A u_s)u_s\right]$$
$$= \left[PA - \left(P + \frac{dP}{dx}\Delta x\right)A\right] - F_a - F_s \quad (4.4)$$

The final expression for the conservation of momentum equation for the solids-gas flows has been obtained by dividing both sides of equation (4.4) by elemental volume $(A\Delta x)$ as shown below:

$$\varepsilon_a \rho_a u_a \frac{du_a}{dx} + \varepsilon_s \rho_{fl} u_s \frac{du_S}{dx} + \frac{dP}{dx} = -f_a - f_s \quad (4.5)$$

Net accumulation of pressure and shear energy in the x-direction equals to

$$= APu_a - A\left[\left(p + \frac{dp}{dx}\Delta x\right)\left(u_a + \frac{du_a}{dx}\Delta x\right)\right] - \left[F_a\left(u_a + \frac{du_a}{dx}\frac{\Delta x}{2}\right) + F_s\left(u_s + \frac{du_s}{dx}\frac{\Delta x}{2}\right)\right] \quad (4.6)$$

The word “shear energy” is intended to mean the energy spent in overcoming the shear forces. These losses are arising due to air-only and particle to particle-air-wall interactions. To overcome these losses, pressure energy is provided (compressed air). In the given study, pressure and shear forces are acting on the cross-sectional area of the pipe and the wall surfaces, respectively. A similar consideration was made by Behera et al. (2013). By solving and neglecting the higher-order terms in equation (4.6), the final expression has been obtained as follows:

Net accumulation of pressure and shear energy in the x-direction equals to

$$= -A\Delta x \left[p\frac{du_a}{dx} + u_a\frac{dp}{dx} + u_a f_a + u_s f_s \right] \tag{4.7}$$

Net accumulation of kinetic energy in x-direction equals to

$$= \frac{1}{2}m_a u_a^2 + \frac{1}{2}m_s u_s^2 - \frac{1}{2}m_a\left(u_a + \frac{du_a}{dx}\Delta x\right)^2 - \frac{1}{2}m_s\left(u_s + \frac{du_s}{dx}\Delta x\right)^2 \tag{4.8}$$

On solving and rearranging the equation (4.8), the final expression has been obtained as follows:

Net accumulation of kinetic energy in x-direction equals to

$$= -A\Delta x \left[\rho_a \varepsilon_a {u_a}^2 \frac{du_a}{dx} + \rho_{fl}\varepsilon_s {u_s}^2 \frac{du_s}{dx} \right] \tag{4.9}$$

Considering there is no net accumulation of energy within the control volume under steady-state condition, the following energy equation (4.10) is obtained from equations (4.7) and (4.9), which shows the net summation under steady-state equals to zero.

$$p\frac{du_a}{dx} + u_a\frac{dp}{dx} + u_a f_a + u_s f_s + \rho_a \varepsilon_a u_a^2 \frac{du_a}{dx} + \rho_{fl}\varepsilon_s {u_s}^2 \frac{du_s}{dx} = 0 \tag{4.10}$$

The energy equation represented in the equation (4.10) addresses the energy dissipation due to the turbulence and frictional resistance of fluid-wall interactions, particle to air, particle to particle,

and particle to wall interactions. Volume fractions for the gas and solid phases obey the following relationship:

$$\varepsilon_a + \varepsilon_s = 1 \tag{4.11}$$

In equations (4.2) to (4.11), the fluidized bulk density has been considered as the representation of solids density, which considers the dune flow nature of the fluidized dense-phase flow. The system of equations (equations 4.2, 4.3, 4.5, 4.10) has been solved for the four variables namely, u_a, u_s, ϵ_s and P. Firstly, the conservation equations, i.e., equations (4.2), (4.3), (4.5), (4.10) have been coupled and transformed into first-order ordinary differential equations (4.12) to (4.15), which show the evolution of an individual parameter with respect to the spatial distance (x) under study. The spatial variation of fluidized bulk density vanishes for the solids phase, as it is considered to be a constant term in the system. The derived equations are represented in the following form:

$$\frac{du_s}{dx} = \frac{u_s}{\varepsilon_s\left(\rho_{fl}u_s^2(u_s-u_a) - \dfrac{u_aP}{(1-\varepsilon_s)}\right)}\left[-(u_s-u_a)f_s + \frac{u_aP}{\rho_a}\frac{d\rho_a}{dx}\right] \tag{4.12}$$

$$\frac{du_a}{dx} = -\frac{u_a}{\rho_a}\frac{d\rho_a}{dx}\frac{u_a}{(1-\varepsilon_s)\left(\rho_{fl}u_s^2(u_s-u_a) - \dfrac{u_aP}{(1-\varepsilon_s)}\right)}\left[-(u_s-u_a)f_s + \frac{u_aP}{\rho_a}\frac{d\rho_a}{dx}\right] \tag{4.13}$$

$$\frac{d\varepsilon_s}{dx} = -\frac{1}{\left(\rho_{fl}u_s^2(u_s-u_a) - \dfrac{u_aP}{(1-\varepsilon_s)}\right)}\left[-(u_s-u_a)f_s + \frac{u_aP}{\rho_a}\frac{d\rho_a}{dx}\right] \tag{4.14}$$

$$\frac{dP}{dx} = -f_a - f_s + (1-\varepsilon_s)u_a^2\frac{d\rho_a}{dx}\frac{\left(\rho_a u_a^2 - \rho_{fl}u_s^2\right)}{\left(\rho_{fl}u_s^2(u_s-u_a) - \frac{u_a P}{(1-\varepsilon_s)}\right)}\left[-(u_s-u_a)f_s + \frac{u_a P}{\rho_a}\frac{d\rho_a}{dx}\right] \quad (4.15)$$

where, $f_a = \left[\left(\lambda_f \rho V^2 L\right)\Big/_{(2D)}\right]$ and $f_s = \left[\left(m^* \lambda_s \rho V^2 L\right)\Big/_{(2D)}\right]$

The set of equations (4.12) to (4.15) present the evolution of the parameters u_s, u_a, ε_s and P, respectively, with respect to the spatial coordinate, i.e., along with the length (x) of the pipeline. The entire length of the pipeline has been divided into several straight pipe segments/sections (6 in numbers) (Figure A1.1). Large straight pipeline sections have been further divided into smaller sections. In the present investigation, the different values of 'x' thus obtained on the horizontal section of pipe for the purpose of study, have been provided in Table 4.2 (starting from the location of the blow tank). For each small section of the pipe, a set of coupled ordinary differential equations have been solved numerically using MATLAB's ode45 solver, which is based on the fourth-fifth-order Runge-Kutta-Fehlberg (RKF45) method (Fehlberg, 1969). The solution proceeded from the pipe inlet to the outlet. In order to calculate the initial value of u_s,u_a, ε_s, the following formulae have been used, represented by the following equations (4.16 to 4.18). It has been assumed that when the material is discharged from the blow tank, the aerated mixture occupies the full cross-section of the pipe. The extent of occupancy decreases subsequently along the direction of flow in the pipeline.

$$u_s = \frac{m_s}{A\rho_{fl}} \quad (4.16)$$

$$u_a = \frac{(m_a/A)}{(\varepsilon_a/\rho_{ai})} \tag{4.17}$$

$$\varepsilon_s = \frac{(m_s/\rho_{fl})}{[m_s/\rho_{fl} + m_a/\rho_{ai}]} \tag{4.18}$$

Numerically determined values of the various parameters, such as u_a, u_s, ϵ_s and P obtained at the end of the first section of pipe was used as the initial conditions for the successive section. This process has been followed in all subsequent sections of the pipe until the outlet section of the pipeline has been reached. Thus, the value of the various parameters $u_s, u_a, u_s/u_a$, ϵ_s and P have been determined at the initial and final point of each section of the pipe, and with the help of these, results corresponding to the mid-point values (at x, given in Table 4.2) were acquired. Calculations have been performed for various operating parameters, i.e., corresponding to different solid flow rates in t/h and airflow rates in kg/s, fluidized bulk density in kg/m^3 (for different products given in Table 4.2). The results of these four parameters, i.e., the variation of $u_s, u_a, u_s/u_a$ and ϵ_s along the length of the pipe section (x) m, are shown in Figures 4.2 to 4.7 for fly ash (Mallick, 2009; Setia et al., 2016) and cement (Setia et al., 2016). Fluidized bulk density values have been obtained from Kaur et al. (2017; 2017a).

Table 4.2: Description of parameters, mid-point values and flow rates of solids and air for numerical simulation

Products	**Calculated parameters**	**Mid-point values x (m)**	**(m_s) (t/h)**	**(m_a) (kg/s)**	**Fluidized bulk density (ρ_{fl}) (kg/m^3)**	**Pipeline conveying length (m)**
Fly ash, (Mallick, 2009)	$u_a\,(m/s), u_s\,(m/s), \epsilon_s, P(kPa)$	6.51, 42.73, 78.94, 83.67, 113.88, 144	19, 14, 9	0.04, 0.09, 0.14	300	168
Cement, (Setia et al., 2016)	$u_a\,(m/s), u_s\,(m/s), \epsilon_s, P(kPa)$	9.1, 20.1, 60.2, 100.3, 144.25, 188.2	18, 14, 10	0.06, 0.16	564	254
Fly ash, (Setia et al., 2016)	$u_a\,(m/s), u_s\,(m/s), \epsilon_s, P(kPa)$	9.1, 20.1, 60.2, 100.3, 144.25, 188.2	18, 14, 10	0.06, 0.16	333	254

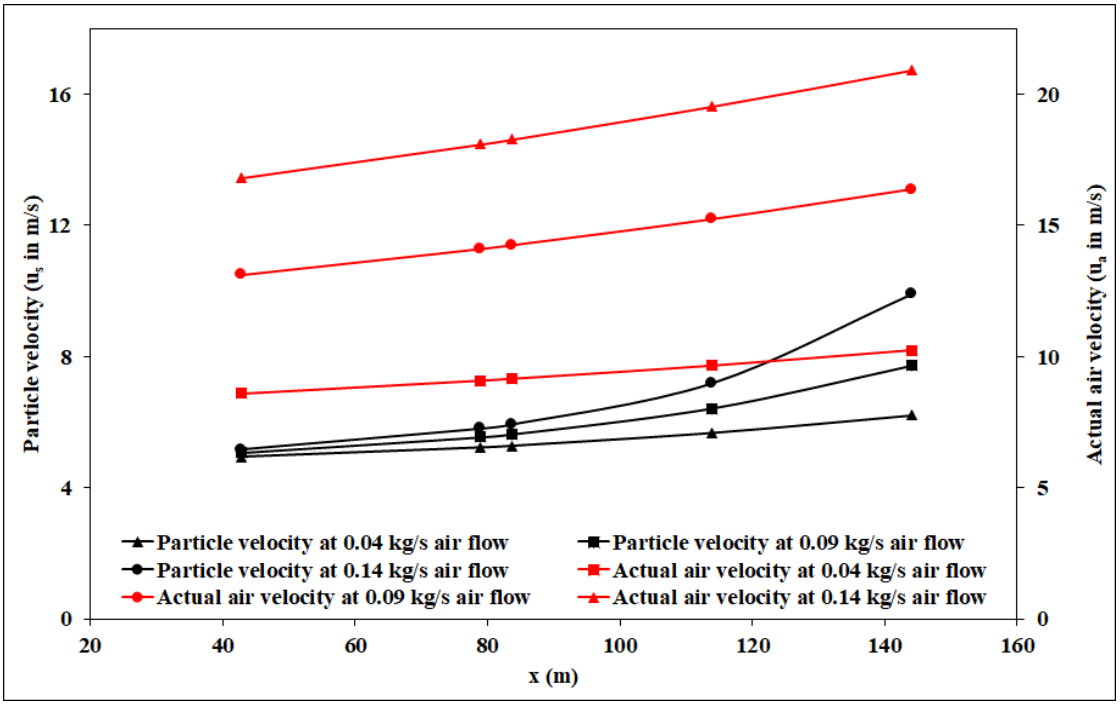

Figure 4.2: Variation of particle velocity and actual air velocity along the pipeline length for fly ash for different airflow rates for m_s = 19 t/h; ρ_{fl} = 300 kg/m^3

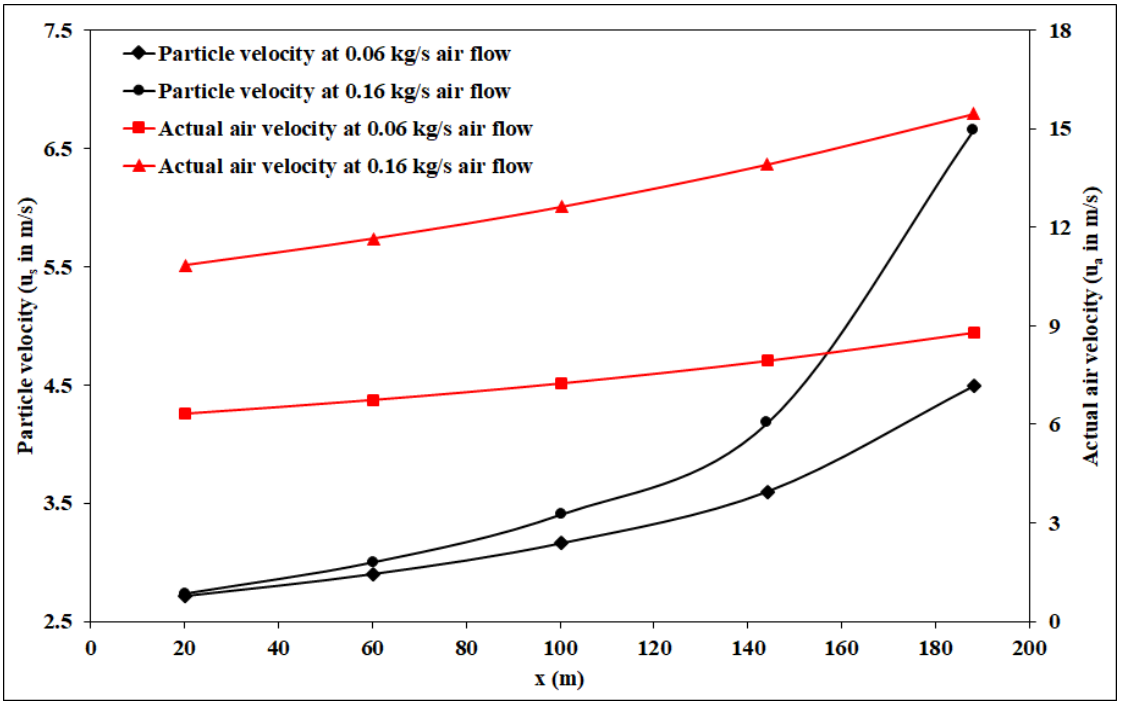

Figure 4.3: Variation of particle velocity and actual air velocity along the pipeline length for cement for different airflow rates for m_s = 18 t/h; ρ_{fl} = 564 kg/m^3

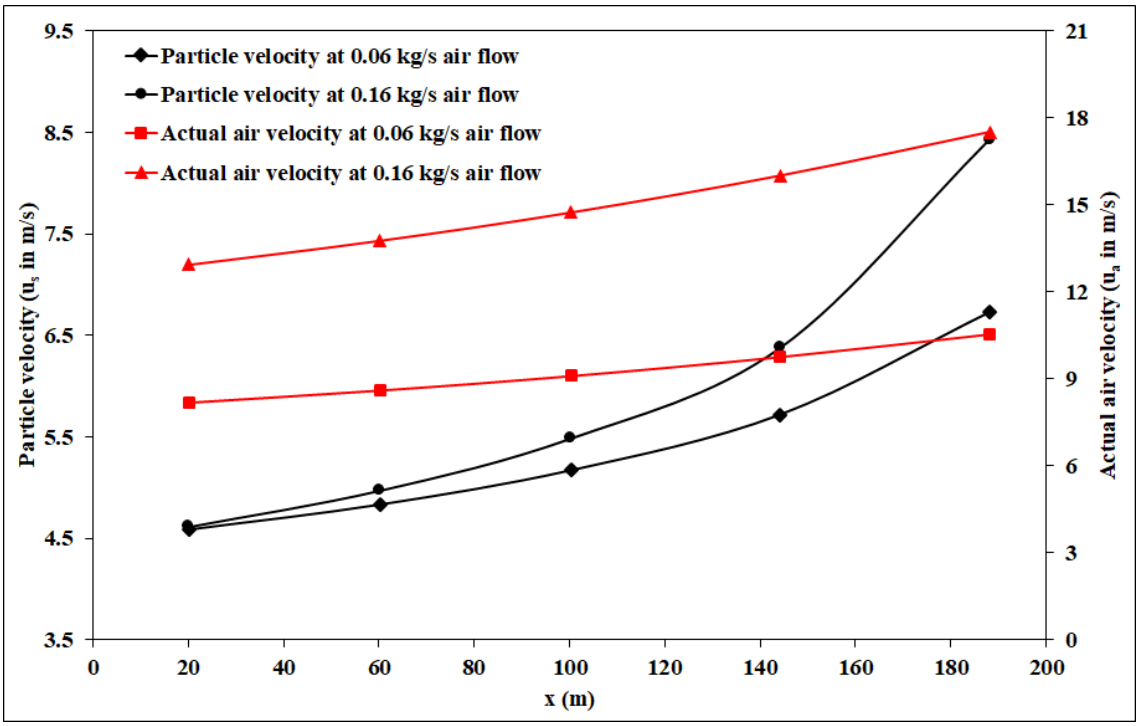

Figure 4.4: Variation of particle velocity and actual air velocity along the pipeline length for fly ash for different airflow rates for m_s = 18 t/h; ρ_{fl} = 333 kg/m^3

Figures 4.2, 4.3, and 4.4 show the variation of particle velocity and actual air velocity for three different products, i.e., fly ash (Mallick, 2009), cement and fly ash (Setia et al., 2016). Particle velocity has been shown along the primary axis and actual air velocity along the secondary axis. It is evident from the figures that there is an overall increasing trend in the values of particle velocity along the direction of flow in the pipeline. It has also been observed that an increased flow rate of air results into higher values of particle velocity. This may be due to the fact that the higher airflow causes the particles to get suspended (i.e., particles do not remain in the non-suspension layer anymore). In the non-suspension mode, the particles experience the impact of adhesive forces and inter-particle locking caused by the pipe wall and the surrounding particles. Hence, the particle velocities would remain relatively smaller as compared to the air velocities at lower airflow rates.

At higher air velocities, the suspended particles remain mostly under the influence of air drag and resistive forces. This is due to the friction occurring at the pipe wall and with the other particles. Hence, the particle velocity values get relatively closure to the air velocity values. There is an overall rising trend observed in the values of actual gas and particle velocities along the direction of flow in the pipeline. Higher particle velocities are observed for higher solids flow rates. Also, higher actual air velocities are observed for higher product flow rates. This could be caused by the higher solid volume occupancy in pipe cross-section at higher product flow rates, which results in a relatively less area available for the gas flows. As a result, there is an increase in the values of actual air velocities with an increase in solids flow rates. Similar results have been obtained for all products conveyed with different solids mass flow rate of 14, 9, and 10 t/h and respective air mass flow rates in kg/s for a constant fluidized bulk density in kg/m^3 (given in Table 4.2). The results are shown in Figures A3.1 to A3.6 (Annexure A3). Figures 4.5, 4.6, and 4.7 show the variation of the ratio of particle to actual air velocity and solids volumetric concentration for these three different products. Particle to actual air velocity ratio has been represented in the primary axis, and solids volumetric concentration has been represented in the secondary axis.

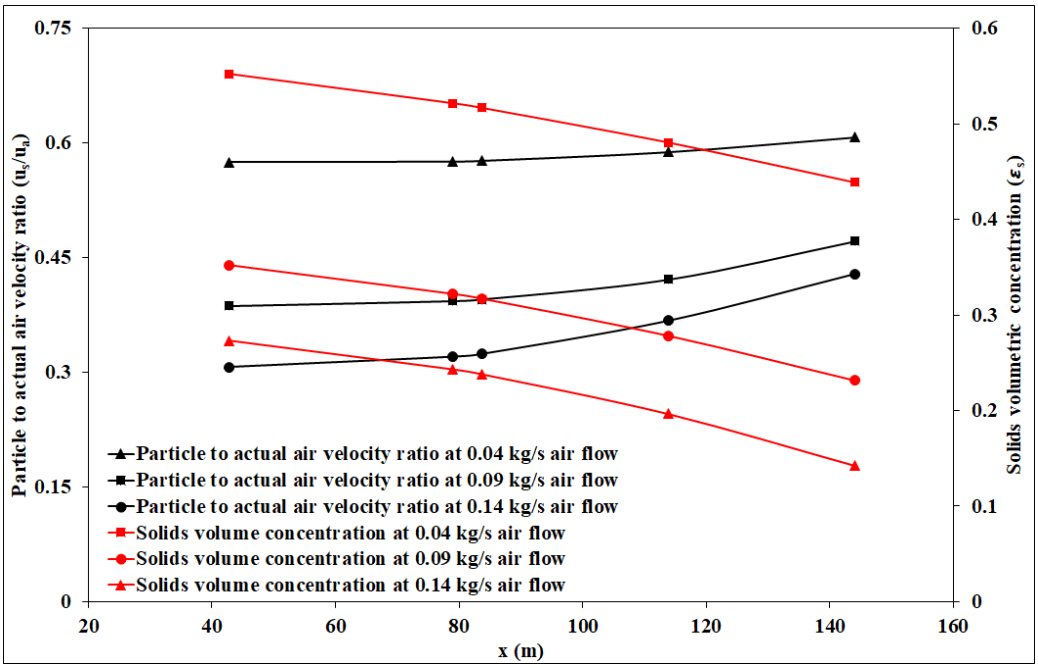

Figure 4.5: Variation of ratio of particle to actual air velocity and solids volumetric concentration along the pipe length for fly ash for different airflow rates for m_s = 19 t/h; ρ_{fl} = 300 kg/m^3

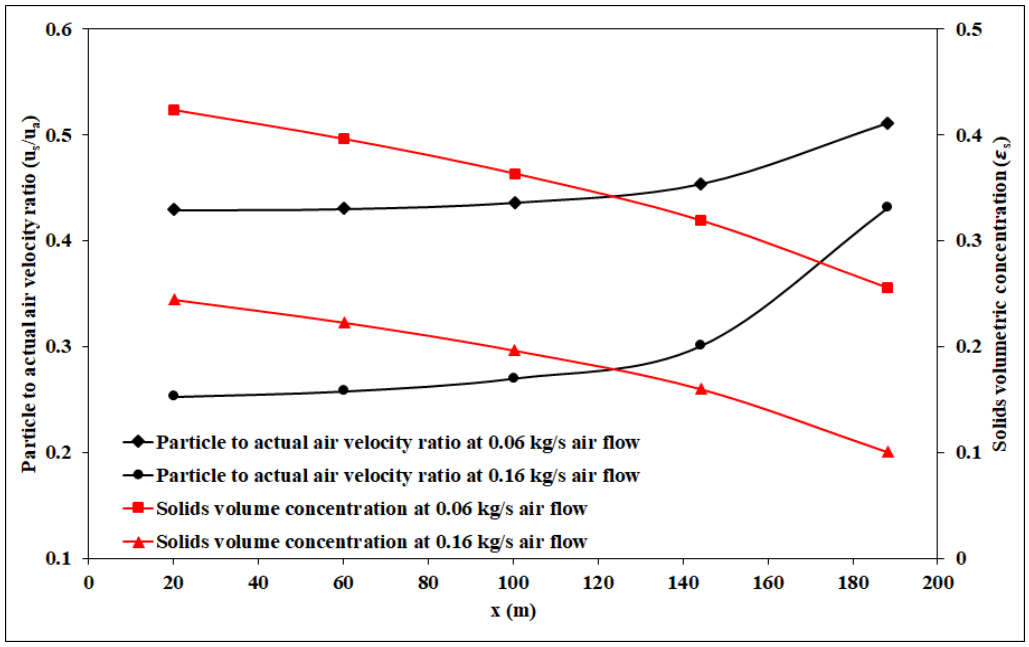

Figure 4.6: Variation of ratio of particle to actual air velocity and solids volumetric concentration along the pipe length for cement for different airflow rates for m_s = 18 t/h; ρ_{fl} = 564 kg/m^3

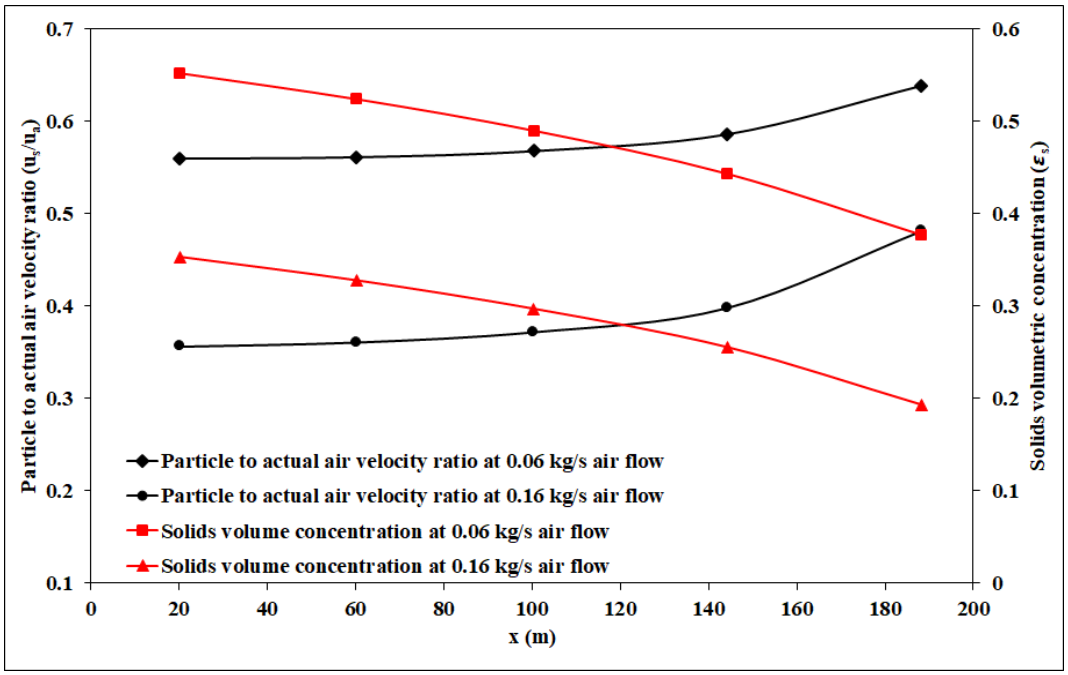

Figure 4.7: Variation of ratio of particle to actual air velocity and solids volumetric concentration along the pipe length for fly ash for different airflow rates for m_s = 18 t/h; ρ_{fl} = 333 kg/m^3

It is evident from the figures that the ratio of particle to actual air velocities increases in the direction of flow, indicating that the rate of increase in the particle velocity is more dominating over the corresponding rise in the actual air velocities (due to gas expansion). This could be due to particles getting into suspension mode along with the direction of flow in the pipeline and/or with an increase in airflow rates, thus experiencing reduced resistive forces due to particle-particle-wall interactions. The results revealed that there is a sharp increase in the value of the solids to actual air velocity ratio towards the end of the pipeline after the closely coupled bends (from 80 to 150 m pipeline length). This is due to the fact that there is a substantial drop in gas pressure due to flow through the closely coupled bend. On the other hand, a decreasing trend in the solids volumetric concentration is observed along the direction of flow, which indicates that there is a gradual transition from dense- to dilute-phase conditions prevailing inside the pipeline. Similar

results have been obtained for all products conveyed with different solids mass flow rate of 14, 9, and 10 t/h and respective air mass flow rates in kg/s for a constant fluidized bulk density in kg/m^3 (given in Table 4.2). The results are shown in Figures A3.7 to A3.12 (Annexure A3). Using the obtained numerical values of the particle to actual gas velocity ratio, a power function-based correlation for particle-to-actual gas velocity has been developed for all three products, namely, fly ash (Mallick, 2009), cement, and fly ash (Setia et al., 2016). The following empirical power function-based models have been obtained using multiple regression method. In these models, the ratio of particle to actual gas velocity has been represented by solids loading ratio (m*) and dimensionless velocity (w_{fo}/V) terms. A high value of the coefficient of determination (R^2) indicates a good fit.

For fly ash of Mallick (2009),

$$\frac{u_s}{u_a} = 10^{-3.561}(m^*)^{1.063}\left(\frac{w_{fo}}{V}\right)^{-0.585},\ R^2 = 0.97 \tag{4.19}$$

For cement of Setia et al. (2016),

$$\frac{u_s}{u_a} = 10^{-4.734}(m^*)^{1.324}\left(\frac{w_{fo}}{V}\right)^{-0.895},\ R^2 = 0.96 \tag{4.20}$$

For fly ash of Setia et al. (2016),

$$\frac{u_s}{u_a} = 10^{-2.981}(m^*)^{0.930}\left(\frac{w_{fo}}{V}\right)^{-0.474},\ R^2 = 0.98 \tag{4.21}$$

An attempt has been made here to improve the existing two-layer model developed by Setia et al. (2016) by including the newly developed particle velocity model in the model. Using steady-state pressure drop data across a straight pipe section, *K, a, b* and λ_s^* values for the newly developed two-layer model (in the form of equation 4.22) were determined. The modified form of the two-layer model has been used for the scale-up validation of solids friction factor and has been shown as follows in equation (4.22).

$$\lambda_s = \tau_1 \left[K(VLR)^a \left(\frac{w_{fo}}{V}\right)^b \right] + \tau_2 \left[\lambda_s^* \left(\frac{u_s}{u_a}\right) + \left(2\beta_o \Big/ \left(\frac{u_s}{u_a}\right) Fr^2 \right) \right] \tag{4.22}$$

where, $\left({}^{u_s}/_{u_a}\right)$ is taken from the newly developed model formats given in equations 4.19, 4.20 and 4.21 (developed with the assumption of constant fluidized bulk density) for cement and fly ash. In the above equation (4.22), VLR (volumetric loading ratio) is determined using equation (1.9) provided in Chapter 1.

The equation (1.10) refer Chapter 1 considers that the particles have the same velocity as that of the superficial gas velocity (V), i.e. $\left({}^{C}/_{V} = 1\right)$, which may be a good approximation for fine powders travelling in very dilute-phase, but not an appropriate assumption for fluidized dense-phase type flow (which is characterized by non-suspension dune flow). Therefore, in order to address the above issues, equation (1.10) has been modified to equation (4.22) by incorporating the term $\left({}^{u_s}/_{u_a}\right)$ (varies from 0 to 1), which replaces the term $\left({}^{C}/_{V} = 1\right)$.

Table 4.3. Newly developed two-layer model (in the form of equation 4.22)

Product	**Models (as per the format provided by equation 4.22)**					**R^2**	**Particle velocity model type**
	K	***a***	***b***	$\boldsymbol{\lambda_s^*}$	$\boldsymbol{w_{fo}}$ **(m/s)**		
Fly ash (Mallick, 2009)	8	-0.40	1.62	0.0164	0.06	0.99	Newly developed model format (equation 4.19)
Cement (Setia et al., 2016)	26.5	-0.62	1.74	0.0384	0.036	0.96	Newly developed model format (equation 4.20)
Fly ash (Setia et al., 2016)	84.5	-0.86	2.10	0.0313	0.038	0.96	Newly developed model format (equation 4.21)

The newly developed improved two-layer models for solids friction factor (refer equation 4.22) has been validated for longer and larger scale-up pipeline conditions viz. 105 mm I.D. × 168 m long and 69 mm I.D. × 554 m long pipelines for fly ash, and 80/100 mm I.D. × 407-m-long pipelines for fly ash and cement for various solids and airflow rates by comparing the predicted pneumatic conveying characteristics against the experimental plots. The results are provided in Figures 4.8 to 4.11. In order to calculate the total pipeline pressure drop, an iterative program using SOLVER and MACRO in Microsoft Excel 2007 has been developed. To evaluate the relative accuracy of the newly developed improved two-layer models (using three different particle velocity models), plots between predicted pneumatic conveying characteristics and experimental pneumatic conveying characteristics have been shown in the Figures 4.8 to 4.11. Predictions obtained from the originally developed two-layer model (Setia et al., 2016) have been superimposed on Figures 4.8 to 4.11 to show the possible improvements obtained by using newly developed particle velocity models in the two-layer model format of solids friction. In Figures 4.8 to 4.11, the "particle specific" term has been used to represent the two-layer model for solids friction that uses particle velocity model given by equation (4.22).

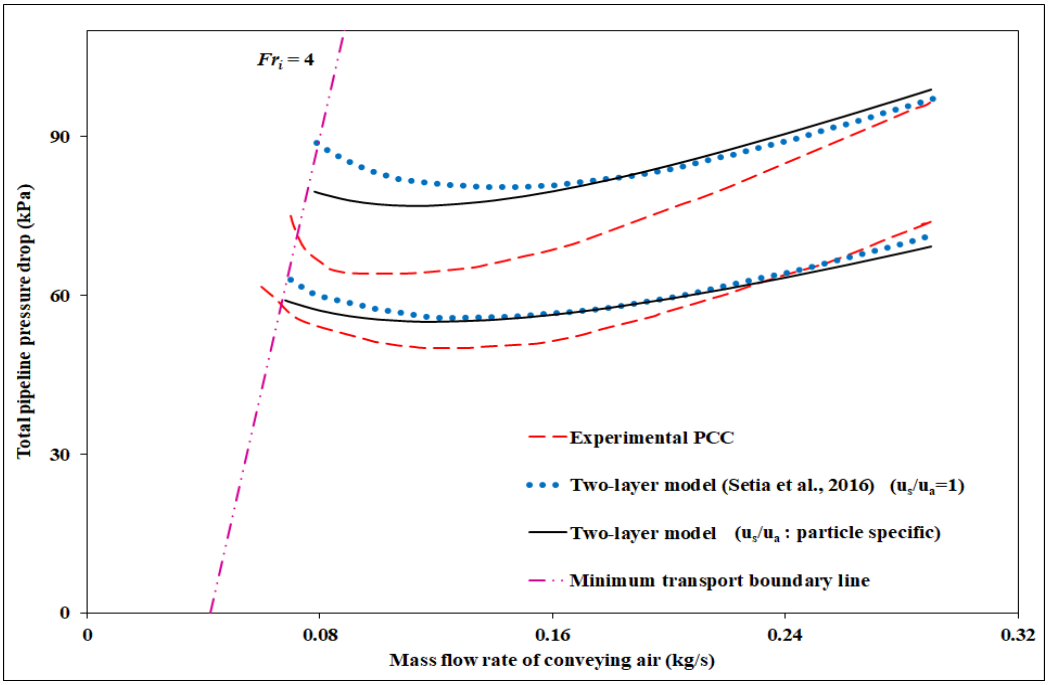

Figure 4.8: Scale-up evaluation for solids friction factor (two-layer specific) for fly ash through 105 mm I.D. × 168 m long pipe

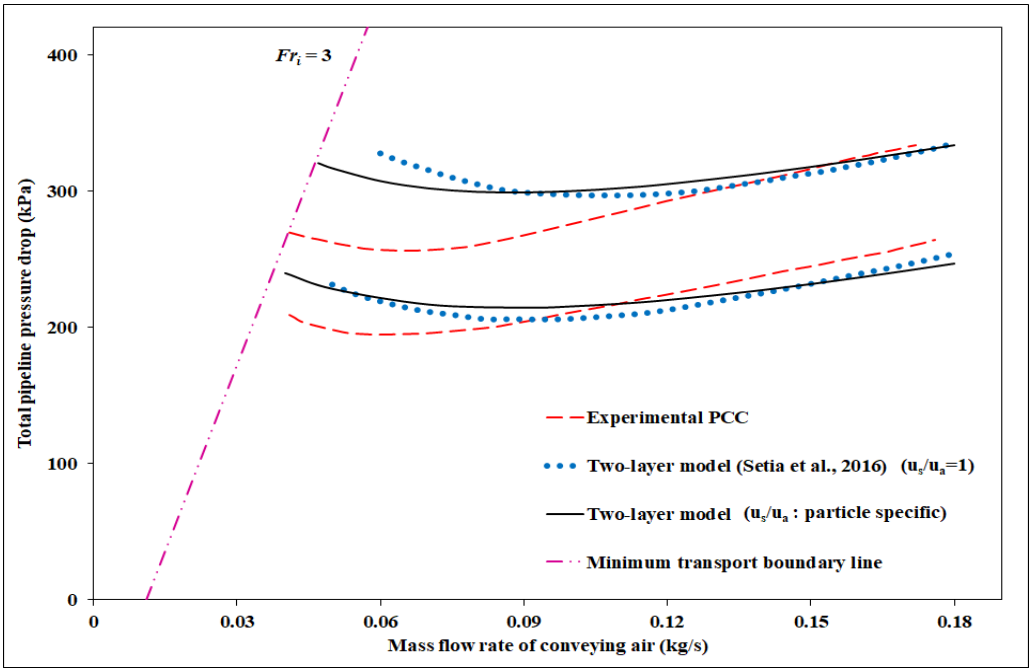

Figure 4.9: Scale-up evaluation for solids friction factor (two-layer specific) for fly ash through 69 mm I.D. × 554 m long pipe

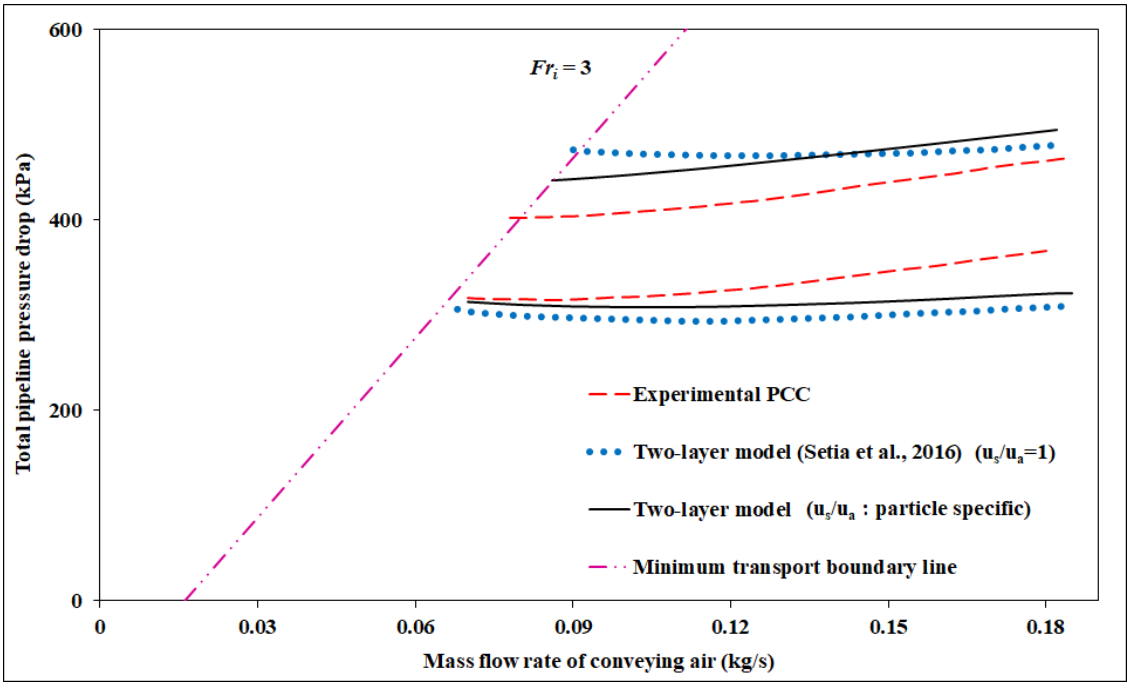

Figure 4.10: Scale-up evaluation for solids friction factor (two-layer specific) for cement through 80/100 mm I.D. × 407 m long pipe

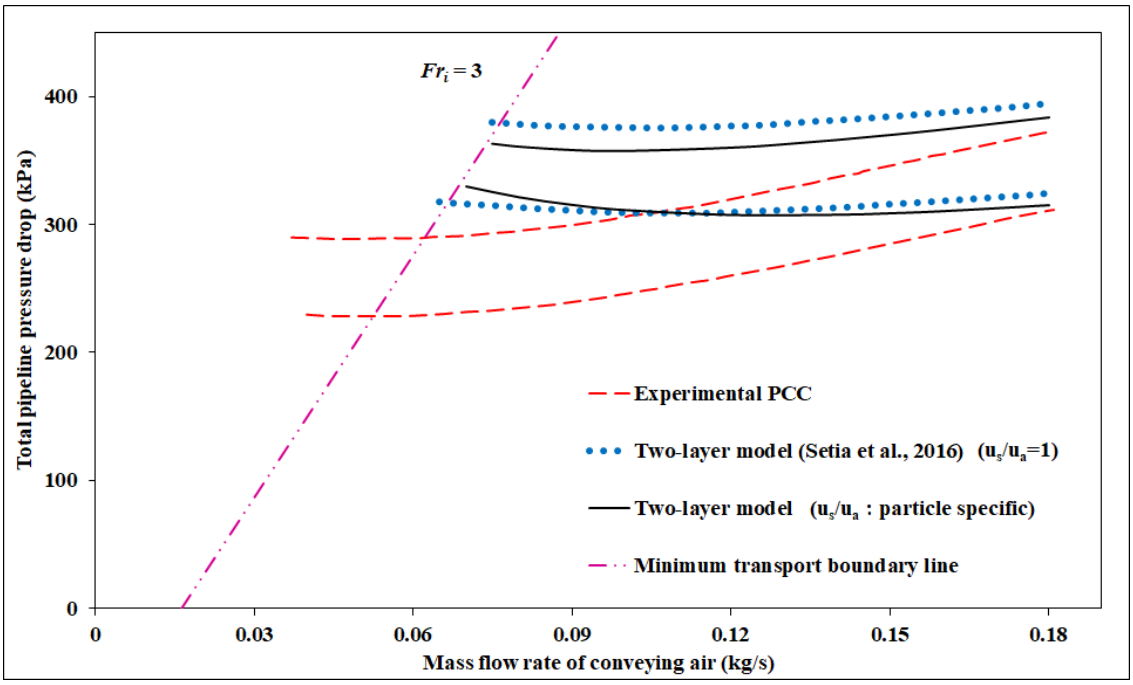

Figure 4.11: Scale-up evaluation for solids friction factor (two-layer specific) for fly ash through 80/100 mm I.D. × 407 m long pipe

Figure 4.8 shows the results of pressure drop evaluations for fly ash conveyed through the 105 mm I.D. × 168 m long pipeline corresponding to the different mass flow rate of solids (18 t/h: bottom lines and 28 t/h: top lines). For the 105 mm I.D. × 168 m long pipe, the two-layer model of equation (4.22) ($^{u_s}/_{u_a}$: particle specific) provides better prediction in dense-phase for both mass flow rate of solids as compared to the predictions obtained from existing two-layer Setia et al. (2016) model. Figure 4.9 shows the results of pressure drop evaluations for fly ash conveyed through the pipeline viz. 69 mm I.D. × 554 m long pipeline corresponding to the different mass flow rate of solids (7 t/h: bottom lines and 11 t/h: top lines). For the 69 mm I.D. × 554 m long pipe, the developed two-layer model using equation (4.22) provides better predictions in the very dense-phase region as compared to the Setia et al. (2016) model for higher mass flow rates of solids. However, for a lower mass flow rate of solids, the model (refer equation 4.22) has provided almost similar results from dense-phase to dilute-phase regime with the two-layer Setia et al. (2016) model. Figure 4.10 shows the results of pressure drop evaluations for cement conveyed through 80/100 mm I.D. × 407 m long pipeline corresponding to a different mass flow rate of solids (18 t/h: bottom lines and 36 t/h: top lines). The results show that for the 80/100 mm I.D. × 407 m long pipe, the newly developed model provides better prediction in very dense-phase region in comparison with Setia et al. (2016) model and provides almost similar prediction in the dilute-phase region for the higher mass flow rate of solids (i.e., 36 t/h). However, for a lower mass flow rate of solids (i.e., 18 t/h), the model (equation 4.22) has provided satisfactory results in the very dense-phase region as compare to the Setia et al. (2016) model and provides almost similar results in the dilute phase regime. Figure 4.11 shows the results of pressure drop evaluations for fly ash conveyed through 80/100 mm I.D. × 407 m long pipeline corresponding to a different mass flow rate of solids (20 t/h: bottom lines and 30 t/h: top lines). The results show that for the 80/100 mm I.D. × 554 m long

pipe, the newly developed model provides better predictions from dense- to dilute-phase flow region in comparison with Setia et al. (2016) model for the higher mass flow rate of solids (i.e., 30 t/h). On the other hand, for the lower mass flow rate of solids (i.e., 20 t/h), the newly developed model provides slight over-prediction in the very dense-phase region and provides almost similar predictions in the dilute-phase region. Overall, it can be inferred that the newly developed two-layer model (equation 4.22, using particle specific model for particle velocity) could provide improved PCC (pneumatic conveying characteristics) predictions from dense- to dilute-phase region for all three products used in the present investigation under scale-up conditions, as compared to the predictions obtained by Setia et al. (2016). This clearly shows the importance of using particle and actual gas velocity ratio term in the model of solids friction factor. Hence, the results demonstrate a step improvement in the existing two-layer model.

Further to developing particle velocity models for individual powders, a combined correlation has been developed for particle-to-actual gas velocity ratio, by combining a large database of particle-to-actual air velocity ratio along the pipeline length obtained from the numerical data of the two samples of fly ash and cement. The correlation for the newly developed particle velocity model is presented in equation (4.23). Higher values of the coefficient of determination (R^2) indicates a good fit. In this model, the ratio of particle to actual gas velocity has been represented by solids loading ratio, dimensionless velocity terms, dimensionless diameter terms, and dimensionless density terms.

$$\frac{u_s}{u_a} = 10^{-0.913}(m^*)^{1.129}\left(\frac{w_{fo}}{V}\right)^{-0.693}\left(\frac{d_p}{D}\right)^{0.534}\left(\frac{\rho_a}{\rho_s}\right)^{0.393}, R^2 = 0.88 \quad (4.23)$$

The correlation presented in equation (4.23) has been included in the model of solids friction factor for the fly ash samples, ESP dust, and cement in the following portion of the thesis. To verify the accuracy of the empirical correlation presented above, comparisons between the predicted results based on the above correlation and numerical data of particle-to-actual gas velocity are shown in Figure 4.12. It has been found that the predicted results $\left({}^{u_s}/_{u_a}\right)$ obtained are in the close agreement with the numerical results $\left({}^{u_s}/_{u_a}\right)$ with the high coefficient of determination R^2 = 0.88.

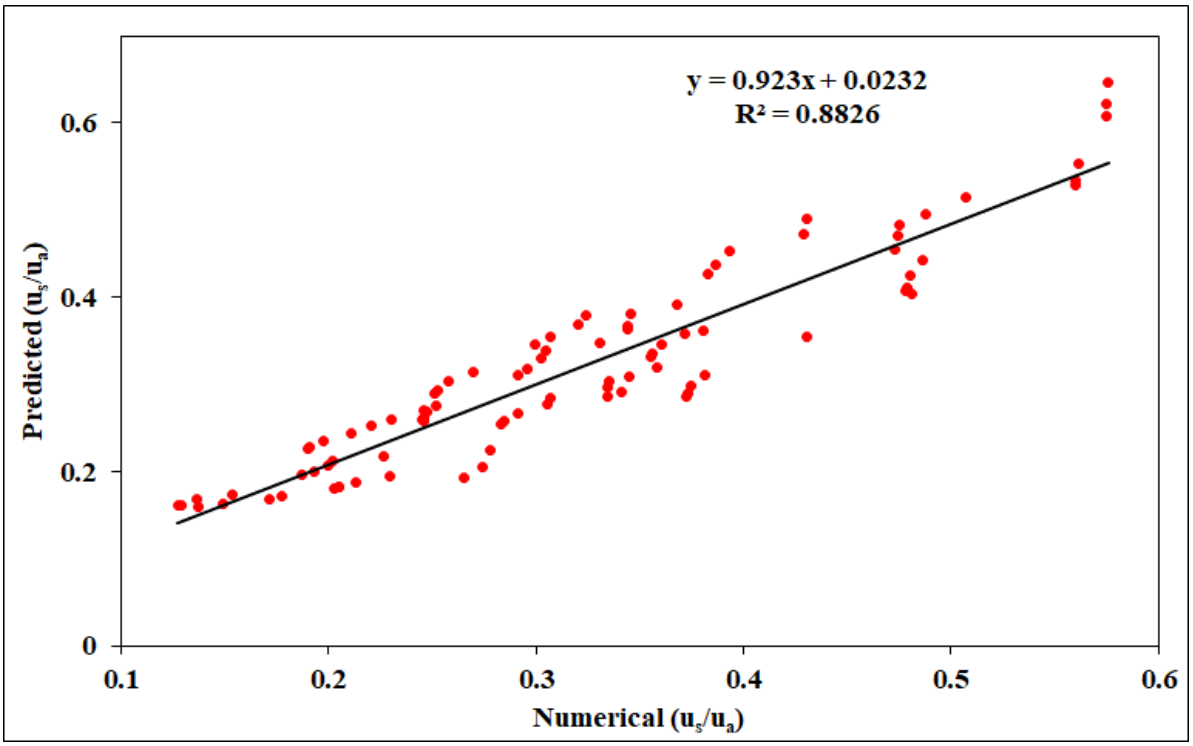

Figure 4.12: Comparison of predicted versus numerical data of particle-to-actual gas velocity for different products with a constant fluidized bulk density

Setia et al. (2016) developed a two-layer model for solids friction factor for the fluidized dense-phase flow of fine powders considering the ratio of particle to air as unity. In the present

investigation, the existing two-layer model (Setia et al., 2016) has been modified with the addition of a newly developed combined particle velocity model. Along with the newly developed model, other existing correlations (available in the literature) have also been employed in Setia et al. (2016) model for solids friction factor for the purpose of scale-up validation for pipeline length and diameter. Table 4.4 lists the two-layer models developed by Setia et al. (2016) for different powders. These are provided here for completeness.

Table 4.4. Two-layer model developed using a "straight pipe" method ("two-layer" format, equation 1.10, Setia et al., 2016)

Product reference	**Models (as per the format provided by equation 1.10)**					**R^2**
	K	**a**	**b**	$\boldsymbol{\lambda_s^*}$	$\boldsymbol{w_{fo}}$ **(m/s)**	
Fly ash (Mallick, 2009)	8.04	−0.22	1.48	0.0043	0.06	0.98
ESP dust (Mallick, 2009)	3018	−0.20	1.72	0.0135	0.005	0.99
Fly ash (Setia et al., 2016)	23.54	−0.61	1.71	0.0074	0.038	0.99
Cement (Setia et al., 2016)	17.31	−0.40	1.54	0.0081	0.036	0.98

Equation (4.22) shows the modified form of the two-layer model (Setia et al., 2016), which has been used for the scale-up validation of solid friction factor in the present investigation. The newly developed two-layer model (in modified form with newly developed particle velocity model and other empirical correlations existing in the literature) for solids friction factor has been validated for longer and larger scale-up pipeline conditions (for fly ash and ESP dust: 105 mm I.D. × 168

m and 69 mm I.D. × 554 m; for cement and fly ash: 80/100 mm I.D. × 407-m-long pipelines) for different solids and airflow rates by comparing the predicted pneumatic conveying characteristics against the experimental plots. The results are provided in Figures 4.13 to 4.18. Predictions obtained from the originally developed two-layer model (Setia et al., 2016) have been superimposed on Figures 4.13 to 4.18 to show any improvement in prediction achieved by using the newly developed particle velocity model in the two-layer model format of solids friction in comparison to the existing correlations cited in the literature. Figure 4.13 shows the results of scale-up evaluations for fly ash conveyed through the pipeline viz. 105 mm I.D. × 168 m long pipeline for the respective mass flow rate of solids, i.e., 28 t/h. The results show that for fly ash (105 mm I.D. × 168 m long pipeline), the modified two-layer format with a newly developed model provides almost similar predictions in the dense-phase region with the other existing correlations and Setia et al. (2016) model. The figure shows some slight under-prediction at the dilute-phase region in comparison with the other existing correlations (by around 10-15 kPa approx.).

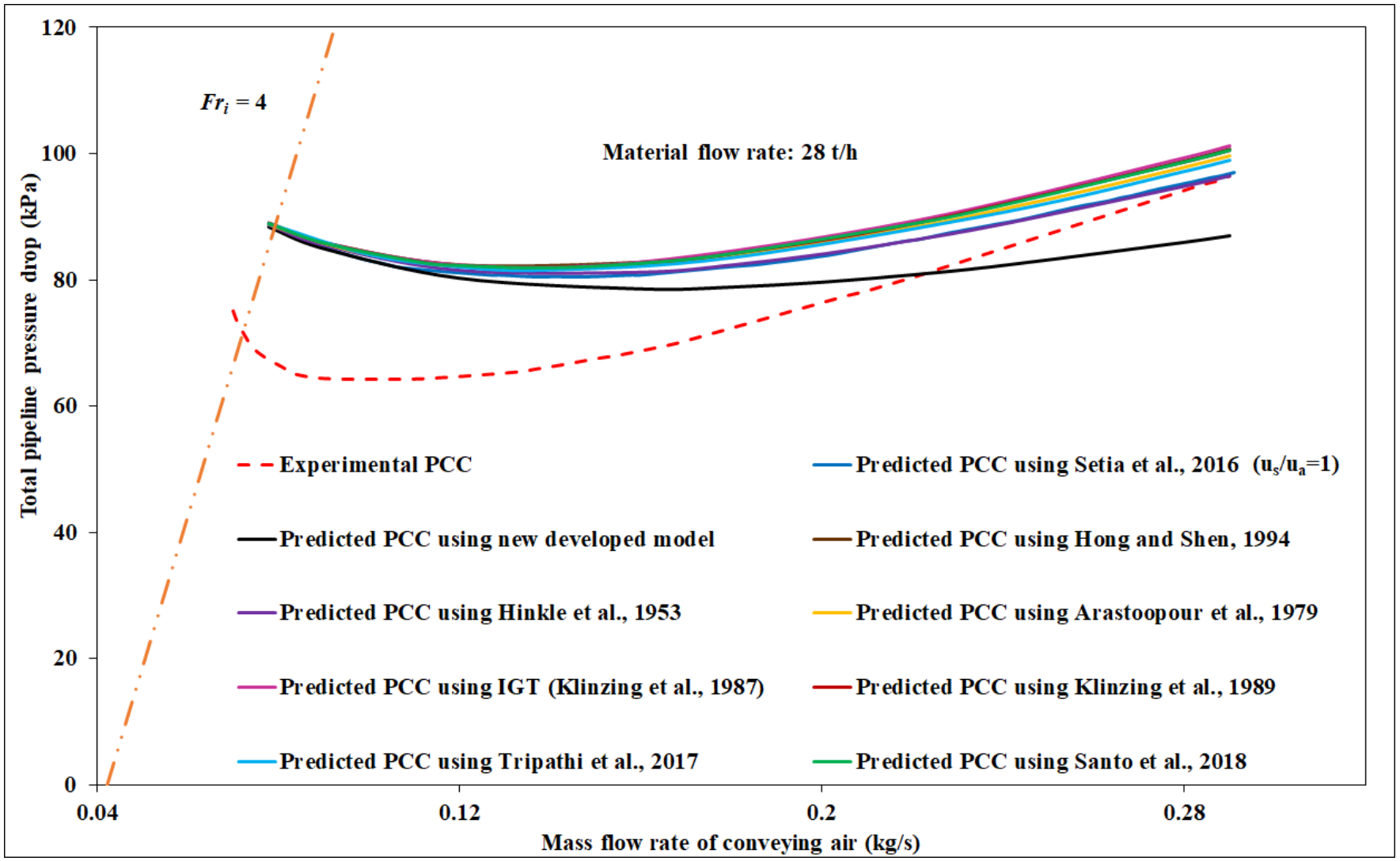

Figure 4.13: Scale-up evaluation for solids friction factor (with particle specific models) for fly ash through 105 mm I.D. × 168 m long pipe

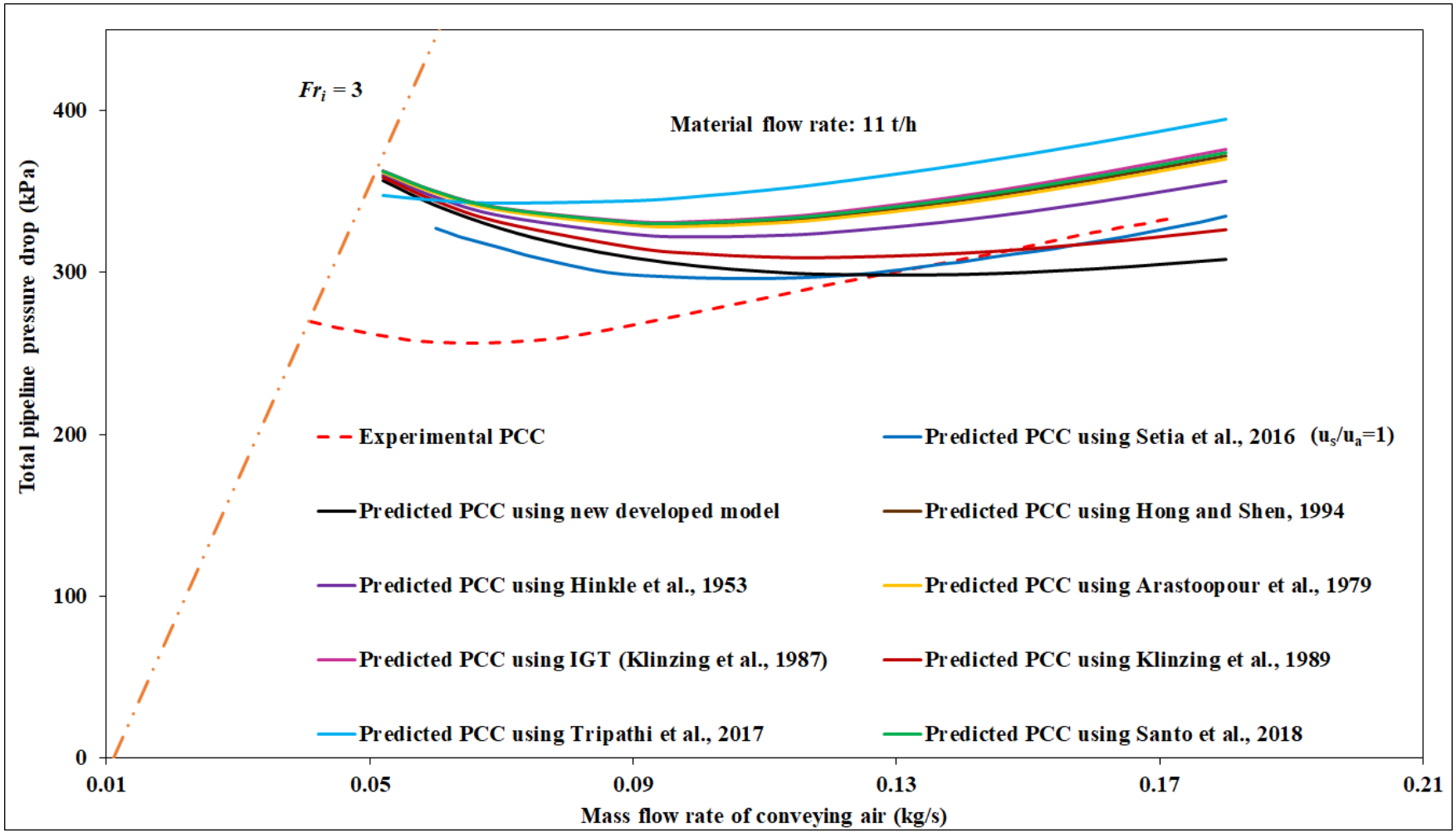

Figure 4.14: Scale-up evaluation for solids friction factor (with particle specific models) for fly ash through 69 mm I.D. × 554 m long pipe

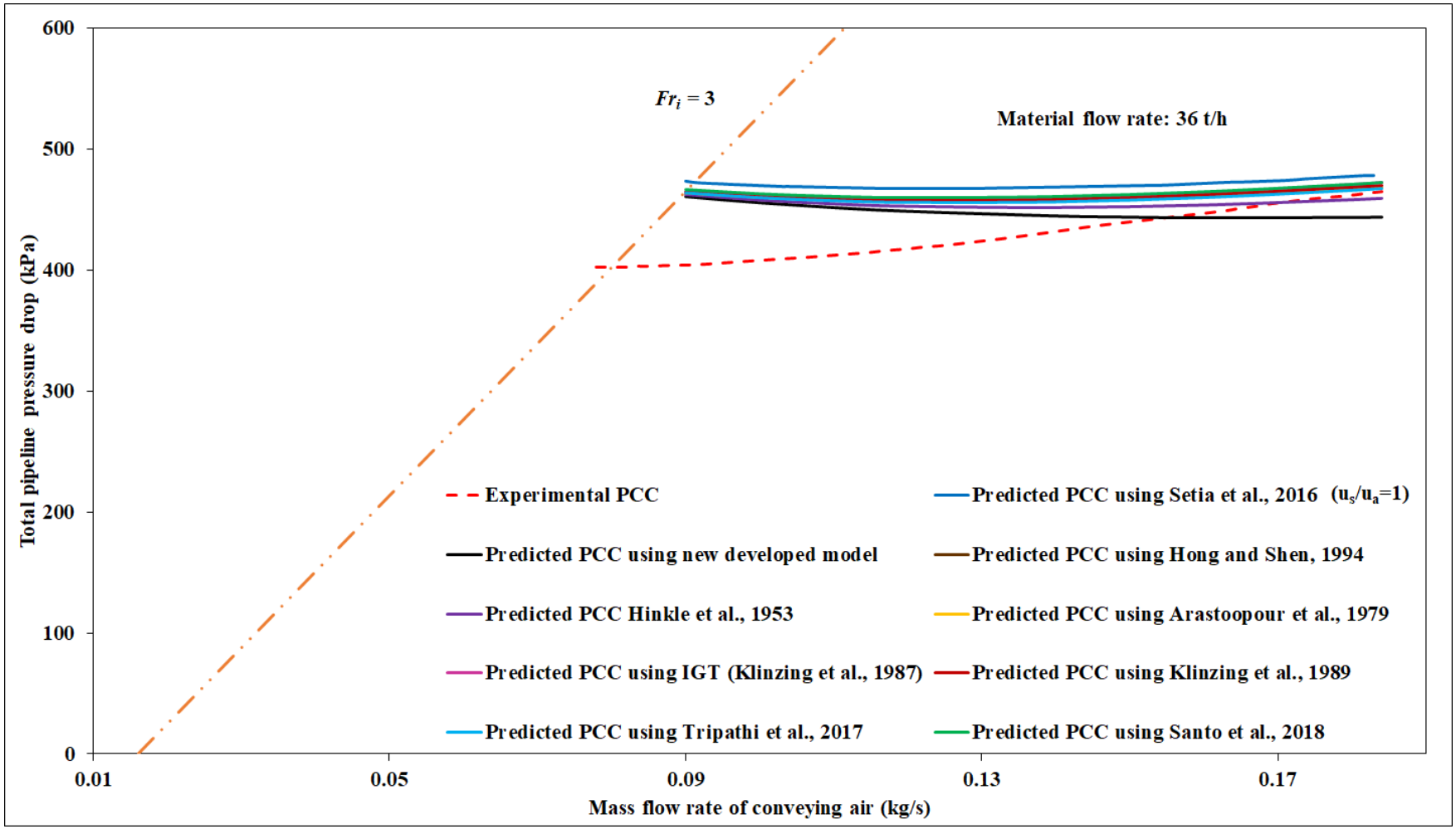

Figure 4.15: Scale-up evaluation for solids friction factor (with particle specific models) for cement through 80/100 mm I.D. × 407 m long pipe

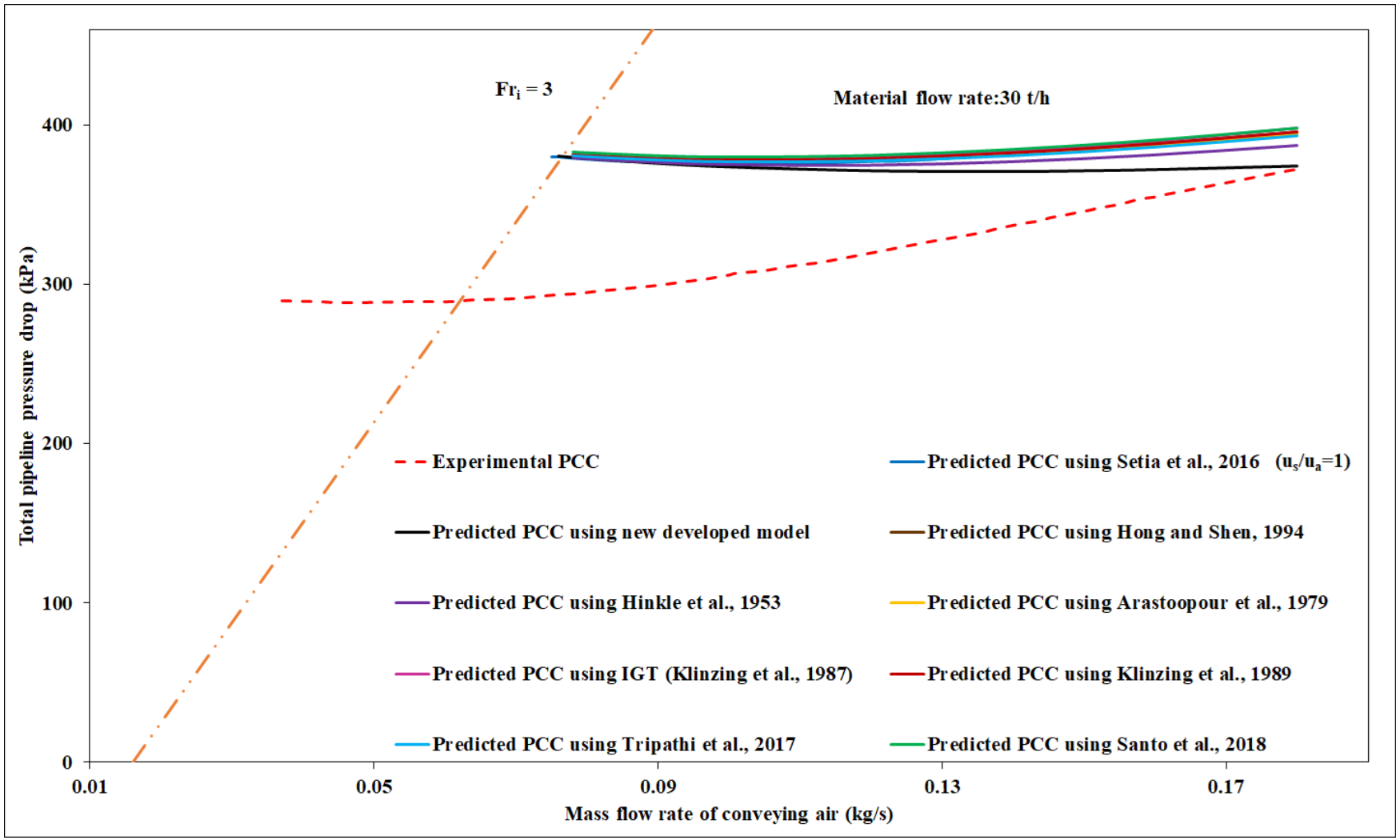

Figure 4.16: Scale-up evaluation for solids friction factor (with particle specific models) for fly ash through 80/100 mm I.D. × 407 m long pipe

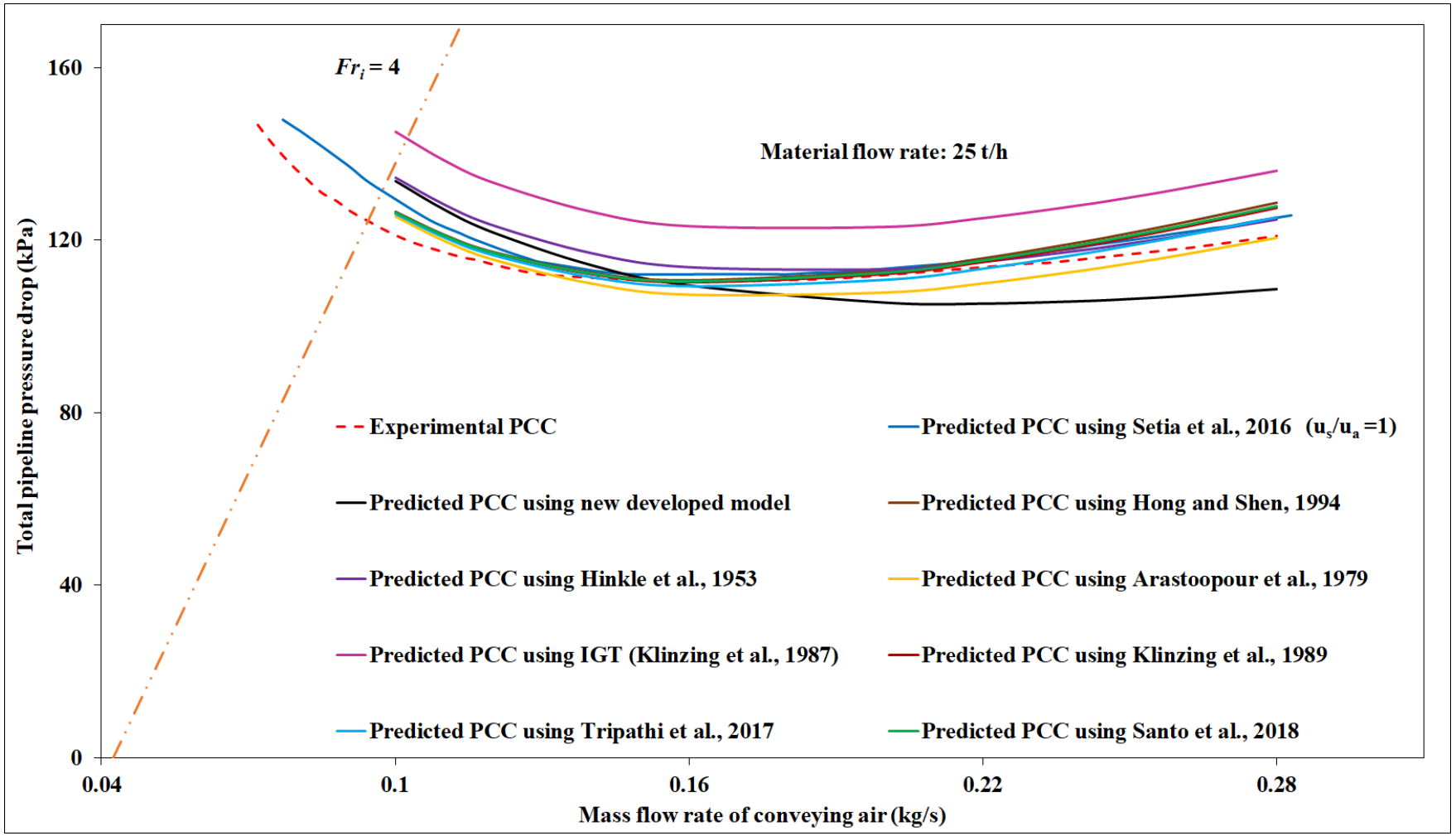

Figure 4.17: Scale-up evaluation for solids friction factor (with particle specific models) for ESP dust through 105 mm I.D. × 168 m long pipe

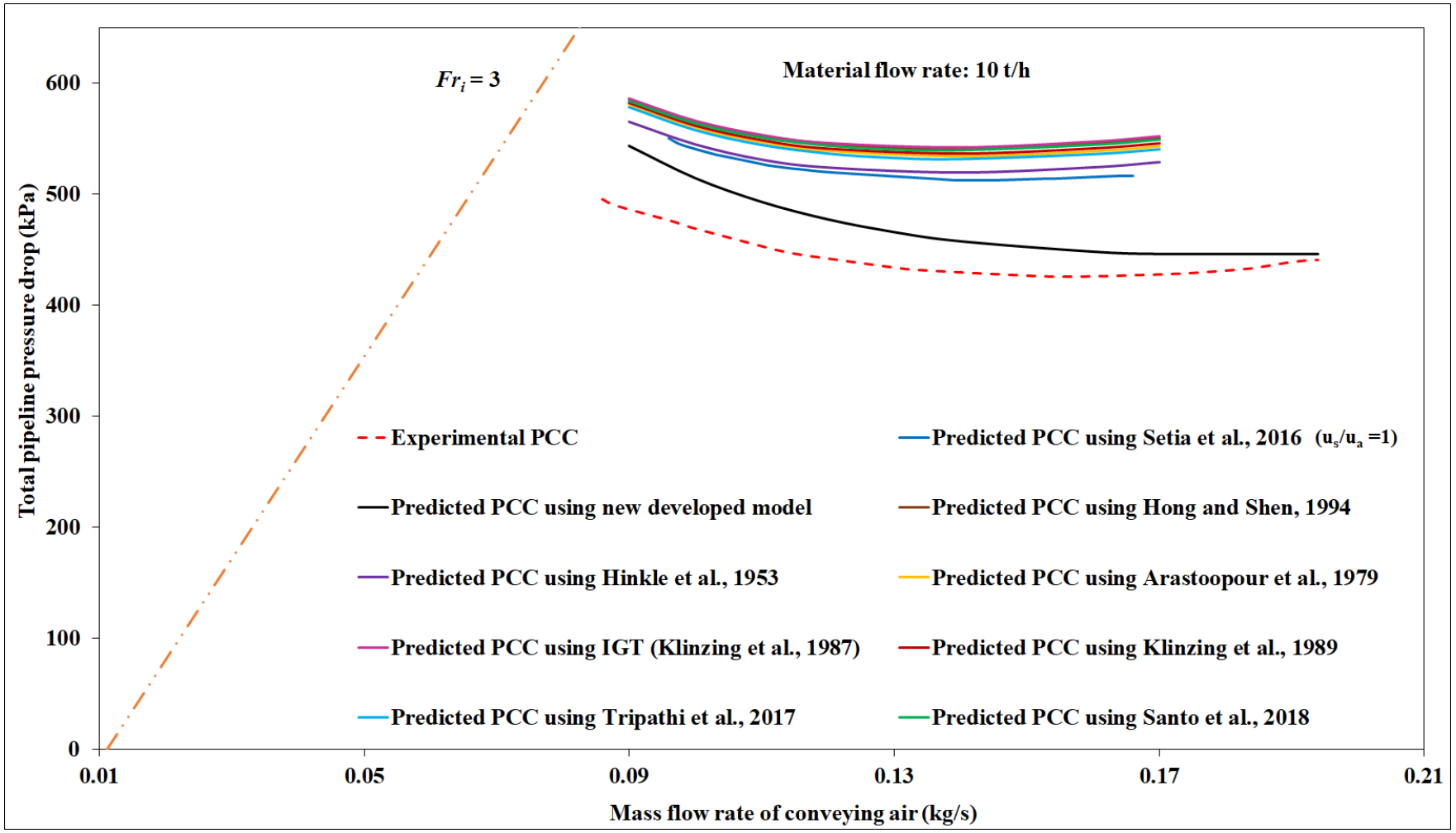

Figure 4.18: Scale-up evaluation for solids friction factor (with particle specific models) for ESP dust through 69 mm I.D. × 554 m long pipe

Figure 4.14 shows the results of scale-up evaluations for fly ash conveyed through the pipeline viz. 69 mm I.D. × 554 m long pipeline for the respective mass flow rate of solids, i.e., 11 t/h. The results show that for fly ash (69 mm I.D. × 554 m long pipeline), the modified two-layer format with newly developed model worked well and provided almost similar predictions in dense-phase region along with the other existing correlations, but provided some slight over-prediction in comparison with Setia et al. (2016) model (i.e., around 15 kPa). On the other hand, all existing correlations showed large over-predictions at dilute-phase region, except Klinzing et al. (1989) and the newly developed model format, which provided some slight under-prediction in the pressure drop predictions (i.e., around 9 to 25 kPa) in comparison to Setia et al. (2016) format in the dilute-phase mode. Figure 4.15 showed the results of scale-up evaluations for cement conveyed through the 80/100 mm I.D. × 554 m long pipeline corresponding to 36 t/h mass flow rate of solids. For the 80/100 mm I.D. × 554 m long pipe, the newly developed model provided almost similar predictions at the dense-phase region along with the existing correlations and better predictions at the dilute-phase region in comparison with the existing correlations, except Hinkle (1953) which provided almost the similar predictions with the newly developed model. On the other hand, the two-layer model format provided over-predictions from dense (i.e., around 8 kPa) to dilute-phase (i.e., around 35 kPa) for the respective mass flow rate of solids. Figure 4.16 shows the results of scale-up evaluations for fly ash conveyed through the pipeline viz. 80/100 mm I.D. × 407 m long pipeline corresponding to 30 t/h mass flow rate of solids. The results show that for fly ash (80/100 mm I.D. × 407 m long pipeline), the newly developed two-layer model provided almost similar predictions at dense-phase and better predictions at the dilute-phase region in comparison to the existing correlations and Setia et al. (2016) model. Whereas on the other hand, the existing two-layer model coincides with the predictions of existing correlations from dense to

dilute-phase. In order to test the accuracy of the newly developed particle velocity model presented in equation (4.23), the scale-up predictions for very fine powder (i.e., for ESP dust) are also investigated. Figure 4.17 shows the results of scale-up evaluations for ESP dust conveyed through 105 mm I.D. × 168 m long pipeline for the respective mass flow rate of solids, i.e., 25 t/h. The results show that for ESP dust (105 mm I.D. × 168 m long pipeline), the new modified two-layer format with particle velocity model included provides slight over-prediction in dense-phase region as compared to Setia et al. (2016) model (by about 4 kPa) and slight over-prediction in comparison with existing correlations (by about 9 kPa). It also shows some slight under-prediction at the dilute-phase region in comparison to the other existing correlations and existing two-layer model format developed by Setia et al. (2016). On the other hand, IGT (Institute of Gas Technology) model (as reported by Klinzing et al., 1987) showed large over predictions from dense to dilute-phase mode. Figure 4.18 shows the results of scale-up evaluations for ESP dust conveyed through 69 mm I.D. × 554 m long pipeline for the respective mass flow rate of solids, i.e., 10 t/h. The results revealed that for ESP dust (69 mm I.D. × 554 m long pipeline), the newly developed model provides improved predictions from dense-phase to very dilute-phase region. The existing correlations and Setia et al. (2016) model provided very large over-predictions from dense-phase to dilute-phase flow regime (in the range of 30 to 70 kPa in dense-phase and 70 to 105 kPa in dilute -phase). It can be concluded that the overall newly developed two-layer model shows satisfactory results from dense to dilute-phase region in comparison with the Setia et al. (2016) model and other correlations existing in the literature.

4.3 Numerical solution for particle velocity for varying fluidized bulk density

In the previous section, it was considered constant value of fluidized bulk density along the length of pipe for numerical modelling of particle velocity; however, in reality, fluidized bulk density may be expected to vary along the length of the pipe (possibly decreasing) because of the expansion of the gas, more mixing of gas by the transport and the intense blending that can happen over the bend. Therefore, the effects of varying fluidized bulk density need to be considered in the model of particle velocity. The following equation (4.24) has been developed, and the results for fluidized bulk density varying along the length of the pipe have been obtained using a MATLAB based program.

$$\frac{d\rho_{fl}}{dx} = -\frac{\rho_{fl}}{u_s}\left[\frac{u_s}{\varepsilon_s\left(\rho_{fl}u_s^2(u_s-u_a)-\frac{u_aP}{(1-\varepsilon_s)}\right)}\left\{-(u_s-u_a)f_s+\frac{u_aP}{\rho_a}\frac{d\rho_a}{dx}\right\}\right] \tag{4.24}$$

A new correlation for particle-to-actual gas velocity ratio has been developed by solving the above equation, with the application of variable fluidized bulk density in the entire pipeline. The developed correlation for cement is presented in equation (4.25) and for fly ash in equation (4.26) obtained using multiple regression technique. Higher values of the coefficient of determination (R^2) indicate a good fit. In these models, the ratio of particle to actual gas velocity has been represented by solids loading ratio and dimensionless velocity terms. The correlations presented in equations (4.25) and (4.26) have been used further to model the solids friction factor for cement and fly ash in the following section.

$$\frac{u_s}{u_a} = 10^{-3.643}(m^*)^{1.032}\left(\frac{W_{fo}}{V}\right)^{-0.612}, R^2 = 0.95 \quad (4.25)$$

$$\frac{u_s}{u_a} = 10^{-3.003}(m^*)^{0.897}\left(\frac{W_{fo}}{V}\right)^{-0.504}, R^2 = 0.95 \quad (4.26)$$

Using steady-state experimental pressure drop data and using the values obtained from equations (4.25) and (4.26) for different experimental conditions, different values of $'\lambda_s'$ have been obtained. Subsequently, a modified two-layer model has been developed with the aid of the newly generated particle velocity model with variable fluidized bulk density (equations 4.25 and 4.26). Table 4.5 shows the K, a, b and λ_s^* values for the newly developed model (in the form of equation 4.22). Equation (4.22) shows the modified form of the two-layer model (Setia et al., 2016), which has been used for the scale-up validation of solid friction factor in the present investigation. The newly developed two-layer model (in modified form with varying fluidized bulk density concept in particle velocity model) for solids friction factor has been validated for longer and larger scale-up pipeline conditions (cement and fly ash: 65 mm I.D. × 254-m-long and 80/100 mm I.D. × 407-m-long pipelines) for different solids and airflow rates by comparing the predicted pneumatic conveying characteristics against the experimental plots. To estimate the relative correctness of the newly developed model, plots between predicted and experimental conveying characteristics have been shown in Figures 4.19 and 4.20. Predictions obtained from the existing two-layer model (Setia et al., 2016) have been superimposed on Figures 4.19 and 4.20 to show the improved results attained with the aid of the newly developed particle velocity model in the two-layer model format of solids friction.

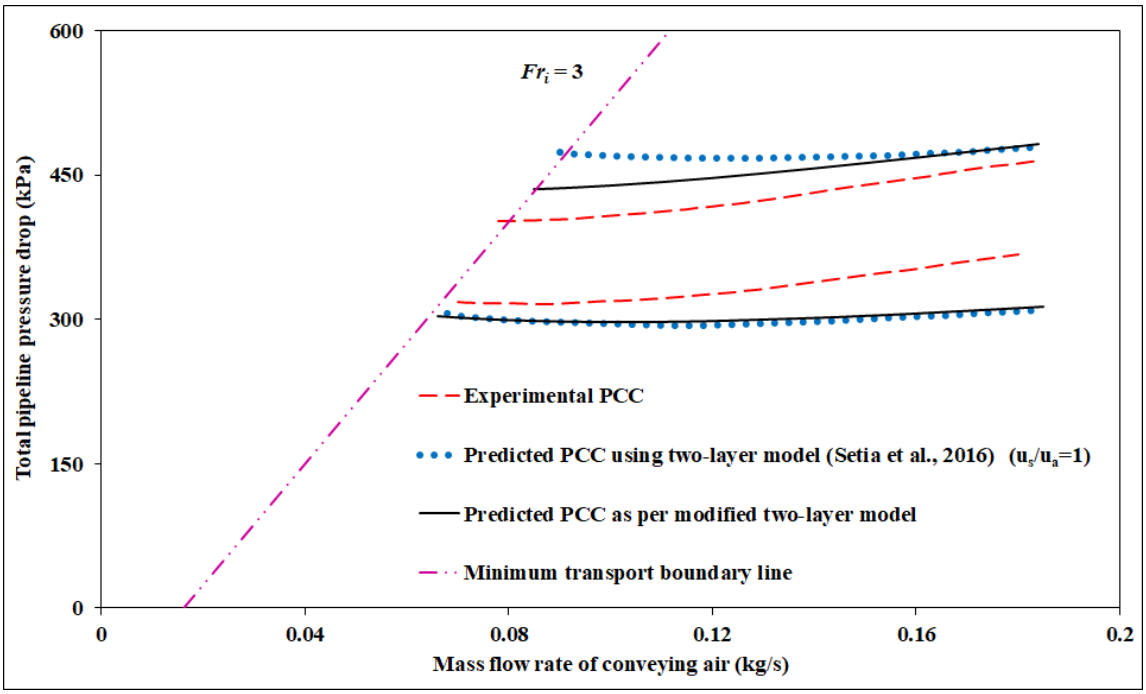

Figure 4.19: Total Pipeline pressure drop depending on a mass flow rate of conveying air for cement through 80/100 mm I.D. × 407 m long pipe

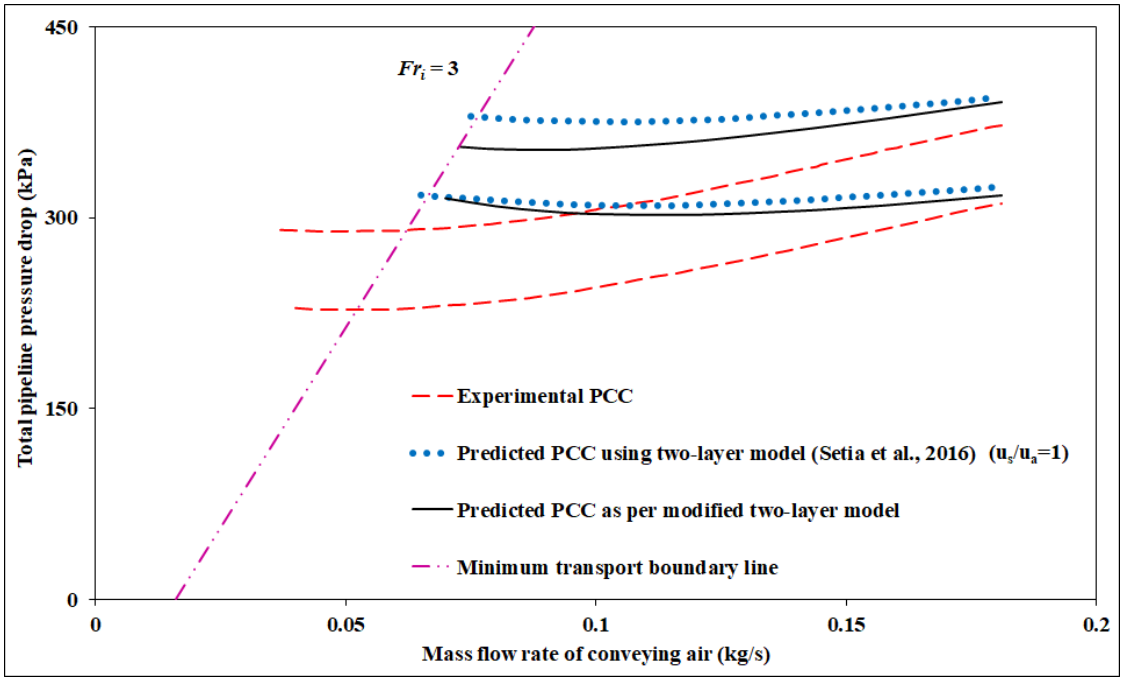

Figure 4.20: Total Pipeline pressure drop depending on a mass flow rate of conveying air for fly ash through 80/100 mm I.D. × 407 m long pipe

Table 4.5. New model developed using a "straight pipe" method (in the form of equation 4.22)

Product	**Pipeline data used for modelling**	**Models (as per the format provided by equation 4.22)**					**R^2**	**Particle velocity model type**
		K	**a**	**b**	**λ_s^***	**w_{fo} (m/s)**		
Cement (Setia et al., 2016)	65 mm I.D. × 254 m	23	−0.55	1.68	0.0402	0.036	0.95	Newly developed model format (equation 4.25)
Fly ash (Setia et al., 2016)	65 mm I.D. × 254 m	74	−0.85	2.07	0.0298	0.038	0.95	Newly developed model format (equation 4.26)

Figure 4.19 shows the results of pressure drop evaluations for cement conveyed through 80/100 mm I.D. × 407 m long pipeline corresponding to a different mass flow rate of solids (18 t/h: bottom lines and 36 t/h: top lines). The results show that for the 80/100 mm I.D. × 407 m long pipe, the newly developed model with variable fluidized bulk density provides better prediction in very dense-phase region in comparison with Setia et al. (2016) two-layer model and provides almost similar prediction in the dilute-phase region for the higher mass flow rate of solids (i.e., 36 t/h). However, for a lower mass flow rate of solids (i.e., 18 t/h), the model (refer equation 4.22) has provided almost similar results from dense- to dilute phase regime with the two-layer (Setia et al., 2016) model. Figure 4.20 shows the results of pressure drop evaluations for fly ash conveyed through 80/100 mm I.D. × 407 m long pipeline corresponding to a different mass flow rate of solids (20 t/h: bottom lines and 30 t/h: top lines). The results show that, for the 80/100 mm I.D. × 554 m long pipe, the newly developed model with variable fluidized bulk density provides better prediction in very dense-phase region in comparison to Setia et al. (2016) two-layer model and provides almost similar prediction in the dilute-phase region for higher mass flow rate of solids (i.e., 30 t/h). On the other hand, for the lower mass flow rate of solids (i.e., 20 t/h), the newly developed model with variable fluidized bulk density provides almost similar predictions from dense- to the dilute-phase regime. Therefore, a newly developed two-layer model based on the concept of variable fluidized bulk density holds good from dense to dilute-phase region in comparison with the Setia et al. (2016) two-layer model.

In the present section, the author attempted to develop a combined correlation for particle-to-actual gas velocity ratio based on the application of variable fluidized bulk density in the entire pipeline using the compilation of numerical data (particle to actual air velocity ratio) which have been

obtained from the products namely, two samples of fly ash and cement. The correlation for newly developed particle velocity model is presented in the equation (4.27) as follows,

$$\frac{u_s}{u_a} = 10^{-1.46}(m^*)^{1.057}\left(\frac{w_{fo}}{V}\right)^{-0.634}\left(\frac{d_p}{D}\right)^{0.415}\left(\frac{\rho_a}{\rho_s}\right)^{0.26}, R^2 = 0.90 \quad (4.27)$$

In this model, the same format has been used as described by equation (4.23). The use of correlation presented in equation (4.27) has been extended further in order to model the solids friction factor for fly ash and cement in the following section (results will be shown in Chapter 5).

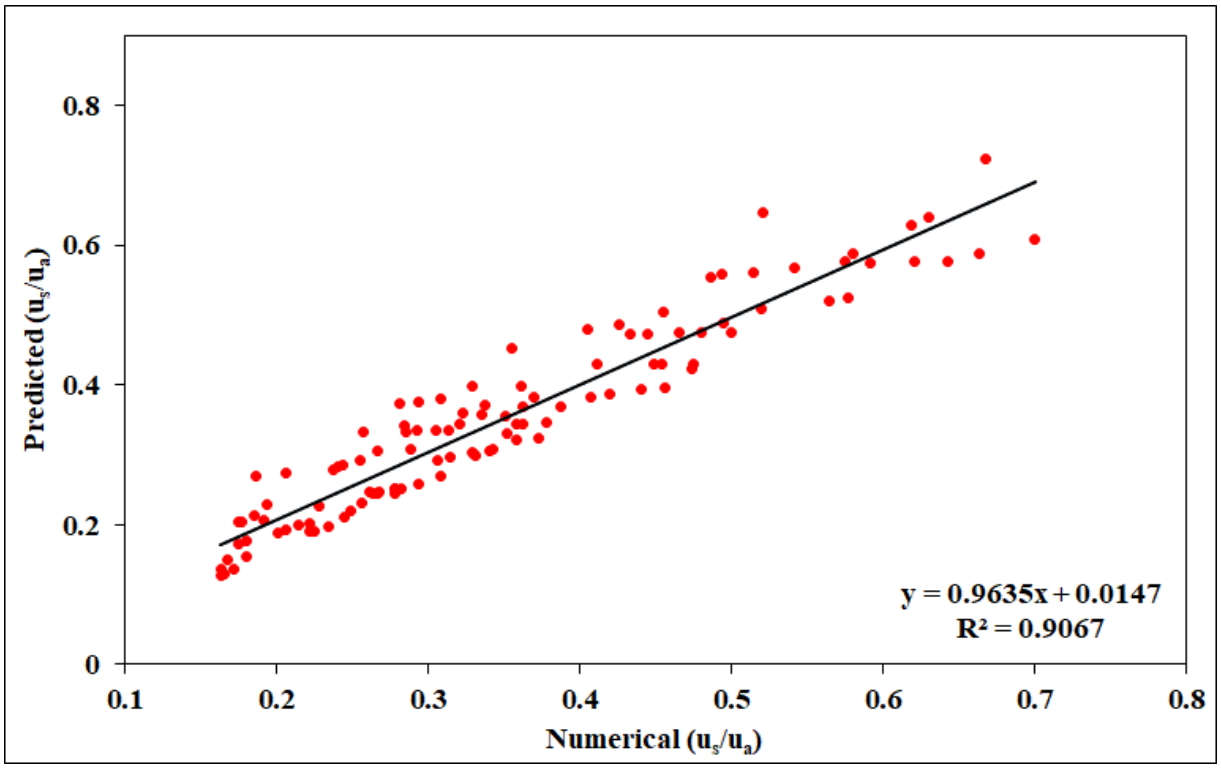

Figure 4.21: Consolidated comparison of predicted and numerical data of particle-to-actual gas velocity for fly ash and cement conveyed data

In order to validate the accuracy of the newly developed empirical correlation presented in equation (4.27), a comparison between the predicted results based on the above correlation and numerical data of particle-to-actual gas velocity have been shown in Figure 4.21. From Figure 4.21, it has been found that, the predicted results $\left({}^{u_s}/_{u_a}\right)$ obtained are in the close agreement with the numerical results $\left({}^{u_s}/_{u_a}\right)$ with the highest coefficient of determination $R^2 = 0.90$.

CHAPTER 5

NEW MODEL DEVELOPMENT FOR SOLIDS FRICTION CONSIDERING PARTICLE-PARTICLE COLLISION EFFECT

This chapter deals with the development of new model for solids friction factor with the aid of (1) apparent rheology of fluidized bed of powders in dense-phase (2) energy loss due to the particle-particle-wall impact and particle bouncing occurring along the internal surface of pipes, (3) newly developed improved unified numerical particle velocity model with variable fluidized bulk density.

5.1 Modelling energy loss due to the collision between particles during dense-phase conveying

Louge et al. (1991) studied the role of particle collisions in pneumatic transport for dilute gas-solids flow in a vertical pipe of 30.5 mm diameter under fully developed steady-state flow. Polystyrene spheres were transported in dilute-phase, with average particle size ranging from 200 μm to 3 mm, particle density of 1020 kg/m^3, mass flow ratio of 3.6. It was concluded that the particle collisions play a significant role in flows involving relatively huge particles, even when the particle phase is in the dilute-phase region. Tanaka and Tsuji (1991) studied the effect of inter-particle collisions for fully developed gas-solid flow in a vertical pipe with the aid of numerical simulation method known as Lagrangian approach. The average particle diameter ranged from 0.406 to 1.50 mm, and the pipe internal diameter was taken as 40 mm. The effect of solid loading ratio on particle concentration was investigated, and it was found that there was a conclusive effect on the particle concentration even at a small loading ratio. Oesterle and Petitjean (1993) examined the interactions between particle to particle in gas-solids flows using Lagrangian simulation method for the dense-phase region. A horizontal straight pipe gas-solids flow (internal diameter: 30 mm) was investigated at loading ratios up to 20 for glass beads with an average diameter of 0.1

mm. It was concluded that the particle collisions play an important role in the entire pipeline, with loading ratio exceeding unity. Huber and Sommerfeld (1998) studied the effects of turbulence, particle-wall collisions including wall roughness, and inter-particle collisions on the development of the two-phase flow in various pipe elements with the aid of using 3-dimensional (3-D) numerical simulation method known as Euler/Lagrangian approach. In the present investigation, the modelling and numerical calculations were done for dilute-phase pneumatic conveying systems. The results obtained from the numerical calculations were presented for various pipe elements, such as horizontal pipes (material: glass and stainless steel), pipe bends $\left({}^{R}/_{D} = 2.54\right)$ and vertical pipes (material: stainless steel) for different pipe diameters (internal diameter.: 80 mm and 150 mm), pipe lengths (4 m and 8 m) and flow conditions, such as conveying velocity (24 and 27 m/s) and particle loading (0.3 and 0.7 kg particles/kg air). Glass beads (shape: spherical) of average particle size: 40 μm were used for the investigation. The numerical results obtained are found to be in close agreement with the experimental results. Sommerfeld (2003) analyzed the collision effects for turbulent gas-solids flow in a horizontal pipe channel (length of 6 m approx.) with the aid of a 2-dimensional numerical simulation technique known as Lagrangian approach. The investigation includes the impact of wall roughness and inter-particle collisions for the particle motion. Mono-sized particles with size ranging from 30 to 700 μm were taken into consideration. It was concluded that the inter-particle collisions and particle collision with the wall, both have a great impact on the particle behaviour in a horizontal pipe channel and on the particle phase characteristics of the developed flow. Bose and Kumaran (2004) studied the velocity distribution for a two-dimensional sheared granular material considering the particle-particle, particle-wall collisions. Bose et al. (2005) studied a two dimensional bi-disperse vibrofluidized granular mixture subject to vertical vibration in the rapid flow regime, where particle interactions occur due to

instantaneous collisions. Schneiderbauer et al. (2012) derive the new boundary conditions for the solid's stresses and the flux of fluctuation energy for collisional granular flows at flat frictional moving walls in non-steady state. Kuang et al. (2012) studied energy dissipation resulting from the interactions between particles, particles, and wall, particles, and fluid and between fluid to fluid. The average diameters of particles were ranging from 3 to 5 mm and a density of 880 kg/m$^{3.}$ The results revealed that the energy loss during steady-state pneumatic conveying consists of particle-fluid energy dissipation, gravitational potential energy (for inclined pneumatic conveying), particle-wall friction energy dissipation and fluid-wall viscous energy dissipation. The energy equations presented in the research (Chapter 4; refer equation (4.10)) addresses the energy dissipation due to the turbulence and frictional resistance of fluid-wall interactions, particle to air, particle to particle and particle to wall interactions. Desu and Annabattula (2019) investigated the force distribution (i.e., contact type) among dissimilar particle sizes in a polydisperse granular assemblies using the discrete element method (DEM) technique. It was found that the larger particles have a higher chance of experiencing stronger contact forces in comparison to the smaller particles.

In this section, the existing Setia et al. (2016) two-layer model has been modified with the inclusion of newly developed combined particle velocity model (represented by equation 4.27) with variable fluidized bulk density concept and kinetic theory of gases showing the energy loss occurs due to the inter-particle collisions, collisions with the wall and velocity fluctuations due to the turbulence in the pipe. The various assumptions that have been made while developing the concept of energy loss during conveying due to the collisions between the particles and with the wall are given below:

- The rapidly moving particles constantly collide among themselves and with the walls of the entire pipeline. All the collisions between the particles are perfectly elastic. This means the particles are considered to be perfectly spherical in shape and elastic in nature.
- The average distance separating the gas particles is large as compared to their dimensions. All the particles have the same mass.
- The number of particles is so large that statistical treatment can be applied.
- The particles are in the state of random motion moving in all directions with velocity $'C_x'$, $'C_y'$, $'C_z'$ and the gas are said to be in the state of molecular disorder.
- There are no intermolecular forces of attraction or repulsion that exist. This means that the energy of a gas is all kinetic.
- Except during collisions, the interactions among the particles are negligible.
- The time spent in a collision is negligible compared to the time during which the particles are moving independently.
- Between collisions, the particles move in a straight line with uniform velocity because of frictionless motion between particles.
- The volume of a particle is so small that it is negligible compared to the total volume of the gas.

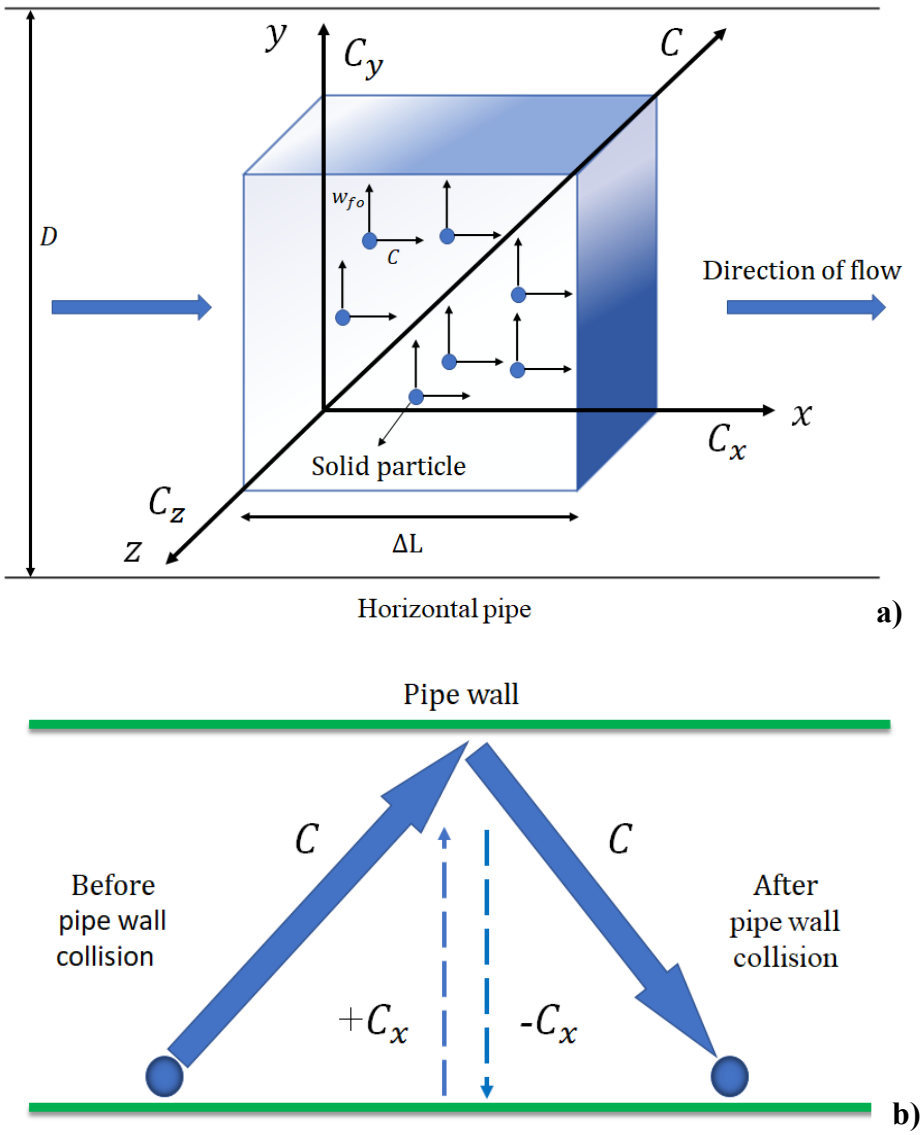

Figure 5.1: (a) Control volume showing single particle movement; (b) bouncing effect of a single particle to the pipe wall

Figure 5.1 shows the control volume (a) single-particle movement; (b) bouncing effect of a single particle to the pipe wall.

Let 'x' be the direction perpendicular to the pipe wall. When a particle bounces off the wall (i.e., in y-z plane), then the projection of velocity of a particle on the 'x' axis is given by:

$$C_{x(after)} = -C_{x(before)} \tag{5.1}$$

(y-z plane with velocity v_x) = (Rebound velocity)

The x-component of velocity is $'C_x'$ and momentum is $'mC_x'$ towards the wall. When a particle hits the wall, it will bounce back with the same speed but in the opposite direction (kinetic energy is conserved, and the collision is being elastic). The x-component of the momentum of the particle changes and will then be -mC_x. Then the change in momentum delivered by the particle to the wall in the 'x' direction is given by:

$$\Delta P_m = 2m_P C_x \tag{5.2}$$

Equation (5.2) presents the total momentum delivered by the particle to the wall.

Let V_T= total volume of gas

N = total number of particles in a control volume having velocities ranging from 0 to ∞

Let dN (C_x): number of particles having velocity greater than (C_x) but $\ll C_x + dC_x$, i.e., colliding on the wall per second. Mathematically can be written as follows:

$$(C_x + dC_x) > C > C_x$$

Consider the particles in the x-component, whose velocity lies in a small interval $[C_x, C_x + dC_x]$, where $dC_x \ll C_x$. Then the contribution of these particles to pressure is:

$$dP\,(C_x) = \Delta P_m\, d\varphi\,(C_x) = 2m_P C_x\, d\varphi\,(C_x) \tag{5.3}$$

where $d\varphi(C_x)$ is the differential particle flux, i.e., the number of particles with velocities in the interval $[C_x, C_x + dC_x]$ hitting the wall per unit time per unit area. Mathematically can be written as follows:

$$d\varphi(C_x) = \frac{dN(C_x)}{At} \tag{5.4}$$

where $dN(C_x)$ is the number of particles with velocity in the interval $[C_x, C_x + dC_x]$ that hits the area 'A' of pipe wall over time t. Hence, mathematically $dN(C_x)$ can be written as follows:

$dN(C_x) =$ [volume, where a particle with velocity (C_x) hitting the wall during time t $\times$ number density of particles in the gas $\times$ fraction of particles whose velocities are in the interval $\{C_x, C_x + dC_x\}$]. Mathematically this can be written as follows:

$$dN(C_x) = A(C_x)t.\,n.\,f(C_x)\, dC_x \tag{5.5}$$

Therefore, we have obtained the following expression as follows:

$$d\varphi(C_x) = n(C_x)\, f(C_x)\, dC_x \tag{5.6}$$

According to the probability theory, normalization of the pdf is given by

$$\int_{-\infty}^{+\infty} f(C_x)\, dC_x = 1 \tag{5.7}$$

Equation (5.7) shows that the probability for a particle to have some velocity lies between -∞ and +∞ is 1. Using equations (5.3) and (5.6), we have,

$$dP\,(C_x) = 2m_P(C_x).\, n(C_x)\, f(C_x)\, dC_x$$

$$dP\,(C_x) = 2m_P n(C_x)^2 f(C_x)\, dC_x \tag{5.8}$$

The total pressure is obtained by integrating overall particles at $C_x > 0$, can be written as follows:

$$P_T = 2m_P n \int_0^{\infty} (C_x)^2 f(C_x)\, dC_x$$

$$P_T = m_P n(C_x)^2 \int_{-\infty}^{+\infty} f(C_x)\, dC_x$$

$$P_T = m_P n(C_x)^2 \tag{5.9}$$

Let us assume all directions are statistically the same (i.e., the system is isotropic). Therefore, the distribution of velocities is isotropic, and the pressure is also isotropic. Then,

$C^2{}_x = C^2{}_y = C^2{}_z$ and $C^2 = C^2{}_x + C^2{}_y + C^2{}_z$

Therefore,

$$C^2{}_x = \frac{C^2}{3}$$

Equation (5.9) can be rewritten as follows:

$P_T = m_P n C^2/3$, where, $n = {N}/{V_{sp}}$

Hence, $P_T V_{sp} = m_P N C^2/3$ (5.10)

The equation (5.10) presented the fundamental equation of the kinetic theory of gases and is often known as the kinetic equation of gases. The term '$P_T V_{sp}$' has a unit of Joule; therefore, it is equivalent to the energy loss due to particle impact against other particles. Energy loss (K.E.) due to particle impact against other particles and further re-acceleration of the decelerated/stopped particle to its original velocity can be represented as follows:

$E_L = m_P N C^2/3$ Since, $m_P N = \Delta M_p$

Then, $E_L = \Delta M_p C^2/3$, here ΔM_p = Total mass of particles in a control volume (kg)

Therefore, kinetic energy loss per unit specific volume = $\left(\Delta M_p C^2/3\right) \Big/ \left(\Delta M_p/\rho^*\right)$

where, $\rho^* = \rho_p(1-\varepsilon)$

Kinetic energy loss per unit specific volume = $C^2\rho^*/3 = C(C.\rho^*/3)$ (5.11)

From Figure 5.1, a single particle motion time (t) is calculated as:

$$t = \frac{\Delta L}{C} = \frac{D}{w_{fo}} \text{ and } C = \frac{\Delta L w_{fo}}{D}$$

Therefore, from equation (5.11), the kinetic energy loss per unit specific volume is:

$$\left(\frac{\Delta L w_{fo}}{D}\right)\left(\frac{C.\rho^*}{3}\right) \tag{5.12}$$

Pressure drop due to the presence of the solids is given by (Klinzing et al., 2010)

$$(\lambda_s m^*)\left(\frac{\rho_a \Delta L V^2}{2D}\right) = (\lambda_S)^* \frac{\rho^* C^2 \Delta L}{2D} + \left(\rho^* g \Delta L \frac{w_{fo}}{V}\right) \tag{5.13}$$

From equation (5.12) adding the kinetic energy loss per unit specific volume in the above expression (5.13), we get,

$$(\lambda_s m^*)\left(\frac{\rho_a \Delta L V^2}{2D}\right) = (\lambda_S)^* \frac{\rho^* C^2 \Delta L}{2D} + \left(\rho^* g \Delta L \frac{w_{fo}}{V}\right) + \left(\frac{\Delta L w_{fo}}{D}\right)\left(\frac{C.\rho^*}{3}\right) \tag{5.14}$$

As

$$m^* = \frac{m_s}{m_a} = \frac{\rho^* C}{\rho_a V} \qquad \text{(Klinzing et al., 2010)}$$

Substituting in equation (5.14) we get

$$\left(\lambda_s.\frac{\rho^* C}{\rho_a V}\right)\left(\frac{\rho_a \Delta L V^2}{2D}\right) = (\lambda_S)^* \frac{\rho^* C^2 \Delta L}{2D} + \left(\rho^* g \Delta L \frac{w_{fo}}{V}\right) + \left(\frac{\Delta L w_{fo}}{D}\right)\left(\frac{C.\rho^*}{3}\right) \quad (5.15)$$

$$(\lambda_s)\left(\frac{CV}{2D}\right) = (\lambda_S)^* \frac{C^2}{2D} + g\frac{w_{fo}}{V} + \left(\frac{C w_{fo}}{3D}\right)$$

$$\lambda_s = (\lambda_S)^* \frac{C^2}{2D}.\left(\frac{2D}{CV}\right) + g\frac{w_{fo}}{V}.\left(\frac{2D}{CV}\right) + \left(\frac{C w_{fo}}{3D}\right).\left(\frac{2D}{CV}\right)$$

$$\lambda_s = \lambda_S{}^* \left(\frac{C}{V}\right) + \frac{2\left({}^{w_{fo}}/_{V}\right)}{Fr^2\left({}^{C}/_{V}\right)} + \left(\frac{2\left(\frac{w_{fo}}{V}\right)}{3}\right)$$

$$\lambda_s = \lambda_S{}^* \left(\frac{C}{V}\right) + \frac{2\beta_o}{Fr^2\left({}^{C}/_{V}\right)} + \left(\frac{2\beta_o}{3}\right) \quad (5.16)$$

In the present investigation, the term $\left({}^{C}/_{V}\right)$ in equation (5.16) has been replaced by the term $\left({}^{u_s}/_{u_a}\right)$; therefore, the modified equation (5.17) can be written in the final form as:

$$\lambda_s = \lambda_S{}^* \left(\frac{u_s}{u_a}\right) + \frac{2\beta_o}{Fr^2\left(\frac{u_s}{u_a}\right)} + \frac{2\beta_o}{3} \quad (5.17)$$

where, λ_S^* is related to the impact and friction of the solid particles (particle to particle/wall). The term $'2\beta_O/\mathrm{Fr}^2\left(\frac{u_s}{u_a}\right)'$ takes into account the influence of weight (i.e., energy loss due to keeping the particles in suspension). β_O refers to the velocity ratio related to particle fall velocity in the undisturbed fluid. An increase in the mass flow rate of solids would cause an increase in the particle/particle/wall interactions, which would cause higher energy losses. The higher energy loss due to keeping the particles in suspension mode has been incorporated by the term $'2\beta_O/\mathrm{Fr}^2\left(\frac{u_s}{u_a}\right)'$ in which the gravity force of the particles is to be overcome by providing sufficient inertia force to keep particles in suspension, with the presence of dimensionless number known as Froude number. However, it is difficult to rationalize the application of the Froude number term to model particle-particle/wall interactions for a non-suspension layer (Mallick, 2009). Turbulent flow condition is prevalent in the suspension flow regime, which would be the main cause for the energy loss of gas, as more of the energy would spend in keeping the particles in turbulent condition. The term $'2\beta_O/3'$ attempts to indicate dense- to dilute-phase transition phenomenon. Larger sized and/or higher particle density products will have increased free settling velocity, and higher velocity will be required to keep them in suspension, which indicates the need for higher energy input. To state, in other words, commonly, the dense-phase regime of flow is attributed to more product turbulence, and the dilute-phase regime is said to be associated with dominant fluid turbulence (Mallick, 2009). However, Mittal (2016) has shown that the pressure fluctuations are more dominating at a higher flow velocity regime, whereas the fluctuations seemed to get suppressed in the low-velocity regime. This is because, at the dense-phase or low-velocity regime of flow, the product to product movements could be suppressed due to rather smaller inter-particle gaps (particles not having too much mean free path to move around and collide with other particles).

The two-layer model format of Setia et al. (2016) has been modified by incorporating the newly developed particle velocity model with variable fluidized bulk density (equation 4.27) and energy loss effect due to the turbulence region occurred in the suspension mode (equation 5.17). The modified two-layer model is given as follows:

$$\lambda_s = \tau_1 \left[K(VLR)^a \left(\frac{w_{fo}}{V} \right)^b \right] + \tau_2 \left[\lambda_s^* \left(\frac{u_s}{u_a} \right) + \left({2\beta_o}\Big/{Fr^2 \left(\frac{u_s}{u_a} \right)} \right) + \frac{2\beta_o}{3} \right] \quad (5.18)$$

Table 5.1 shows the exponents values obtained during modelling obtained through regression analysis. The modified two-layer model (incorporated with particle velocity model with variable fluidized bulk density and energy loss due to impact) for solids friction factor has been validated for longer and larger scale-up pipeline conditions (fly ash and ESP dust: 105 mm I.D. × 168 m and 69 mm I.D. × 554 m; cement and fly ash: 80/100 mm I.D. × 407-m-long pipelines) for different solids and airflow rates by comparing the predicted pneumatic conveying characteristics against the experimental plots. Predictions obtained using the two-layer model of Setia et al. (2016) have been superimposed on the plots to highlight the improvement in the prediction capability of the new model (5.18), if any.

Table 5.1. Modified two-layer model developed using a "straight pipe" method (equation 5.18)

Product	**Pipeline data used for modelling**	**Models (as per the format provided by equation 5.18)**					**R^2**
		K	**a**	**b**	λ_s^*	w_{fo} **(m/s)**	
Fly ash (Mallick, 2009)	69 mm I.D. × 168 m	9.5	−0.39	1.67	0.0103	0.06	0.98
ESP dust (Mallick, 2009)	69 mm I.D. × 168 m	1072	−0.23	1.59	0.0150	0.005	0.98
Fly ash (Setia et al., 2016)	65 mm I.D. × 254 m	81	−0.89	2.12	0.0305	0.038	0.96
Cement (Setia et al., 2016)	65 mm I.D. × 254 m	26	−0.57	1.72	0.0314	0.036	0.97

To evaluate the relative accuracy of the newly developed model, plots between predicted pneumatic conveying characteristics and experimental pneumatic conveying characteristics have been shown in Figures 5.2 to 5.7. Figure 5.2 shows the results of scale-up validation for fly ash conveyed through the 105 mm I.D. × 168 m long pipeline corresponding to different mass flow rates of solids (18 t/h: bottom lines and 28 t/h: top lines).

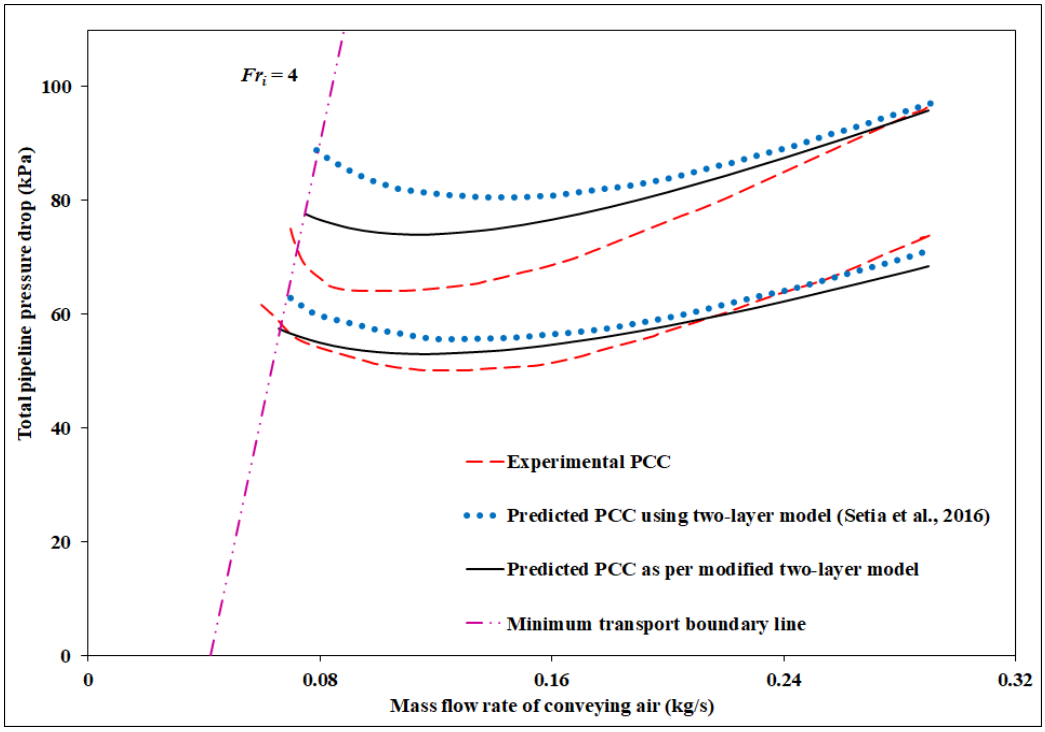

Figure 5.2: Scale-up validation for solids friction factor (modified two-layer model with impact friction, variable fluidized bulk density) for fly ash through 105 mm I.D. × 168 m long pipe

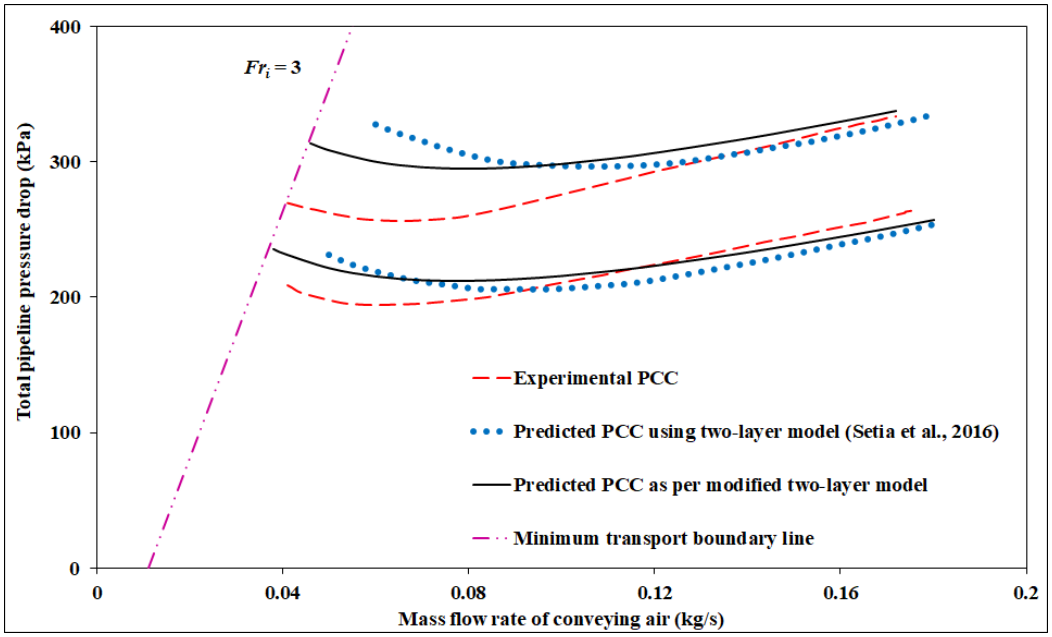

Figure 5.3: Scale-up validation for solids friction factor (modified two-layer model with impact friction, variable fluidized bulk density) for fly ash through 69 mm I.D. × 554 m long pipe

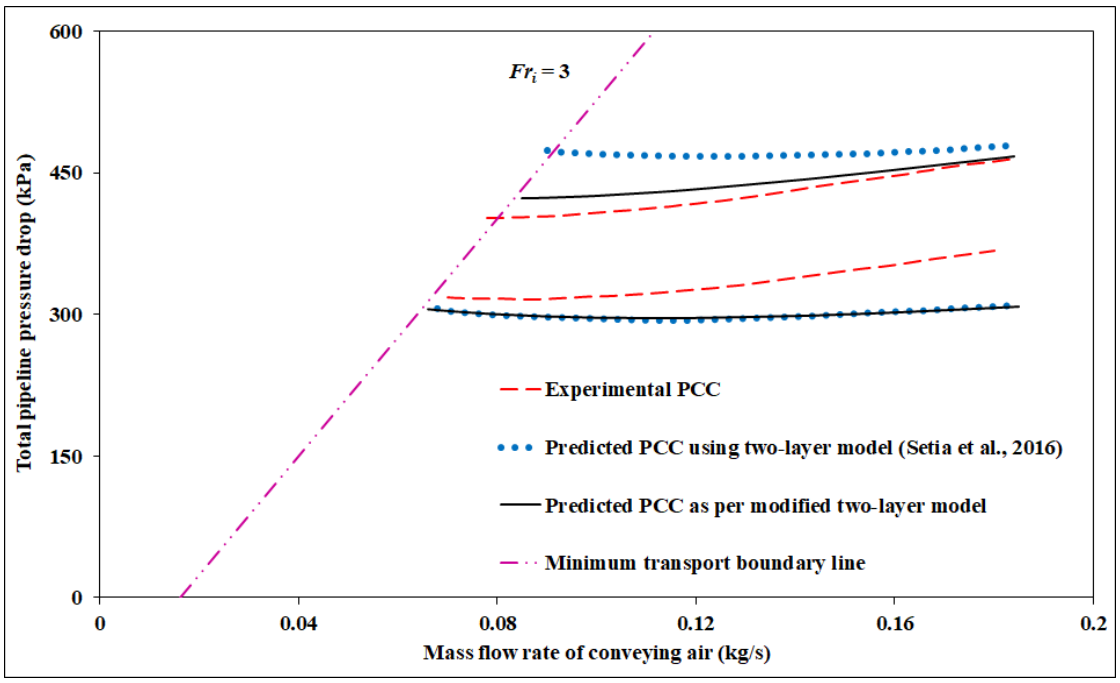

Figure 5.4: Scale-up validation for solids friction factor (modified two-layer model with impact friction, variable fluidized bulk density) for cement through 80/100 mm I.D. × 407 m long pipe

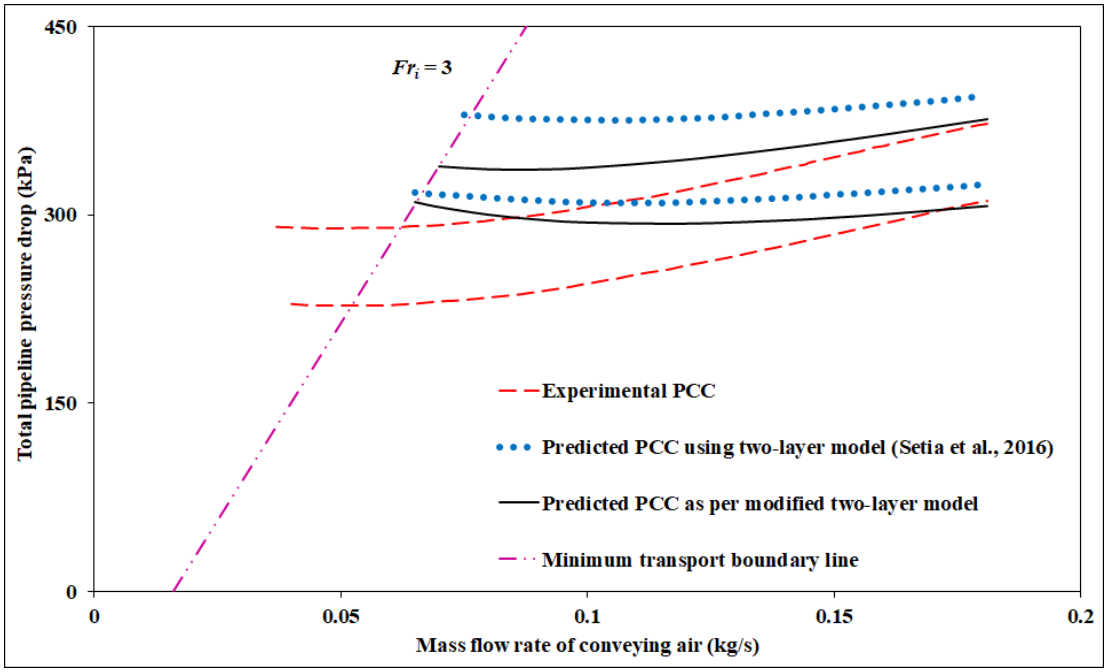

Figure 5.5: Scale-up validation for solids friction factor (modified two-layer model with impact friction, variable fluidized bulk density) for fly ash through 80/100 mm I.D. × 407 m long pipe

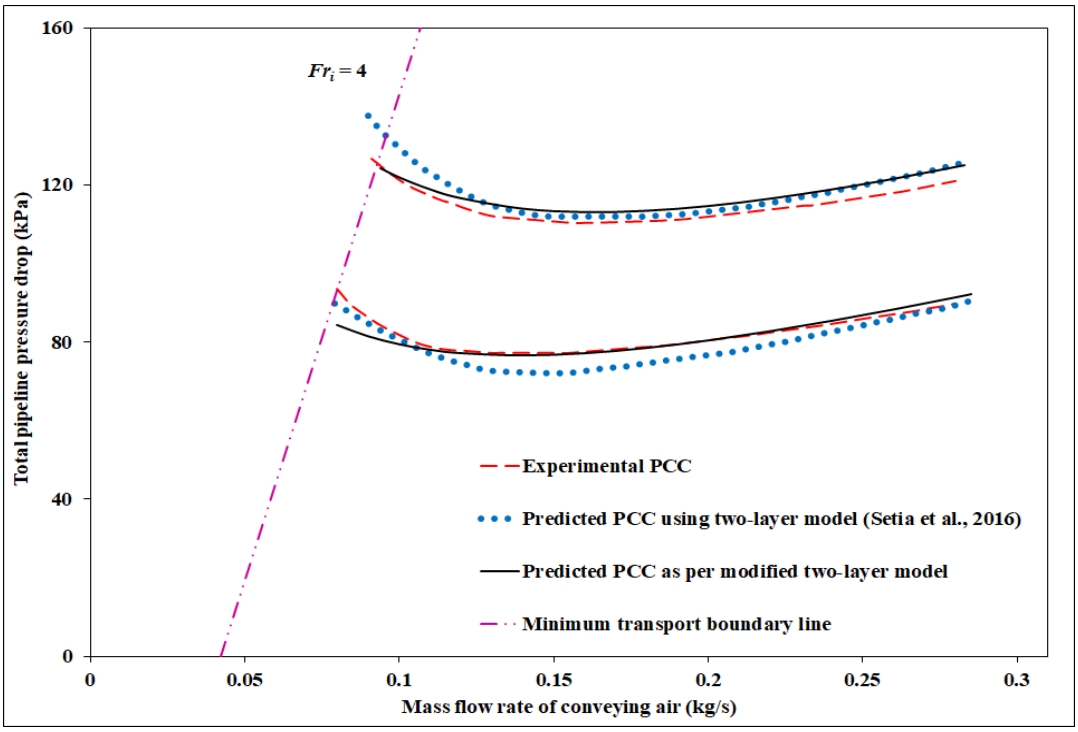

Figure 5.6: Scale-up validation for solids friction factor (modified two-layer model with impact friction, variable fluidized bulk density) for ESP dust through 105 mm I.D. × 168 m long pipe

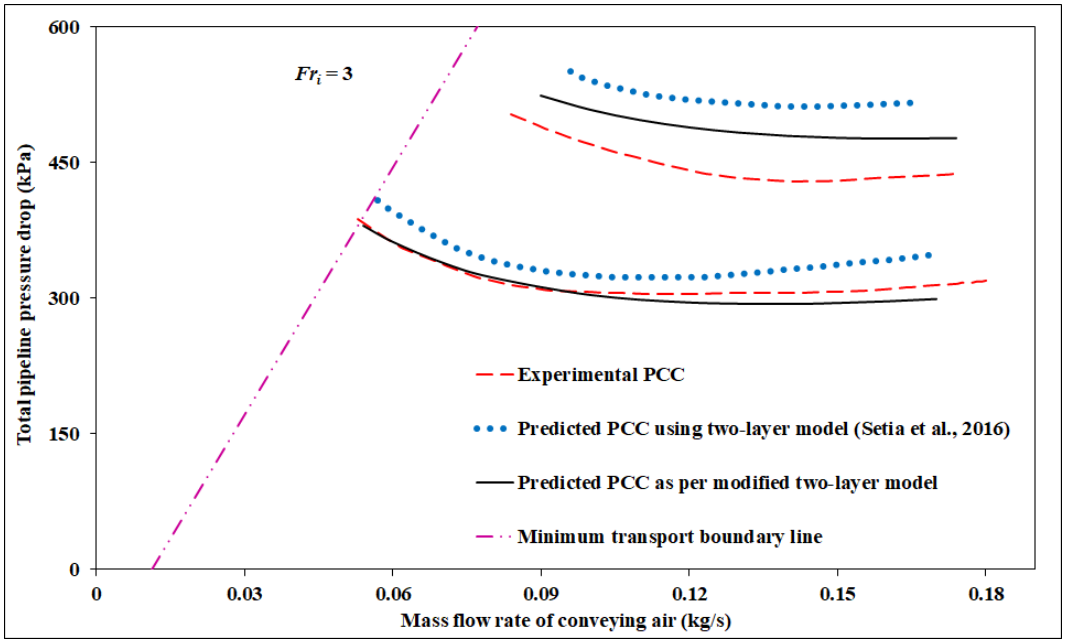

Figure 5.7: Scale-up validation for solids friction factor (modified two-layer model with impact friction, variable fluidized bulk density) for ESP dust through 69 mm I.D. × 554 m long pipe

The results show that for this fly ash, the modified two-layer format with newly developed particle specific model with variable fluidized bulk density and energy loss impact provides better prediction from dense- to dilute-phase region in comparison with the Setia et al. (2016) model for the higher mass flow rates (28 t/h: top lines). On the other hand, for lower (18 t/h: bottom lines) mass flow rates it shows better predictions in very dense-phase region and some very slight under-prediction (i.e., around 2 to 3 kPa) at dilute-phase region in comparison with the existing two-layer model format developed by Setia et al. (2016). Figure 5.3 shows the results of scale-up validation for fly ash conveyed through the pipeline viz. 69 mm I.D. × 554 m long pipeline corresponding to the different mass flow rate of solids (7 t/h: bottom lines and 11 t/h: top lines). The results show that for fly ash (69 mm I.D. × 554 m long pipeline), the modified two-layer format with newly developed particle specific model with variable fluidized bulk density and energy loss impact provides better predictions from dense- to dilute-phase region in comparison with the Setia et al. (2016) model for higher (11 t/h: top lines) mass flow rate. On the other hand, for lower (7 t/h: bottom lines) mass flow rate, it shows satisfactorily better predictions in very dense-phase and almost similar-prediction in the dilute-phase region with the existing two-layer model format developed by Setia et al. (2016). Figure 5.4 shows the results of scale-up validation for cement conveyed through the pipeline viz. 80/100 mm I.D. × 407 m long pipeline corresponding to the different mass flow rate of solids (18 t/h: bottom lines and 36 t/h: top lines). The results show that for cement (80/100 mm I.D. × 407 m long pipeline), the modified two-layer format with newly developed particle specific model with variable fluidized bulk density and energy loss impact provides better predictions from dense- to dilute-phase region in comparison with the Setia et al. (2016) model for higher (36 t/h: top lines) mass flow rate. On the other hand, the modified two-layer model shows almost similar prediction from dense to dilute-phase region for lower mass flow

rate (18 t/h: bottom lines) with the existing two-layer model format developed by Setia et al. (2016). Figure 5.5 shows the results of scale-up validation for fly ash conveyed through the pipeline viz. 80/100 mm I.D. × 407 m long pipeline corresponding to the different mass flow rate of solids (20 t/h: bottom lines and 30 t/h: top lines). The results show that for fly ash (80/100 mm I.D. × 407 m long pipeline), the modified two-layer format with newly developed particle specific model with variable fluidized bulk density and energy loss impact provides better predictions from dense- to dilute-phase region in comparison with the existing two-layer model format developed by Setia et al. (2016) for almost both mass flow rates (20 t/h: bottom lines and 30 t/h: top lines). In order to test the accuracy of the modified two-layer model presented, the scale-up predictions for very fine powder (i.e., for ESP dust) were also investigated. Figure 5.6 shows the results of scale-up validation for ESP dust conveyed through 105 mm I.D. × 168 m long pipeline corresponding to the different mass flow rate of solids (15 t/h: bottom lines and 25 t/h: top lines). The results show that for ESP dust (105 mm I.D. × 168 m long pipeline), the modified two-layer format with newly developed particle specific model with variable fluidized bulk density and energy loss impact provides better predictions in dense-phase and almost shows the similar prediction in the dilute-phase region for higher mass flow rate (25 t/h: top lines) compared to the existing two-layer model format developed by Setia et al. (2016). On the other hand, it shows some slight under-prediction (i.e., around 4 to 7 kPa) at dense-phase and almost shows the similar predictions in the dilute-phase region for lower (15 t/h: bottom lines) mass flow rate compared to the existing two-layer model format developed by Setia et al. (2016). Figure 5.7 shows the results of scale-up validation for ESP dust conveyed through the pipeline viz. 69 mm I.D. × 554 m long pipeline corresponding to the different mass flow rate of solids (6 t/h: bottom lines and 10 t/h: top lines). The results show that for ESP dust (69 mm I.D. × 554 m long pipeline), the modified two-

layer format with newly developed particle specific model with variable fluidized bulk density and energy loss impact provides better predictions from dense- to dilute-phase region in comparison with the existing two-layer model format developed by Setia et al. (2016) for almost both mass flow rates (6 t/h: bottom lines and 10 t/h: top lines). It has been seen from the Figures 5.2 to 5.7 that the modified two-layer model could provide better predictions from dense to the dilute-phase region for the used mass flow rate of solids in the present investigation and products under scale-up conditions. Therefore, the modified two-layer model holds good and shows great improvements from dense- to dilute-phase region in comparison with the Setia et al. (2016) model for scale-up configurations.

In addition to this, the modified two-layer model format developed in equation (5.18) has also been used to model the fly ash conveyed in the newly developed test rig under the NTPC project shown in Chapter 2 (see Figure 2.3). NTPC power station fly ash was conveyed in the test rig (105 mm I.D. × 130 m long pipeline) at Particle and Bulk Solids Technologies Laboratory of Thapar Institute of Engineering & Technology, India. The physical properties are given in Chapter 2 (refer to Table 2.2). The obtained *K, a*, *b* values are shown in Table 5.2 as follows: -

Table 5.2. Modified two-layer model developed using equation (5.18)

Product	**Pipeline data used for modelling**	**Model (as per the format provided by equation 5.18)**					**R^2**
		K	**a**	**b**	$\boldsymbol{\lambda_s^*}$	$\mathbf{w_{fo}}$ **(m/s)**	
Fly ash	105 mm I.D. × 130 m	10	-1.122	2.195	0.02126	0.123	0.97

Similarly, different grade of products (i.e., fly ash) obtained from other NTPC super thermal power stations have been modelled with the same format represented by equation (5.18) using multiple regression method (not shown in the present thesis research work).

5.2 Modelling solids friction using apparent rheology of powdered bed

Anjaneyulu and Khakhar (1994) experimentally studied the rheology of granular materials (i.e., glass beads) with Brookfield, Synchro-Lectric viscometer. The average particle size of glass beads ranges from 400 to 1000 μm. It was concluded that the yield stress decreases with an increase in the amount of aeration. Zhao and Wei (2000) studied the rheological behaviours of gas-solid fluidized beds. The viscosity of fluidized beds was measured with the help of solid-settling experiments. The inner diameter and height of the fluidized bed were 46 mm and 240 mm. The average particle size of silica sand was 88 μm, whereas, for glass beads, average particle size ranges from 88 to 175 μm. The plastic viscosity and yield stress values of fluidized beds were obtained with the aid of the linear regression technique, which was applied to the obtained experimental data. The calculated results were found to be in a close agreement with the experimental data. It was also concluded that both plastic viscosity and yield stress values increase with an increase in particle size. Bruni et al. (2005) studied the flow properties of aerated/fluidized granular powders below the minimum fluidization condition and when the powders are just fluidized using torque measurements using a mechanically stirred fluidized bed rheometer (msFBR). The average particle size of glass ballotini was 350 μm, and particle density was 2500 kg/m^3, whereas for Alumina powders, average particle size was 75 μm and particle density was 1730 kg/m^3. It was observed that below the minimum fluidization, the torque profiles obtained for

both powders were independent of impeller speed, and at minimum fluidization condition, torque profiles obtained were dependent on the impeller speed and found to increase linearly with increasing depth of the impeller. Barletta et al. (2007) experimentally studied the effect of aeration on the yield strength, rheology, and on the shear stress of various cohesive powders. In this work, for experimental purposes, two different cohesive powder samples were taken into account, i.e., silica: average particle size: 21 μm, particle density: 2650 kg/m^3 and magnesium carbonate: average particle size: 15 μm, particle density: 2600 kg/m^3. He designed and fabricated a new rotational shear cell tester for the measurement of flow properties of aerated fine powders for respective internal diameter: 61.8 mm and height: 15 mm. It was found that aeration does not affect the unconfined yield strength of the powder and its inherent rheological properties. It only modifies the effective state of shear stress of the powder. Bruni et al. (2007, 2007a) experimentally studied the rheology of fine powders aerated below the minimum fluidization with the help of using mechanically stirred fluid-bed rheometer. Glass ballotini, silica and alumina (A0, A3, A4, A5, A6) powders with different fine contents were tested. The average particle size of glass ballotini was 350 μm, and that of silica powders alumina (A0, A3, A4, A5, A6) powders ranged from 36 to 75 μm. At various impeller depths of immersions, aeration rates and rotational speeds of the impeller, the torque required to spin an impeller immersed in a bed of aerated powders was measured near minimum fluidization velocities. This investigation mainly focusses on studying the influence of the IPFs on the fluidization behaviour and rheology of alumina powders when adding big fines (25–45 μm) or small fines (0–25 μm) using fluidization tests and shear cell measurements. Results obtained from pressure drop profiles, bed expansion profiles, and bed collapse tests were linked to the rheological examination of materials. The results obtained from the cohesion and the effective angle of internal friction showed that the alumina sample containing small fines (0–25 μm), A6,

was more cohesive, means increased effect of interparticle forces (IPFs) and maximum resistance to flow, hence less flowable, than the alumina sample containing the same amount of big fines (25–45 μm) having lower resistance to flow. Colafigli et al. (2008) attempted to determine the viscosity of fine powders in a homogeneous gas-fluidized bed using ambient nitrogen as the aeration medium. In this work, the powder sample used was silica (falling under Geldart Group-C category) of average particle size of 26 μm, particle density of 460 kg/m^3. He designed and fabricated a Couette fluidized-bed rheometer (CFBR) set-up having Pyrex cylindrical vessel of width 13.8 cm, height: 30 cm and the wall thickness of 0.2 cm, capable of measuring the viscosity of a fluidized suspension under variable conditions of applied shear stress. It was observed that the viscosity decreases with increased shear rate. Tripathi and Khakhar (2011) used the discrete element method (DEM) simulation technique to study the rheology of granular mixtures in a steady, fully developed, gravity-driven flow on an inclined plane. Barletta and Poletto (2013) developed a new experimental device for the measurement of the horizontal to vertical stress ratio for free-flowing (65 to 373 μm) non-compressible powders and for, cohesive (3 to 25 μm) and compressible powders. Chen (2013) experimentally studied the rheology of aerated fine powders. He designed and fabricated a new testing apparatus using a combination of a fluidization chamber and a rotary viscometer, which utilized the Couette method to measure the rheology of gas-solid systems. In his set-up, the rheology of homogenous laminar flow was considered. Chen (2013) carried out rheology testing of fine powders, such as fly ash and alumina. Based on rheology, conveying models of aerated fine powders (fly ash and alumina) were derived for straight pipelines. The newly derived conveying models are presented below by equations (5.19), (5.20), and (5.21).

The power-law fluid conveying model is given as follows:

$$\frac{\Delta P}{2L} = A_{sp} + \left(\frac{\Delta P}{2L}\right)_{air} \tag{5.19}$$

The yield power-law fluid conveying model is given as follows:

$$\frac{\Delta P}{2L} = A_{sy} + \left(\frac{\Delta P}{2L}\right)_{air} \tag{5.20}$$

Combined material conveying model is given as follows:

$$\frac{\Delta P}{2L} = A_{sy} + A_{sp} + \left(\frac{\Delta P}{2L}\right)_{air} \tag{5.21}$$

Out of three above derived conveying models, the yield power-law fluid conveying model was selected to describe the pneumatic flow of fine powders. Afterwards, the newly developed conveying model based on the concept of rheology was evaluated and validated by comparing the pressure drop obtained from the conveying model with the pressure drop measured from a 79 mm I.D. × 7 m long pilot-scale pneumatic conveying loop. The results of the final validation revealed that, for alumina, the overall error between the experimental observations and the newly predicted model was around 11.7 %, which was considered to be in good agreement. Whereas, on the other hand, for fly ash, the new model predictions showed good agreement (i.e., error < 20%) with the experimental results only at low to intermediate dense-phase flow mode conditions (m* < 130). For highly dense-phase flow conditions, the predicted model under-estimated the pressure drop values, while for highly dilute-phase flow conditions, the predicted model over-predicted the pressure drop values. It was concluded that the selected rheology based conveying model (i.e., yield power-law fluid) has a good potential to estimate the straight pipeline pressure drops for the

fine aerated flow of powders. Chaudhry (2015) tried to investigate the rheology of fine powders in order to develop a rheological model for fluidized dense-phase pneumatic conveying systems with the help of designed and fabricated powder rheological tester in the lab. In this work, yield stress and viscosity were measured under fluidized and unfluidized conditions. Five different power station fly ash samples with average particle size ranging from 19-139 μm, particle density from 1950-2370 kg/m^3 and bulk density from 660-950 kg/m^3 were taken into account along with the cement sample with particle size of 19 μm, particle density of 2910 kg/m^3 and bulk density of 1080 kg/m^3 in order to carry out the rheological experimentations for respective fluidization chamber of internal diameter: 105 mm. From the experimental results, it was concluded that with fluidization, the yield stress and viscosity decreases. On the other hand, in the unfluidized state, yield stress increases with an increase in the mean particle size of the powders. It was also found that the yield stress and viscosity values increased with the increase in depth of spindle immersion but decreased with the increase in the rotational speed of the spindle. Moscardini et al. (2017) simulated the mechanical behaviour of particles (ellipsoidal shape) with the aid of the discrete element method (DEM) approach. It was concluded that the DEM simulations are essential to study the stress-strain behaviour of particles having non-spherical nature. Salehi et al. (2018) performed the torque measurements with the powder cell mounted on an Anton Paar rheometer using glass beads of two different sizes (2 to 4 mm) and different impeller geometries. The scope of the research work of Salehi et al. (2018) was only limited up to granular products, and hence, no data was generated to study the rheology of fine powders.

In the present work, results have been obtained from the rheology of fine powders performed at Anton Paar Powder Rheometer for different rotational speeds, aeration amounts, and direction of

the rise of rotational speeds. The details of the Rheometer device used and the experimental conditions are given in Chapter 2 (see Table 2.3). Figures 5.8 to 5.12 shows the results obtained for the variation of shear stress along with the shear rates (increasing spindle speed: 0-200) for 3 to 15 l/min airflow rates. Whereas, Figures 5.13 to 5.17 shows the results obtained for the variation of shear stress along with the shear rates (decreasing spindle speed: 200-0) for 3 to 15 l/min airflow rates. Different products such as fly ash 1, fly ash 2, grey cement 1, grey cement 2, and white cement have been taken into consideration while doing the rheology tests. The details of all products tested for apparent powder rheology are shown in Chapter 2 (see Table 2.4). The shear rate is shown in all figures has been divided into three zones, i.e., low shear rate, medium shear rate, high shear rate zones. Figure 5.8 shows the variation of shear stress along with the shear rates (0-200) for 3 l/min air flow rate. It has been seen that the powder sample grey cement 1 shows higher shear stress values at the low shear rate in comparison to the other powder samples, which shows lower values of shear stresses at the same condition (i.e., low shear rate). Overall, the same trend has been continued in the higher shear rate as well. It has been observed that, as the shear rate from the origin point increased with the uniform increment, the gradient of the shear stress curves reduces accordingly, which exhibited a shear-thinning effect. In other words, pseudo-plastic behaviour has been displayed by all powders. Figure 5.9 shows the variation of shear stress along with the shear rates (0-200) for 6 l/min air flow rate. It has been seen that the powder sample grey cement 1 shows higher shear stress values as compared to the other powder samples, which show lower values of shear stresses at the low shear rate zone. In the higher shear rate zone, it has been seen that the sample fly ash 1 exhibits higher values of shear stress in comparison to the other used powder samples in the investigation. It has been observed that, as the shear rate from the origin point increased with the uniform increment, the gradient of the shear stress curves reduces

accordingly, which exhibited a shear-thinning effect. It has been critically reviewed by the authors that, in Figure 5.9 more reduced gradient has been observed (in the shear stress curves) in case of samples grey cement 1 and fly ash 1, which essentially reflects the more shear-thinning effect. On the other hand, for the remaining powder samples, the less shear-thinning effect has been pronounced due to the less curvilinear structure of the shear stress curves with increasing shear rate on the x-axis. It has been concluded that, more or less, the pseudo-plastic behaviour has been displayed by all powders. Figure 5.10 shows the variation of shear stress along with the shear rates (0-200) for 9 l/min air flow rate. It has been seen that, at a very low shear rate zone, the values of powder samples grey cement 1 and fly ash 1 have got almost similar values of shear stress. But overall, the results indicated that the powder sample fly ash 1 shows higher shear stress values in comparison to the other powder samples, which shows lower values of shear stresses at the low shear rate zone. The same trend has been continued in the higher shear rate zone as well. It has been observed that, as the shear rate from the origin point increased with the uniform increment, the gradient of the shear stress curves reduces accordingly for samples grey cement 1 and fly ash 1 which exhibited a shear-thinning effect. On the other hand, for other powder samples, as the shear rate from the origin point increased with the uniform increment on the x-axis, the shear stress curves rose correspondingly, which also reflects the pseudo-plastic behaviour or shear thinning behaviour. Figure 5.11 shows the variation of shear stress along with the shear rates (0-200) for 12 l/min air flow rate. The results indicated that the powder sample fly ash 1 shows higher shear stress values in comparison to the other powder samples, which shows lower values of shear stresses at the low shear rate zone. The same trend has been continued in the higher shear rate zone as well. The shear-thinning effect or pseudo-plastic effect for powder samples grey cement 1 and fly ash 1, and other powder samples used in the present investigation is similar, as described in Figure

5.10. Figure 5.12 shows the variation of shear stress along with the shear rates (0-200) for 15 l/min air flow rate. It has been seen that, overall, the powder sample grey cement 1 shows higher shear stress values in comparison to the other powder samples, which shows lower values of shear stresses at the low shear rate zone. The same trend has been displayed in the higher shear rate zone as well. It has been observed that, for all powders, as the shear rate from the origin point increased with the uniform increment on the x-axis, the gradient of the shear stress curves rose correspondingly, which in turn exhibited a shear thinning behaviour or pseudo-plastic behaviour. Likewise, a similar trend has been observed with the decreasing spindle speed from 200-0 rpm, i.e., for all powder samples Figures 5.13 (variation of shear stress along the shear rates (200-0) for 3 l/min air flow rate), 5.14 (variation of shear stress along the shear rates (200-0) for 6 l/min air flow rate) and 5.17 (variation of shear stress along the shear rates (200-0) for 15 l/min air flow rate) shows shear-thinning or pseudo-plastic behaviour (gradient of the shear stress curves reduces correspondingly) with the uniform increment of shear rate from the origin point (from low shear rate zone to high shear rate zone). Whereas, in Figures 5.15 (variation of shear stress along the shear rates (200-0) for 9 l/min air flow rate) an 5.16 (variation of shear stress along the shear rates (200-0) for 12 l/min air flow rate) for major of the powder samples the gradient of the shear stress curves rises correspondingly to the uniform increment of shear rate from the origin point on x-axis, which in turn also reflect the shear thinning behaviour. Finally, it has been concluded that almost all test samples used in the investigation exhibit a shear-thinning or pseudo-plastic behaviour with increasing shear rate a uniform rate on the x-axis. It has also been evident from all figures that the shear stress (Pa) remains constant after 125 shear rate value in seconds. This has been observed towards increasing shear rate values in the higher shear rate zone. It has also been

observed that with an increase in fluidization airflow, the yield stress (starting stress values at low rotational speeds) values show a decreasing trend.

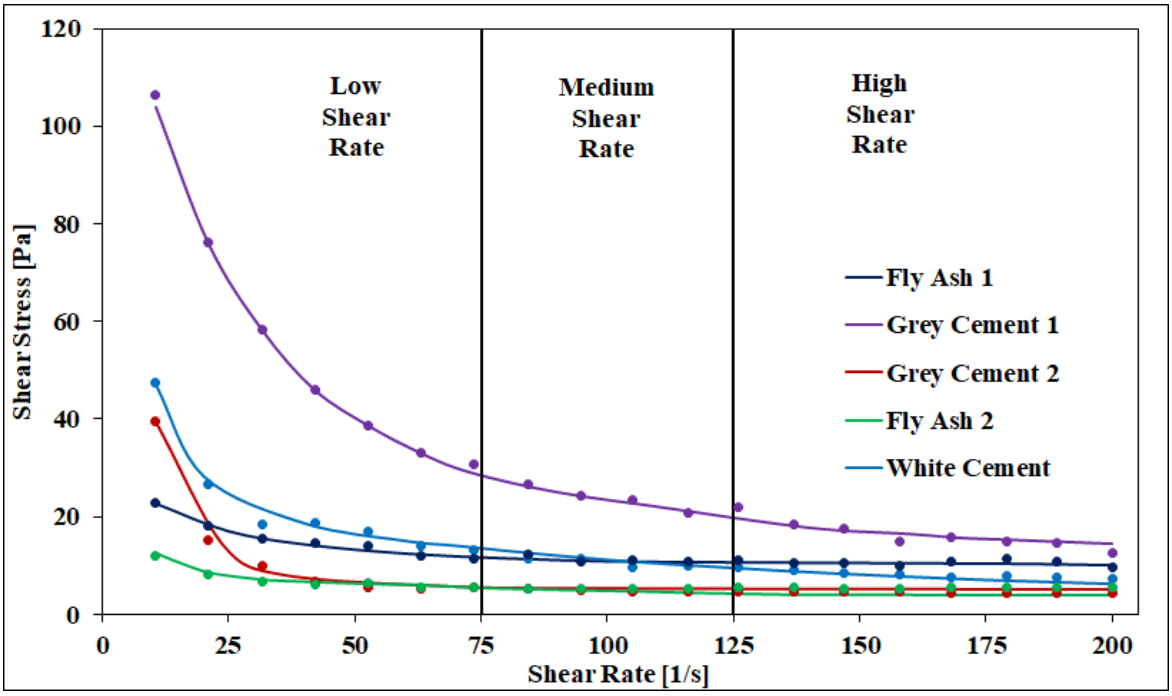

Figure 5.8: Variation of shear stress along with the shear rates (0-200) for 3 l/min air flow rate

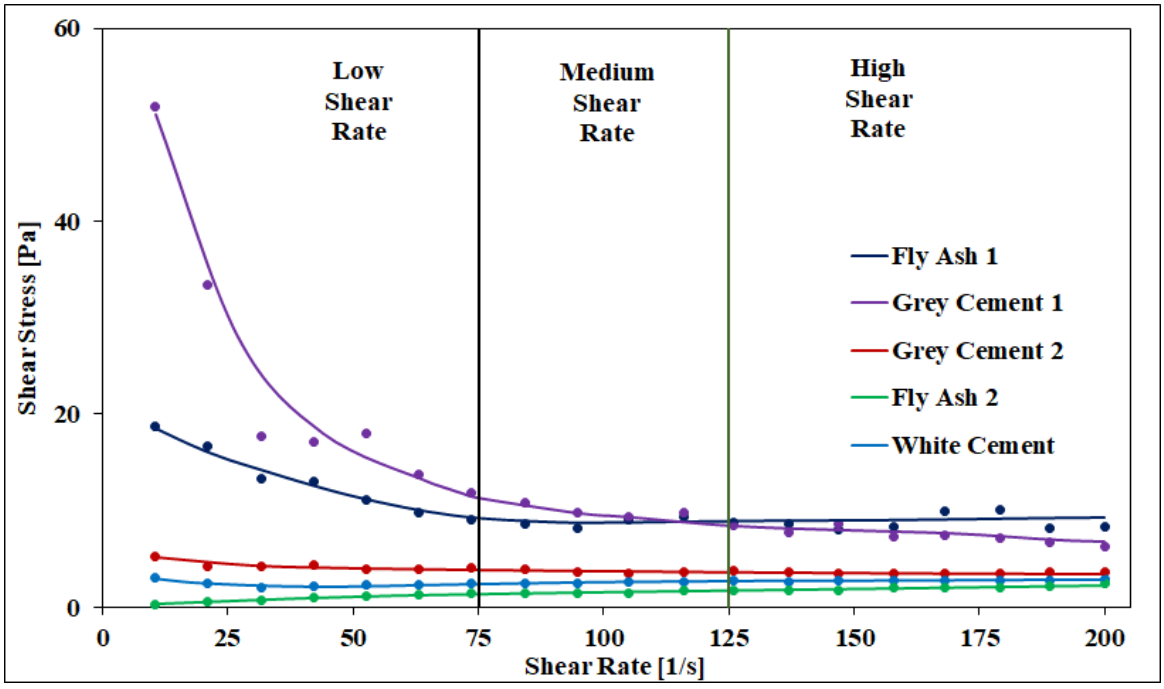

Figure 5.9: Variation of shear stress along with the shear rates (0-200) for 6 l/min air flow rate

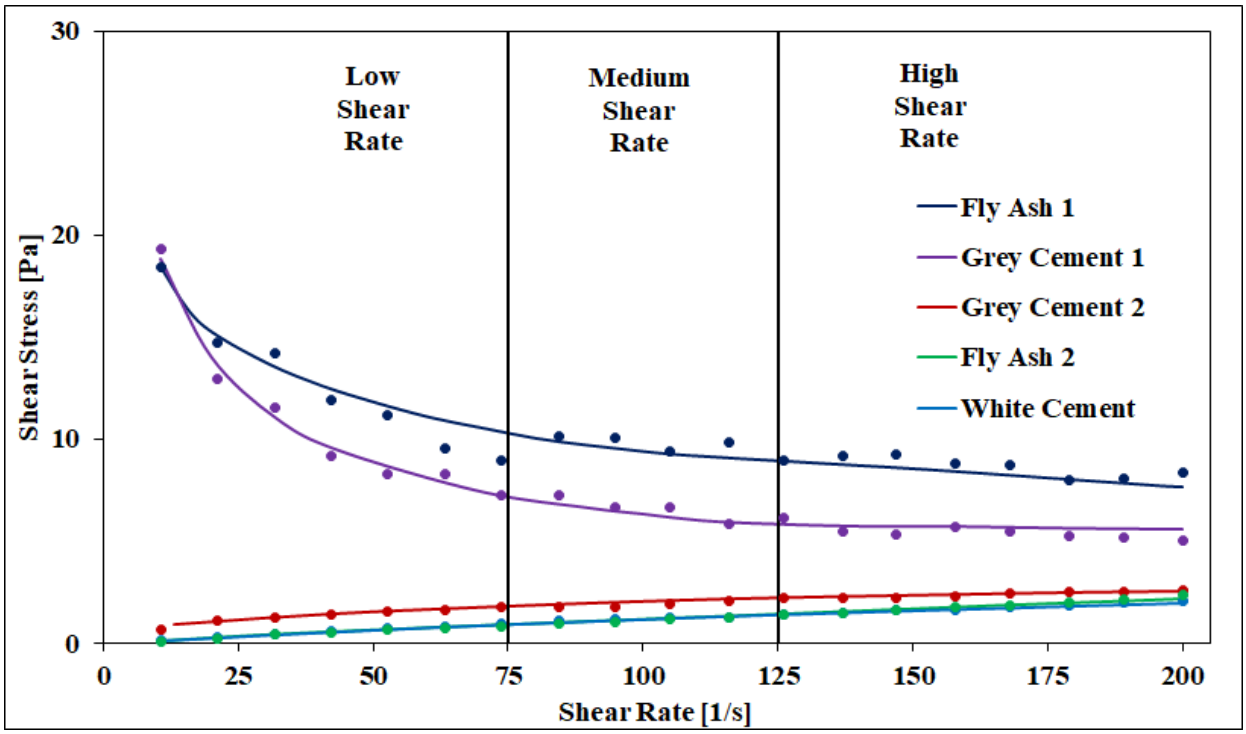

Figure 5.10: Variation of shear stress along with the shear rates (0-200) for 9 l/min air flow rate

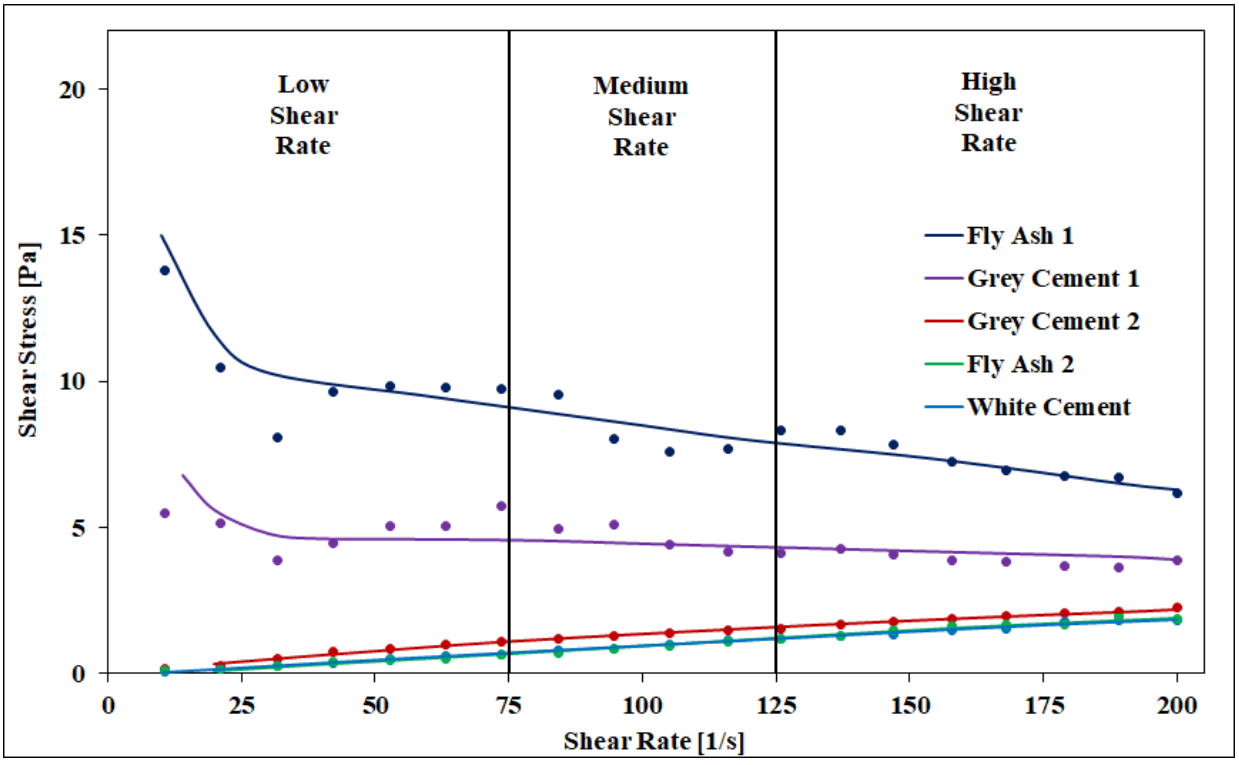

Figure 5.11: Variation of shear stress along with the shear rates (0-200) for 12 l/min air flow rate

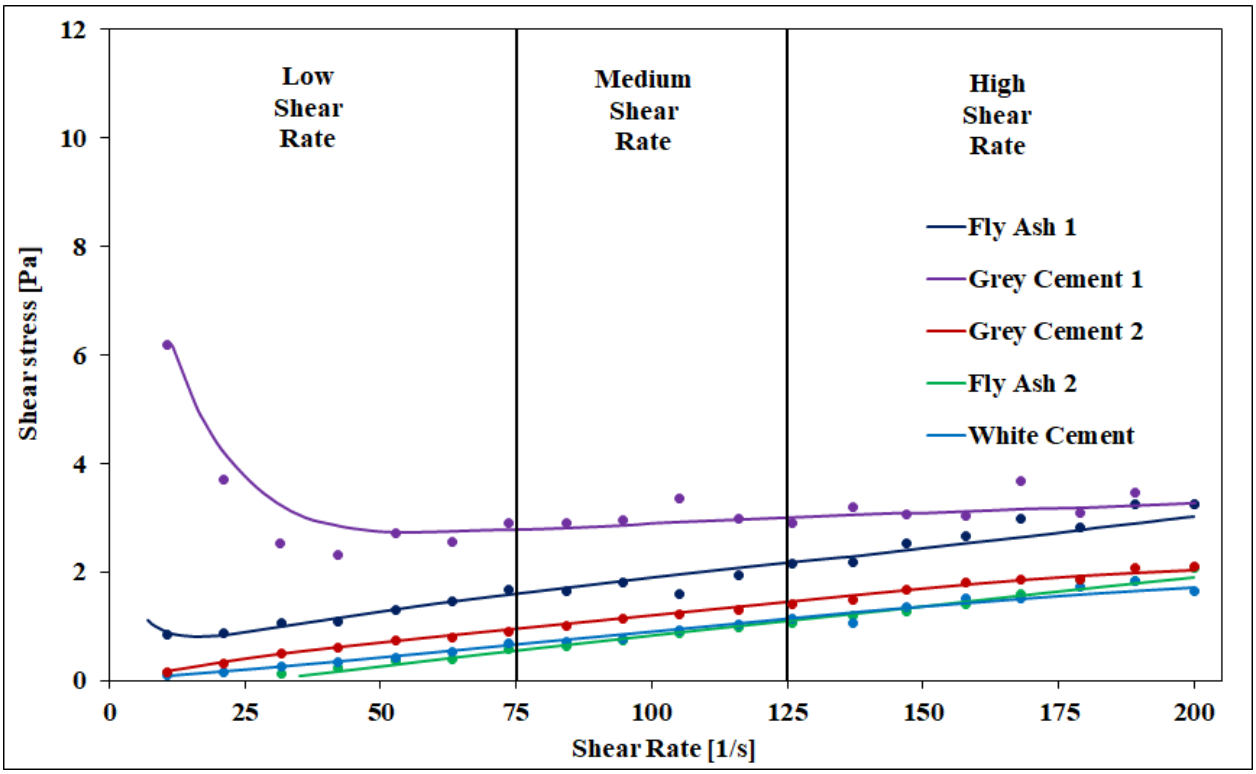

Figure 5.12: Variation of shear stress along with the shear rates (0-200) for 15 l/min air flow rate

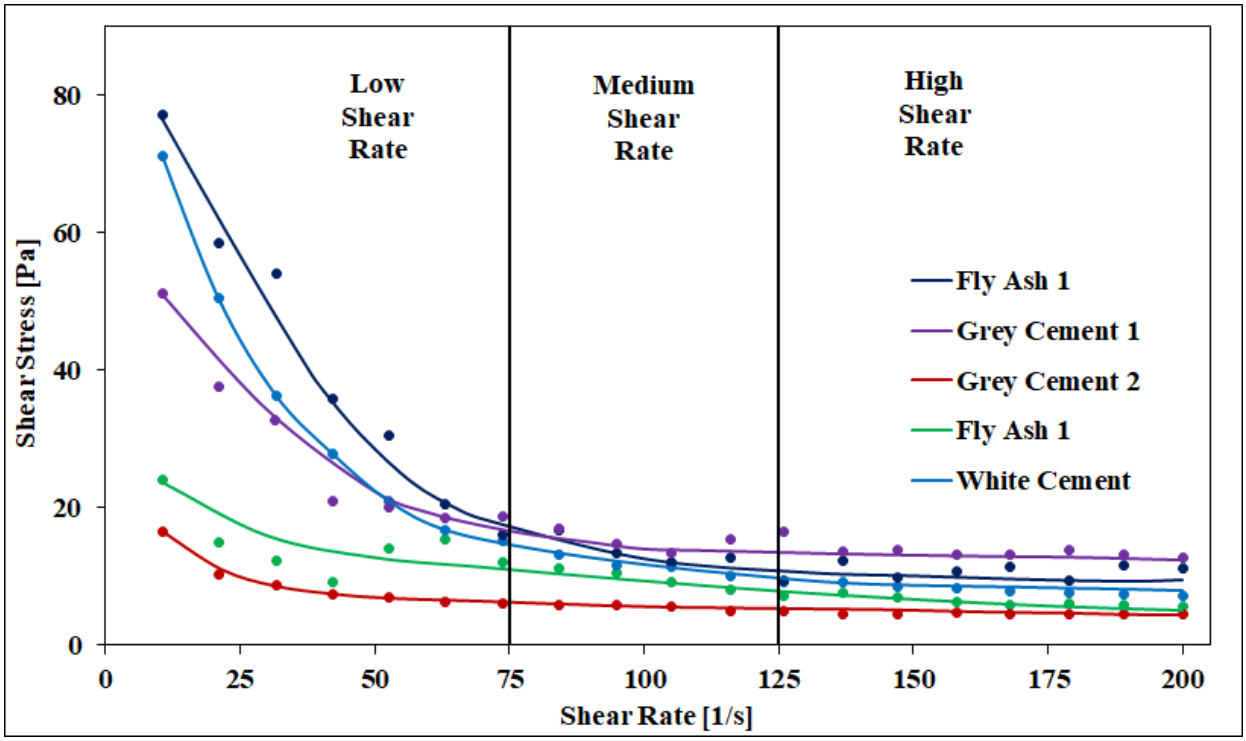

Figure 5.13: Variation of shear stress along with the shear rates (200-0) for 3 l/min air flow rate

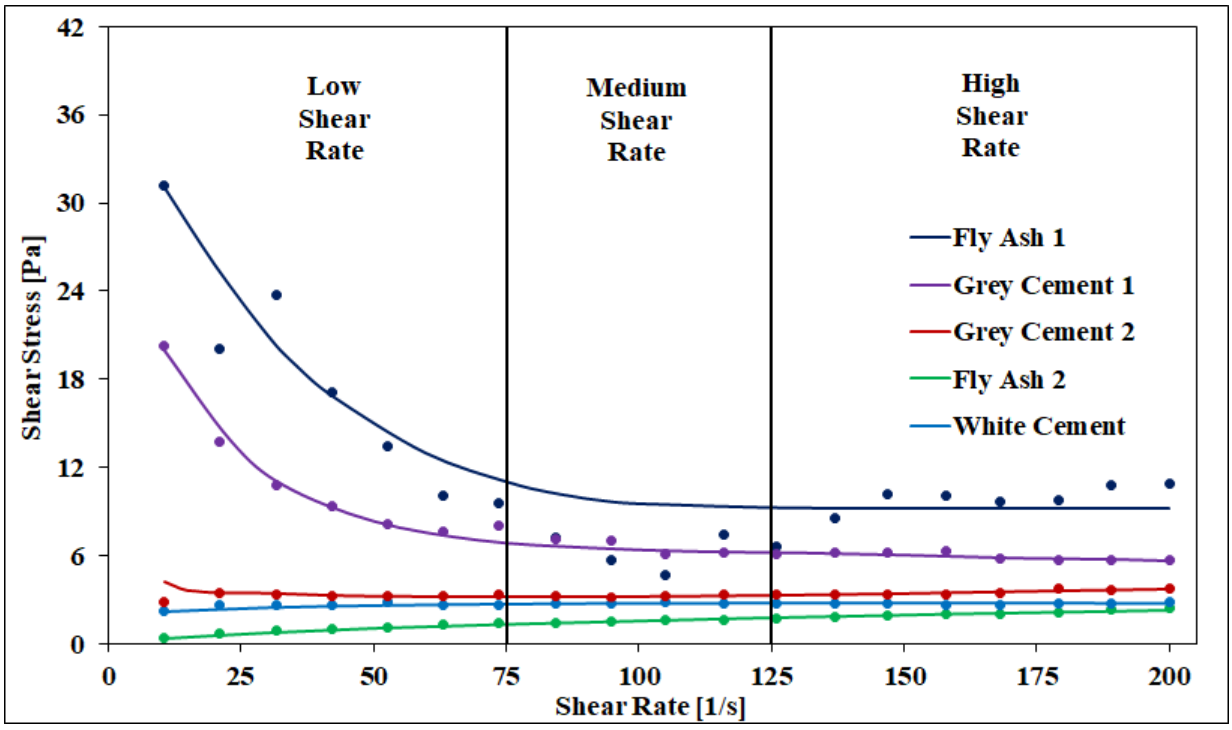

Figure 5.14: Variation of shear stress along with the shear rates (200-0) for 6 l/min air flow rate

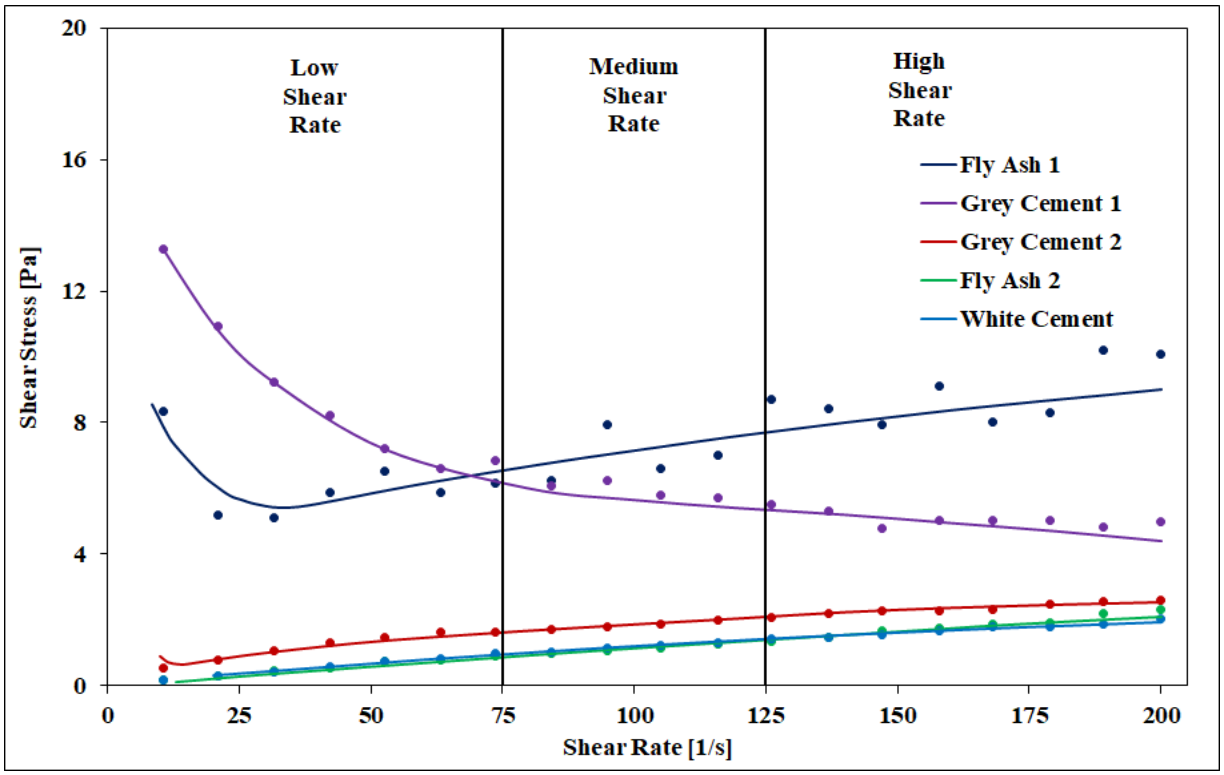

Figure 5.15: Variation of shear stress along with the shear rates (200-0) for 9 l/min air flow rate

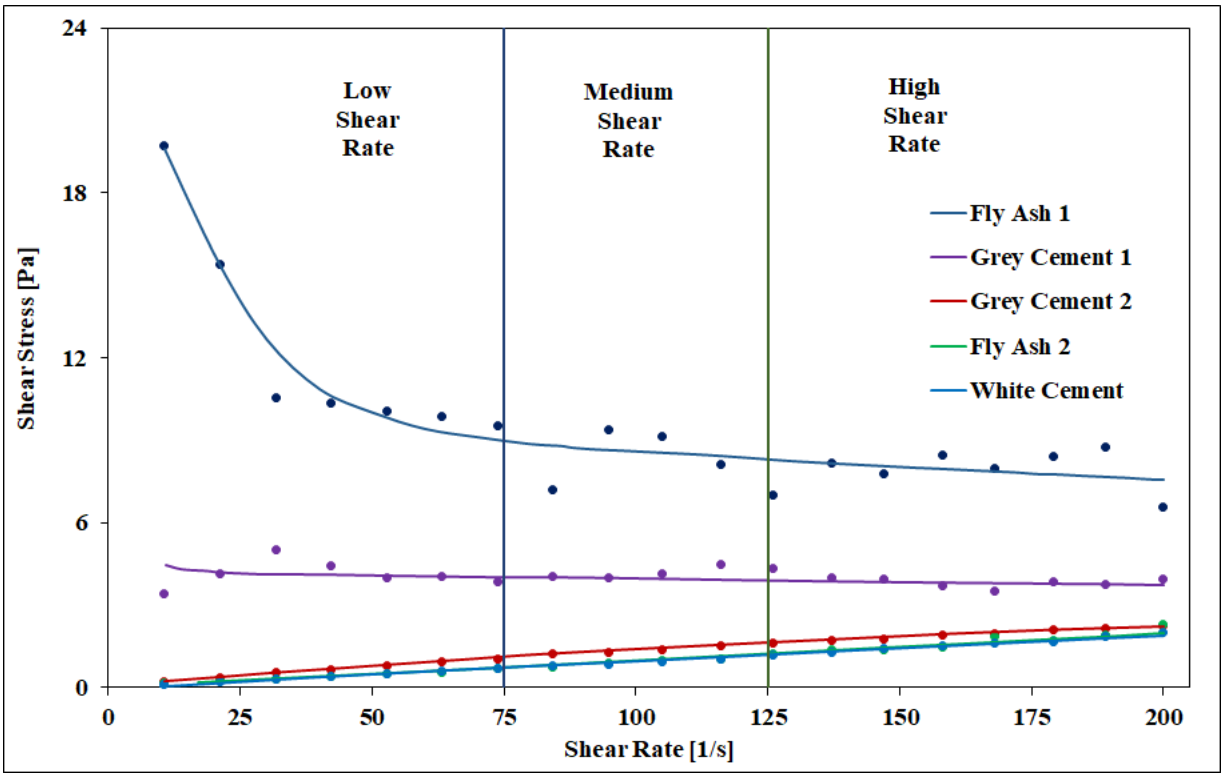

Figure 5.16: Variation of shear stress along with the shear rates (200-0) for 12 l/min air flow rate

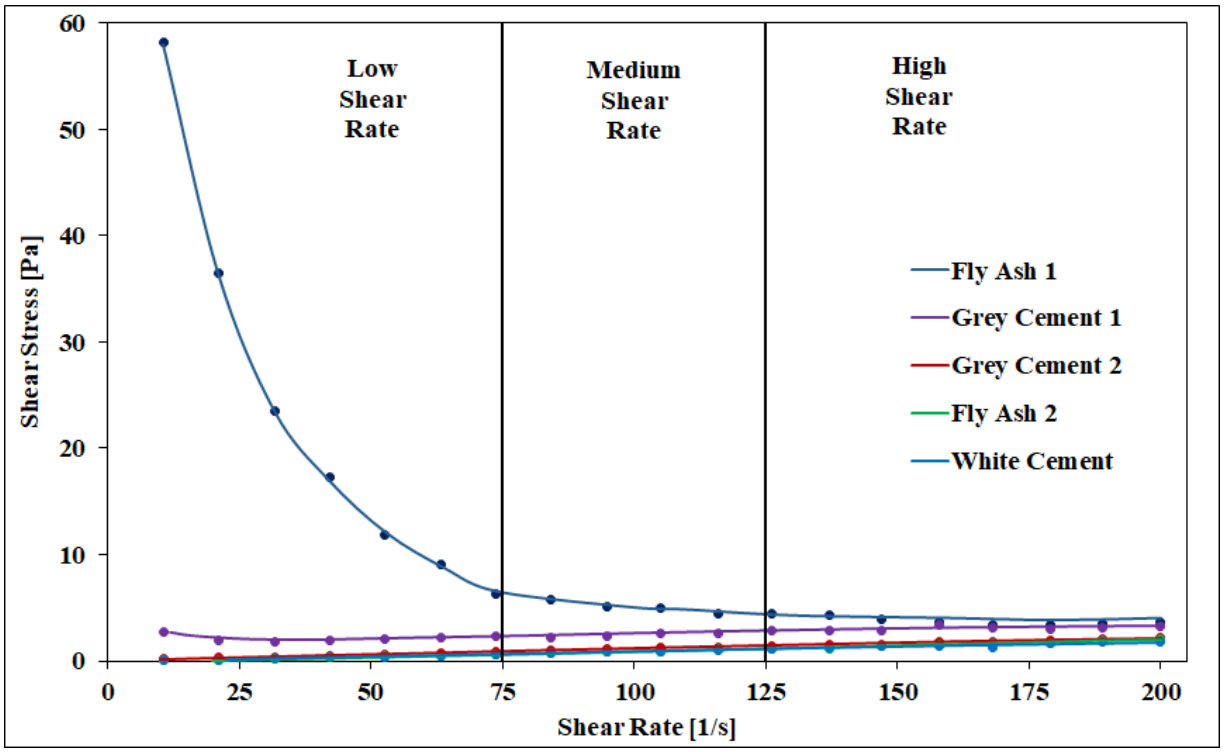

Figure 5.17: Variation of shear stress along with the shear rates (200-0) for 15 l/min air flow rate

The authors developed a power function-based rheological model. The empirical correlation for newly developed models based on rheology is presented in the equation (5.22). This correlation has been obtained using the large database of fine powders (see corresponding Table 2.4 in Chapter 2), namely different fly ash and cement samples, with the aid of multiple regression technique. Higher values of the coefficient of determination (R^2) indicates a good fit. In addition to this, in the present investigation, the accuracy of the newly developed models has been tested for the solids friction factor in a two-layer model format. The rheological model is given as:

$$\frac{\tau}{{w_{fo}}^2 \rho_s} = K \left[\frac{\mu}{V \rho_s d_p}\right]^a [Ar]^b \tag{5.22}$$

$$Ar = \left[\frac{(\rho_b - \rho_a)\rho_a g (d_p)^3}{\mu^2}\right]$$

where, K = 10, a = 0.627, b = -0.978, R^2 = 0.93

Very few researchers have put efforts towards linking outcomes obtained from the rheological investigations with the fluidized dense-phase pneumatic conveying of fine powders. In the view of this, in the present thesis work, authors tried to link the rheological studies with the determination of solid friction factor of fluidized dense-phase pneumatic conveying of fine powders. Therefore, in this section, the Setia et al. (2016) two-layer model has been modified with the inclusion of rheology effects.

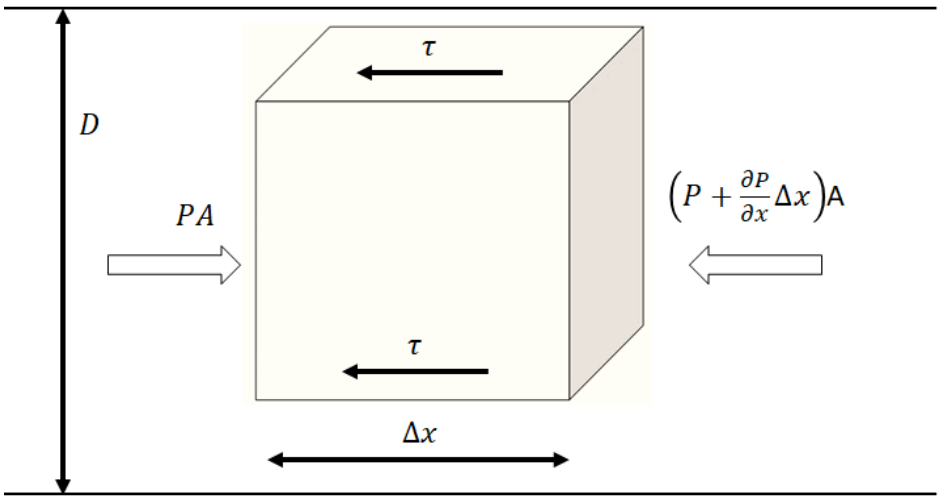

Figure 5.18: Shear energy interactions across a control volume

The derived expression in order to incorporate the rheology effects from the control volume (see Figure 5.18) is given as follows:

From the control volume shown in Figure 5.18, the net accumulation of shear energy in the x-direction can be written as follows:

$$PA - \left(P + \frac{dP}{dx}\Delta x\right)A = \tau(\pi D)(\Delta x) \tag{5.23}$$

On solving and rearranging the equation (5.23), the final expression has been obtained as follows:

$$\frac{dP}{dx} = \frac{4\tau}{D} \tag{5.24}$$

On rearranging the Barth (1958) model format represented by equation (1.1), the following expression has been obtained as follows for solids component of pressure loss:

$$\frac{dP}{dx} = \frac{(m^* \lambda_s)\rho_s V^2}{2D} \tag{5.25}$$

On equating the expressions represented by equations (5.24) and (5.25) the following final expression has been obtained as follows:

$$\lambda_s = \frac{8\tau}{m^* \rho_s V^2} \tag{5.26}$$

where the term 'τ' is the shear stress, 'm^*' is the solids loading ratio, 'ρ_s' is the particle density, and '*V*' is the superficial air or gas velocity. The equation (5.26) shows the inclusion of rheology effects with the term 'τ' in solids friction factor. Therefore, the derived expression represented by equation (5.26) has been incorporated in the Setia et al. (2016) two-layer model in dense-phase flow region in order to encounter the effects of rheology. In fluidized non-suspension mode, the powders having aeration capability when conveyed behave as pseudo-fluid (fluid-like appearance). In order to understand the flow mechanism and modelling fluidized non-suspension type of conveying, the rheological term 'τ' has been considered to be the most significant parameter to address the apparent rheology phenomenon.

Setia et al. (2016) have modelled a two-layer model presented in equation (1.10) using the steady-state pressure drop of fly ash, ESP dust, and cement conveying. In the present investigation, the Setia et al. (2016) two-layer model format has been modified by incorporating the rheology effects (developed in equation (5.26)) with the newly developed rheological model from Anton Paar experiments on Rheometer, varying fluidized bulk density and energy loss effect due to turbulence region.

The modified two-layer model is given as follows:

$$\lambda_s = \tau_1 \left[\frac{8\tau}{m^* \rho_s V^2} + K(VLR)^a \left(\frac{w_{fo}}{V} \right)^b \right] + \tau_2 \left[\lambda_s^* \left(\frac{u_s}{u_a} \right) + \left(2\beta_o \Big/ \left(\frac{u_s}{u_a} \right) Fr^2 \right) + \frac{2\beta_o}{3} \right] \qquad (5.27)$$

where the rheological term 'τ' has been obtained from the newly developed rheological model provided in equation (5.22). The modified form of Setia et al. (2016) two-layer model presented in equation (5.27) has been used for the scale-up validation of solid friction factor in the present investigation. Table 5.3 shows the constant and exponent values obtained during modelling obtained through regression analysis.

Table 5.3. Modified two-layer developed using a "straight pipe" method (equation 5.27)

Product reference	Pipeline data used for modelling	Models (as per the format provided by equation 5.27)					R^2
		K	a	b	λ_s^*	w_{fo} (m/s)	
Fly ash (Mallick, 2009)	69 mm I.D. × 168 m	10.2	−0.38	1.68	0.0103	0.06	0.98
ESP dust (Mallick, 2009)	69 mm I.D. × 168 m	1109	−0.22	1.59	0.0150	0.005	0.98
Fly ash (Setia et al., 2016)	65 mm I.D. × 254 m	83	−0.88	2.12	0.0305	0.038	0.96
Cement (Setia et al., 2016)	65 mm I.D. × 254 m	27.5	−0.56	1.73	0.0314	0.036	0.97

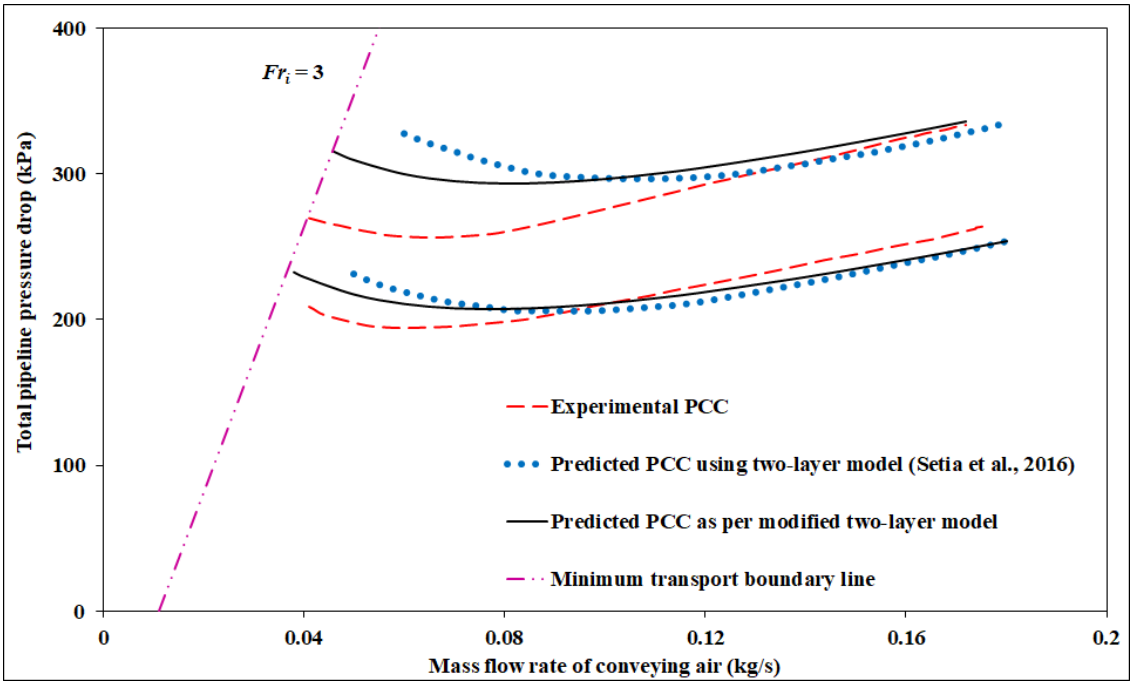

Figure 5.19: Scale-up validation for solids friction factor (modified two-layer model with rheology) for fly ash through 69 mm I.D. × 554 m long pipe

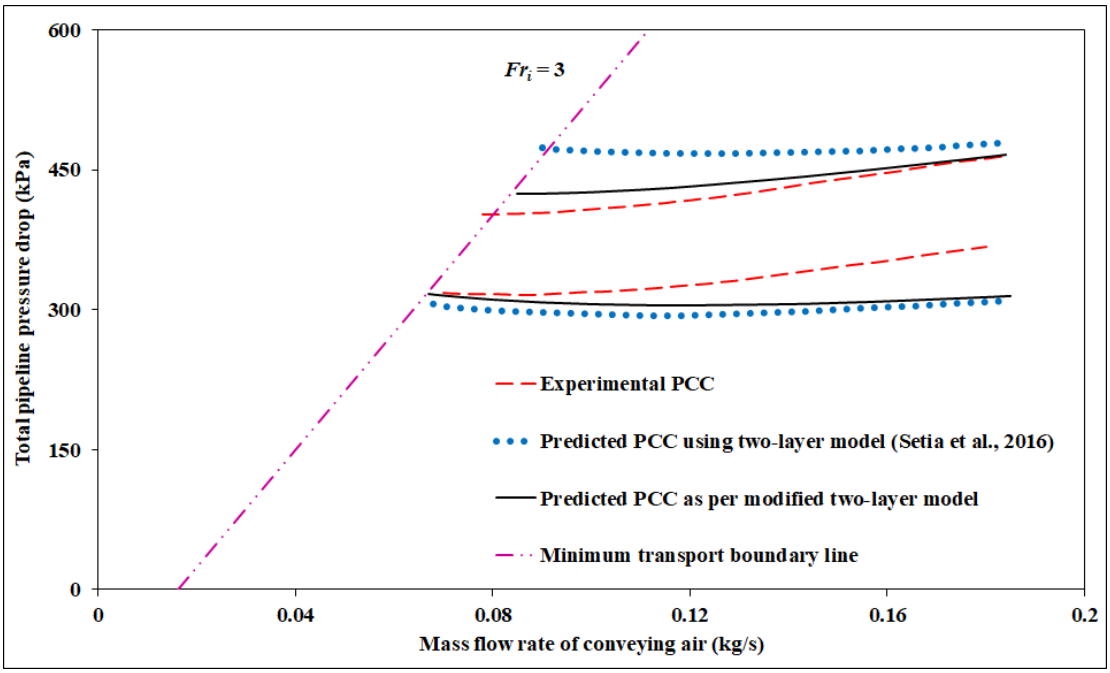

Figure 5.20: Scale-up validation for solids friction factor (modified two-layer model with rheology) for cement through 80/100 mm I.D. × 407 m long pipe

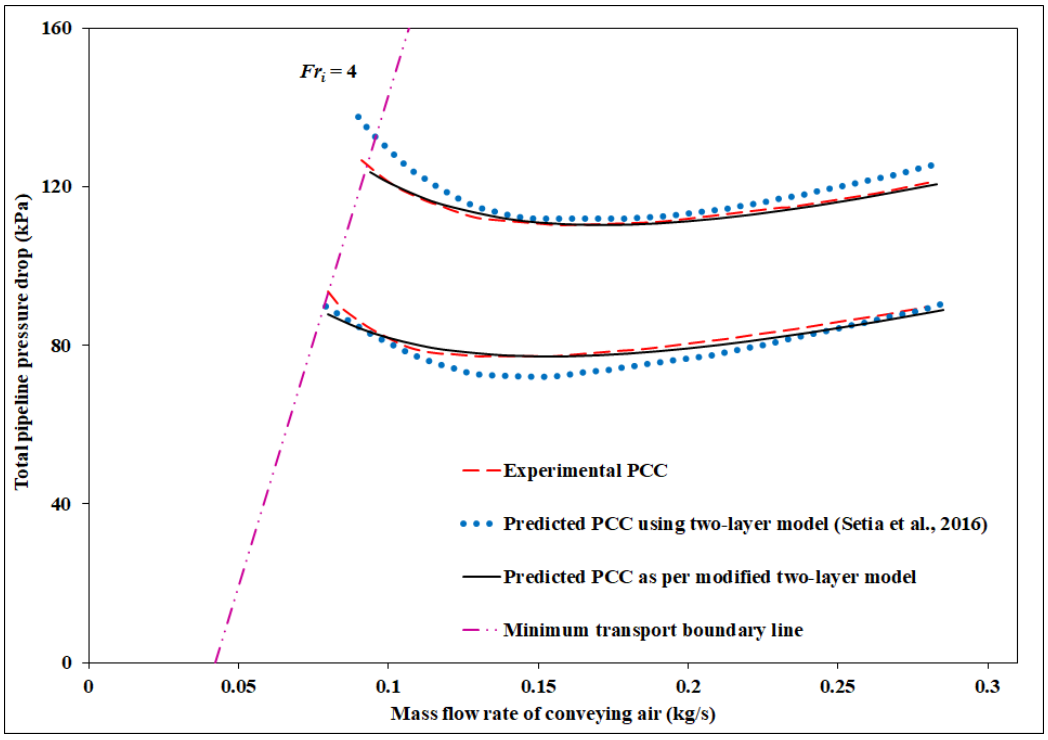

Figure 5.21: Scale-up validation for solids friction factor (modified two-layer model with rheology) for ESP dust through 105 mm I.D. × 168 m long pipe

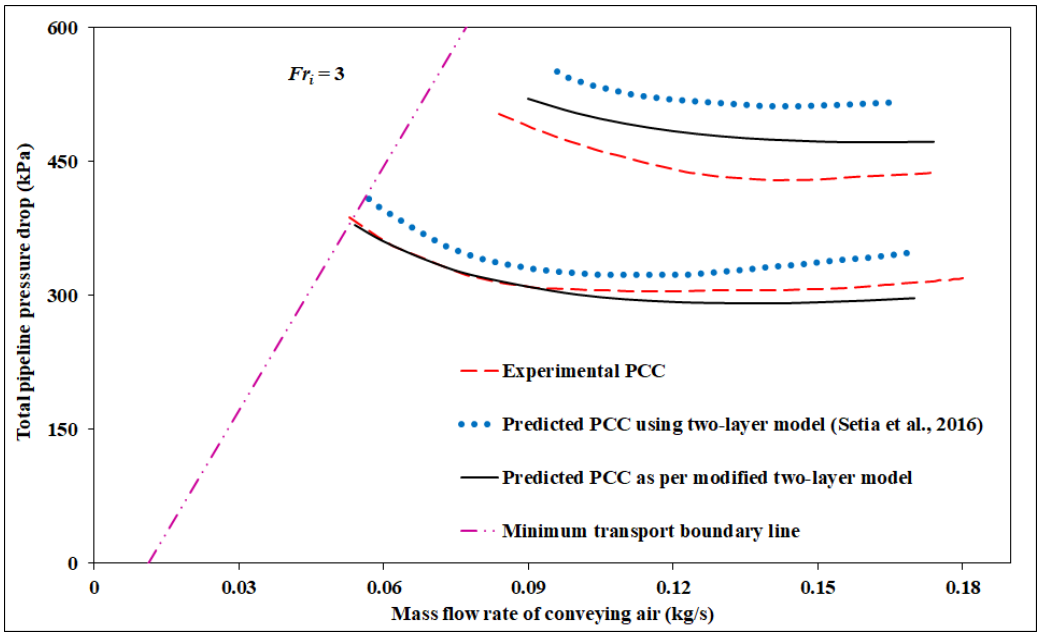

Figure 5.22: Scale-up validation for solids friction factor (modified two-layer model with rheology) for ESP dust through 69 mm I.D. × 554 m long pipe

Figure 5.19 shows the results of scale-up validation for fly ash conveyed through the pipeline viz. 69 mm I.D. × 554 m long pipeline corresponding to the different mass flow rate of solids (7 t/h: bottom lines and 11 t/h: top lines). The results indicate that for fly ash in 69 mm I.D. × 554 m long pipeline configuration, the newly developed rheological two-layer model format with inclusion of developed unified particle velocity model with variable fluidized bulk density and energy loss impact provides better predictions from dense to dilute-phase region in comparison with the Setia et al. (2016) model for almost both mass flow rates of solids (7 t/h: bottom lines and 11 t/h: top lines). The results of scale-up validation for fly ash conveyed through the pipeline viz. 105 mm I.D. × 168 m long pipeline for the different mass flow rate of solids (18 t/h: bottom lines and 28 t/h: top lines) are shown in A4.1 (Annexure A4). Figure 5.20 shows the results of scale-up validation for cement conveyed through 80/100 mm I.D. × 407 m long pipeline corresponding to

the different mass flow rate of solids (18 t/h: bottom lines and 36 t/h: top lines). The results show that for cement (80/100 mm I.D. × 407 m long pipeline), the newly developed rheological two-layer model format with inclusion of developed unified particle velocity model with variable density and energy loss impact provides better predictions from dense to dilute-phase region in comparison with the Setia et al. (2016) model for higher (36 t/h: top lines) mass flow rate. On the other hand, the newly developed rheological two-layer model format shows satisfactorily better prediction in the very dense-phase region and almost similar prediction in the dilute-phase region for lower mass flow rate (18 t/h: bottom lines) with the existing two-layer model format developed by Setia et al. (2016). The results of scale-up validation for fly ash conveyed through the pipeline viz. 80/100 mm I.D. × 407 m long pipeline corresponding to the different mass flow rate of solids (20 t/h: bottom lines and 30 t/h: top lines) are shown in A4.2 (Annexure A4). In order to test the accuracy of the newly developed rheological two-layer model format presented in equation (5.27), the scale-up predictions for very fine powder (i.e., for ESP dust) are also investigated. Figure 5.21 shows the results of scale-up validation for ESP dust conveyed through 105 mm I.D. × 168 m long pipeline corresponding to the different mass flow rate of solids (15 t/h: bottom lines and 25 t/h: top lines). The results show that for ESP dust (105 mm I.D. × 168 m long pipeline), the newly developed rheological two-layer model format with inclusion of developed unified particle velocity model with variable density and energy loss impact provides better prediction in very dense-phase and shows similar prediction in the dilute-phase region with the experimental curve for higher mass flow rate (25 t/h: top lines) in comparison with the existing two-layer model format developed by Setia et al. (2016), which shows slight over-prediction. On the other hand, it provides the almost same predictions from dense to dilute-phase flow regime for lower (15 t/h: bottom lines) mass flow rate, with the existing two-layer model format developed by Setia et al. (2016). Figure

5.22 shows the results of scale-up validation for ESP dust conveyed through the pipeline viz. 69 mm I.D. × 554 m long pipeline corresponding to the different mass flow rate of solids (6 t/h: bottom lines and 10 t/h: top lines). The results show that for ESP dust (69 mm I.D. × 554 m long pipeline), the newly developed rheological two-layer model format with inclusion of developed unified particle velocity model with variable density and energy loss impact provides better predictions from dense to dilute-phase region in comparison with the existing two-layer model format developed by Setia et al. (2016) for both mass flow rates (6 t/h: bottom lines and 10 t/h: top lines). In the present investigation, it has been observed from the Figures 5.19 to 5.22 that the newly developed rheological two-layer model format with effect of particle velocity with variable density and energy loss impact is able to predict better PCC (pneumatic conveying characteristics) results from dense to dilute-phase region for the respective mass flow rate of solids for the products conveyed under scale-up conditions.

CHAPTER 6

CONCLUSIONS AND FUTURE SCOPE OF WORK

6.1 Conclusions

The relative error values of predictions obtained using the "back-calculation" method are generally larger than that obtained using a "straight pipe" method by a maximum of 15%. The absolute error values obtained using the "back-calculation" method have been drastically reduced to a range of 3 to 35% from the earlier reported values of 40 to 150% inaccuracy. This significant improvement has been made possible due to the selection of an accurate format of modelling solids friction factor (two-layer modelling format) in the first place. Therefore, the selection of a better format of the model for solids friction factor could significantly improve the reliability of the "back-calculation" method. While the "straight pipe" modelling approach will remain as the preferred method for studying pneumatic conveying and solids friction from a more research/fundamental point of view, the significant improvement of accuracy of "back-calculation" technique could promote the "back-calculation" approach as a quicker method for conducting testing and modelling pressure drop for industrial designs considering the several practical benefits of performing pneumatic conveying trails, data analysis, cost, time, etc. associated with "back-calculation method". Based on the results presented in this chapter, it can be said that the "back-calculation" method generally provides up to 15% over-prediction compared to the straight-pipe model. This could be beneficial from an industrial system design point of view as this could provide a natural safety factor in predicting total pipeline pressure drop. However, while developing solids friction factor model using the "back-calculation" method, the pilot plant in the laboratory should not have too many bends or verticals, and the significant amount of pressure drops should come from the straight-horizontal pipe sections.

The author has numerically developed particle velocity models for different powders with and without the conditions of variable fluidized bulk densities using solid loading ratio and dimensionless velocity terms. Subsequently, the author developed a unified model for particle velocity model using solids loading ratio, dimensionless terms for velocity, diameter, and density. These particle velocity models, when employed in the existing two-layer model format for solids friction factor, has provided improved scale-up predictions (under diameter and length scale-up conditions) compared to the original two-layer model. The results indicated the importance of incorporating particle and actual gas velocity terms while modelling solids friction factor, especially for fluidized dense-phase (non-suspension) mode.

The authors developed a modified two-layer model with the inclusion of energy loss impact (occurred due to the particle-particle collision, particle-wall collision, and turbulence velocity fluctuations) and variable fluidized bulk density throughout the pipeline. Later on, the author linked the rheological studies with the fluidized dense-phase mode of pneumatic conveying with the aid of the newly developed model based on the concept of rheology. The predicted PCC (pneumatic conveying characteristics) results obtained from the modified two-layer model format have been validated for scale-up configurations of various pipeline lengths and diameters, respectively. The newly developed model incorporating the effects of rheology has been employed in the existing two-layer model format along with the concept of energy loss impact and variable fluidized bulk density. The results revealed that the modified two-layer model for solids friction factor provided better predictions under scale-up conditions (under diameter and length scale-up) in the non-suspension mode as compared to the existing two-layer model format.

6.2 Future scope of work

Further scope of work will include:

1. Experimental determination of particle velocity and volume fraction of solids and the inclusion of particle to particle agglomeration effect in the flow models for describing the pneumatic conveying of fine powders.
2. The future model of particle velocity should include the effects of the concentration gradient across the diameter of the pipe and coupling between solid to solid and gas to solid particles.
3. An attempt should be made to incorporate the effects of the particle size distribution (other than median particle diameter, d_{50}) in the future two-layer model format for determining solids friction factor.

REFERENCES

Ahmed, A. M., and Elghobashi, S., 2000. On the mechanisms of modifying the structure of turbulent homogeneous shear flows by dispersed particles. Physics of Fluids. 12 (11): 2906–2930.

Anjaneyiulu, P., and Khakhar, D.V., 1995. Rheology of a gas-fluidized bed. Powder Technology. 83: 29-34.

Arastoopour, H., Modi, M.V., Punwani, D.V., Talwalkar, A.T., 1979. A review of design equations for dilute-phase gas–solids horizontal conveying systems for coal and related materials. Philadephia. 339–355.

Barth, W., 1958. Flow processes during the transport of solid particles and liquid particles in gases, with special consideration of the processes of pneumatic conveying. Chemistry - Ing. – Techn. 30 (3): 171-180.

Barletta, D., and Poletto, M., 2013. A device for the measurement of the horizontal to vertical stress ratio in powders. Granular Matter. 15: 487–497.

Barletta, D., Donsì, G., Ferrari, G., Poletto, M., 2007. A rotational tester for the characterization of aerated shear flow of powders. Particle & Particle Systems Characterization. 24: 259–270.

Behera N., Agarwal V. K., Jones M.G., Williams K. C., 2013. Modeling and analysis of solids friction factor for fluidized dense phase pneumatic conveying of powders. Particulate Science and Technology. 31 (2): 136-146.

Behera, N., Agarwal, V. K., Jones, M.G., Williams, K. C., 2013a. Modeling and analysis for fluidized dense phase conveying including particle size distribution. Powder Technology. 235: 386–394.

Behera N., Agarwal V. K., Jones M., 2015. A model of solids friction factor for fluidized dense phase pneumatic conveying. Powder Technology. 284: 403-410.

Bose, M., and Kumaran, V., 2004. Velocity distribution for a two-dimensional sheared granular flow. Physical Review E. 69, 061301: 1-16.

Bose, M., Kumar, U. U., Nott, P. R., Kumaran, V., 2005. Brazil nut effect and excluded volume attraction in vibrofluidized granular mixtures. Physical Review E. 72, 021305: 1-9.

Bosse, T., Kleiser, L., and Meiburg, E., 2006. Small particles in homogeneous turbulence. Physics of Fluids. 18 (027102): 1-17.

Bruni, G., Barletta, D., Poletto, M. Lettieri, P., 2007. A rheological model for the flowability of aerated fine powders. Chemical Engineering Science. 62 (1–2): 397–407.

Bruni, G., Lettieri, P., Newton, D., Barletta, D., 2007a. An investigation of the effect of the interparticle forces on the fluidization behaviour of fine powders linked with rheological studies. Chemical Engineering Science. 62(1–2): 387–396.

Bruni, G., Colafigli, A., Lettieri, P., Elson, T., 2005. Torque measurements in aerated powders using a mechanically stirred fluidized bed rheometer (MSFBR). Chemical Engineering Research and Design, 83(A11): 1311–1318.

Cai L., Liu S., Pan X., Guiling X., Gaoyang Y., Xiaoping C., Changsui Z., 2014. Comparison of pressure drops through different bends in dense-phase pneumatic conveying system at high pressure. Experimental Thermal and Fluid Science. 57: 11-19.

Chambers, A.J., and Marcus, R.D., 1986. Pneumatic conveying calculations. In the proceedings of 2nd International Conference on Bulk Materials Storage and Transportation, Wollongong, Australia, 7–9 July: 49-52.

Chaudhry, B., 2015. Master's Dissertation: An experimental investigation into the rheology of fine powders for modelling fluidized dense-phase pneumatic conveying. Thapar University, India.

Chen, W., 2013. Ph.D. Dissertation: The rheology of aerated fine powders: Theory and Application in pneumatic conveying systems. The University of Newcastle, Australia.

Chunhui H., Xianmei C., Jianhao W., Hongliang N., Yupeng X., Haijun Z., Yuanquan X., Xianglin S., 2012. Conveying characteristics and resistance characteristics in dense phase pneumatic conveying of rice husk and blending of rice husk and coal at high pressure. Powder Technology. 227: 51-60.

Colafigli, A., Mazzei, L., Lettieri, P., Gibilaro, L., 2009. Apparent viscosity measurements in a homogeneous gas-fluidized bed. Chemical Engineering Science. 64: 144–152.

Desu, R. K., and Annabattula, R. K., 2019. Particle size effects on the contact force distribution in compacted polydisperse granular assemblies. Granular Matter. 21:29. https:// doi.org/10.1007/s10035-019-0883-9.

Fehlberg, E., 1969. Low-order classical Runge-Kutta formulas with step size control and their application to some heat transfer problems. NASA Technical Report 315.

Frank, T., Schade, K.P., and Petrak, D., 1993. Numerical simulation and experimental investigation of a gas-solid two-phase flow in a horizontal channel. International Journal of Multiphase Flow. 19 (1): 187-198.

Hong, J., and Shen, Y.S., 1994. Flow characteristics of high-density continuous conveying of solids. Engineering Chemistry and Metallurgy. 15: 122-128 (in Chinese).

Hinkle, B.L., 1953. Ph.D. Dissertation: Acceleration of particles and pressure drops encountered in horizontal pneumatic conveying, Institute of Technology, Georgia.

Huber, N., and Sommerfeld, M., 1998. Modelling and numerical calculation of dilute-phase pneumatic conveying in pipe systems. Powder Technology. 99: 90-101.

Jones, M. G., and Williams K. C., 2003. Solids friction factors for fluidized dense phase conveying. Particulate Science and Technology. 21: 45–56.

Jones, M.G., Mills, D., and Mason, J.S., 1987. Pneumatic conveying of high bulk density products. In the Proceedings of the Technical Program, Pneumatech 3, International Conference on pneumatic Conveying technology, Jersey, Channel Islands, England, 24-26 Mar: 371-396, Organized by the Powder Advisory Centre, London, England.

Kaur, B., Mittal A., Wypych P., Mallick, S.S., Jana, S., 2017. On developing improved modelling and scale-up procedures for pneumatic conveying of fine powders. Powder Technology 305, 270–278.

Kaur, B., Mittal, A., Mallick, S.S., Pan, R., Jana, S., 2017a. Numerical simulation of fluidized dense-phase pneumatic conveying of powders to develop improved model for solids friction factor. Particuology. 35:42-50.

Klinzing, G.E., Rohatgi, N.D., Zaltash, A., Myler, A., 1987. Pneumatic transport—a review (Generalized phase diagram approach to pneumatic transport). Powder Technology. 51: 135–149.

Klinzing, G.E., Myler, C.A., Zaltash, A., Dhodapkar, S., 1989. A simplified correlation for solids friction factor in horizontal conveying systems based on Yang's unified theory. Powder Technology. 58: 187-193.

Klinzing, G.E., Marcus, R.D., Rizk, F., Leung, L.S., 2010. Pneumatic Conveying of Solids – A Theoretical and Practical Approach. 3rd Edition. Springer.

Kuang, S. B., Li, K., Zou, R. P., Pan, R. H., Yu, A. B., 2013. Application of periodic boundary condition to CFD-DEM simulation of gas-solid flow in pneumatic conveying. Chemical Engineering Science. 93: 214–228.

Kuang, S. B., Zou, R. P., Pan, R. H., Yu, A. B., 2012. Gas solid flow and energy dissipation in inclined pneumatic conveying. Industrial & Engineering Chemistry Research. 51: 14289-302.

Levy, A., 2000. Two-fluid approach for plug flow simulations in horizontal pneumatic conveying. Powder Technology. 112: 263–272.

Li, H., and Tomita Y., 2000. Particle velocity and concentration characteristics in a horizontal dilute swirling flow pneumatic conveying. Powder Technology. 107: 144–152.

Li, K., Kuang, S.B., Pan, R.H., Yu, A.B., 2014. Numerical study of horizontal pneumatic conveying: effect of material properties. Powder Technology. 251: 15–24.

Liu, Z., Duan, G., and Wang, K., 2011. Numerical simulation of dense phase pneumatic conveying in long-distance pipe. Computational Simulations and Applications, Chapter 17, ISBN: 978-953-307-430-6, Available from: http://www.intechopen.com/books/computational-simulations-andapplications/numerical-simulation-of-dense-phase-pneumatic-conveying-in-long-distance-pipe. In Tech. 373–394.

Louge, M. Y., Mastorakos, E., and Jenkins, J. T., 1991. The role of particle collisions in pneumatic transport. Journal of Fluid Mechanics. 231: 345-359.

Mallick, S.S., 2009. Ph.D. Dissertation: Modelling dense-phase pneumatic conveying of powders, University of Wollongong, Australia.

Mi, B., and Wypych, P.W., 1994. Pressure drop prediction in low-velocity pneumatic conveying. Powder Technology 81: 125-137.

Mi, B., and Wypych P.W., 1995. Investigations into wall pressure during slug-flow pneumatic conveying. Powder Technology. 84: 91-98.

Mills, D., 2016. Pneumatic conveying design guide. Elsevier/Butterworth-Heinemann, 3rd Edition. ISBN: 978-0-08-100649-8.

Mills, D., Jones, M.G., and Agarwal, V.K., 2004. Handbook of Pneumatic Conveying Engineering, Marcel Dekker, Inc., ISBN: 0-8247-4790-9.

Mittal, A., 2016. Ph.D. Dissertation: Investigation into pressure signal fluctuations during fluidized dense-phase pneumatic conveying of powders, Thapar University, Patiala, India.

Miyazaki, K., Chen, G., Yamamoto, F., Ohta J., Murai, Y., Horii, K., 1999. PIV measurement of particle motion in spiral gas-solid two-phase flow. Experimental Thermal and Fluid Science. 19: 194–203.

Moscardini, M., Gan, Y., Annabattula, R.K., Kamlah, M., 2017. A Discrete Element Method to simulate the mechanical behavior of ellipsoidal particles for a fusion breeding blanket. Fusion Engineering and Design. 121: 22–31.

Oesterle, B., and Petitjean, A., 1993. Simulation of particle-to-particle interactions in gas-solid flows. International Journal of Multiphase Flow. 19 (1): 199-211.

Pan, R., and Wypych, P.W., 1992. Scale up procedures for pneumatic conveying design. Powder Handling and Processing. 4 (2): 167-172.

Pan, R., and Wypych, P.W., 1997. Pressure drop and slug velocity in low-velocity pneumatic conveying of bulk solids. Powder Technology. 94: 123-132.

Pan, R., 1992. Ph.D. Dissertation: Improving scale-up procedures for the design of pneumatic conveying systems, University of Wollongong, Australia.

Pan, R., and Wypych, P. W., 1998. Dilute and dense phase pneumatic conveying of fly ash. In the Proceedings of 6th International Conference on Bulk Materials Storage and Transportation, Wollongong, NSW, Australia:183–189.

Pu, W., Zhao, C., Xiong, Y., Liang, C., Chen, X., Lu, P., Fan, C., 2008. Three-dimensional numerical simulation of dense pneumatic conveying of pulverized coal in a vertical pipe at high pressure. Chemical Engineering Technology. 31 (2): 215–223.

Pu, W., Zhao, C., Xiong, Y., Liang, C., Chen, X., Lu, P., Fan, C., 2010. Numerical simulation on dense phase pneumatic conveying of pulverized coal in horizontal pipe at high pressure. Chemical Engineering Science. 65: 2500–2512.

Ratnayake, C., Datta, B.K., and Melaaen, M. C., 2007. A Unified scaling-up technique for pneumatic conveying systems. Particulate Science and Technology. 25 (3): 289-302.

Ratnayake, C., 2005. Ph.D. Dissertation: A Comprehensive Scaling Up Technique for Pneumatic Transport Systems, Norwegian University of Science and Technology (NTNU).

Rautiainen, A., Stewart, G., Poikolainen, V., and Sarkomaa, P., 1999. An experimental study of vertical pneumatic conveying. Powder Technology. 104: 139-150.

Rizk, F., 1982. Pneumatic transport in dilute and dense phase. Bulk Solids Handling. 2 (2): 235-241.

Saether, A., Arakaki C., Ratnayake C., and Di Ruscio D., 2009. Prediction of mass flow rate in pneumatic conveying using a system identification modeling approach. Particulate Science and Technology. 27 (4): 314-326.

Salehi, H., Sofia, D., Schütz, D., Barletta, D., and Poletto, M., 2018. Experiments and simulation of torque in Anton Paar powder cell. Particulate Science and Technology. 36 (4): 501-512.

Santo, N., Portnikov, D., Eshel, I., Taranto, R., Kalman, H., 2018. Experimental study on particle steady state velocity distribution in horizontal dilute phase pneumatic conveying. Chemical Engineering Science. 187: 354-366.

Schneiderbauer, S., Schellander, D., Löderer, A., Pirker, S., 2012. Non-steady state boundary conditions for collisional granular flows at flat frictional moving walls. International Journal of Multiphase. Flow 43: 149–156.

Setia, G., Mallick, S.S., Wypych, P.W., Pan, R., 2016. Modeling solids friction factor for fluidized dense-phase pneumatic transport of powders using two-layer flow theory. Powder Technology. 294: 80-92.

Setia, G., 2016a. Ph.D. Dissertation: Improving scale-up procedures for solids friction and minimum transport boundary for fluidized dense-phase pneumatic conveying systems. Thapar University, India.

Setia, G., and Mallick, S.S., 2015. Modelling fluidized dense-phase pneumatic conveying of fly ash. Powder Technology. 270: 39-45.

Setia, G., and S.S. Mallick., 2015a. Improved scale-up procedures for fluidized dense-phase pneumatic conveying systems. In the proceedings of 8th International Conference on Conveying and Handling of Particulate Solids, Tel-Aviv, Israel.

Setia, G., Mallick, S.S., and Wypych, P.W., 2014. On improving solid friction factor modelling for fluidized dense-phase pneumatic conveying systems. Powder Technology. 257: 88-103.

Sommerfeld, M., 2003. Analysis of collision effects for turbulent gas-particle flow in a horizontal channel: Part I. Particle transport, International Journal of Multiphase Flow. 29: 675-699.

Stegmaier, W., 1978. Zur berechnung der horinentalen pneumatischen forderung feinkorniger feststoffe - for the calculation of horizontal pneumatic conveying of fine-grained solids. Fordern and Heben. 28: 363-366.

Tanaka, T., and Tsuji, Y., 1991. Numerical simulation of gas-solid two-phase flow in a vertical pipe: on the effect of inter-particle collision. The American Society of Mechanical Engineers. 123-128.

Tripathi, A., and Khakhar, D. V., 2011. Numerical simulation of the sedimentation of a sphere in a sheared granular fluid: A granular stokes experiment. Physical Review Letters: American Physical Society 107: 108001:1-4.

Tripathi, A., and Khakhar, D. V., 2011. Rheology of binary granular mixtures in the dense flow regime. Physics of Fluids. 23, 113302:1-12.

Tripathi, N. M., Levy, A., and Kalman, H., 2018. Acceleration pressure drop analysis in horizontal dilute phase pneumatic conveying system. Powder Technology. 327: 43–56.

Tsuji, Y., Oshima, T., and Morikawa, Y., 1985. Numerical simulation of pneumatic conveying in a horizontal pipe. KONA Powder and Particle Journal. 3: 38–51.

Vångö, M., Pirker, S., and Lichtenegger, T., 2018. Unresolved CFD–DEM modeling of multiphase flow in densely packed particle beds. Applied Mathematical Modelling. 56: 501–516.

Weber, M., 1981. Principles of hydraulic and pneumatic conveying in pipes. Bulk Solids Handling. 1: 57-63.

Weber, M., 1991. Friction of the air and the air/solid mixture in pneumatic conveying. Bulk Solids Handling. 11 (1): 99-102.

Wei, W., Qingliang, G., Yuxin, W., Hairui, Y., Jiansheng, Z., Junfu. L., 2011. Experimental study on the solid velocity in horizontal dilute phase pneumatic conveying of fine powders. Powder Technology 212: 403-409.

Williams, K.C., and Jones, M.G., 2004. Numerical model velocity profile of fluidized dense phase pneumatic conveying. In the proceedings of 8th International Conference on Bulk Materials Storage and Transportation, Wollongong, NSW, Australia, 5-8 July: 354-358.

Wypych, P.W., 1989. Ph.D. Dissertation: Pneumatic conveying of bulk solids, University of Wollongong, Australia.

Wypych, P.W., Kennedy, O.C., and Arnold, P.C., 1990. The future potential of pneumatically conveying coal through pipelines. Bulk Solids Handling. 10 (4): 421-427.

Wypych, P.W., Kennedy, O.C., and Arnold, P.C., 1990a. Pneumatic conveying of pulverized and crushed R.O.M. coal. In the proceedings of 4th International Conference on Pneumatic Conveying Technology, Glasgow, Scotland, 26-28 June: 159-173.

Wypych, P.W., and Arnold, P.C., 1984. The use of powder and pipe properties in the prediction of dense phase pneumatic transport behaviour. In the Proceedings of the Technical Program, Pneumatech 2, International Conference on Pneumatic Conveying Technology, University of Kent, Canterbury, England, 4-6 September, Organized by the Powder Advisory Centre, London, England.

Wypych, P.W., and Arnold, P.C., 1987. On improving scale-up procedures for pneumatic conveying design. Powder Technology, 50: 281–294.

Yan, F., and Rinoshika, A., 2011. Application of high-speed PIV and image processing to measuring particle velocity and concentration in a horizontal pneumatic conveying with dune model. Powder Technology. 208 (1): 158–165.

Zhao, Y., and Wei, L., 2000. Rheology of gas-solid fluidized bed. Fuel Processing Technology. 68: 153–160.

ANNEXURE A1

LAYOUTS OF DIFFERENT EXPERIMENTAL SET-UPS (OF OTHER RESEARCH LABORATORIES) USED IN THE PRESENT THESIS WORK

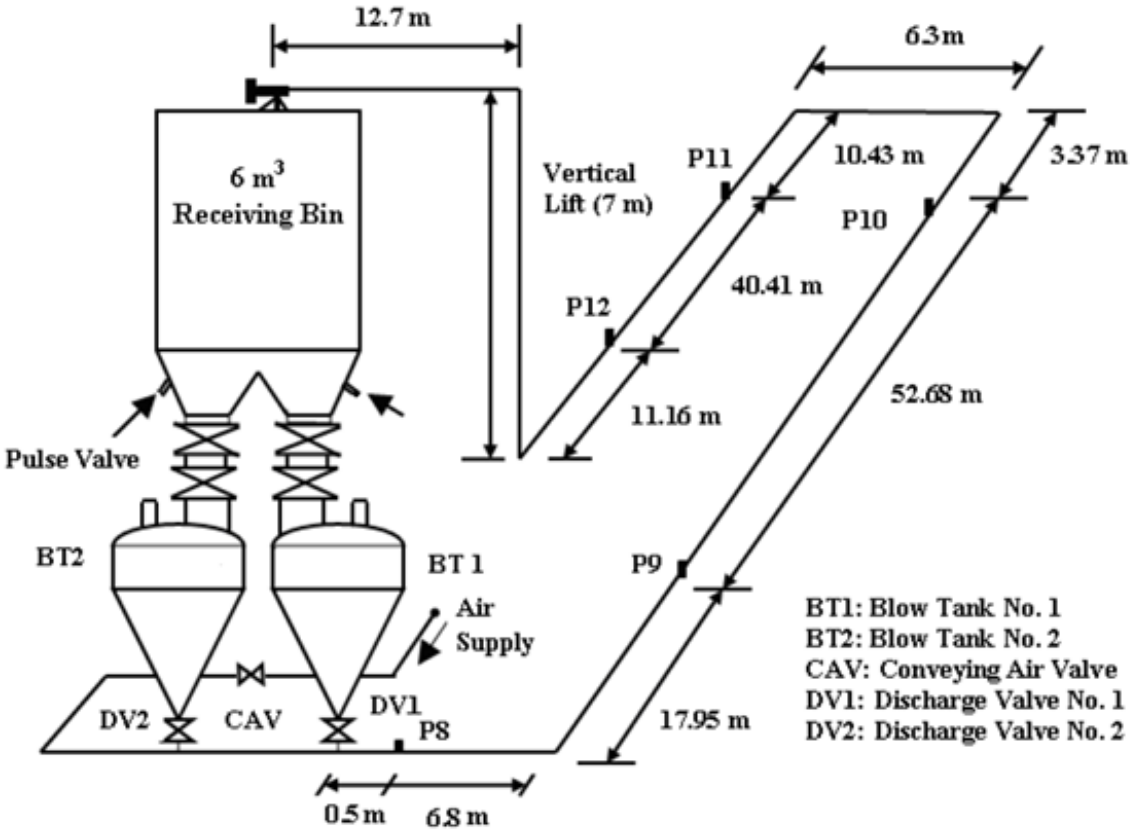

Figure A1.1: Layout of the 69 mm I.D. x 168 m test rig (for fly ash) (Mallick, 2009)

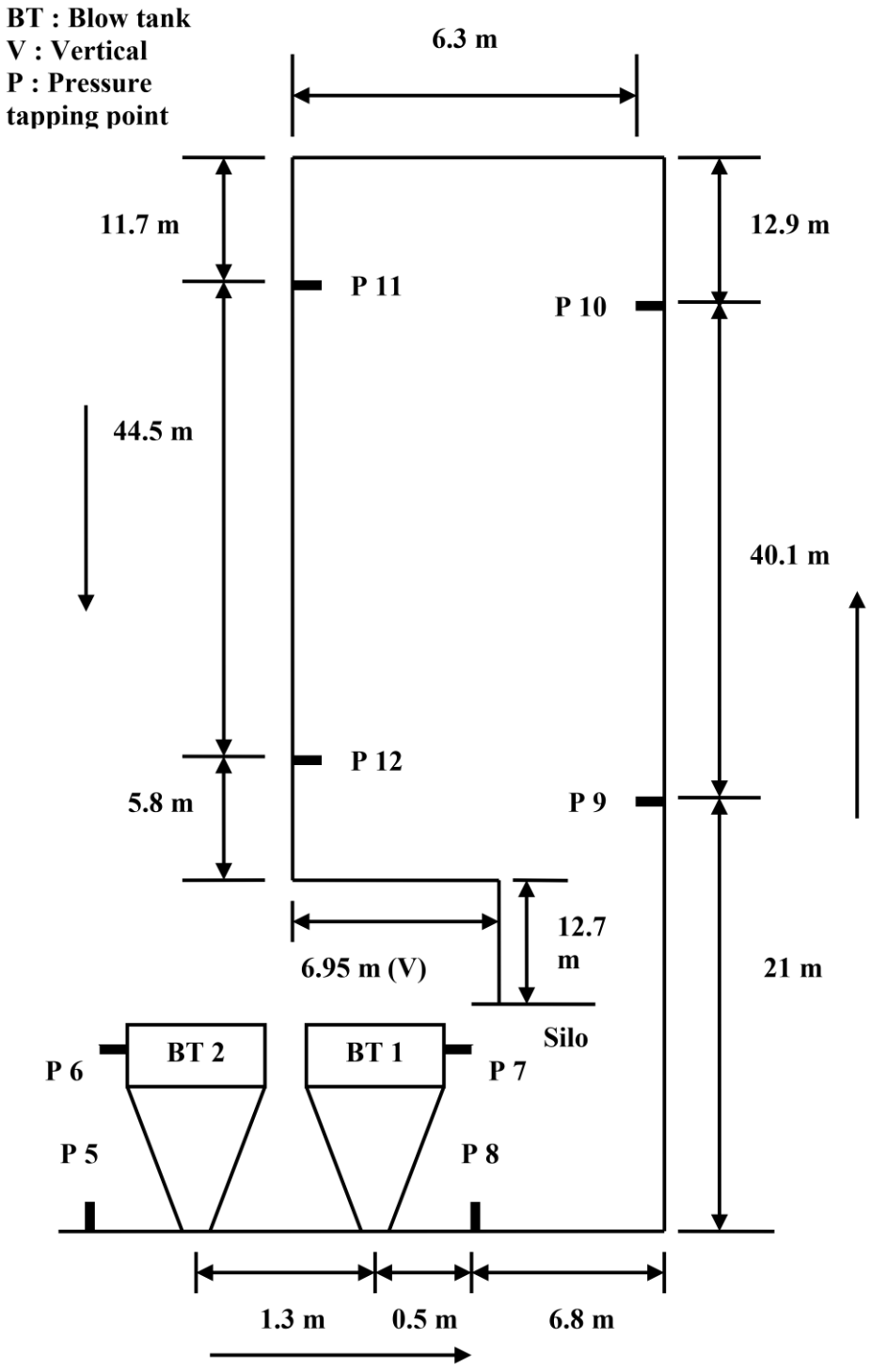

Figure A1.2: Layout of the 105 mm I.D. x 168 m test rig (for fly ash) (Mallick, 2009)

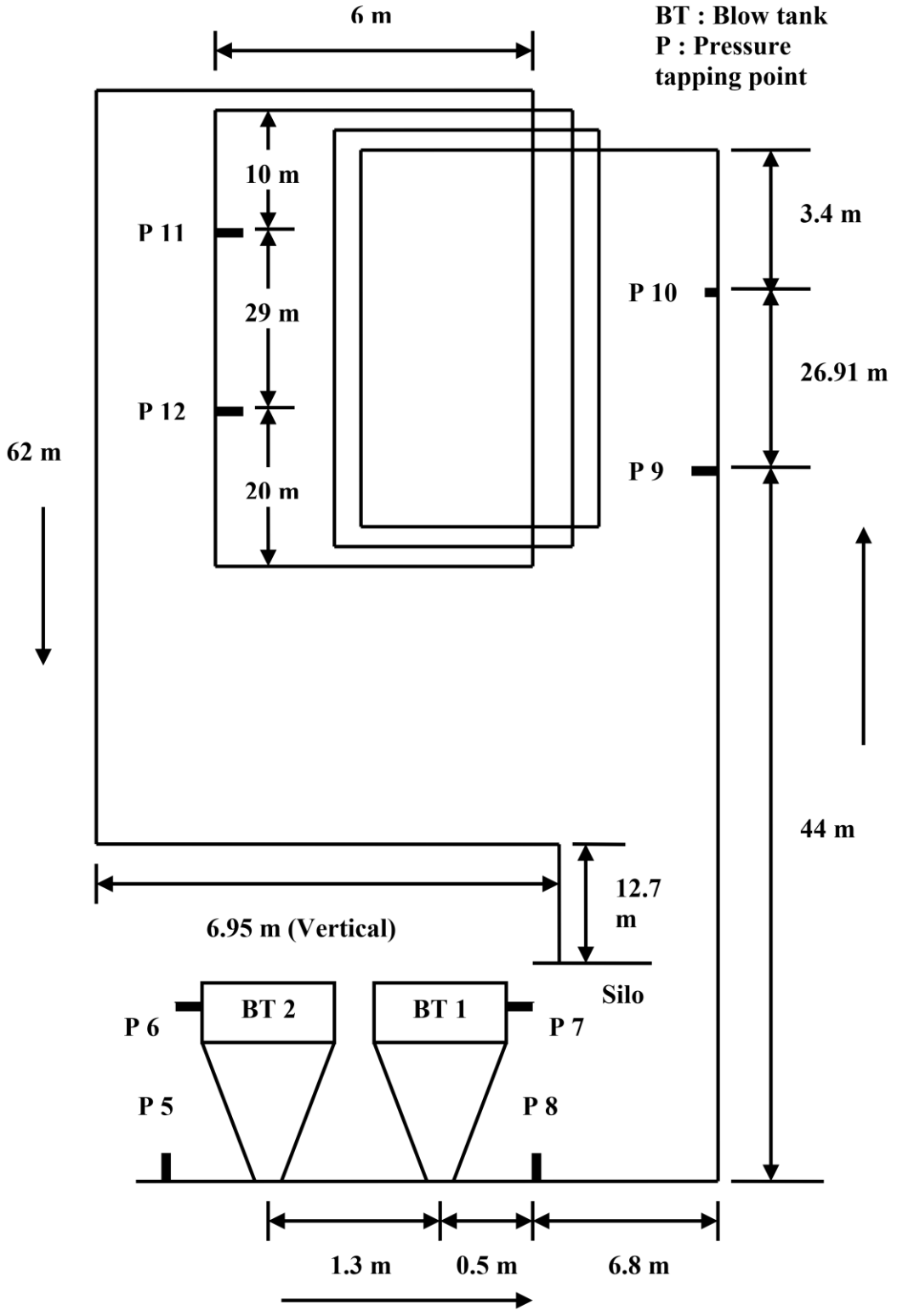

Figure A1.3: Layout of the 105 mm I.D. x 168 m test rig (for fly ash) (Mallick, 2009)

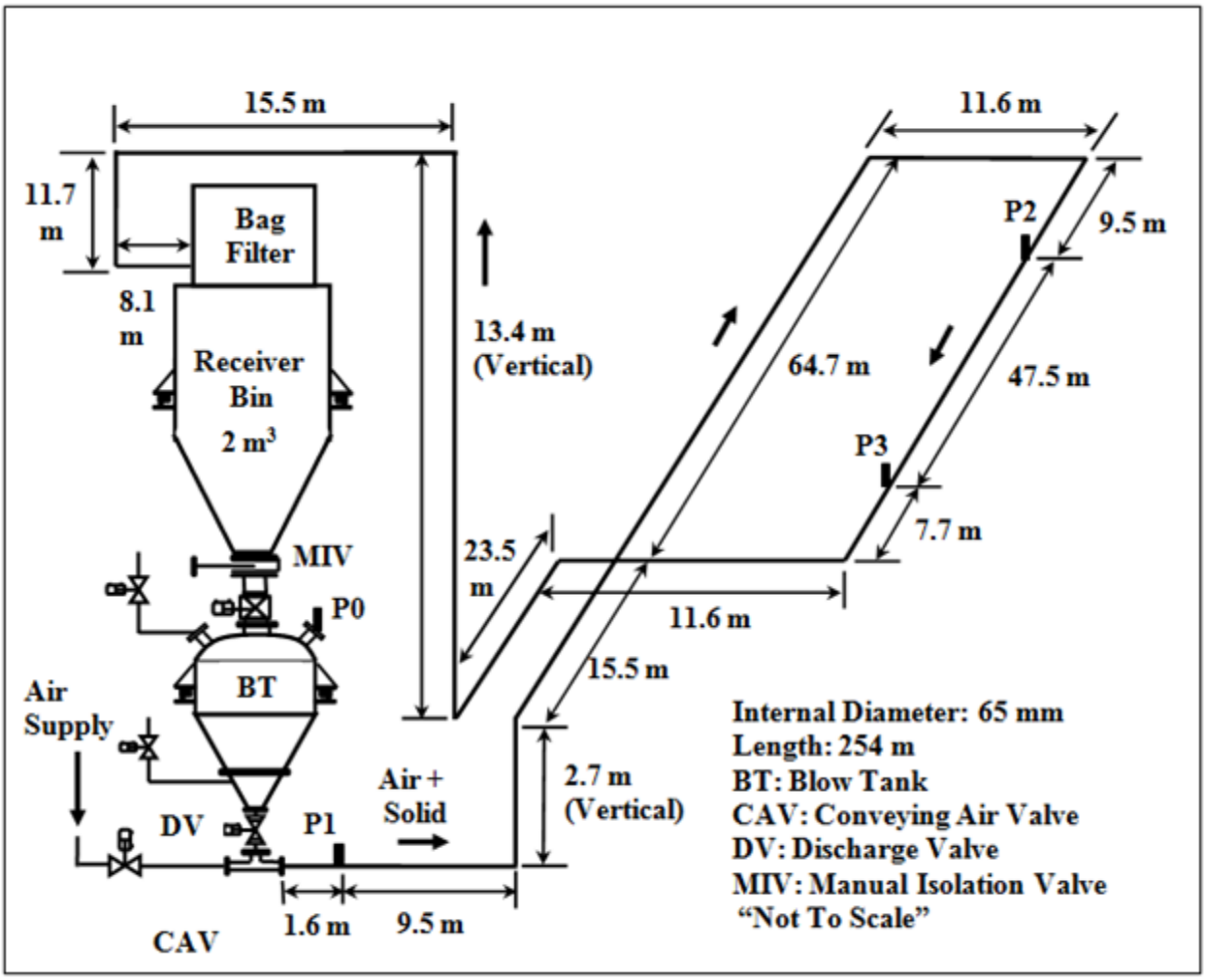

a) 65 mm I.D. × 254 m long pipeline test rig

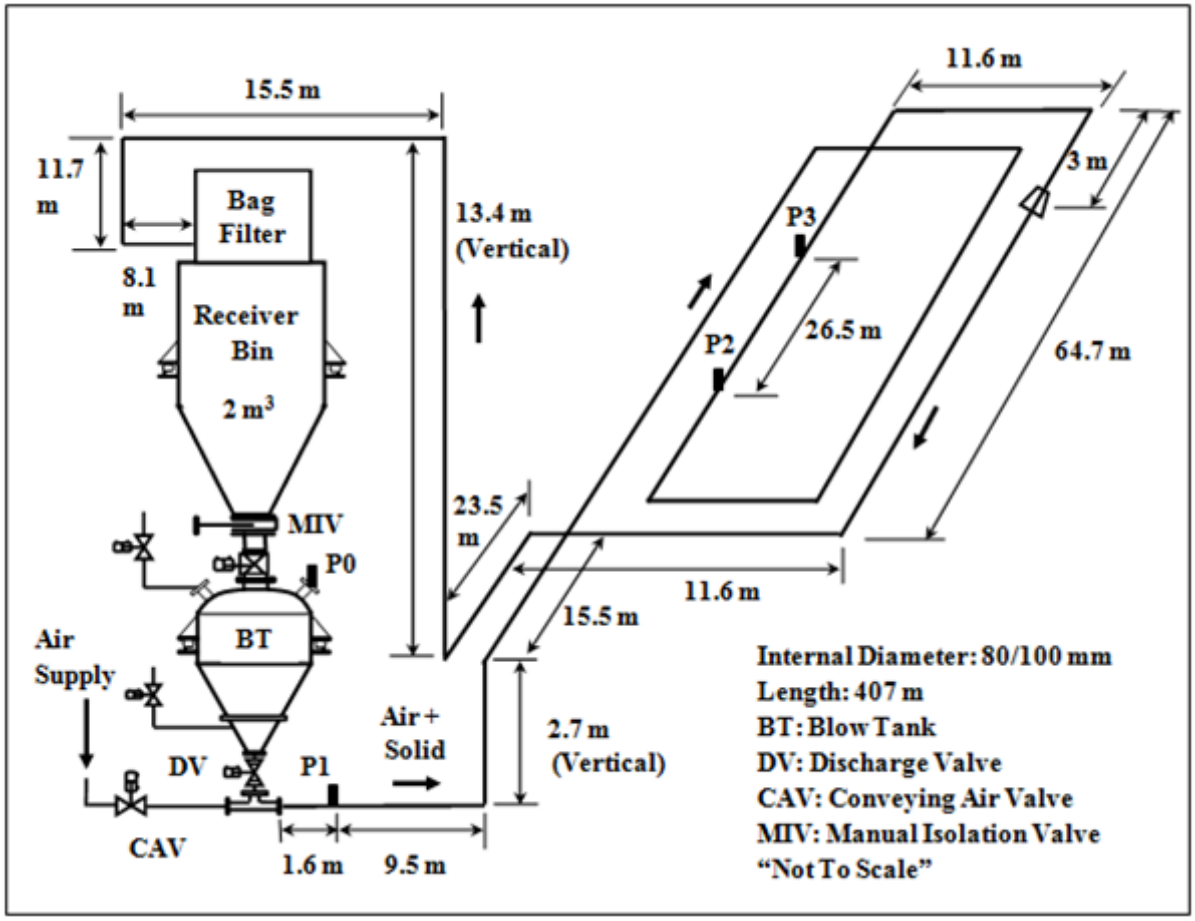

b) 80/100 mm I.D. × 407 m long stepped pipeline test rig

Figure A1.4: Schematic diagrams of the test rigs at Fujian Longking Co., Ltd., China (Setia, 2016)

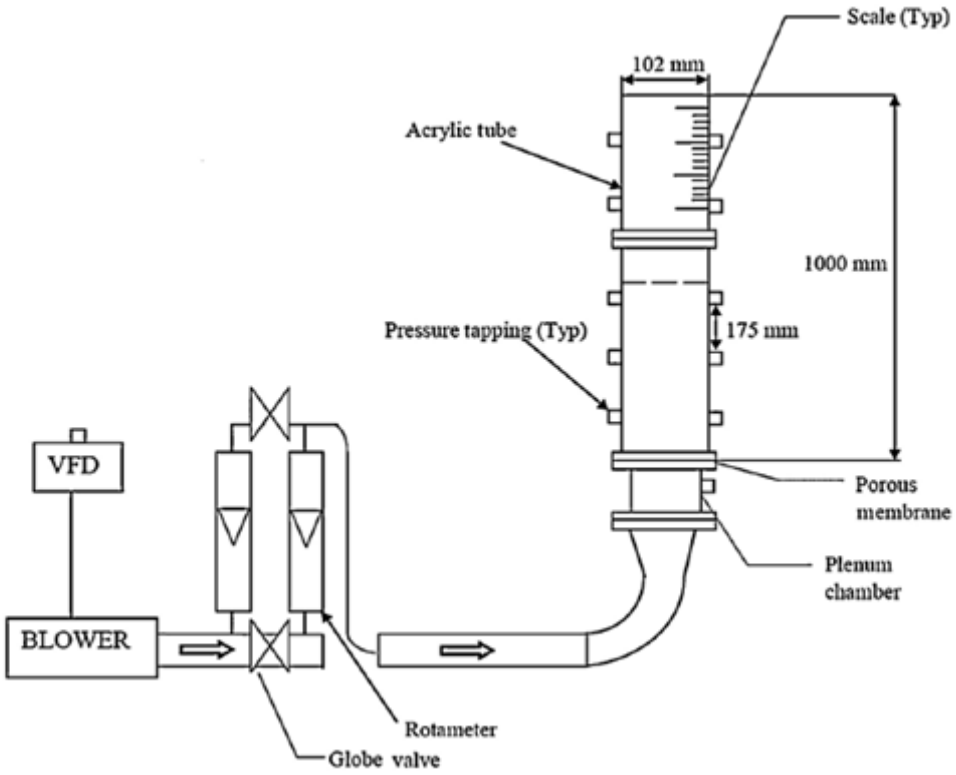

Figure A1.5: Fluidization and de-aeration chamber used to determine fluidized bulk density of fly ash powders (Kaur et al., 2017)

ANNEXURE A2

PRELIMINARY INVESTIGATION TO MODEL

SOLIDS FRICTION FACTOR

This section deals with the estimation and evaluation of solids friction factor term with various proposed approaches, such as combined solids-gas friction approach and modified Barth equation approach. This work was carried out in the initial part of the thesis. The attempt was to carry out certain basic changes in the format of Barth equation and the way solids and gas friction factors are approached separately while modelling pipeline pressure drop due to solids-gas flows. Unfortunately, such attempts did not result in any improvement in modelling prediction capabilities, and it was decided that effort should be focused to improve the two-layer modelling approach of Setia et al. (2016) to achieve step-wise better in prediction capability in a definite direction. However, for the purpose of completeness, some portion of these initial attempts have been included in this thesis in Annexure.

A2.1 Combined solids-gas friction approach

Weber (1991) introduced a unique approach to represent the pressure drop in the pipeline (as already discussed in Chapter 1). He suggested that the pressure drop of the solids air mixture was inseparable in nature (i.e., the pressure drop due to solids-only and that due to the air-only were difficult to separate individually). This happens due to the intense mixing nature of the non-suspension flow mode regime. Therefore, in 1991, Weber developed a new format of representing pressure drop, which is represented in Chapter 1 (refer equation 1.11). The model format presented in the equation (1.11) has been validated by Mallick (2009) under scale-up configurations. He validated with the help of using dimensionless numbers based on the format of equation (1.4) given in Chapter 1. It has been found that using the model represented by equation (1.12), pressure drop predictions under significant scale-up conditions of respective pipeline lengths and diameter did

not come well (i.e., gross inaccurate predictions). However, an effort should be made to discover the usage of other dimensionless terms (Volumetric Loading ratio and w_{fo}/V) provided by equation (1.8) in Chapter 1, because in the opinion of various researchers (Setia et al., 2015) this model format has a good potential to provide promising predictions under scale-up situations. Therefore, there is a probability that the format given by equation (1.8) is more appropriate for fluidized dense-phase flow, and it is only the selection of dimensionless terms that are causing the inaccurate predictions associated with equation (1.4). The first main objective of this chapter is to examine the reliability of the format given by equation (1.8) by using the terms volumetric loading ratio (VLR) and dimensionless velocity (w_{fo}/V) in the combined model (considering solid and air as an integral mixture). The modified form of Barth (1958) equation with the combined model (λ_T) approach is shown by equation (A2.1).

$$\lambda_T = K\,(VLR)^a\,\left(\frac{w_{fo}}{V}\right)^b \qquad (A2.1)$$

where VLR is represented by equation (A2.2):

$$VLR = \left\{\left(m_s/\rho_{fl}\right)/\left(m_a/\rho_a\right)\right\} \qquad (A2.2)$$

The above-proposed model format represented by equation (A2.1) has been used to estimate the combined solids-gas friction factor term. Rautiainen et al. (1999) used solids volume fraction to model pneumatic conveying of solids and stated that the slip velocity of particles is greatly influenced by the solids volume concentration. The free gas path is affected by the occupied volume of solids as the gas would need to follow the circuitous path available through the solid

particles. This non-linear gas path would contribute to the pressure drop of the gas-phase. In the opinion of Bosse et al. (2006), “two-way coupling” is appropriate for the non-suspension type of flow, where the gas and fine solids are expected to influence the turbulence of each other. Similar conclusions were made by Ahmed and Elghobashi (2000), who concluded that the gas and fine solids would influence the turbulence of each other and vorticity dynamics of the flow. Huber and Sommerfield (1998) concluded that the volume concentration of solids would influence the turbulence pattern of the gas-phase. Therefore, the volumetric loading ratio (VLR) has been considered as a suitable dimensionless parameter to model solids-air combined friction factor. To identify whether the flow mode is in non-suspension or suspension mode, another dimensionless term w_{f0}/V has been introduced in the model. The least-square technique has been used to model the combined solids-air friction factor (λ_T) using steady-state P11-P12 data (i.e., straight pipe pressure tapping data) of fly ash conveying through the 69 mm I.D. x 168 m long pipe (see Figure A1.1). The newly developed model for fly ash has been shown in Table A2.1. The format of the newly developed model has been represented by equation (A2.1). The high values of R^2 indicate a good fit. The high values of ‘K’ may induce unstable predictions during scale-up validations.

Table A2.1: New model developed using combined solids-gas friction format

(in the form of equation A2.1)

Product	Model (as per the format provided by equation A2.1)				R^2	Model type
	K	a	b	w_{fo} (m/s)		
Fly ash (Mallick, 2009)	$10^{4.256}$	0.417	1.825	0.06	0.99	Combined solids-gas friction model format (equation A2.1)

To evaluate the relative accuracy of the newly developed combined model approach for solids-gas, predictions obtained from a recently developed uniform flow model format by Setia et al. (2015) have been superimposed on Figure A2.1. The model developed by Setia et al. (2015) has been provided by Table A2.2 for comprehensiveness for fly ash, respectively. Note that the format used by Setia et al. (2015) is as per Barth equation, i.e., it considers the losses due to air and solids separately.

Table A2.2: Model developed using uniform flow format (Setia et al., 2015)

Product	Model (as per the format provided by equation 1.8)				R^2	Model type
	K	a	b	w_{fo} (m/s)		
Fly ash, Mallick (2009)	7.94	-0.26	1.51	0.06	0.98	Uniform flow model format (equation 1.8)

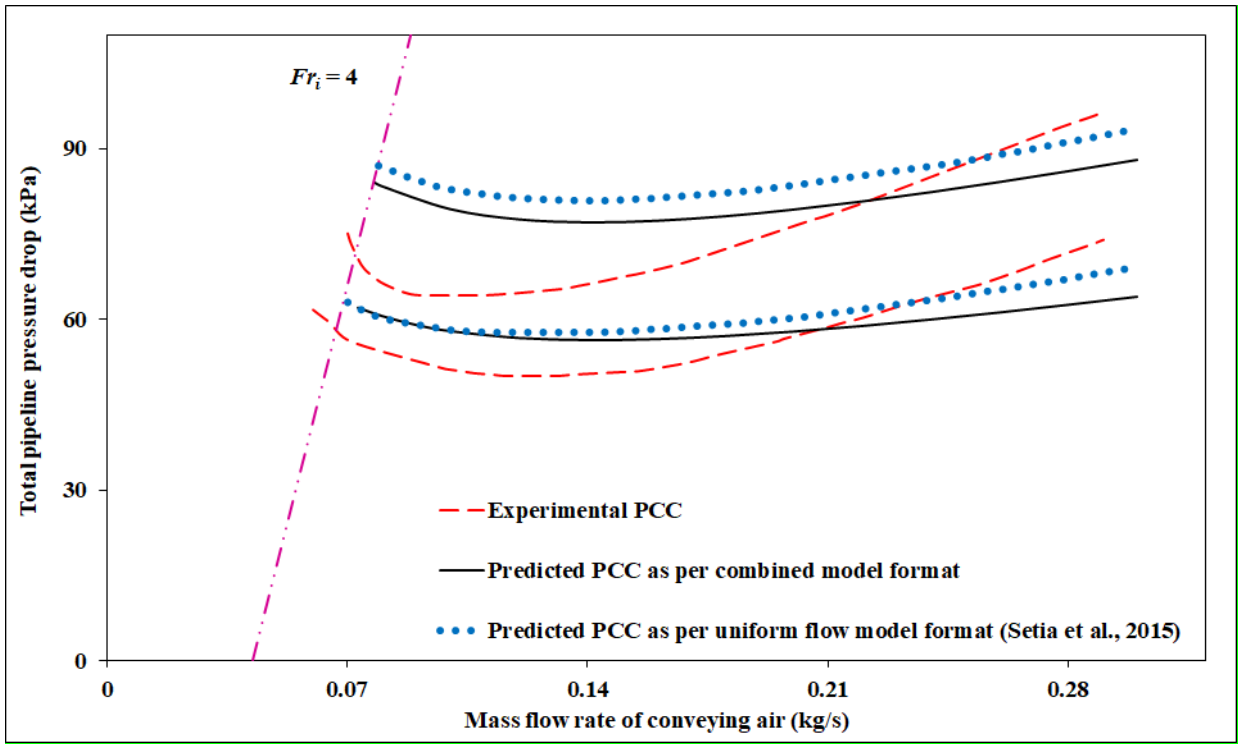

Figure A2.1: Scale-up evaluation for combined solids-gas friction factor for fly ash through 105 mm I.D. × 168 m long pipe

Figure A2.1 shows the results of pressure drop evaluations in scale-up conditions for combined solids-gas friction factor for fly ash conveyed through the 105 mm I.D. × 168 m long pipeline corresponding to the different mass flow rate of solids (18 t/h: bottom lines and 28 t/h: top lines). For the 105 mm I.D. × 168 m long pipe, the combined model approach provides almost similar predictions in very dense-phase region and some very slight under-prediction at dilute-phase region in comparison with the uniform flow model format developed by Setia et al. (2015) for a lower mass flow rate of solids (i.e., 18 t/h). However, for a higher mass flow rate of solids (i.e., 28 t/h), the combined model approach (equation A2.1) provides better predictions in the very dense-phase region and slight under-prediction at the dilute-phase region in comparison with the uniform flow model format developed by Setia et al. (2015). Subsequently, the combined solids-gas friction

model approach is further evaluated by applying it to predict the total pipeline pressure losses for fly ash (69 mm I.D. × 554 m long pipes). The results are shown in Figure A2.2. It can be seen that the combined model format resulted in highly inaccurate results for length scale-up conditions. It was decided not to pursue this format any further.

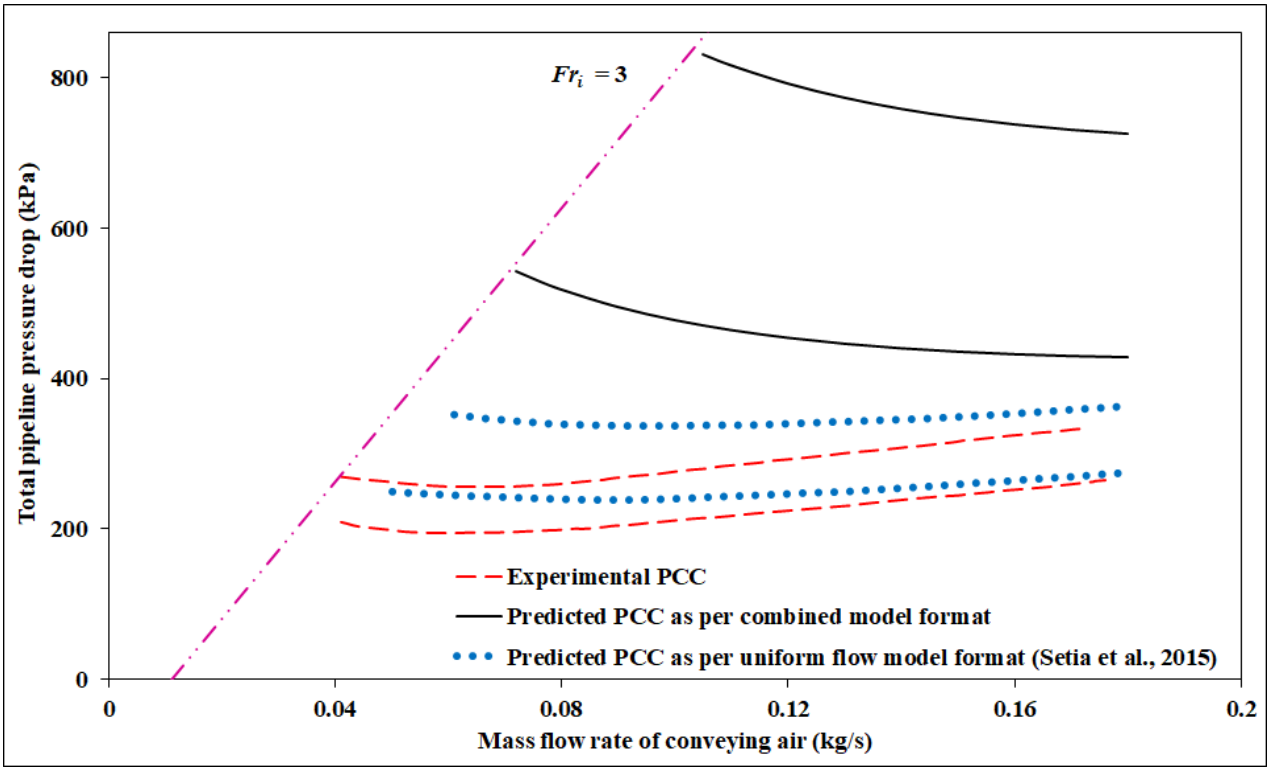

Figure A2.2: Scale-up evaluation for combined solids-gas friction factor for fly ash through 69 mm I.D. × 554 m long pipe

A2.2 Amended Barth equation approach

The existing pressure drop models are based on the Barth's approach (Barth 1958) provided by equation (1.1) in Chapter 1 and using the "straight pipe" pressure drop data in order to model the solids friction factor (Mallick 2009). In the opinion of Mallick (2009), Barth equation format

mainly depends on the solids loading ratio term, which is then multiplied by solids friction factor (which shows direct or indirect involvement of solids loading ratio term). As a result, it is believed that the Barth equation format is integrally influenced by the solids loading ratio term. Therefore, it is significant to evaluate a model format that will not include solids loading ratio term. A proposed format is provided by equation (1.16) in Chapter 1, which is termed here as the amended Barth format. The proposed model format represented by equation (1.16) has been used to estimate the solids friction factor term. The least-square technique has been used to model the solids friction using an amended Barth equation approach using steady-state P11-P12 data (i.e., straight pipe pressure tapping data) of fly ash conveying through the 69 mm I.D. x 168 m long pipe (Mallick 2009, see Figure A1.1). The newly developed model for fly ash has been shown in Table A2.3. The format of the newly developed model based on the equation represented by equation (1.10). The high values of R^2 indicate a good fit.

Table A2.3: New model developed using two-layer modelling format

(in the form of equation 1.10)

Product	**Model (as per the format provided by equation 1.10)**					**R^2**	**Model type**
	K	a	b	w_{fo} (m/s)	λ_s^*		
Fly ash (Mallick, 2009)	10^4	0.464	1.656	0.06	0.0273	0.995	Two-layer flow model format (equation 1.10)

To evaluate the relative accuracy of the newly developed amended Barth equation approach for solids-gas, predictions obtained from a recently developed two-layer flow model format by Setia et al. (2016) have been superimposed on Figure A2.3. The model developed by Setia et al. (2016) has been provided by Table A2.4 for comprehensiveness for fly ash, respectively. Note that the format used by Setia et al. (2016) is as per Barth equation, i.e., it considers the inclusion of solids loading ratio term (m^*).

Table A2.4: Model developed using two-layer modelling format (Setia et al., 2016)

Product	**Model (as per format based on the equation 1.10)**					**R^2**	**Model type**
	K	a	b	w_{fo} (m/s)	λ_s^*		
Fly ash (Mallick, 2009)	8.04	-0.22	1.48	0.06	0.0043	0.98	Two-layer flow model format (Setia et al., 2016)

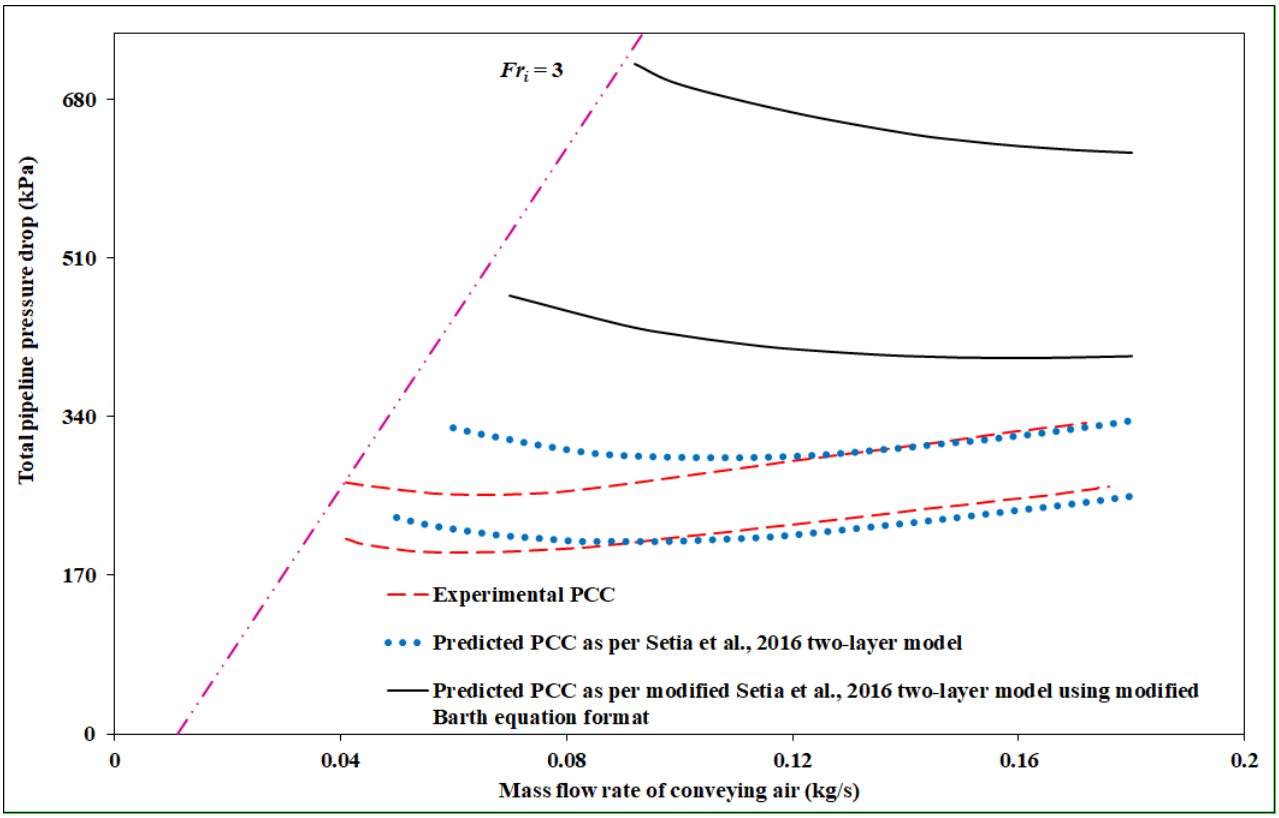

Figure A2.3: Scale-up evaluation using a modified Barth equation format (Two-layer) for fly ash through 69 mm I.D. × 554 m long pipe

Figure A2.3 shows the results of pressure drop evaluations in scale-up conditions for modified Barth equation format for fly ash conveyed through the 69 mm I.D. × 554 m long pipeline corresponding to the different mass flow rate of solids (7 t/h: bottom lines and 11 t/h: top lines). For the 69 mm I.D. × 105 m long pipe, the modified Barth equation model approach provides large over-predictions from dense- to dilute-phase flow phase flow regimes in comparison with the existing two-layer flow model format developed by Setia et al. (2016) for both mass flow rate of solids (7 t/h: bottom lines and 11 t/h: top lines). Subsequently, it was decided not to pursue the amended Barth equation approach.

A2.3 Development of VLR curves

This section deals with the development of VLR curves for straight pipeline pressure drop per unit length vs mass flow rate of air. Figures A2.4 to 2.20 shows “straight-pipe” pneumatic conveying characteristics with constant volumetric loading ratio (VLR) curves for fly ash and cement with various pipeline configurations along with the different straight pipe sections. It has been observed that with progressively increased mass flow rates of air, all constant VLR curves become straight with slowly decreasing of VLR values (from fluidized dense-phase to dilute-phase). This is due to the fact that, in accordance with the concept of VLR model presented in equation (1.8) given by Setia et al. (2015), the concept of volumetric loading ratio approach works well only in the dense-phase (already discussed in Chapter 1), hence higher values of volumetric loading ratio can be seen in dense-phase zone (more curvilinear structure) in the Figures A2.4 to 2.20 which decreases as we entered in the dilute-phase zone (less curvilinear structure).

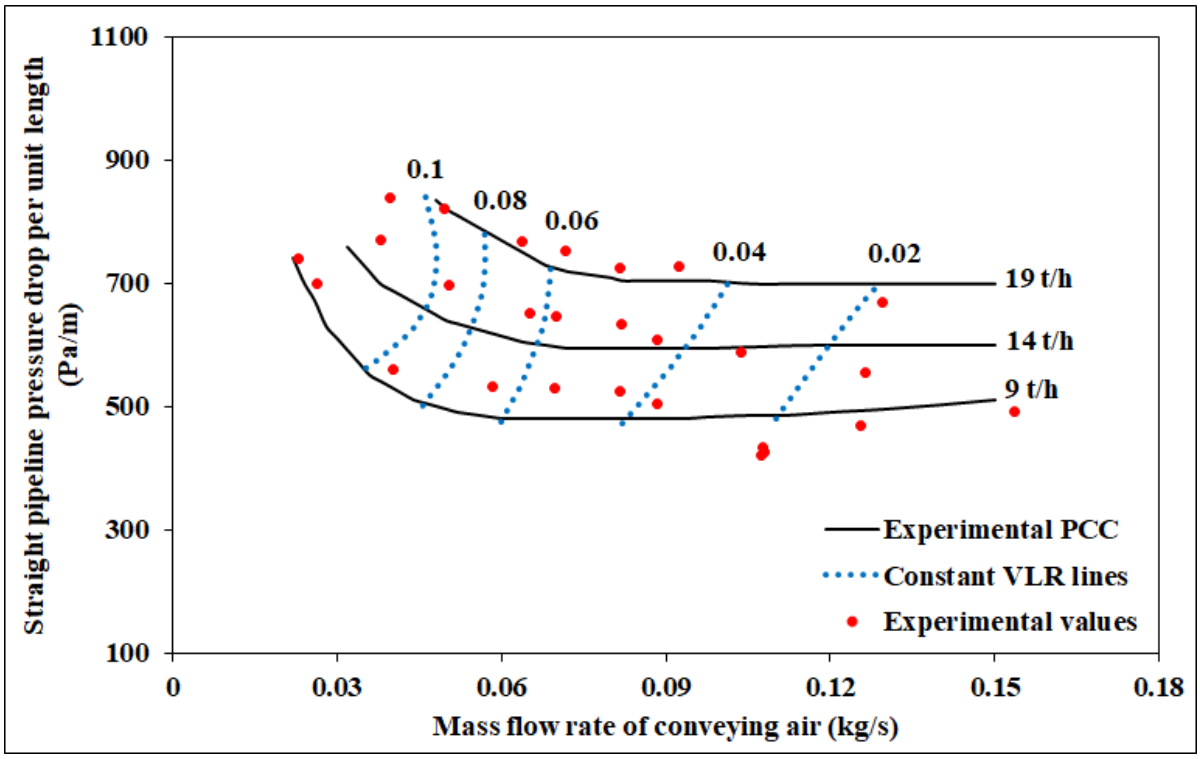

Figure A2.4: VLR curves for fly ash through 69 mm I.D. × 168 m long pipe (P9-P10 section)

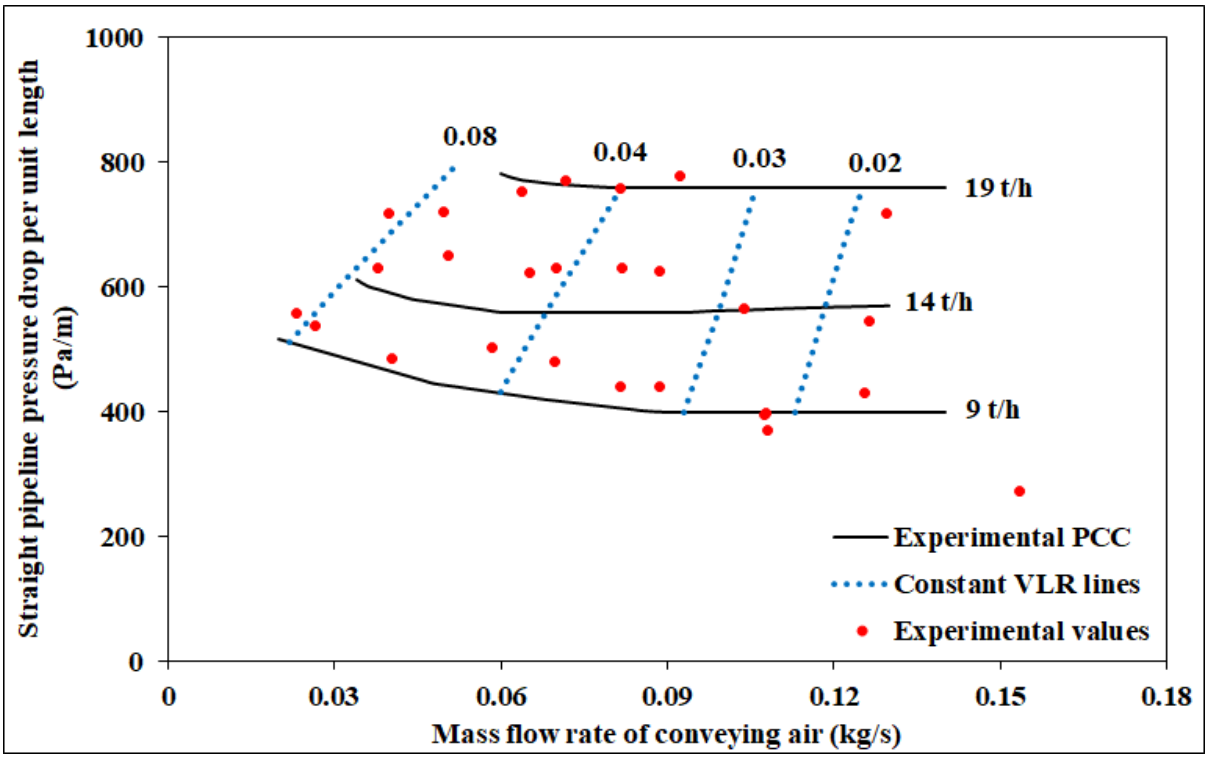

Figure A2.5: VLR curves for fly ash through 69 mm I.D. × 168 m long pipe (P11-P12 section)

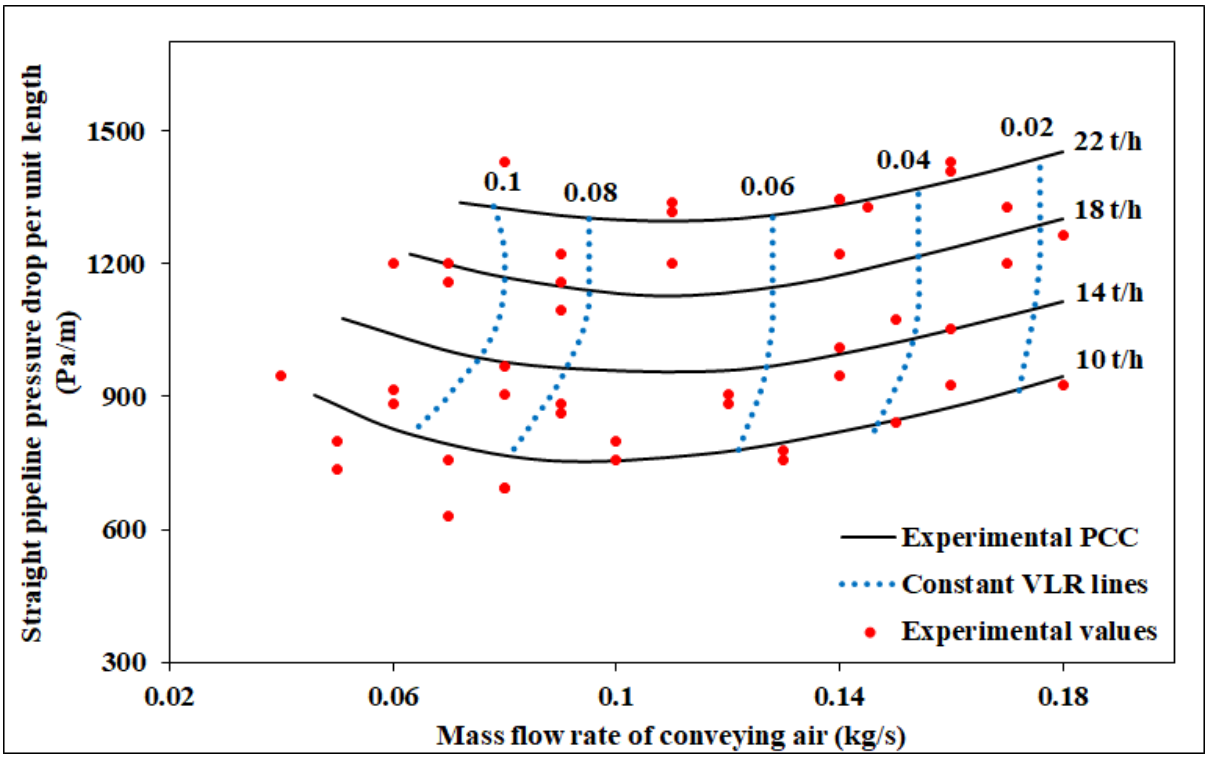

Figure A2.6: VLR curves for cement through 65 mm I.D. × 300 m long pipe

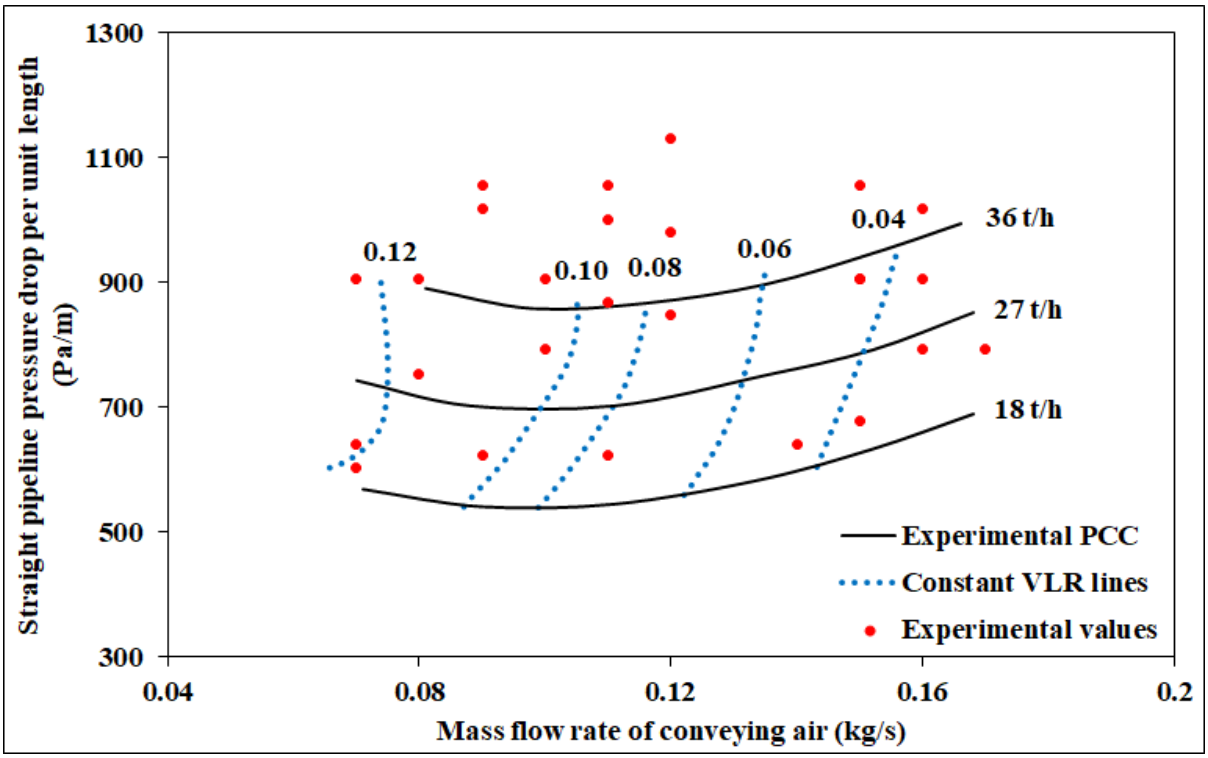

Figure A2.7: VLR curves for cement through 80/100 mm I.D. × 407 m long pipe

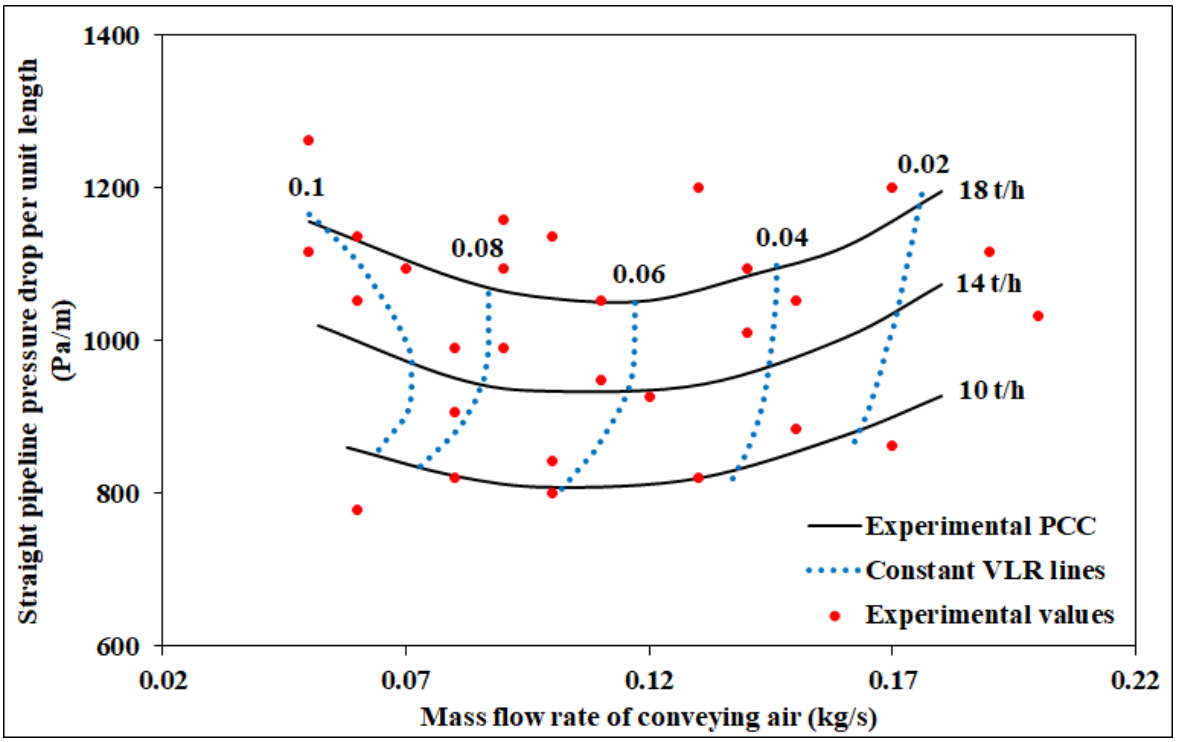

Figure A2.8: VLR curves for fly ash through 65 mm I.D. × 300 m long pipe

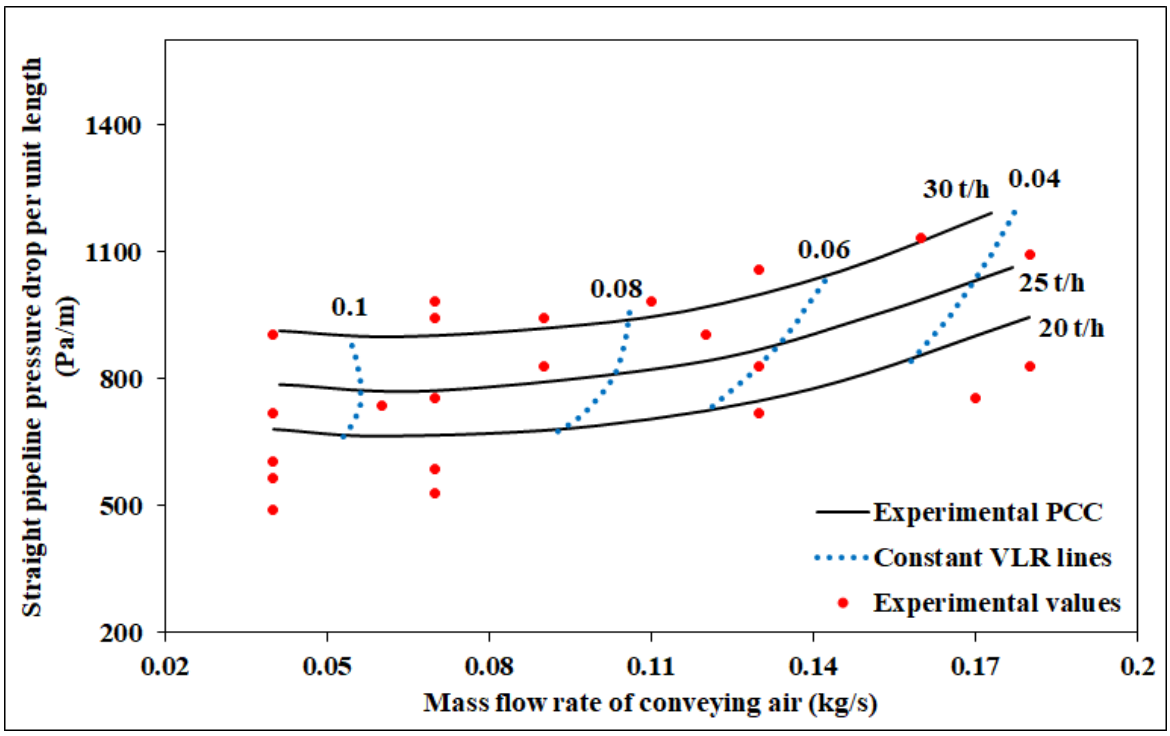

Figure A2.9: VLR curves for fly ash through 80/100 mm I.D. × 407 m long pipe

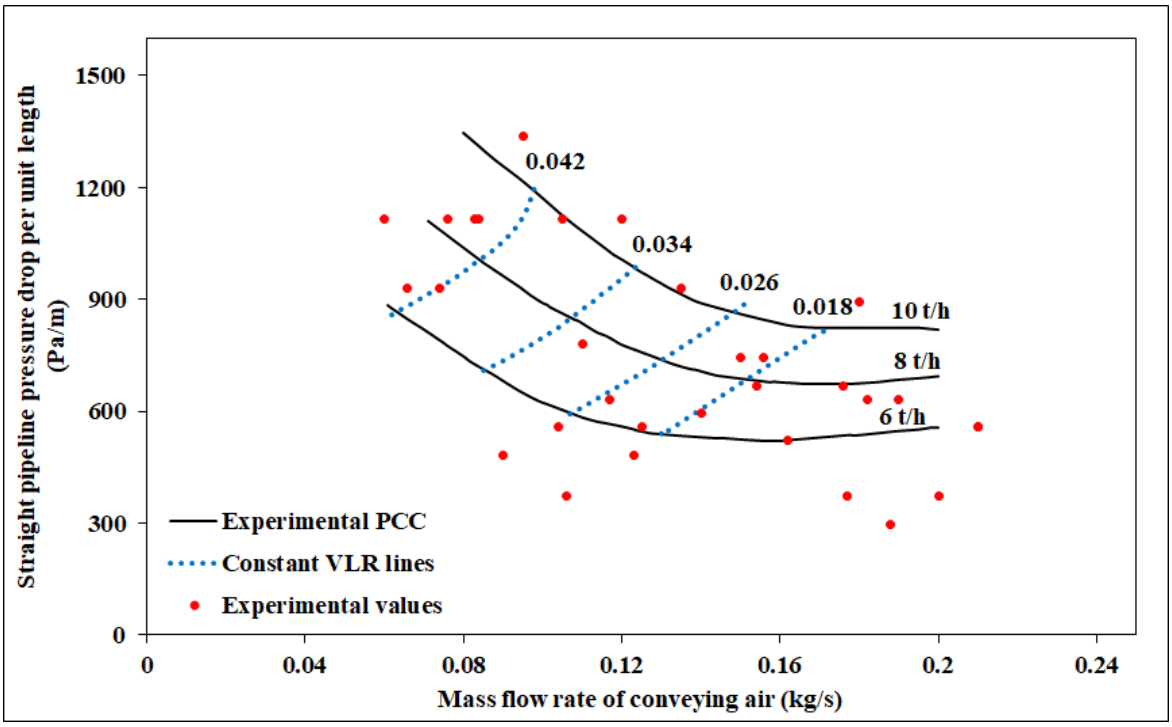

Figure A2.10: VLR curves for ESP dust through 69 mm I.D. × 554 m long pipe

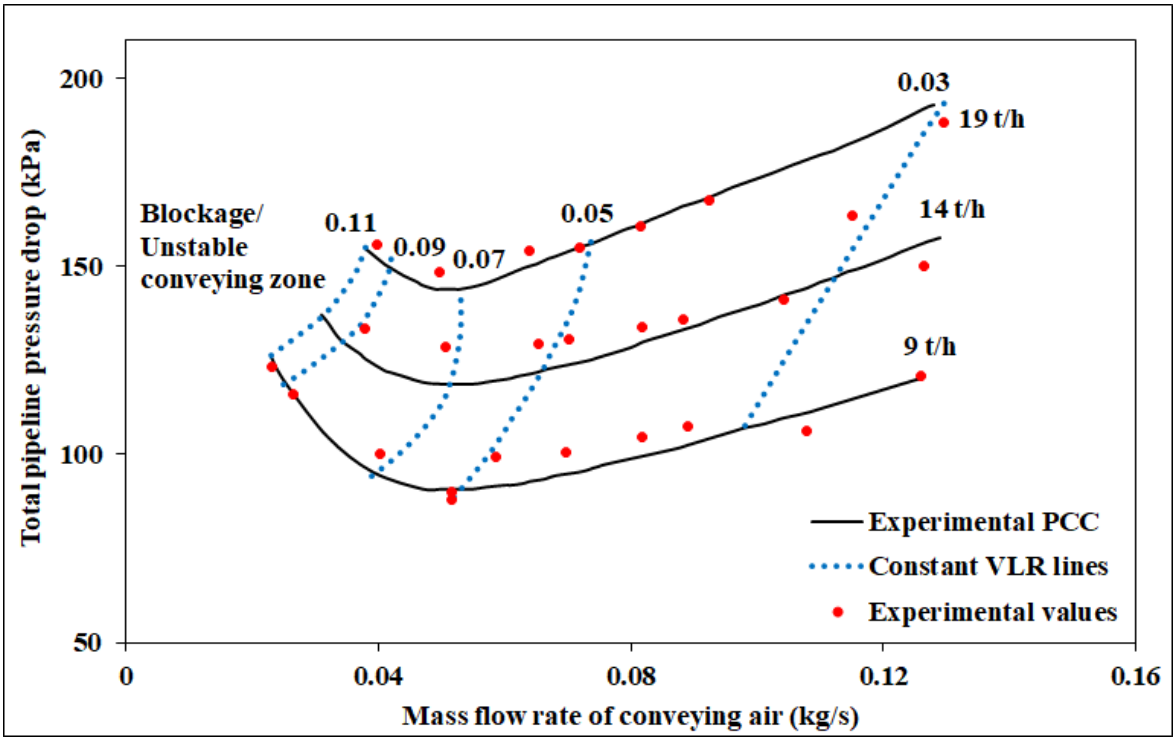

Figure A2.11: VLR curves for fly ash through 69 mm I.D. × 168 m long pipe

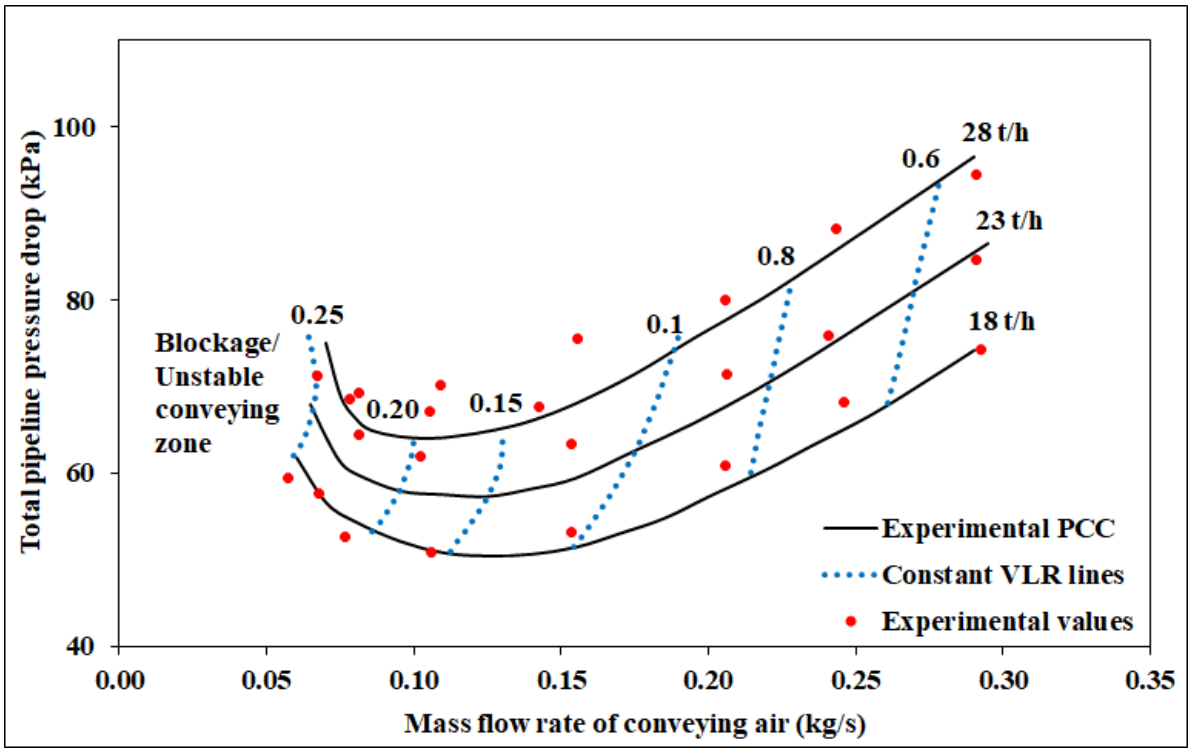

Figure A2.12: VLR curves for fly ash through 105 mm I.D. × 168 m long pipe

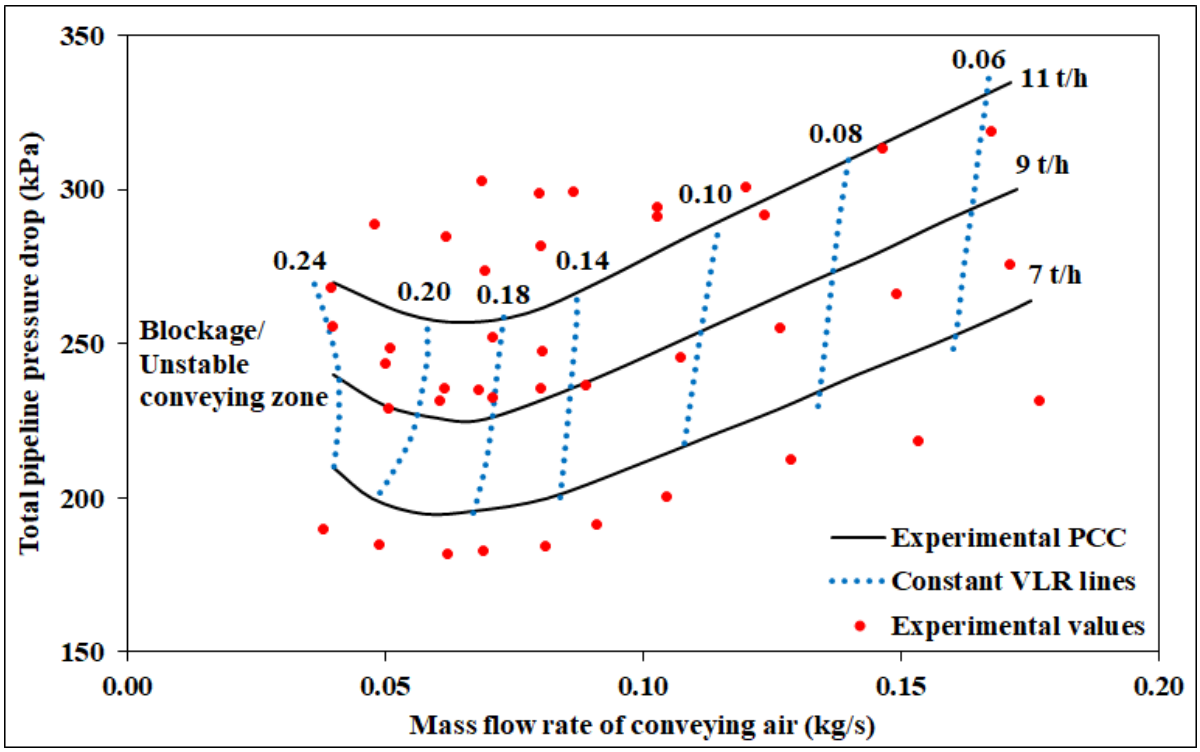

Figure A2.13: VLR curves for fly ash through 69 mm I.D. × 554 m long pipe

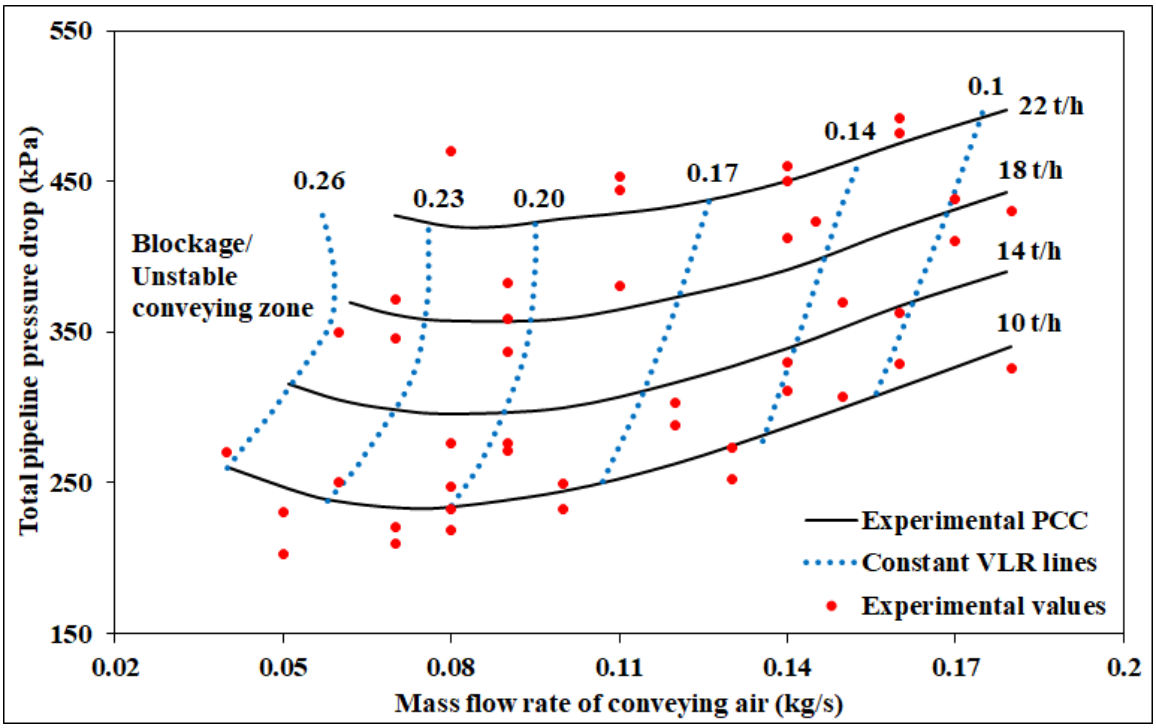

Figure A2.14: VLR curves for cement through 65 mm I.D. × 300 m long pipe

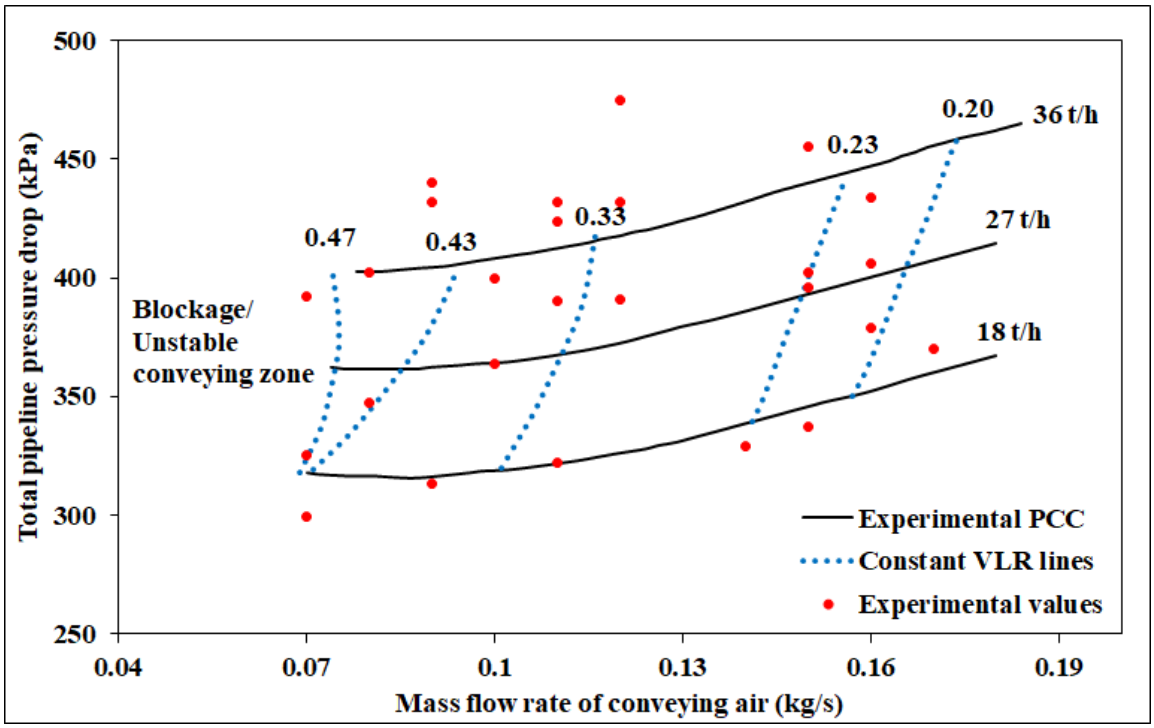

Figure A2.15: VLR curves for cement through 80/100 mm I.D. × 407 m long pipe

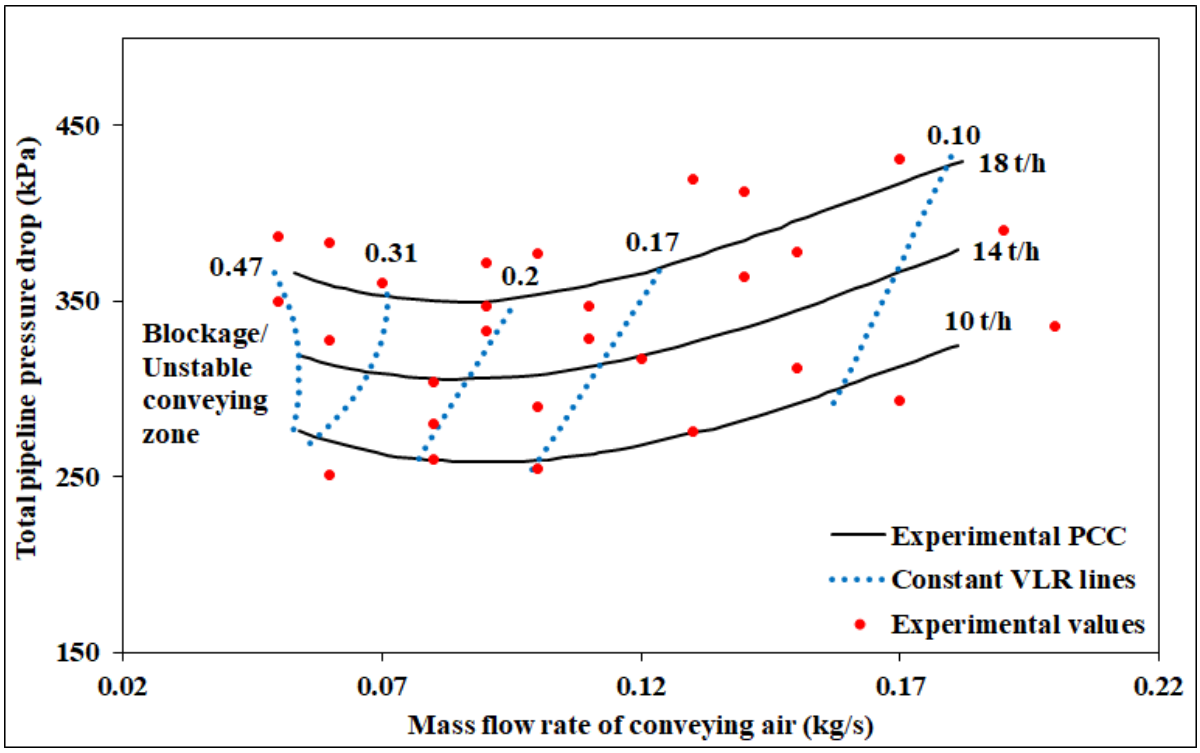

Figure A2.16: VLR curves for fly ash through 65 mm I.D. × 300 m long pipe

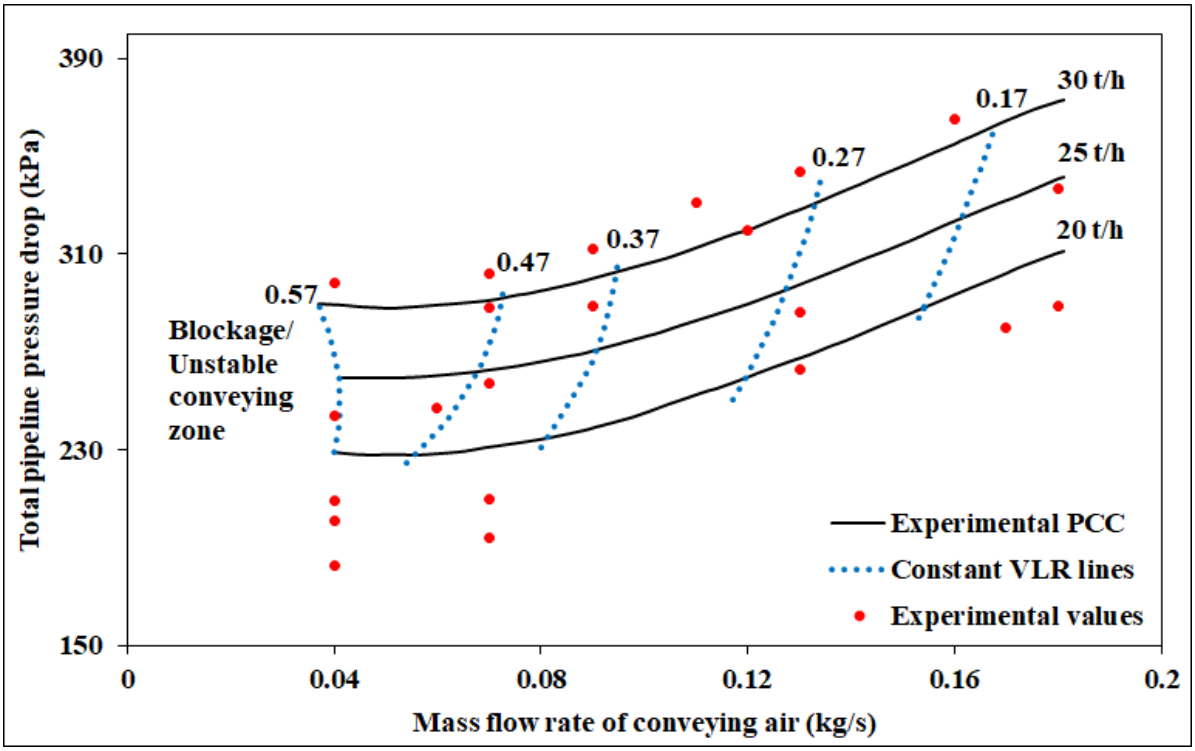

Figure A2.17: VLR curves for fly ash through 80/100 mm I.D. × 407 m long pipe

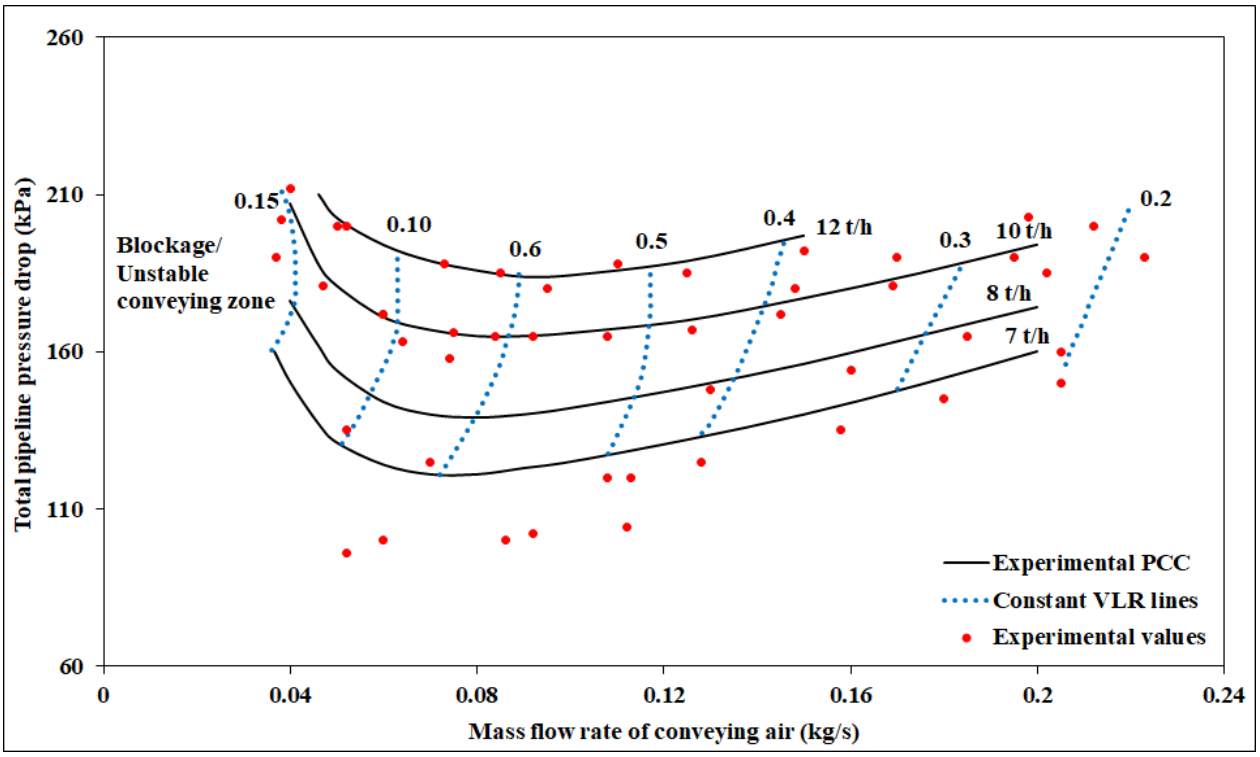

Figure A2.18: VLR curves for ESP dust through 69 mm I.D. × 168 m long pipe

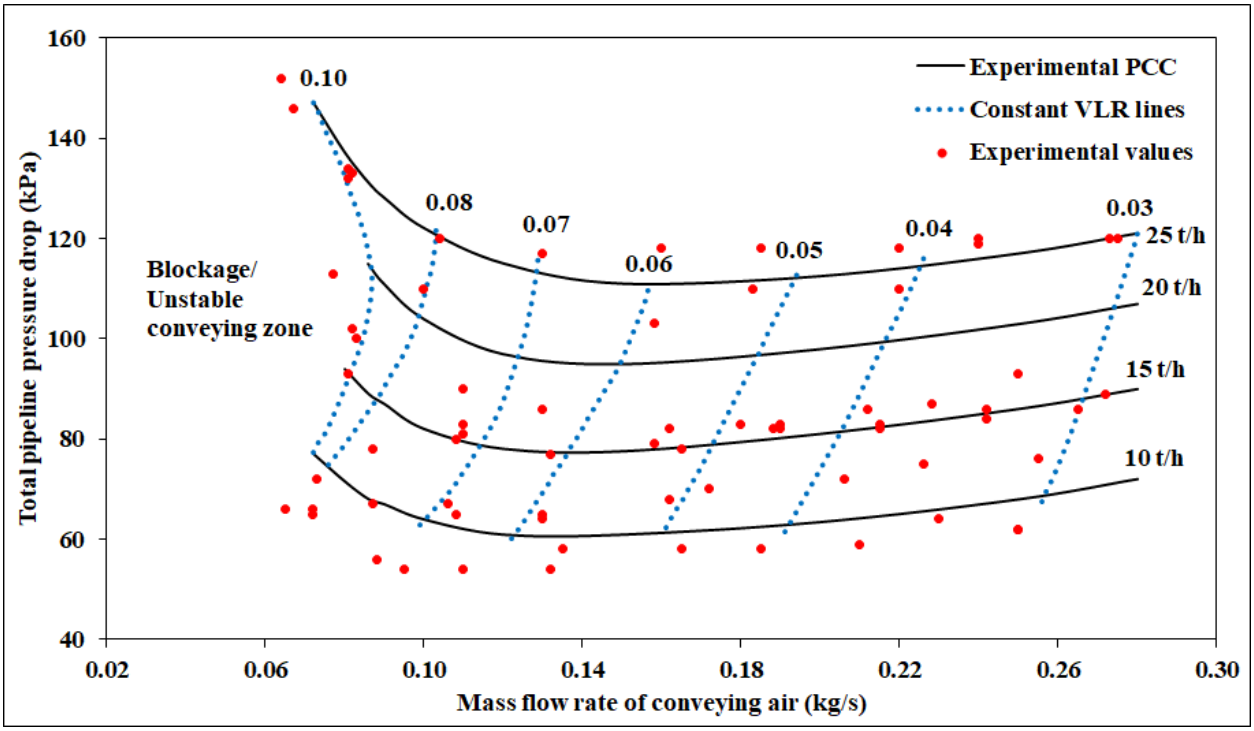

Figure A2.19: VLR curves for ESP dust through 105 mm I.D. × 168 m long pipe

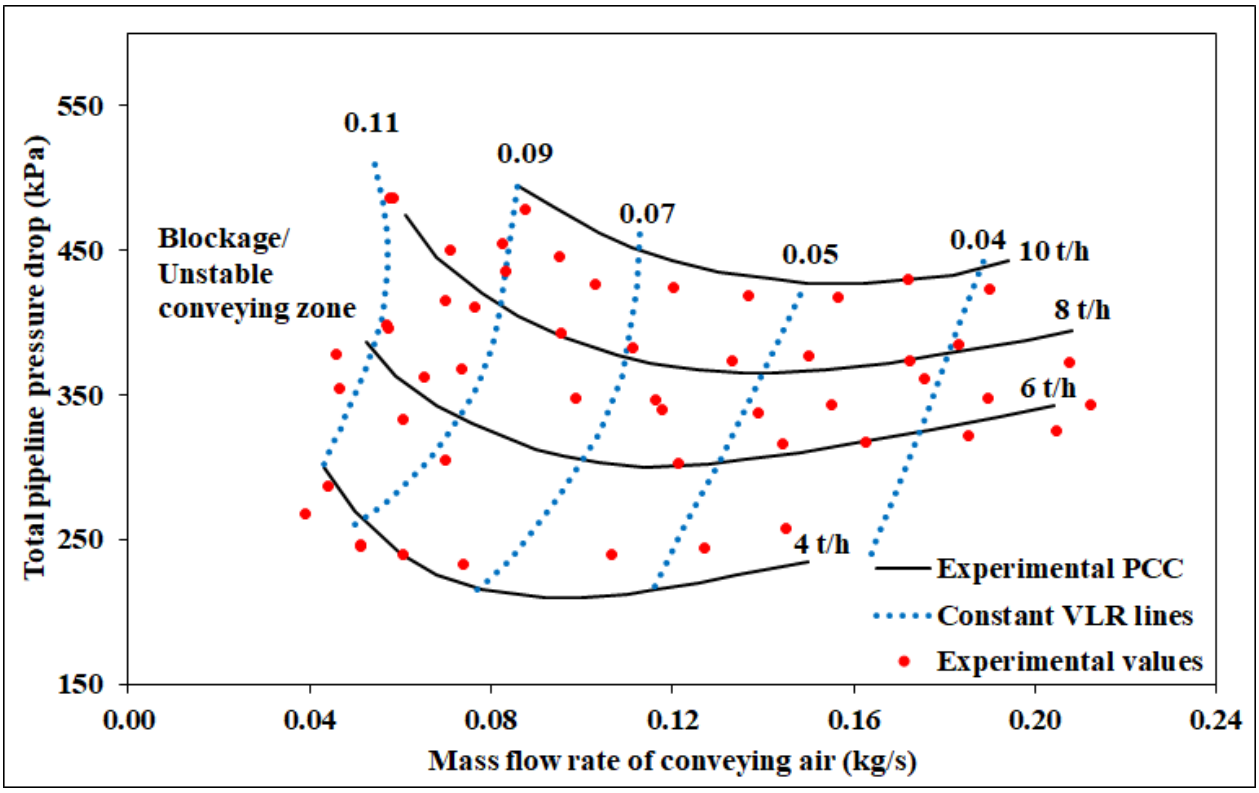

Figure A2.20: VLR curves for ESP dust through 69 mm I.D. × 554 m long pipe

A2.4 Solids friction factor values from literature

This section deals with the development of characterization diagram which shows solids friction factor per unit solid loading ratio $\left({}^{\lambda_s}/_{m^*}\right)$ on y-axis & Archimedes number (Ar) and Stokes number (Stk) on the x-axis. Figures A2.21 and A2.22 have been developed with a large number of an extensive database, including 57 different products and 107 pipeline configurations with various lengths and diameters, respectively. The complete summary of 57 different products and 107 pipeline configurations are given in Table A2.5. The coloured experimental data points have been obtained from the total pipeline pressure drop PCC (pneumatic conveying characteristics) predictions through the minimum transport boundary conditions beyond which the blockage

happens in the pipeline. In the present investigation, cohesive, very cohesive, and coarse-grained particles have been taken into account. It has been evident from the graphs that, with increasing the size of the powder the logarithmic values of Archimedes number (Ar) and Stokes number (Stk) progressively increasing with some asymptotic varied values of solids friction factor per unit solid loading ratio $\left({\lambda_s}/{m^*}\right)$.

It has also been observed that, in case of increasing Archimedes number (Ar) in the x-axis, more gravity effects have been pronounced with larger values of terminal (w_{fo}) velocity for progressively larger particle sizes. However, in case of increasing Stokes number (Stk) in the x-axis, large particle size powders will have higher superficial velocity (V) in the pipeline.

The expressions for Archimedes number and Stokes number are given by the following equations:

$$Ar = \frac{\rho_a(\rho_s - \rho_a) g {d_p}^3}{\mu^2} \qquad (A2.3)$$

$$Stk = \frac{\rho_S V {d_p}^2}{18\mu D} \qquad (A2.4)$$

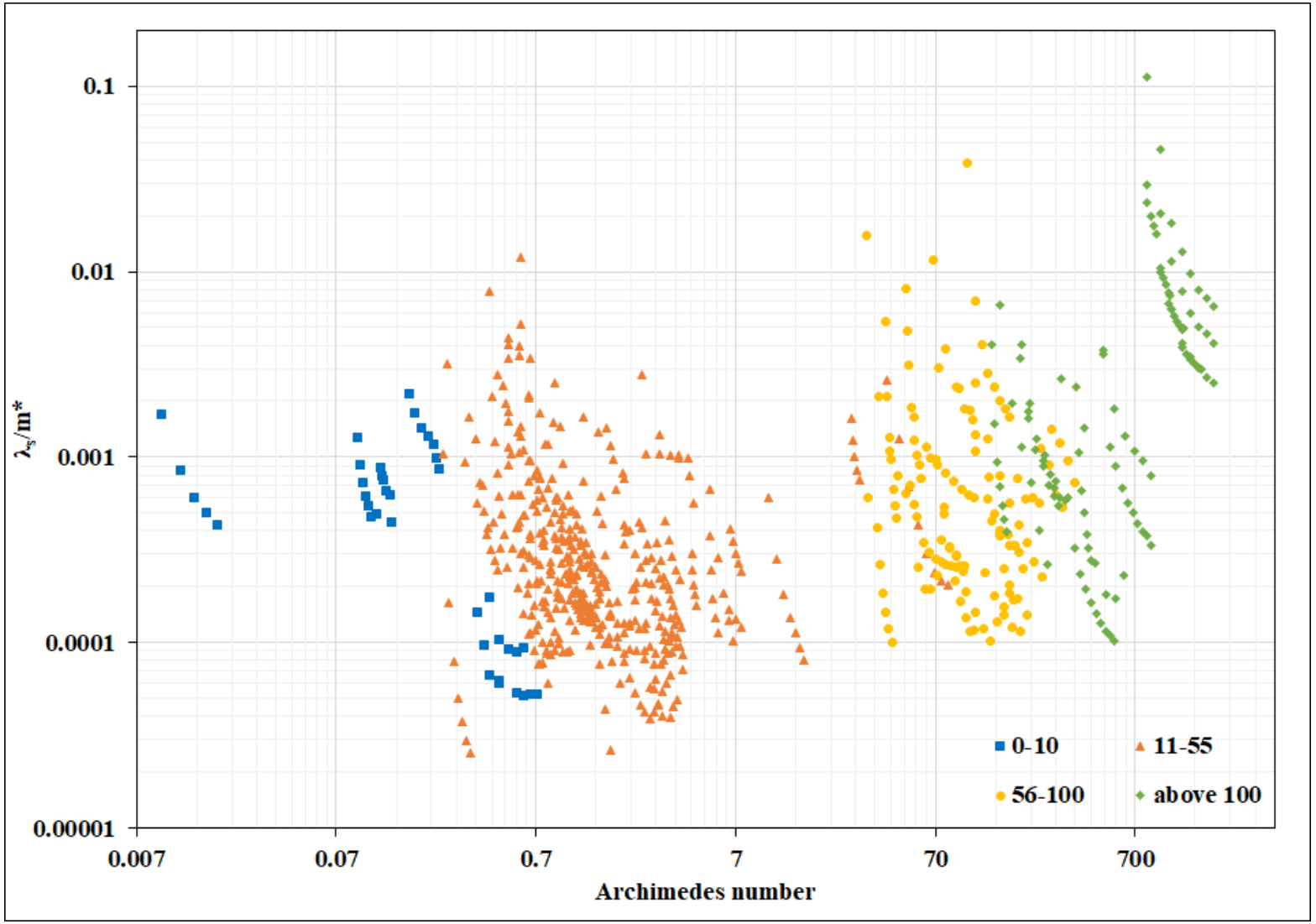

Figure A2.21: Different solids friction factor per unit solid loading ratio with Archimedes number

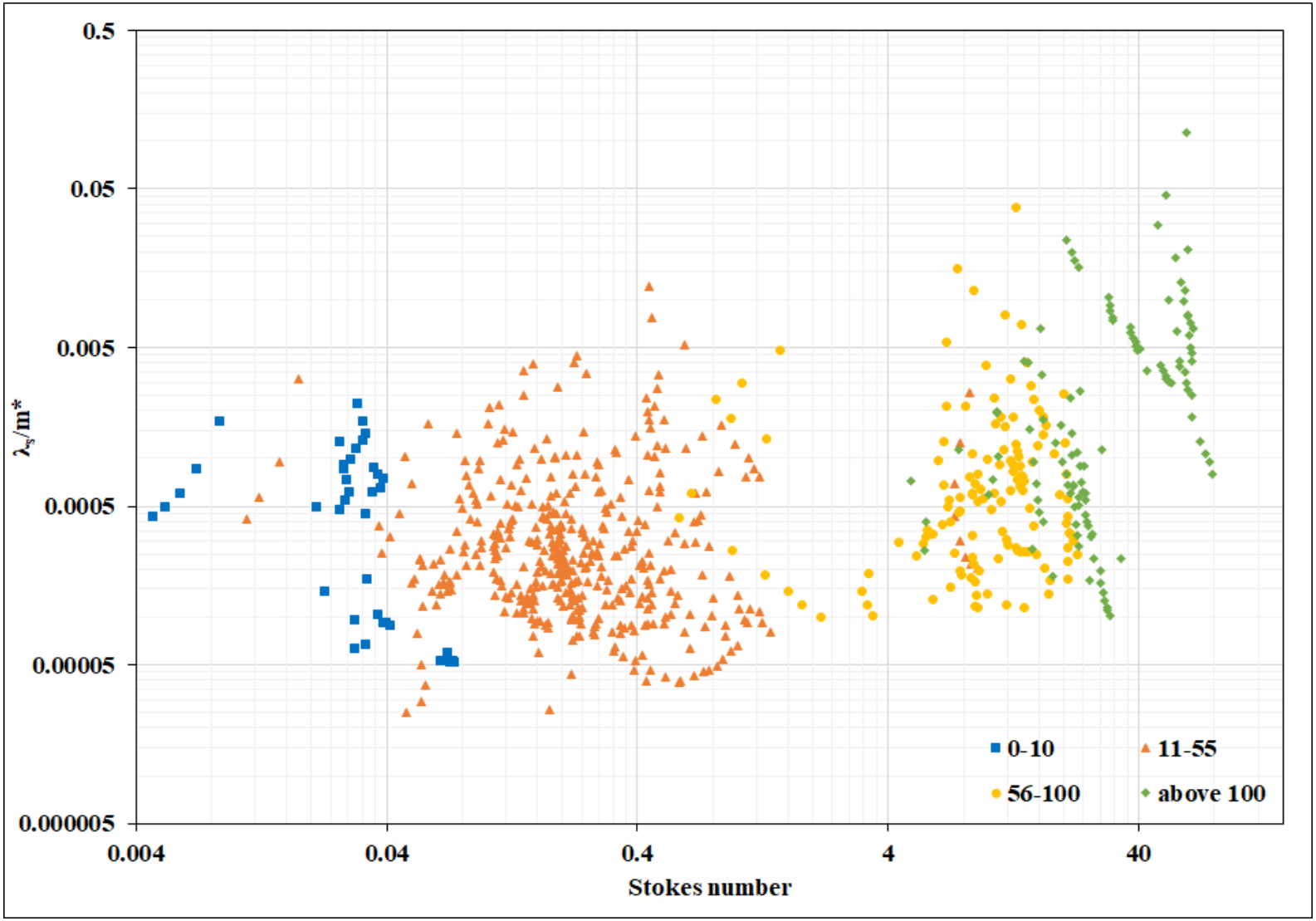

Figure A2.22: Different solids friction factor per unit solid loading ratio with Stokes Number

Table A2.5: Summary of 57 products conveyed and 107 pipeline configurations

No.	Product Reference	d_{50} (µm)	ρ_s (kg/m^3)	ρ_{bl} (kg/m^3)	w_{fo} (m/s)	Blow tank type	D (mm)	L (m)	L_h (m)	L_v (m)	No. of bends
1	ESP dust (Mallick, 2009)	7	3637	610	0.005	BD	69 69 105	168 554 168	161 547 161	7 7 7	5 17 5
2	Fly ash (Mallick, 2009)	30	2300	700	0.06	BD	69 69 105	168 554 168	161 547 161	7 7 7	5 17 5
3	White powder (Mallick, 2009)	55	1600	620	0.145	BD	69	148	142	6	6
4	Barytes (Ratnayake, 2005)	12	4200	*	0.0182	TD	75 75 100 125	72 66 66 68	64 66 66 68	8 0 0 0	5 4 4 4
5	Cement (Ratnayake, 2005)	15.5	3100	*	0.0224	TD	75 75 100 125	72 66 66 68	64 66 66 68	8 0 0 0	5 4 4 4

No.	Product Reference	d_{50} (µm)	ρ_s (kg/m^3)	ρ_{bl} (kg/m^3)	w_{fo} (m/s)	Blow tank type	D (mm)	L (m)	L_h (m)	L_v (m)	No. of bends
6	Ilmenite (Ratnayake, 2005)	9.5	4600	*	0.0125	TD	75 100 125	66 66 68	66 66 68	0 0 0	4 4 4
7	Bentonite (Ratnayake, 2005)	25	2500	*	0.047	TD	75	72	64	8	5
8	Alumina 1 (Ratnayake, 2005)	59.2	2800	*	0.295	TD	75	138	130	8	9
9	Alumina 2 (Ratnayake, 2005)	72	2800	*	0.4368	TD	75	138	130	8	9
10	Alumina 3 (Ratnayake, 2005)	79.3	2800	*	0.53	TD	75	138	130	8	9
11	Alumina 4 (Ratnayake, 2005)	86.7	2800	*	0.633	TD	75	138	130	8	9
12	Alumina 5 (Ratnayake, 2005)	90.5	2800	*	0.69	TD	75	138	130	8	9

No.	Product Reference	d_{50} (µm)	ρ_s (kg/m^3)	ρ_{bl} (kg/m^3)	w_{fo} (m/s)	Blow tank type	D (mm)	L (m)	L_h (m)	L_v (m)	No. of bends
13	Cement (Mills, 2004)	14	3060	1070	0.018	TD	81 53	95 101	95 101	0 0	9 17
14	Fly ash (Pan, 1992)	15.5	2197	634	0.0158	BD	52.5 52.5 69 69	102 135 172 553	96 129 165 547	6 6 7 6	4 4 5 17
15	Tallawarra fly ash (Wypych, 1989)	20	2350	500	0.02828	BD	52	71	67.4	3.6	11
16	Eraring fly ash (Wypych, 1989)	27	2160	880	0.0473	BD	52	71	67.4	3.6	11
17	Munmorah fly ash (Wypych, 1989)	25	2100	650	0.0395	BD	52	71	67.4	3.6	11
18	Vales Point fly ash (Wypych, 1989)	19	2130	700	0.02313	BD	52	71	67.4	3.6	11
19	Gladstone fly ash (Wypych, 1989)	18	2250	1030	0.02193	BD	52	71	67.4	3.6	11

No.	Product Reference	d_{50} (µm)	ρ_s (kg/m^3)	ρ_{bl} (kg/m^3)	w_{fo} (m/s)	Blow tank type	D (mm)	L (m)	L_h (m)	L_v (m)	No. of bends
20	Wallerawang fly ash (Wypych, 1989)	12	2195	455	0.0095	BD	52	71	67.4	3.6	11
21	Liddell fly ash (Wypych, 1989)	13	2415	640	0.01228	BD	52	71	67.4	3.6	11
22	Cement (Setia et al., 2016)	19	2910	1080	0.036	BD	65	254	241	13	10
23	Fly ash (Setia et al., 2016)	22	2370	660	0.038	BD	65	254	241	13	10
24	Cement (Wypych & Arnold, 1984)	20	3100	950	0.0373	BD	65	162	157.6	4.4	5
25	Pulverized coal (Wypych & Arnold, 1984)	30	1600	760	0.0433	BD	50	25	21.4	3.6	5

No.	Product Reference	d_{50} (µm)	ρ_s (kg/m^3)	ρ_{bl} (kg/m^3)	w_{fo} (m/s)	Blow tank type	D (mm)	L (m)	L_h (m)	L_v (m)	No. of bends
26	Power station fly ash (Wypych & Arnold, 1984)	43	2100	880	0.1168	BD	50	71	67.4	3.6	13
27	PVC powder (Wypych & Arnold, 1984)	130	1400	575	0.7118	BD	50	71	67.4	3.6	13
28	Fly ash 1 (Pan & Wypych, 1998)	16	2197	634	0.0169	BD	69 128	554 760	547 735	7 25	17 4
29	Fly ash 2 (Pan & Wypych, 1998)	12	2215	955	0.00959	BD	105 128	168 760	161 735	7 25	5 4
30	Fly ash 3 (Pan & Wypych, 1998)	3.5	2540	670	0.000936	BD	128	760	736	24	4
31	Fly ash 4 (Pan & Wypych, 1998)	58	2180	730	0.22069	BD	128 53	760 70	736 65	24 5	4 8
32	Fly ash (Setia et al., 2015)	19	1950	950	0.02118	BD	54	70	67	3	4
33	Fly ash + Cement (Wypych, 1989)	19	2237	728	0.0243	BD	60 105	158 158	153 153	5 5	5 5

No.	Product Reference	d_{50} (µm)	ρ_s (kg/m^3)	ρ_{bl} (kg/m^3)	w_{fo} (m/s)	Blow tank type	D (mm)	L (m)	L_h (m)	L_v (m)	No. of bends
34	Cement (Jones et al., 1987)	21	3060	1070	0.04	BD	53	50	50	0	9
35	Copper ore (Jones et al., 1987)	75	3950	1660	0.6688	BD	53	50	50	0	9
36	Pulverized coal (Wypych et al., 1990a)	37	1680	*	0.0692	BD	52	71	67.4	3.6	11
37	PVC powder (Wypych & Arnold, 1987)	130	1400	575	0.7118	BD	52 105	71 162	67.4 157.4	3.6 4.6	11 5
38	Calcined alumina (Mills et al., 2004)	66	3920	750	0.5139	TD	81	95	95	0	9
39	Hydrated alumina (Mills et al., 2004)	60	2420	1110	0.2621	TD	53	98	98	0	13
40	Sandy alumina (Mills, 2016)	79	3600	1040	0.6762	BD TD TD	53 53 81	47 50 95	47 50 95	0 0 0	6 8 9
41	Bentonite (Mills et al., 2004; Mills, 2016)	24	2300	760	0.0398	TD TD	53 53	70 70	70 70	0 0	9 9 (6 L+3 S)

No.	Product Reference	d_{50} (µm)	ρ_s (kg/m^3)	ρ_{bl} (kg/m^3)	w_{fo} (m/s)	Blow tank type	D (mm)	L (m)	L_h (m)	L_v (m)	No. of bends
42	Barites (Mills et al., 2004; Mills, 2016)	12	4250	1590	0.0184	BD	53	34	34	0	7
						BD	53	43	43	0	6
						TD	53	50	50	0	8
						TD	53	70	70	0	9
						TD	53	101	101	0	17
						TD	53	163	163	0	17
						BD	81	50	50	0	9
						BD	102	50	50	0	9
43	Portland cement (Mills et al., 2004; Mills, 2016)	14	3060	1070	0.018	BD	53	43	43	0	6
						TD	53	50	50	0	8
						TD	53	70	70	0	9
						TD	53	95	95	0	9
						TD	53	163	163	0	17
						BD	81	95	95	0	9
						BD	102	95	95	0	9
44	PVC powder (Mills, 2016)	90	990	615	0.2411	BD	53	34	34	0	7
45	PVC resin (Mills et al., 2004)	120	1400	490	0.6065	BD	53	34	34	0	7
						TD	53	50	50	0	8

No.	Product Reference	d_{50} (µm)	ρ_s (kg/m^3)	ρ_{bl} (kg/m^3)	w_{fo} (m/s)	Blow tank type	D (mm)	L (m)	L_h (m)	L_v (m)	No. of bends
46	Silica sand (Mills et al., 2004; Mills, 2016)	70	2630	1250	0.3878	BD TD TD	53 53 53	35 50 70	35 50 70	0 0 0	8 8 9 (6+3)
47	Potassium sulphate (Mills, 2016)	170	2625	1240	2.283	TD TD TD TD TD TD TD	81 81 81 100 125 150 200	95 150 200 95 95 95 95	95 150 200 95 95 95 95	0 0 0 0 0 0 0	9 9 9 9 9 9 9
48	Granulated coal (degraded) (Mills, 2016)	146	1550	700	0.994	TD	53	50	50	0	8
49	Granulated sugar (degraded) (Mills, 2016)	170	1580	655	1.373	TD	53	50	50	0	8
50	Copper concentrate (Mills et al., 2004)	55	3950	1660	0.3596	TD	53	50	50	0	8

No.	Product Reference	d_{50} (µm)	ρ_s (kg/m^3)	ρ_{bl} (kg/m^3)	w_{fo} (m/s)	Blow tank type	D (mm)	L (m)	L_h (m)	L_v (m)	No. of bends
51	Fine fly ash (Mills & Mason, 1985; Mills, 2016)	25	1700	700	0.03196	BD TD TD TD	53 53 53 63	34 101 116 133	34 101 116 133	0 0 0 0	7 17 10 10
52	Fluorspar (Mills, 2016)	66	3700	1580	0.4851	TD	53	70	70	0	9 (6+3)
53	Iron powder (Mills, 2016)	64	5710	2380	0.704	TD	53	50	50	0	9
54	Pearlite (Mills et al., 2004)	200	800	100	0.962	BD TD	53 53	35 50	35 50	0 0	8 9
55	Pulverized coal (Mills, 2016)	84	1550	393	0.329	TD	53	50	50	0	9
56	Wheat flour (Mills, 2016)	90	1470	510	0.3582	TD	53	50	50	0	9
57	Zircon sand (Mills et al., 2004)	120	4600	2600	1.993	TD	53	50	50	0	9

ANNEXURE A3

ADDITIONAL RESULTS OF NUMERICAL WORK

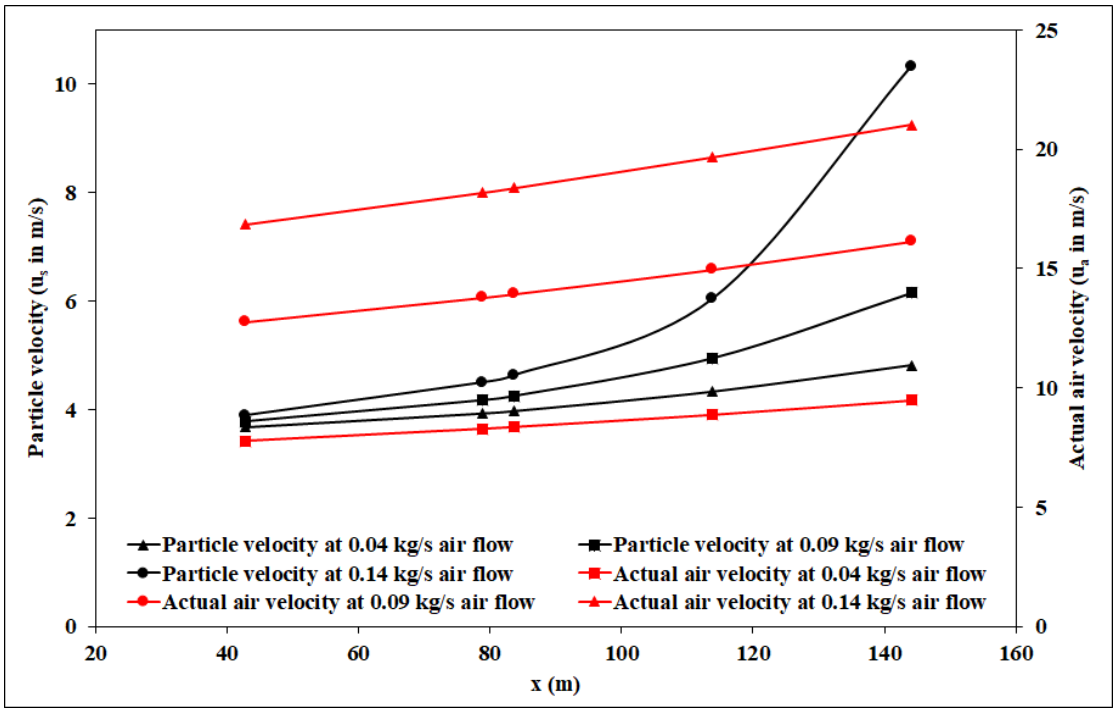

Figure A3.1: Variation of particle velocity and actual air velocity along the pipeline length for fly ash for different airflow rates for m_s = 14 t/h; ρ_{fl} = 300 kg/m^3

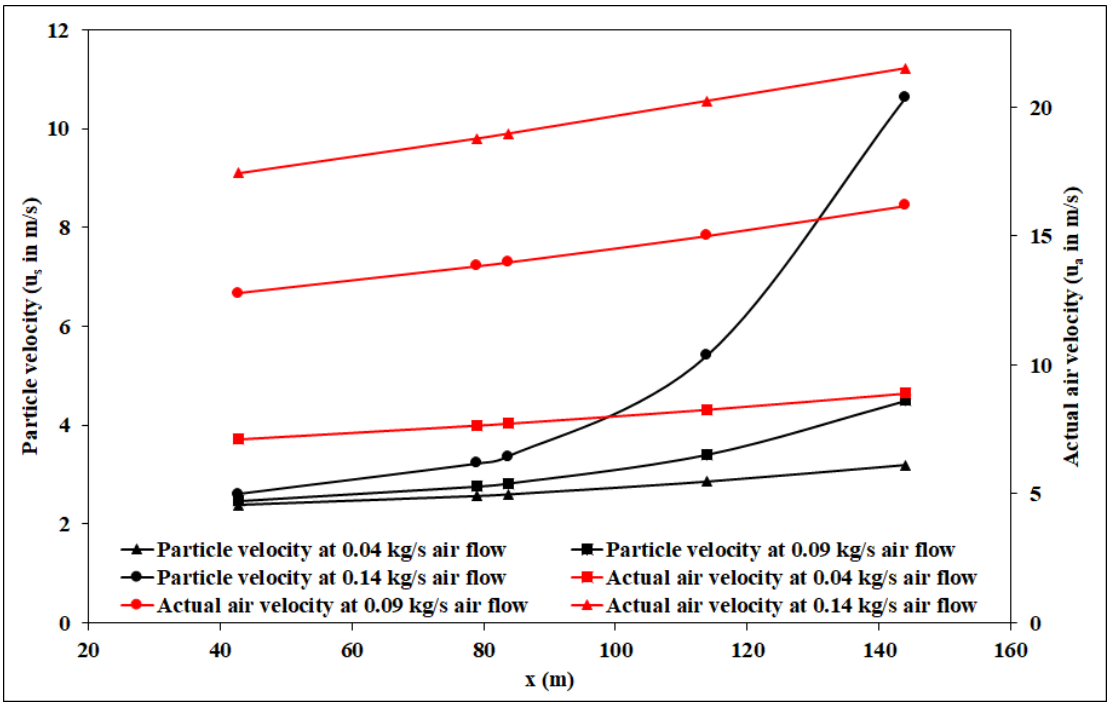

Figure A3.2: Variation of particle velocity and actual air velocity along the pipeline length for fly ash for different airflow rates for m_s = 9 t/h; ρ_{fl} = 300 kg/m^3

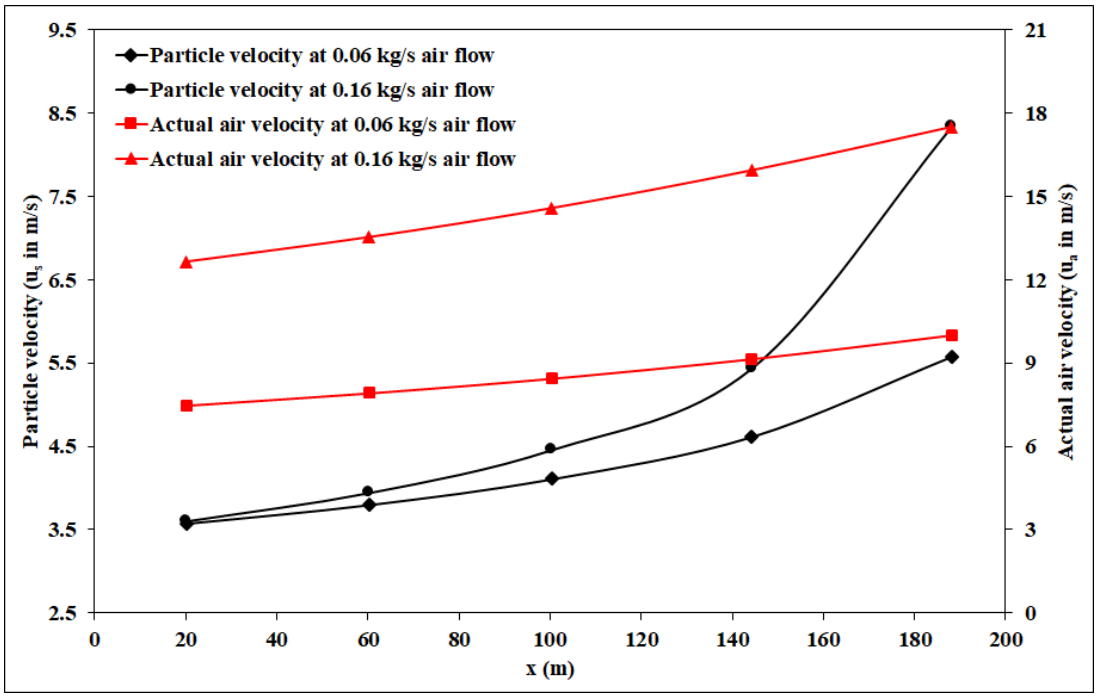

Figure A3.3: Variation of particle velocity and actual air velocity along the pipeline length for fly ash for different airflow rates for m_s = 14 t/h; ρ_{fl} = 333 kg/m^3

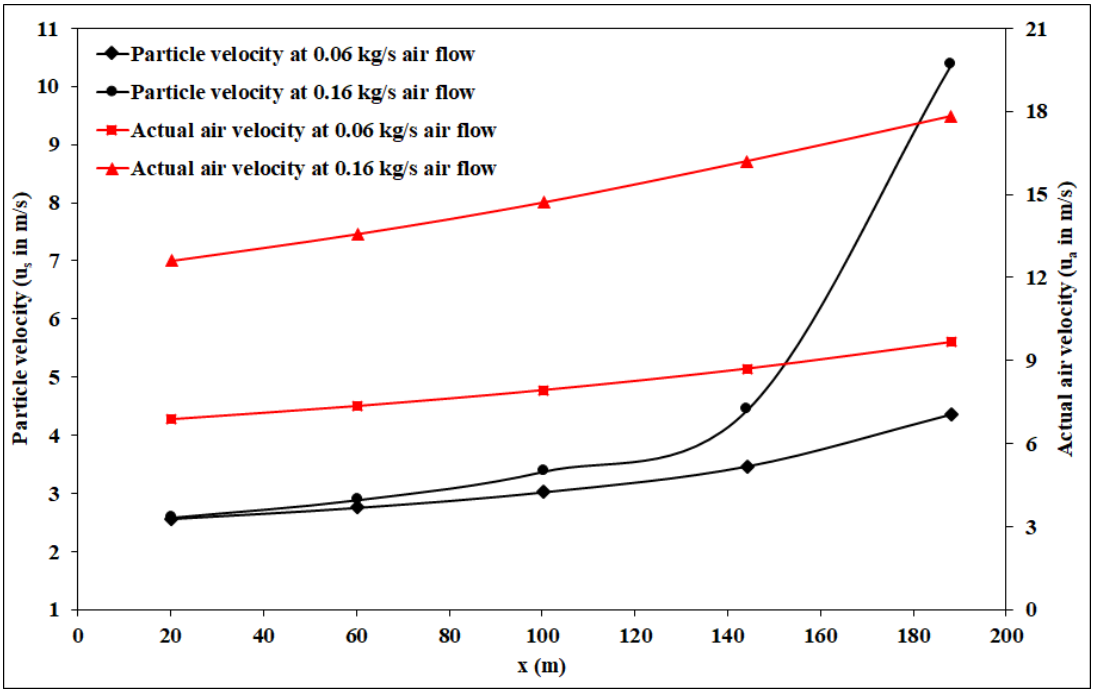

Figure A3.4: Variation of particle velocity and actual air velocity along the pipeline length for fly ash for different airflow rates for m_s = 10 t/h; ρ_{fl} = 333 kg/m^3

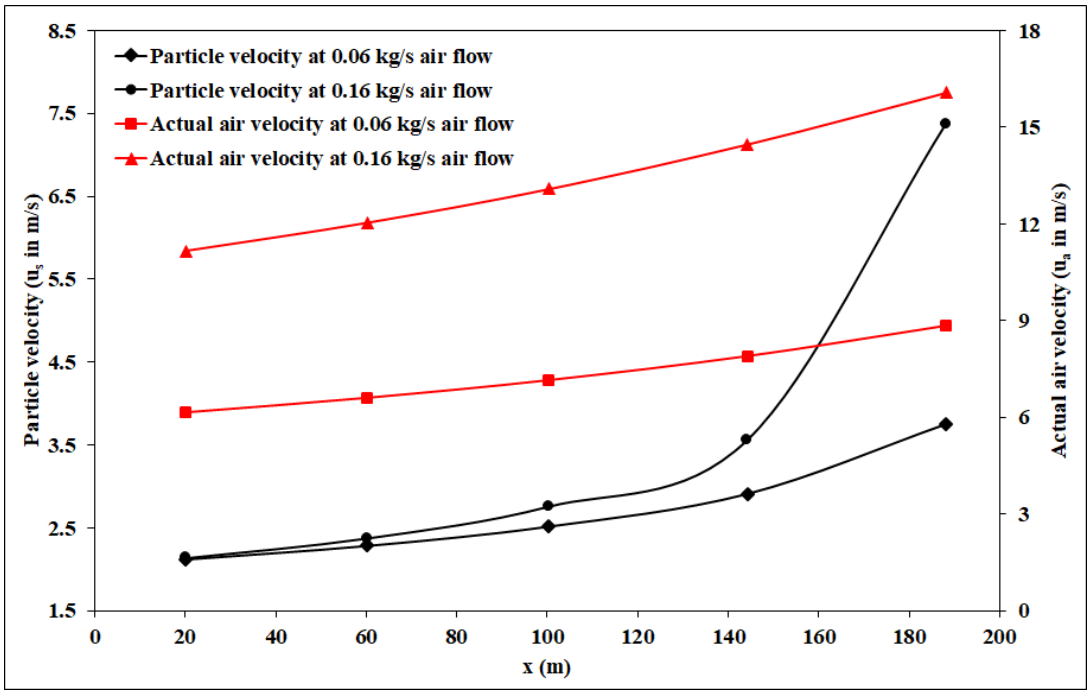

Figure A3.5: Variation of particle velocity and actual air velocity along the pipeline length for cement for different airflow rates for m_s = 14 t/h; ρ_{fl} = 564 kg/m^3

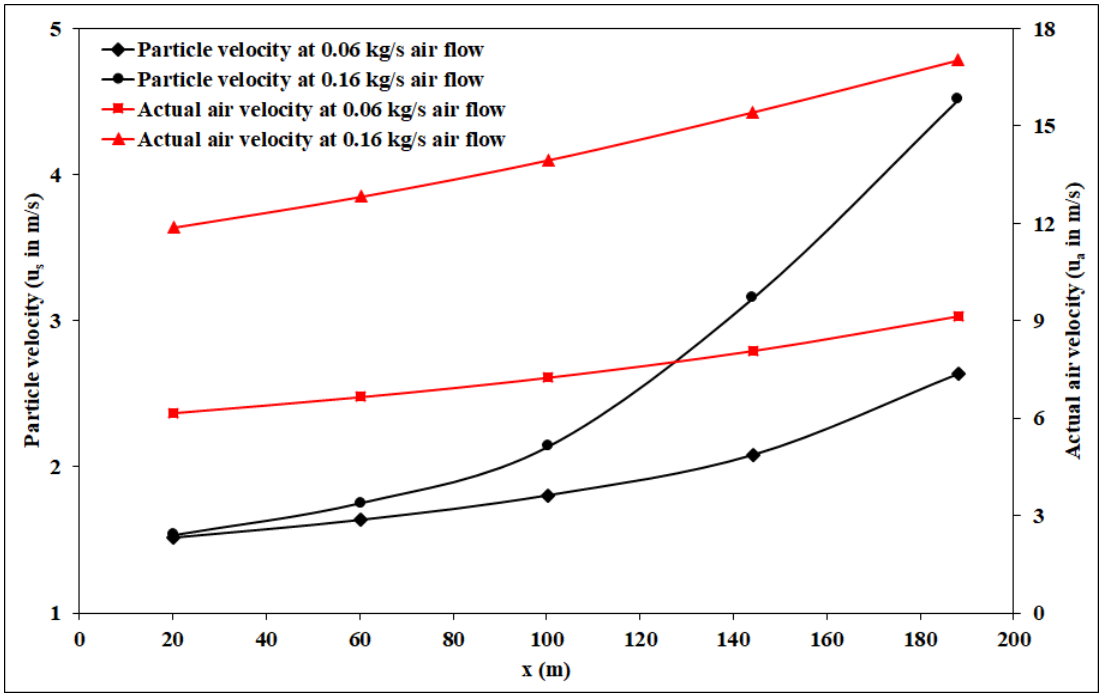

Figure A3.6: Variation of particle velocity and actual air velocity along the pipeline length for cement for different airflow rates for m_s = 10 t/h; ρ_{fl} = 564 kg/m^3

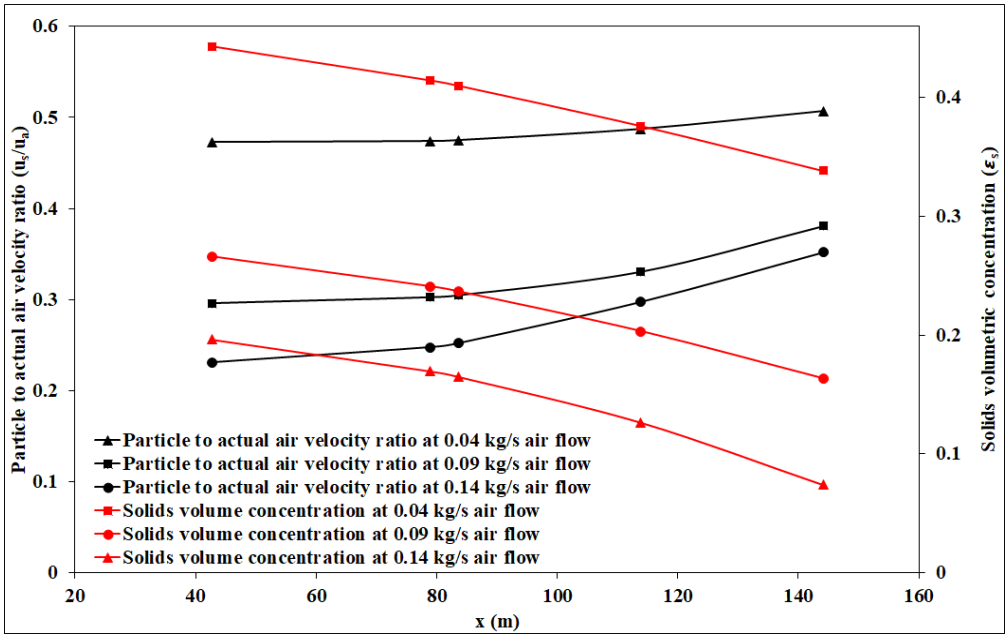

Figure A3.7: Variation of ratio of particle to actual air velocity and solids volumetric concentration along the pipeline length for fly ash for different airflow rates for m_s = 14 t/h; ρ_{fl} = 300 kg/m^3

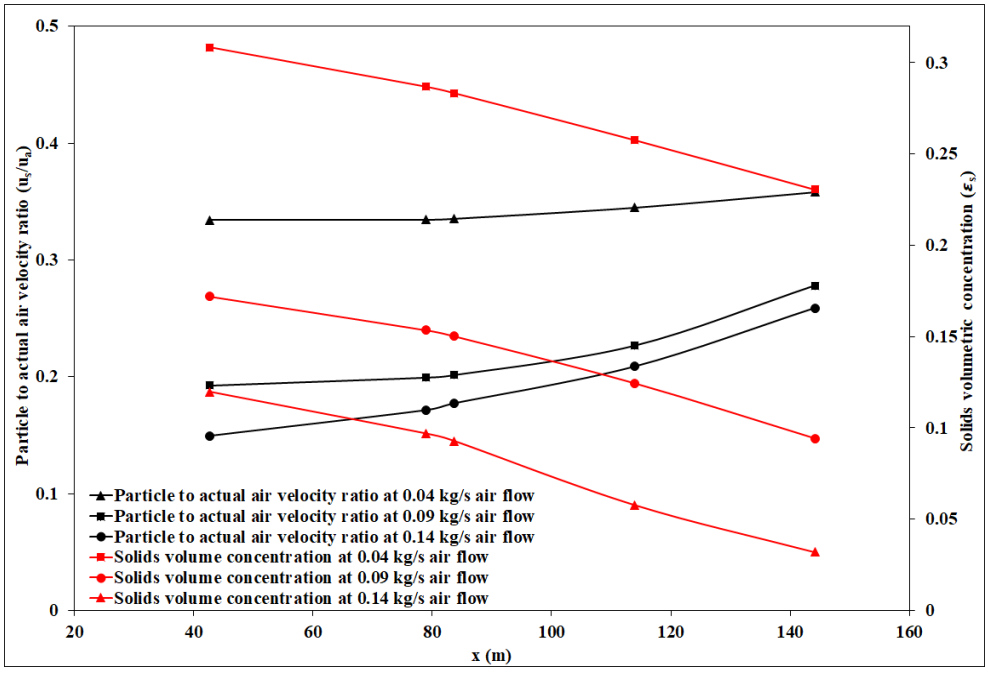

Figure A3.8: Variation of ratio of particle to actual air velocity and solids volumetric concentration along the pipeline length for fly ash for different airflow rates for m_s = 9 t/h; ρ_{fl} = 300 kg/m^3

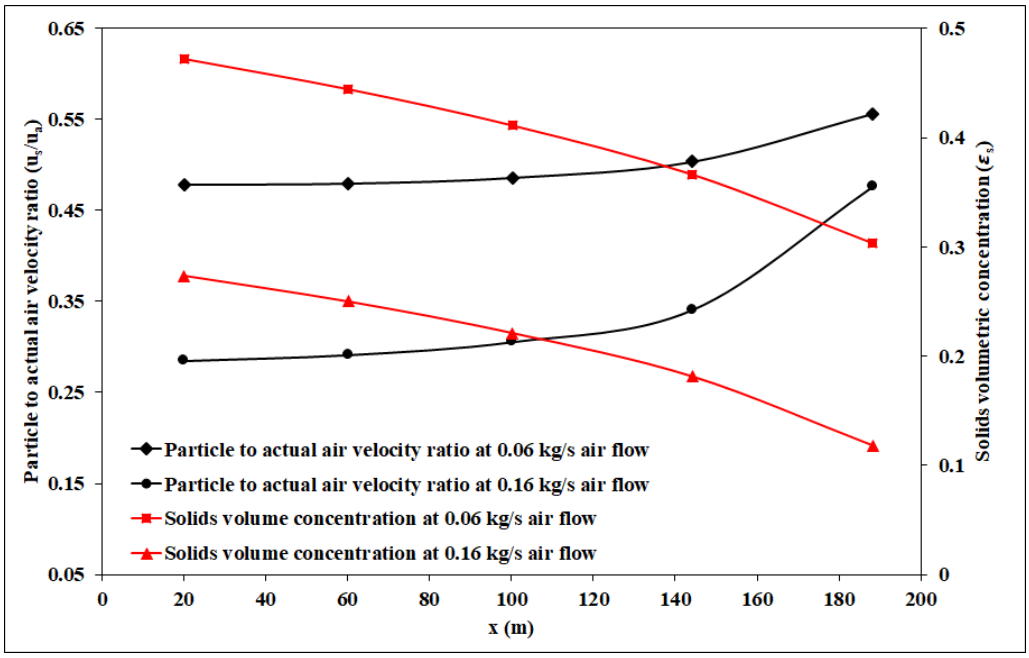

Figure A3.9: Variation of ratio of particle to actual air velocity and solids volumetric concentration along the pipeline length for fly ash for different airflow rates for m_s = 14 t/h; ρ_{fl} = 333 kg/m^3

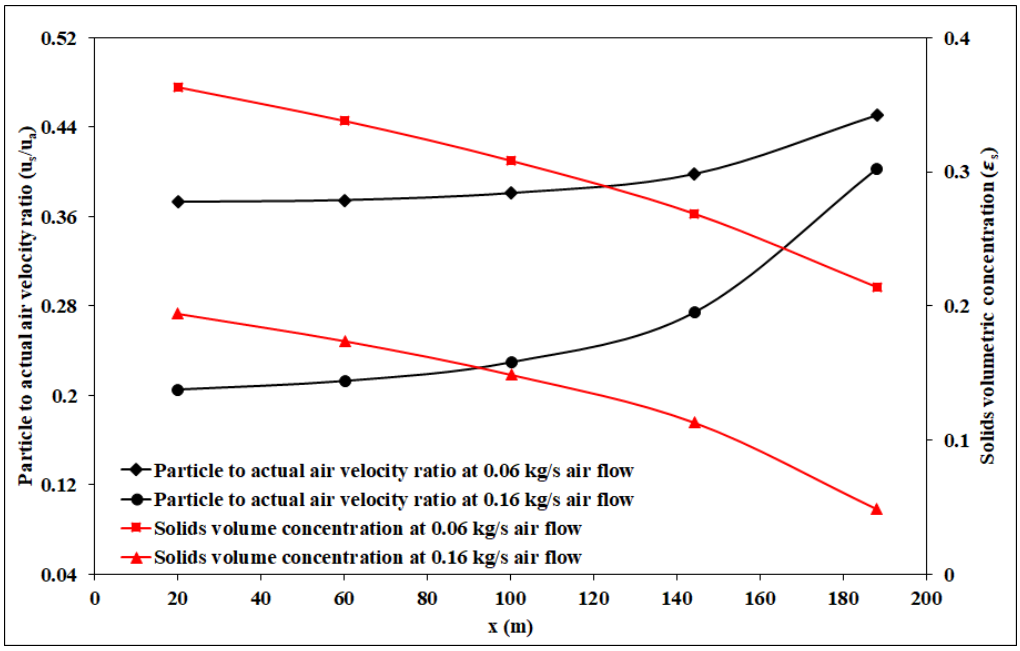

Figure A3.10: Variation of ratio of particle to actual air velocity and solids volumetric concentration along the pipeline length for fly ash for different airflow rates for m_s = 10 t/h; ρ_{fl} = 333 kg/m^3

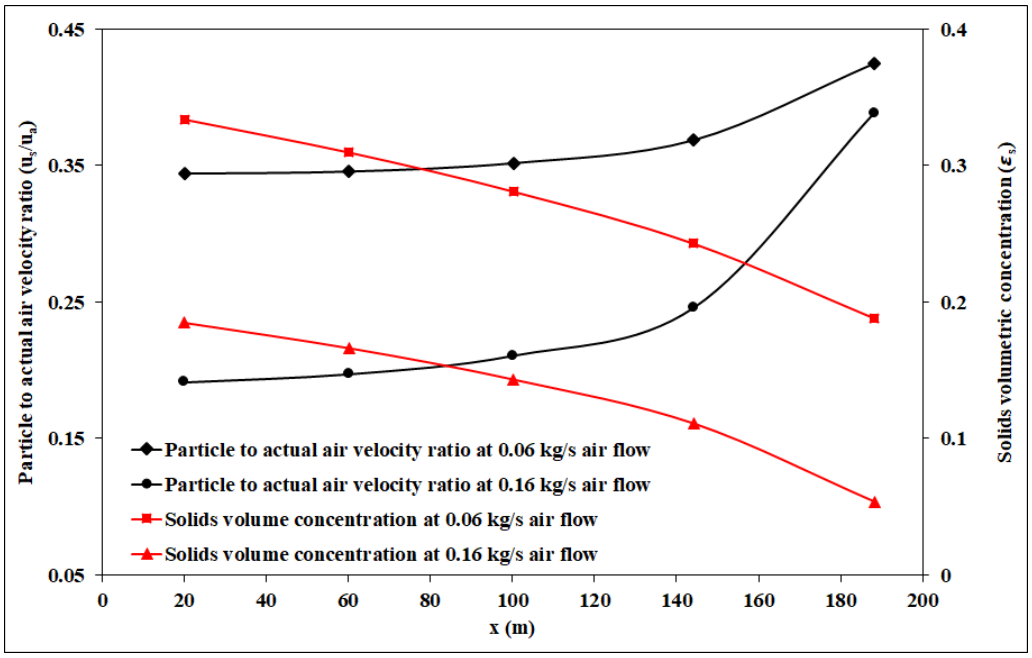

Figure A3.11: Variation of ratio of particle to actual air velocity and solids volumetric concentration along the pipeline length for cement for different airflow rates for m_s = 14 t/h; ρ_{fl} = 564 kg/m^3

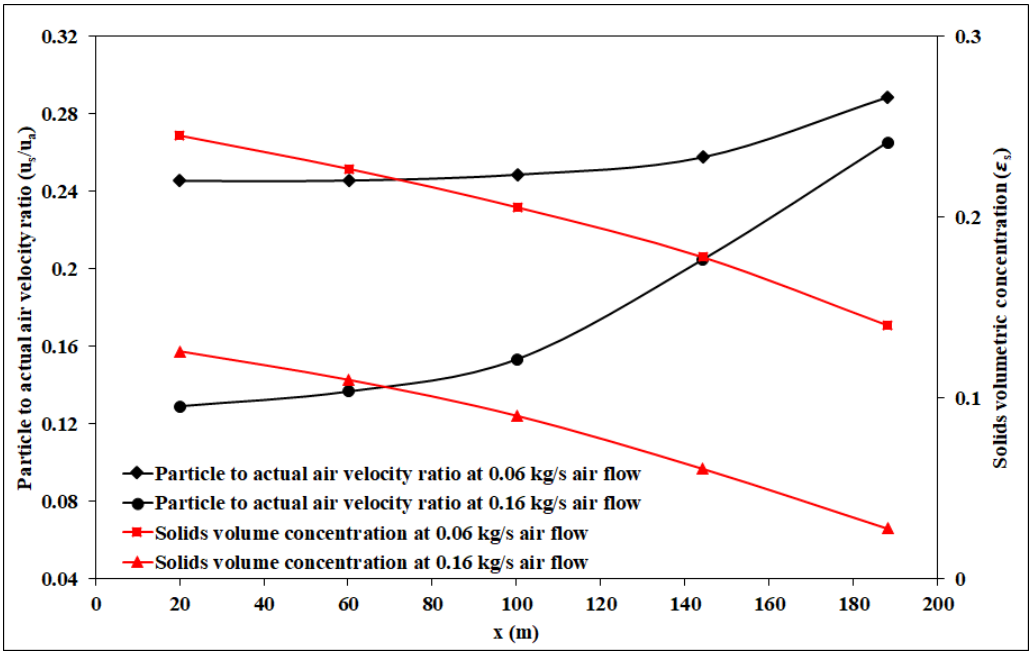

Figure A3.12: Variation of ratio of particle to actual air velocity and solids volumetric concentration along the pipeline length for cement for different airflow rates for m_s = 10 t/h; ρ_{fl} = 564 kg/m^3

A3.1 Model for particle velocity for varying dune bed area

In this section, an attempt has been made to develop the particle velocity model with the variable area and constant fluidized bulk density. In addition to the assumptions listed in section 4.2 (see Chapter 4), additional considerations are provided as below:

- Variable cross-section area ($A \neq c$) in the entire cross-section of the pipeline.
- The first layer (i.e., the lower section in the control volume) will be considered as a pure non-suspension layer (dense-phase).
- The second layer (i.e., the middle section in the control volume) will be considered as a suspension layer (dilute-phase) carrying solids with some amount of air.
- The third layer (i.e., the upper section in the control volume) will be considered as a pure suspension layer (dilute-phase) carrying only air without the presence of solids.
- Particle density will be taken in case of the first layer.
- Fluidized bulk density will be taken in case of the second layer.

For developing the energy equation, energy balance across a control volume is as given below (Figure A3.13).

Conservation of mass for the gas-phase is represented by equation (A3.1) as,

$$\frac{d}{dx}(\varepsilon_a A_a \rho_a u_a) = 0 \qquad (A3.1)$$

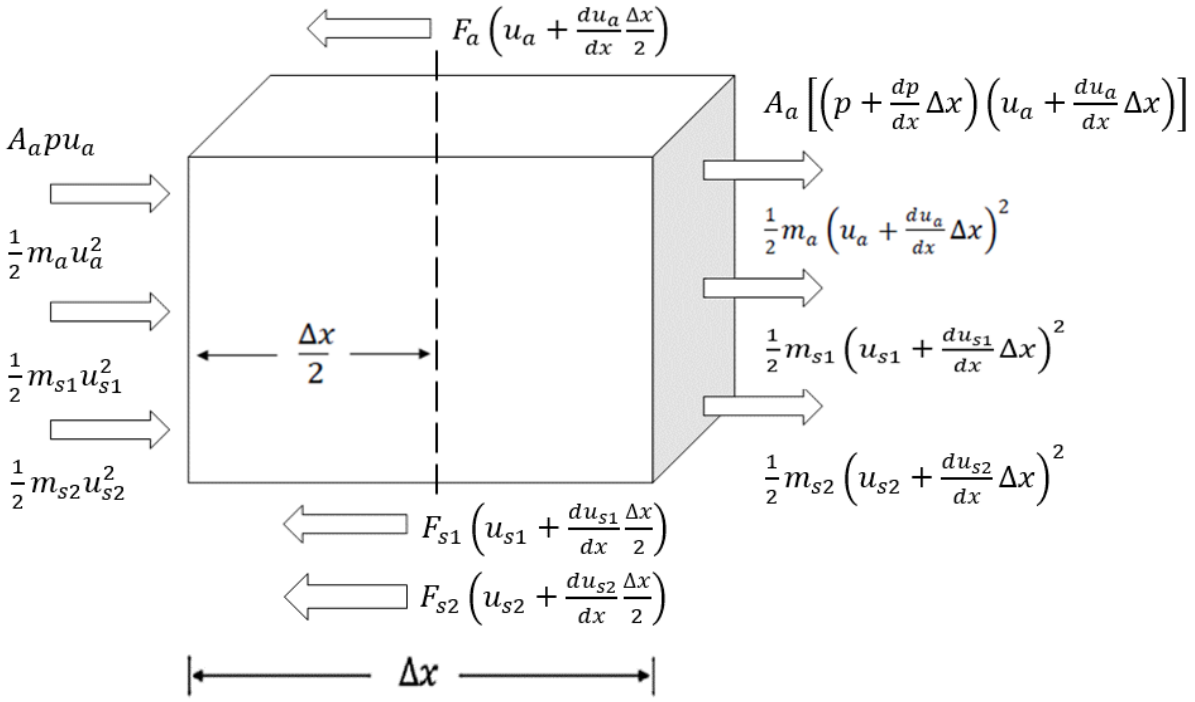

Figure A3.13: Mass and momentum interactions across a control volume

Conservation of mass equation for solids phase is represented by equations A3.2, and A3.3 as,

$$\frac{d}{dx}(\varepsilon_{s1}\rho_{s1}A_{s1}u_{s1}) = 0 \qquad (A3.2)$$

$$\frac{d}{dx}(\varepsilon_{s2}\rho_{s2}A_{s2}u_{s2}) = 0 \qquad (A3.3)$$

Equation (A3.4) for the conservation of momentum has been derived from the control volume shown in Figure A3.13, as shown below:

$$\left[(\rho_a \varepsilon_a A u_a)\left(u_a + \frac{du_a}{dx}\Delta x\right) - (\rho_a \varepsilon_a A u_a)u_a\right] + \left[(\rho_s \varepsilon_s A u_s)\left(u_s + \frac{du_s}{dx}\Delta x\right) - (\rho_s \varepsilon_s A u_s)u_s\right]$$

$$= \left[PA - \left(P + \frac{dP}{dx}\Delta x\right)A\right] - F_a - F_s \qquad (A3.4)$$

The final expression for the conservation of momentum equation for the solids-gas flows has been obtained by dividing both sides of equation (A3.4) by elemental volume $(A\Delta x)$ as shown below:

$$\varepsilon_a \rho_a A_a u_a \left(\frac{du_a}{dx}\right) + \varepsilon_{s1}\rho_{s1}A_{s1}u_{s1}\frac{du_{S1}}{dx} + \varepsilon_{s2}\rho_{fl}A_{s2}u_{s2}\left(\frac{du_{S2}}{dx}\right) + A_a\left(\frac{dP}{dx}\right)$$

$$= -f_a A_a - f_{s1}A_{s1} - f_{s2}A_{s2} \qquad (A3.5)$$

Net accumulation of pressure and shear energy in the x-direction equals to

$$= A_a P u_a - A_a\left[\left(p + \frac{dp}{dx}\Delta x\right)\left(u_a + \frac{du_a}{dx}\Delta x\right)\right]$$

$$- \left[F_a\left(u_a + \frac{du_a}{dx}\frac{\Delta x}{2}\right) + F_{s1}\left(u_{s1} + \frac{du_{s1}}{dx}\frac{\Delta x}{2}\right) + F_{s1}\left(u_{s2} + \frac{du_{s2}}{dx}\frac{\Delta x}{2}\right)\right] \qquad (A3.6)$$

Net accumulation of kinetic energy in x-direction equals to

$$= \frac{1}{2}m_a u_a^2 + \frac{1}{2}m_{s1}u_{s1}^2 + \frac{1}{2}m_{s2}u_{s2}^2 - \frac{1}{2}m_a\left(u_a + \frac{du_a}{dx}\Delta x\right)^2 - \frac{1}{2}m_{s1}\left(u_{s1} + \frac{du_{s1}}{dx}\Delta x\right)^2$$

$$- \frac{1}{2}m_{s2}\left(u_{s2} + \frac{du_{s2}}{dx}\Delta x\right)^2 \qquad (A3.7)$$

Neglecting the higher-order terms and considering that there is no net accumulation of energy within the control volume under steady-state condition, the following energy equation (A3.8), which shows the net summation under steady-state equals to zero.

$$\left[A_a\left\{p\left(\frac{du_a}{dx}\right)+u_a\left(\frac{dp}{dx}\right)+u_a f_a\right\}+u_{s1}A_{s1}f_{s1}+u_{s2}A_{s2}f_{s2}+\rho_a A_a \varepsilon_a {u_a}^2\left(\frac{du_a}{dx}\right)\right.$$
$$\left.+\rho_{s1}A_{s1}\varepsilon_{s1}{u_s}^2\left(\frac{du_{s1}}{dx}\right)+\rho_{fl}A_{s2}\varepsilon_{s2}{u_s}^2\left(\frac{du_{s2}}{dx}\right)\right]=0 \qquad (A3.8)$$

The energy equation represented in the equation (A3.8) addresses the energy dissipation due to the turbulence and frictional resistance of fluid-wall interactions, particle to air, particle to particle, and particle to wall interactions. Volume fractions for the gas and solid phases obey the following relationship:

$$\varepsilon_a+\varepsilon_{s1}+\varepsilon_{s2}=1 \qquad (A3.9)$$

The system of equations (equations A3.1 to A3.3, A3.5, A3.8) have been solved for the eight variables namely, $u_a,\ u_{s1},\ u_{s2},\ \epsilon_{s1}, \epsilon_{s2},\ A_{s1},\ A_{s2}$ and P. Firstly, the conservation equations, i.e., equations A3.1 to A3.3, A3.5, A3.8, have been coupled and transformed into first-order ordinary differential equations (A3.10) to (A3.17), which show the evolution of an individual parameter with respect to the spatial distance (x) under study. The derived equations are represented in the following form:

$$\frac{du_a}{dx} = \left[\frac{\left\{-\frac{u_a}{\varepsilon_a}\frac{\varepsilon_{s2}}{u_{s2}}\right\}\left\{\frac{X_1 - X_2}{Y_1 + Y_2}\right\} - \frac{u_a}{\rho_a}\left(\frac{d\rho_a}{dx}\right) + \frac{u_a}{A_a}\left\{\frac{dA_{s1}}{dx} + \frac{dA_{s2}}{dx}\right\}}{\left[\left(1 + c\frac{u_a}{\varepsilon_a}\frac{\varepsilon_{s1}}{u_{s1}}\right)\right]}\right] \quad (A3.10)$$

$$\frac{du_{s1}}{dx} = c.\left[\frac{\left\{-\frac{u_a}{\varepsilon_a}\frac{\varepsilon_{s2}}{u_{s2}}\right\}\left\{\frac{X_1 - X_2}{Y_1 + Y_2}\right\} - \frac{u_a}{\rho_a}\left(\frac{d\rho_a}{dx}\right) + \frac{u_a}{A_a}\left\{\frac{dA_{s1}}{dx} + \frac{dA_{s2}}{dx}\right\}}{\left[\left(1 + c\frac{u_a}{\varepsilon_a}\frac{\varepsilon_{s1}}{u_{s1}}\right)\right]}\right] \quad (A3.11)$$

$$\frac{du_{s2}}{dx} = \left\{\frac{X_1 - X_2}{Y_1 + Y_2}\right\} \quad (A3.12)$$

$$\frac{d\varepsilon_{s1}}{dx} = c.\left[\frac{\left\{-\frac{u_a}{\varepsilon_a}\frac{\varepsilon_{s2}}{u_{s2}}\right\}\left\{\frac{X_1 - X_2}{Y_1 + Y_2}\right\} - \frac{u_a}{\rho_a}\left(\frac{d\rho_a}{dx}\right) + \frac{u_a}{A_a}\left\{\frac{dA_{s1}}{dx} + \frac{dA_{s2}}{dx}\right\}}{\left[\left(1 + c\frac{u_a}{\varepsilon_a}\frac{\varepsilon_{s1}}{u_{s1}}\right)\right]}\right]\left[-\frac{\varepsilon_{s1}}{u_{s1}} + \frac{\varepsilon_{s1}}{A_{s1}}\left(\frac{A_{s1}}{u_{s1}}\right)\right] \quad (A3.13)$$

$$\frac{d\varepsilon_{s2}}{dx} = \left\{\frac{X_1 - X_2}{Y_1 + Y_2}\right\}\left[-\frac{\varepsilon_{s2}}{u_{s2}} + \frac{\varepsilon_{s2}}{A_{s2}}\left(\frac{A_{s2}}{u_{s2}}\right)\right] \quad (A3.14)$$

$$\frac{dA_{s1}}{dx} = \left[-\frac{A_{s1}}{u_{s1}}\ c.\left[\frac{\left\{-\frac{u_a}{\varepsilon_a}\frac{\varepsilon_{s2}}{u_{s2}}\right\}\left\{\frac{X_1 - X_2}{Y_1 + Y_2}\right\} - \frac{u_a}{\rho_a}\left(\frac{d\rho_a}{dx}\right) + \frac{u_a}{A_a}\left\{\frac{dA_{s1}}{dx} + \frac{dA_{s2}}{dx}\right\}}{\left[\left(1 + c\frac{u_a}{\varepsilon_a}\frac{\varepsilon_{s1}}{u_{s1}}\right)\right]}\right]\right] \quad (A3.15)$$

$$\frac{dA_{s2}}{dx} = -\frac{A_{s2}}{u_{s2}}\left\{\frac{X_1 - X_2}{Y_1 + Y_2}\right\} \quad (A3.16)$$

$$\frac{dP}{dx} = -f_a - f_{s1}\left(\frac{A_{s1}}{A_a}\right) - f_{s2}\left(\frac{A_{s2}}{A_a}\right)$$

$$+\left[\frac{\left\{-\frac{u_a}{\varepsilon_a}\frac{\varepsilon_{s2}}{u_{s2}}\right\}\left\{\frac{X_1 - X_2}{Y_1 + Y_2}\right\} - \frac{u_a}{\rho_a}\left(\frac{d\rho_a}{dx}\right) + \frac{u_a}{A_a}\left\{\frac{dA_{s1}}{dx} + \frac{dA_{s2}}{dx}\right\}}{\left[\left(1 + c\frac{u_a}{\varepsilon_a}\frac{\varepsilon_{s1}}{u_{s1}}\right)\right]}\right]\left\{-\rho_a\varepsilon_a u_a\right.$$

$$\left. - \rho_{s1}u_{s1}\varepsilon_{s1}\left(\frac{A_{s1}}{A_a}\right).c\right\} - \rho_{fl}u_{s2}\varepsilon_{s2}\left(\frac{A_{s2}}{A_a}\right)\left[\left\{\frac{X_1 - X_2}{Y_1 + Y_2}\right\}\right] \qquad (A3.17)$$

where,

$$X_1 = \left[-(u_{s1} - u_a)f_{s1}A_{s1} - (u_{s2} - u_a)f_{s2}A_{s2} + A_aP\left(\frac{u_a}{\rho_a}\right)\left(\frac{d\rho_a}{dx}\right)\right]$$

$$X_2 = \left[c.\varepsilon_{s1}\frac{u_a}{\rho_a}\left(\frac{d\rho_a}{dx}\right)\left\{A_aP\left(\frac{u_a}{\varepsilon_a u_{s1}}\right) - \rho_{s1}A_{s1}u_{s1}(u_{s1} - u_a)\right\}\right]$$

$$Y_1 = \left[\left\{\frac{c\varepsilon_{s1}\left(\frac{u_a}{\varepsilon_a}\frac{\varepsilon_{s2}}{u_{s2}}\right)}{\left(1 + c\frac{u_a}{\varepsilon_a}\frac{\varepsilon_{s1}}{u_{s1}}\right)}\right\}\left\{A_a\frac{P}{\varepsilon_a}\frac{u_a}{u_{s1}} - \rho_{s1}A_{s1}u_{s1}(u_{s1} - u_a)\right\}\right]$$

$$Y_2 = \left[\varepsilon_{s2}\left\{\rho_{fl}A_{s2}u_{s2}(u_{s2} - u_a)\right\} - A_aP\left(\frac{u_a}{\varepsilon_a u_{s2}}\right)\right]$$

The set of equations (A3.10) to (A3.17) present the evolution of the parameters u_a, u_{s1}, u_{s2}, ϵ_{s1}, ϵ_{s2}, A_{s1}, A_{s2} and P respectively, along with the length (x) of the pipeline. The entire length of the pipeline has been divided into several straight pipe segments (6 in numbers) (Figure A1.1). Large

straight pipeline segments have been divided into smaller segments. In the present investigation, the different values of 'x ' thus obtained on the horizontal segments of pipe for the purpose of study, have been provided in Table 4.2 (starting from the location of the blow tank). For each small segment of the pipe, a set of coupled ordinary differential equations have been solved numerically using MATLAB's ode45 solver, which is based on the fourth-fifth-order Runge-Kutta-Fehlberg (RKF45) method (Fehlberg, 1969). The solution proceeded from the pipe inlet to the outlet. In order to calculate the initial value of $u_a,\ u_{s1},\ u_{s2},\ \epsilon_{s1}, \epsilon_{s2}$ and $A_{s1},\ A_{s2}$ the following formulae have been used, represented by the following equations (A3.18 to A3.24). It has been assumed that when the material is discharged from the blow tank, the aerated mixture occupies the full cross-section of the pipe. The extent of occupancy decreases subsequently along the direction of flow in the pipeline.

$$\mathrm{u_{s1}} = u_a \left[1 - 0.02 \left[Ar \left(\frac{\rho_p - \rho_a}{\rho_a}\right)\left(\frac{D}{D_{50}}\right)^{-2}\right]^{0.14}\right] \qquad \text{(Santo et al., 2018)} \qquad (A3.18)$$

$$u_{s2} = \frac{m_{s2}}{\rho_{fl}.A_{s2}} \qquad (A3.19)$$

$$u_a = \frac{(m_a/A_a)}{(\varepsilon_a/\rho_{ai})} \qquad (A3.20)$$

$$\varepsilon_{s1} = \frac{(m_{s1}/\rho_s)}{[m_{s1}/\rho_s + m_a/\rho_{ai}]} \qquad (A3.21)$$

$$\varepsilon_{s2} = \frac{(m_{s2}/\rho_{fl})}{[m_{s2}/\rho_{fl} + m_a/\rho_{ai}]} \quad (A3.22)$$

$$A_{s1} = \left[\frac{(m_{s1}/\rho_s)}{[m_{s1}/\rho_s + m_a/\rho_{ai}]}\right] * A_{Total} \quad (A3.23)$$

$$A_{s2} = \left[\frac{(m_{s2}/\rho_{fl})}{[m_{s2}/\rho_{fl} + m_a/\rho_{ai}]}\right] * A_{Total} \quad (A3.24)$$

Numerically calculated values of the different parameters, such as u_a, u_{s1}, u_{s2}, ϵ_{s1}, ϵ_{s2}, A_{s1}, A_{s2} and P obtained at the end of the first segment of the pipe were considered as the initial conditions for the successive segment. This process has been followed in all subsequent segments of pipe up to the last segment of the pipeline. Thus, the value of the different parameters u_a, u_{s1}, u_{s2}, ϵ_{s1}, ϵ_{s2}, A_{s1}, A_{s2} and P have been calculated at the initial and final point of each segment of the pipe and with the help of these, results corresponding to the mid-point values (at x, given in Table 4.2) were acquired. Calculations have been performed for different operating parameters, i.e., corresponding to different solid flow rates in t/h, airflow rates in kg/s, and fluidized bulk density in kg/m^3 (for different products given in Table 4.2). While performing the numerical simulations in MATLAB program, it was found that the program becomes unstable after 4th/5th segment for almost all respective solids flow rates in t/h and airflow rates in kg/s for all 3 products used in the investigation. Therefore, using the proposed 3-layer approach, valid results for the parameters under consideration could not be obtained. It was decided to consider this topic as the future scope of the study.

ANNEXURE A4

ADDITIONAL RESULTS OF TWO-LAYER MODEL DEVELOPMENT WITH RHEOLOGY EFFECTS

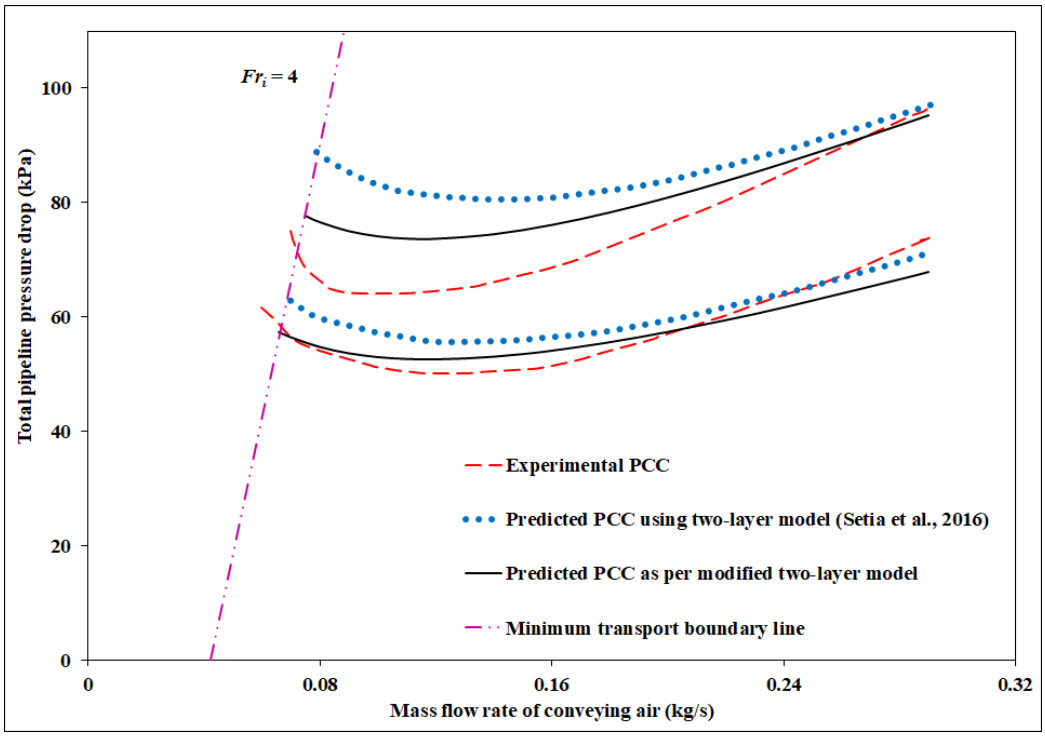

Figure A4.1: Scale-up validation for solids friction factor (modified two-layer model with rheology) for fly ash through 105 mm I.D. × 168 m long pipe

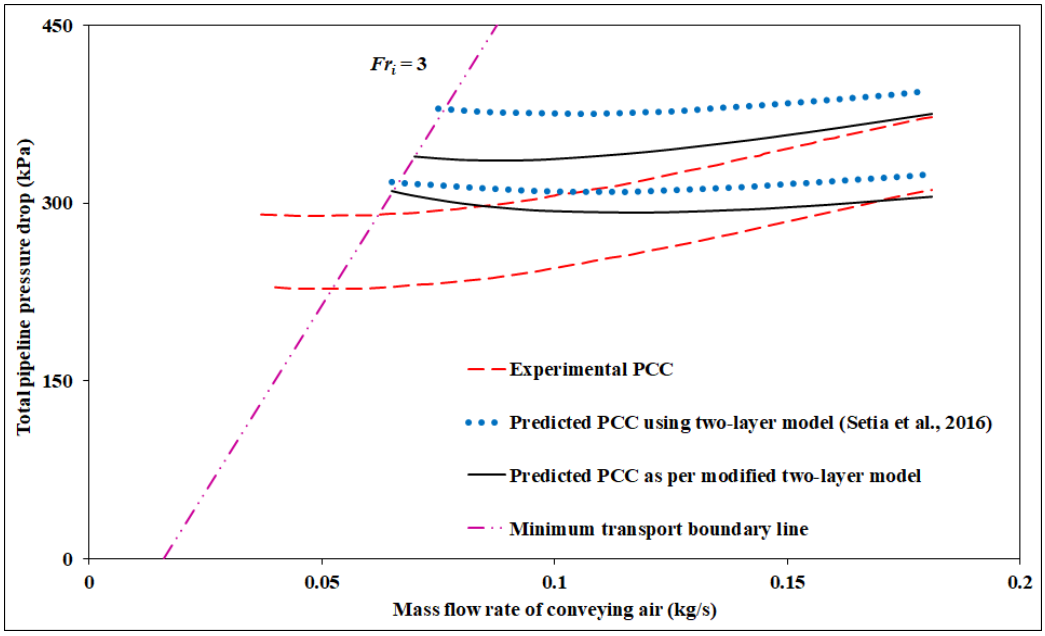

Figure A4.2: Scale-up validation for solids friction factor (modified two-layer model with rheology) for fly ash through 80/100 mm I.D. × 407 m long pipe

LIST OF PUBLICATIONS DURING COURSE OF PhD

Referred SCI journal papers (published/accepted) – 4 Nos.

Sr. No.	Title of paper	Author's Names	Journal Name	Publisher	Volume, Year, Page no.	Impact factor
1.	On developing improved modelling for particle velocity and solids friction for fluidized dense-phase pneumatic transport systems	**K. Sharma,** S.S. Mallick, A. Mittal, R. Pan	Powder Technology	Elsevier	332, 2018, 41-55	3.413
2.	Modelling Solids Friction for Fluidized Dense-Phase Pneumatic Conveying	**K. Sharma,** S.S. Mallick, A. Mittal, P.W. Wypych	Particulate Science & Technology	Taylor and Francis	DOI: 10.1080/ 02726351. 2018. 1545712	1.424
3.	An evaluation of testing and modeling procedure for solids friction factor for fluidized dense-phase pneumatic conveying of fine powders	**K. Sharma,** S.S. Mallick, A. Mittal	Particulate Science & Technology	Taylor and Francis	DOI: 10.1080/ 02726351. 2019. 1662527	1.424
4.	A study of energy loss due to particle to particle and wall collisions during fluidized dense-phase pneumatic transport	**K. Sharma,** S.S. Mallick, A. Mittal	Powder Technology	Elsevier	362, 2020, 707-716	3.413